universität wien

DISSERTATION

Titel der Dissertation

Experimental data guided ligand docking at the benzodiazepine binding site of $GABA_A$ receptors

Verfasser

Mag. pharm. Lars Richter

angestrebter akademischer Grad

Doktor der Naturwissenschaften (Dr.rer.nat.)

Wien, 2012

Studienkennzahl lt. Studienblatt:	A 091 449
Dissertationsgebiet lt. Studienblatt:	Pharmazie
Betreuer:	Prof. Gerhard F. Ecker

In liebevoller Erinnerung

an meinen Vater Emil, meine Schwester Michaela und meinen Bruder Kay

First and foremost I offer my sincerest gratitude to my supervisor, Prof. Dr. Gerhard Ecker. I had the great luck to work with such an extraordinary personality. Those who know Prof. Ecker know his passion and commitment to science and peak performance that is so impressive as infectious. Furthermore, I strongly admire his distinguished interpersonal competences, making him an excellent group leader, and mixed with his deep scientific knowledge, a valuable enrichment in the scientific community of computer-aided drug design. In total I can state that Prof. Ecker is an idol for me and other group members in many facets of life. Thank you, Gerhard.

I want to thank Dr. Margot Ernst for her kind introduction into the field of $GABA_A$ receptors. I learned a lot in the cooperation with such an intelligent and creative scientist. Let the nightly “Sternenhaufen” remind us of this very productive time.

I'm very proud that I can mention that I was also supervised by Prof. Dr. Werner Sieghart, one of the world top scientist, if not the top scientist at the $GABA_A$ receptor. I expected his deep knowledge in the $GABA_A$ receptor field but I was astonished about his curiosity and openness towards computational methodologies. I want to thank him for his trust and his unbelievable endurance that finally led to a publication in a top journal.

I was in the lucky position to cooperate with a further world top scientist at the $GABA_A$ field, Prof. Erwin Sigel. I want to thank him for the helpful critical discussions and his support in many fields that strongly influenced this thesis.

Further I want to thank Zdravko Varagic who performed the experimental testing of selected compounds working late often. All the best to this hard worker and great volleyball player.

I would like to thank all my friends and colleagues at Pharmacoinformatics Research Group. Thanks to Barbara Zdrazil, Dominik Kaiser, Rita Schwaha, Michael Demel, Khac-Minh Thai, Daniela Digles, Ishrat Jabeen, Nathan Poongavanam, René Weissensteiner, Andrea Schiesaro, Andreas Jurik, Freya Klepsch, Marta Pinto, Amir Seddik, Daria Tsareva, Rainer Dangl, Katharina Prokes, Christoph Waglechner for their wonderful company during my PhD thesis.

Furthermore I also want to address special thanks to my friends Christoph Kerschbaum and Markus Mayerhofer, which accompanied me in every life situation. I will never forget that.

My personal "hit" during this PhD-study was not found in virtual screening runs, instead I instantly met her in reality. I want to thank my "hit" Victoria Slubowski for all her love and support during my PhD-thesis.

Mein größter Dank gilt meiner Familie, die mich zu der Persönlichkeit formte, die ich heute bin. Ich möchte mich bei meinen Eltern, Tabea Mueller Richter und Emil Friedrich Richter, vor allem für ihre bedingungslose Liebe bedanken, aus der ich viel geschöpft habe und sicherlich noch viel schöpfen werde. Desweiteren möchte ich mich bei meiner Schwester Michaela und bei meinem Bruder Kay für all die schönen unvergesslichen Momente bedanken, die wir gemeinsam erlebt haben. Ich vermisse euch und Papa.

Benzodiazepines exert their anxiolytic, anticonvulsant, muscle relaxant, and sedative-hypnotic properties by allosterically enhancing the action of GABA at $GABA_A$ receptors via their benzodiazepine binding site. After 50 years of clinical use, the molecular basis of this interaction still is not known as all attempts for structural resolution failed so far. In the absence of a crystal structure, protein homology modeling and molecular dockings are the only source for structure-based binding mode hypotheses for benzodiazepines. But two obstacles make this undertaking extraordinary challenging. First, the homology models were quite uncertain due to the low target-to-template sequence identity. And secondly, although standard docking tools are capable of reproducing the correct binding mode, they regularly fail to select this out of the produced pose list.

In this thesis, the obstacles were tackled in a two step approach. Primarily, the model uncertainty was faced by an *explorative step,* where nine benzodiazepines were docked into an array of $\alpha1\beta2\gamma2$ $GABA_A$ homology models, considering flexible sidechains and keeping the 100 best scored poses per ligand per model. Consequently in the *selection step*, exhaustive implementations of various validation sources in an orchestrated and integrative manner were necessary to filter the gigantic pose space. A key criterion in this filtering process was the common binding mode (CBM) hypothesis, which assumes that diazepam and its close structural analogues exhibit a common binding mode within the binding site. Therefore, ligand poses were clustered according to their common scaffold, which led to three common binding mode geometries, CBM I–III. Then, the integrative qualities of CBM came into effect by incorporating experimental information from nine benzodiazepines for CBM I-III validation. The evaluation clearly demonstrated that CBM I is convincingly supported by a large variety of structural, computational and experimental evidence. The CBM I ligand-receptor complex was then used in structure-based virtual screening runs and led to the successful discovery of three novel, experimentally validated, benzodiazepine binding site ligand classes. The structural models were also used to investigate mechanistic receptor features and finally identified $\alpha1$Y168 to be important for the mechanistic coupling from benzodiazepine binding to $GABA_A$ channel modulation.

In a broader view, the gained structural models for $\alpha1\beta2\gamma2$ $GABA_A$ receptors can be used for modelling other $GABA_A$ receptor subtypes that will ultimately improve our understanding of the structural determinants for subtype selectivity of $GABA_A$ receptors, leading to drugs excluding subtypes known to be responsible for addicting. Finally, the underlying computational workflow can stimulate other groups to integrate various information pieces in binding mode elucidation of structurally unresolved membrane proteins.

Die anxiolytische, antikonvulsive, muskelrelaxierende und sedative-hypnotische Wirkung von Benzodiazepinen wird durch allosterische Verstärkung der GABA Aktivität am $GABA_A$ Rezeptor ausgeübt. Nach 50 Jahren in klinischer Verwendung ist die molekulare Basis für diese Interaktion immer noch ungeklärt, da alle Maßnahmen zur strukturellen Aufklärung scheiterten. In Abwesenheit einer Kristallstruktur sind Homology Modeling und Molekulares Docking die einzigen Möglichkeiten zur Darstellung von Bindungshypothesen für Benzodiazepine. Zwei Tatsachen erschweren diesen Weg aber deutlich: Erstens sind die Homology Modelle ungenau da die Sequenzidentität zwischen Target und Template gering ist. Und zweites, obwohl Molekulares Docking den richtigen Bindungsmodus generieren kann, kann es ihn selten aus der Menge an produzierten Posen selektieren. In dieser Dissertation wurden diese Probleme in zwei Schritten gelöst. Zuerst stellte man sich der Modellungenauigkeit in einem *explorativem Schritt*, indemneun Benzodiazepine in einen Array von $\alpha1\beta2\gamma2$ $GABA_A$ Homologie Modellen gedockt wurden, unter Berücksichtigung von flexiblen Seitenketten und Einbeziehung der besten 100 Posen pro Ligand pro Modell. Im folgenden *Selektionsschritt* waren eine ausführliche Implementierung von verschiedenen Validierungsquellen in einem orchestrierten und integrativen Verfahren notwendig, um den sehr umfangreichen Poseraum zu filtern. Ein Schlüsselkriterium in diesem Prozess war die *common binding mode* (CBM) Hypothese. Diese nimmt an, dass Diazepam und seine strukturellen Analoga einen gemeinsamen Bindungsmodus in der Bindetasche haben. Anschließendes Clustern der Posen führte zu drei *common binding mode* Cluster, CBM I-III. Die nachfolgende Validierung der drei CBMs erfolgte durch Inkorporation von experimentellen Informationen von neun Benzodiazepinen . Die Bewertung zeigte eindeutig, dass CBM I durch eine Reihe von strukturellen, energetisch-rechnerischen und experimentellen Befunden gestützt wird und somit als korrekter Bindungsmodus angesehen wird. Der CBM I Ligand-Rezeptor Komplex wurde dann für Virtuelles Screening verwendet und führte zur Entdeckung von drei neuen, experimentell bestätigten Substanzklassen, die an der Benzodiazepine Bindetasche binden. Die Strukturmodelle wurden auch für die Untersuchung von Rezeptor Mechanismen verwendet, die letztendlich die Bedeutung von $\alpha1$Y168 in der Transduktion von Benzodiazepine Bindung zu $GABA_A$ Kanal Modulation zeigten. Die gewonnen Modelle für $\alpha1\beta2\gamma2$ $GABA_A$ Rezeptoren können die Modellierung anderer Subtypen verbessern und damit die Entwicklung von Arzneistoffen vorantreiben welche nicht mehr mit Subtypen reagieren welche bekanntermaßen für die Abhängigkeit verantwortlich sind. Schließlich kann der Workflow von Gruppen mit ähnlichen Problemstellungen aufgegriffen werden.

A. Background

I. Motivation

Benzodiazepines belong to the most widely prescribed drugs in current therapeutic use and exert their anxiolytic, anticonvulsant, muscle relaxant, and sedative hypnotic properties by allosterically enhancing the action of GABA at $GABA_A$ receptors[1]. In spite of being used clinically for 50 years, their exact mode of interaction with the benzodiazepine binding site of $GABA_A$ receptors still is not known.

All experimental attempts to structurally resolve the $GABA_A$ receptor has failed so far. In particular the hydrophobic transmembrane domain of the protein aggravates the elsewhere quite successful X-ray crystallography.

In the absence of the $GABA_A$ receptor structure, a bunch of experimental methodologies were applied to gain knowledge of the spatial arrangement of ligands within the benzodiazepine site of the $GABA_A$-receptor. Over the years, methodologies like receptor mutation and ligand labelling have contributed a lot to this understanding[2,3]. But also affinity data from ligand binding assays which become manifest in structure-activity relationships gave valuable hints about the orientation of ligands in the benzodiazepine binding site[4]. However, these findings gave only a vague schematic idea of the benzodiazepine binding mode.

Suddenly new hope emerged in the year 2001 when a crystal structure from a functional and structural homologue of the extracellular ligand binding domain of the $GABA_A$ receptor, the ACh-binding protein (AChBP), became available[5].

Shortly after, the first homology models based on this crystal structure (AChBP) were generated and computational docking was used to generate structural hypotheses about the binding mode of benzodiazepines in the benzodiazepine binding site[3,6-9]. Overall, however, conclusions remained contradictory and unsatisfactory. Also after the resolution of other, more distant structural homologues, the quality of the hypotheses did not improve. The low success in the elucidation of the binding mode of 1,4-benzodiazepines with structure based approaches were based mainly on two shortcomings:

1. High ambiguity in the $GABA_A$ receptor homology models due to the low sequence identity to the templates of around 18%. Models that are built on such a low sequence identity are considered speculative at best for structure based studies[10] (**"ambiguity problem"**).

2. Even if a correct model is available and molecular docking is able to generate the correct binding mode, docking scoring functions are not competent to identify this orientation out of other solutions[11] (**"evaluation problem"**).

The fact that 60% of today's drug targets are membrane proteins[12], make the described constellation of poor structural target models in line with intensive research and accumulation of experimental data, a quite frequent problem in the drug discovery field.

The ambiguity in the models **("ambiguity problem")** could be faced by broadly sampling protein and ligand flexibility during docking. This results in an enormous amount of possible ligand-receptor complexes, but with a high likelihood of generating the correct binding mode for benzodiazepines.

However, the great challenge of this thesis lies in the subsequent step, i.e. the selection of the correctly generated binding mode out of an ocean of ligand-receptor complexes **("evaluation problem"**). Here a protocol has to be established that supports docking scoring functions in the evaluation of ligand-receptor complexes. This protocol should implement various knowledge sources (mutagenesis data, labeling data, structure-activity relationships) in an orchestrated and integrative manner, leading to the selection of one single benzodiazepine binding mode.

In a broader view the gained structural model of the benzodiazepine binding site will also improve our understanding of the molecular determinants for subtype selectivity of experimental ligands on $GABA_A$ receptors. This knowledge will aid the development of subtype selective benzodiazepine binding site ligands, avoiding interactions with subtypes known to be responsible for benzodiazepine addiction[13].

But these models and the established methodology should also stimulate structure based approaches beyond the $GABA_A$ receptor field. Together with the nicotinic acetylcholine receptors (nAChR), glycine, and serotonin type3 receptors, the $GABA_A$ receptors belong to the pharmacological important protein class of ligand gated ion channels. All members of this class share a sequence identity of at least 30% to each other[14]. So the findings of this study could be of interest for researches in this important field. After all, 10% of all currently approved drug targets belong to the class of ligand gated ion channels[15], highlighting once again the pharmacological relevance of this protein class.

References:

1. Sieghart, W. Structure and pharmacology of gamma-aminobutyric acidA receptor subtypes. *Pharmacol Rev* **47**, 181-234 (1995).
2. Sigel, E. Mapping of the benzodiazepine recognition site on GABA(A) receptors. *Curr Top Med Chem* **2**, 833-9 (2002).
3. Clayton, T. et al. An updated unified pharmacophore model of the benzodiazepine binding site on gamma-aminobutyric acid(a) receptors: correlation with comparative models. *Curr. Med. Chem.* **14**, 2755-2775 (2007).
4. Zhang, W., Koehler, K.F., Zhang, P. & Cook, J.M. Development of a comprehensive pharmacophore model for the benzodiazepine receptor. *Drug. Des. Discov.* **12**, 193-248 (1995).
5. Brejc, K. et al. Crystal structure of an ACh-binding protein reveals the ligand-binding domain of nicotinic receptors. *Nature* **411**, 269-276 (2001).
6. Mokrab, Y. et al. Exploring ligand recognition and ion flow in comparative models of the human GABA type A receptor. *J. Mol. Graph. Model.* **26**, 760-774 (2007).
7. Ci, S., Ren, T. & Su, Z. Investigating the putative binding-mode of GABA and diazepam within GABA A receptor using molecular modeling. *Protein J.* **27**, 71-78 (2008).
8. Berezhnoy, D., Gibbs, T.T. & Farb, D.H. Docking of 1,4-benzodiazepines in the alpha1/gamma2 GABA(A) receptor modulator site. *Mol. Pharmacol.* **76**, 440-450 (2009).
9. Sancar, F., Ericksen, S.S., Kucken, A.M., Teissére, J.A. & Czajkowski, C. Structural determinants for high-affinity zolpidem binding to GABA-A receptors. *Mol. Pharmacol.* **71**, 38-46 (2007).
10. Cavasotto, C.N. & Phatak, S.S. Homology modeling in drug discovery: current trends and applications. *Drug Discov Today* **14**, 676-83 (2009).
11. Warren, G.L. et al. A critical assessment of docking programs and scoring functions. *J. Med. Chem.* **49**, 5912-31 (2006).
12. Yildirim, M.A., Goh, K.I., Cusick, M.E., Barabasi, A.L. & Vidal, M. Drug-target network. *Nat Biotechnol* **25**, 1119-26 (2007).
13. Tan, K.R., Rudolph, U. & Luscher, C. Hooked on benzodiazepines: GABAA receptor subtypes and addiction. *Trends Neurosci* **34**, 188-97 (2011).
14. Sieghart, W. et al. Structure and subunit composition of GABA(A) receptors. *Neurochem Int* **34**, 379-85 (1999).
15. Rask-Andersen, M., Almen, M.S. & Schioth, H.B. Trends in the exploitation of novel drug targets. *Nat Rev Drug Discov* **10**, 579-90 (2011).

II. Biological Background

Current Medicinal Chemistry, 2007, *14*, 2755-2775

An Updated Unified Pharmacophore Model of the Benzodiazepine Binding Site on γ-Aminobutyric Acid$_a$ Receptors: Correlation with Comparative Models

T. Clayton[1], J.L. Chen[1], M. Ernst[4], L. Richter[4,5], B.A. Cromer[2], C.J. Morton*[,2], H. Ng[2], C.C. Kaczorowski[1], F.J. Helmstetter[2], R. Furtmüller[4], G. Ecker[5], M.W. Parker[3], W. Sieghart[4] and J.M. Cook*[,1]

[1]Departments of Chemistry & Biochemistry and [2]Psychology, University of Wisconsin-Milwaukee, Milwaukee, WI 53201; [3]St. Vincent's Institute of Medical Research, Victoria 3065, Australia; [4]Division of Biochemistry & Molecular Biology, Center for Brain Research, Medical University Vienna, A-1090, Vienna, Austria; [5]Department of Medicinal Chemistry, University Vienna, A-1090 Vienna, Austria

Contribution of the thesis author to this review:

The thesis author contributed to the computational section of this review (p. 2770 – 2774) with the aim of positioning the ligand based pharmacophore model into homology models of the benzodiazepine binding site of the α1β2γ2 $GABA_A$ receptor. The homology models were provided by M. Ernst and W. Sieghart. The molecular docking of diazepam into the homology models and the subsequent pose analysis was undertaken by the thesis author. Computational tools were programmed that aided the pose selection towards a diazepam pose that fit also the orientation and residue assignments of the ligand based pharmacophore model.

An Updated Unified Pharmacophore Model of the Benzodiazepine Binding Site on γ-Aminobutyric Acid$_a$ Receptors: Correlation with Comparative Models

T. Clayton[1], J.L. Chen[1], M. Ernst[4], L. Richter[4,5], B.A. Cromer[2], C.J. Morton*[,2], H. Ng[2], C.C. Kaczorowski[1], F.J. Helmstetter[2], R. Furtmüller[4], G. Ecker[5], M.W. Parker[3], W. Sieghart[4] and J.M. Cook*[,1]

[1]Departments of Chemistry & Biochemistry and [2]Psychology, University of Wisconsin-Milwaukee, Milwaukee, WI 53201; [3]St. Vincent's Institute of Medical Research, Victoria 3065, Australia; [4]Division of Biochemistry & Molecular Biology, Center for Brain Research, Medical University Vienna, A-1090, Vienna, Austria; [5]Department of Medicinal Chemistry, University Vienna, A-1090 Vienna, Austria

Abstract: A successful unified pharmacophore/receptor model which has guided the synthesis of subtype selective compounds is reviewed in light of recent developments both in ligand synthesis and structural studies of the binding site itself. The evaluation of experimental data in combination with a comparative model of the α1β2γ2 $GABA_A$ receptor leads to an orientation of the pharmacophore model within the Bz BS. Results not only are important for the rational design of selective ligands, but also for the identification and evaluation of possible roles which specific residues may have within the benzodiazepine binding pocket.

Keywords: Aminobutyric acid(A) receptors, gated ion channels, GABA-A, computer-assisted analysis, benzodiazepine.

The $GABA_A$ receptor is the major inhibitory neurotransmitter receptor of the central nervous system (CNS) and the site of action of a variety of pharmacologically and clinically important drugs, such as benzodiazepines, barbiturates, neuroactive steroids, anesthetics and convulsants [1]. It is now clear that these receptors regulate the excitability of the brain, anxiety, muscle tone, circadian rhythms, sleep, vigilance, memory, and learning [1]. There are several disease states associated with the improper functioning of this protein, including anxiety, epilepsy [2], insomnia [3], depression and bipolar disorder [4, 5], schizophrenia [6], as well as mild cognitive impairment and Alzheimer's disease [7]. A role of $GABA_A$ receptors in drug and alcohol abuse has also been reported [8-10].

$GABA_A$ receptors are composed of 5 subunits that form a central chloride channel and can belong to different subunit classes. A total of 19 subunits ($6\alpha, 3\beta, 3\gamma, 1\delta, 1\varepsilon, 1\pi, 1\theta, 3\rho$) of the $GABA_A$ receptor have been cloned and sequenced from the mammalian nervous system [11, 12]. All these polypeptides possess an approximate molecular mass of ~ 50 kD and are structurally related. Each subunit consists of a large extracellular region, which contains several potential glycosylation sites and a characteristic "cys-loop" formed by a covalent bond between two conserved cysteines. This extracellular region is also important in contributing to the agonist GABA and modulatory benzodiazepine binding sites. The protein then traverses the lipid bilayer four times and has a large intracellular loop located between transmembrane regions 3 and 4 (M3 and M4). This intracellular region contains possible phosphorylation sites necessary for regulation of the receptor. The homology within each subunit class is about 60 – 80 %, while the homology between subunit classes is about 30 – 40 %. In Fig. (**1**) the proposed topology of a single $GABA_A$ receptor subunit is shown. The pentameric structure of a ligand-gated ion channel is shown in Fig. (**2**) [13, 14].

The existence of multiple $GABA_A$ receptor subunits can give rise to a large number of different $GABA_A$ receptor subtypes [15]. The majority of $GABA_A$ receptors, however, is composed of 1γ and 2α and 2β subunits. The presence of a γ subunit within a $GABA_A$ receptor is necessary for the formation of a benzodiazepine binding site that is located at the interface of an α and γ subunit. Whereas the classical benzodiazepines, such as diazepam or flunitrazepam, exhibit a high affinity for receptors composed of α1βγ2, α2βγ2, α3βγ2 or α5βγ2 subunits (diazepam sensitive (DS) receptors), as well as for their less intensively investigated analogues containing the γ3 subunit, other benzodiazepine binding site ligands are also able to interact with α4βγ2 or α6βγ2 receptors (diazepam insensitive (DI) receptors), or with receptors containing γ1 subunits [1]. Receptors containing γ1 or γ3 subunits exhibit a quite low abundance in the brain [16-18] and their contribution to the "*in vivo*" effects of benzodiazepine binding site (BZ BS) ligands currently is unclear.

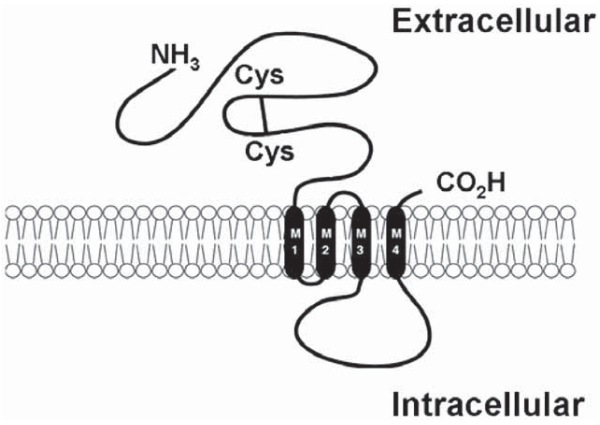

Fig. (1). Proposed topology of a $GABA_A$ receptor subunit. The extracellular domain begins with the N-terminus and M1-M4 represent the four transmembrane domains. Figure reprinted with permission [13].

The concept of receptor multiplicity has been extremely valuable, in that different receptor subtypes reside within anatomically distinct regions of the brain and are responsible for different physiological and pathological processes [15, 19, 20]. For example, the α1βγ2 receptor subtype has a prominent role in seizure susceptibility and sedation [21-23], the α2βγ2 and possibly also the α3βγ2 subtypes are involved in anxiety, whereas the α5βγ2 subtype has a prominent role in memory and learning (Table **1**) [15, 24-26]. These distinctions have thus become a motivation for the design of subtype selective ligands in order to elicit a single specific response [15, 27-34]. Differences observed in the action of such drugs may be due to subtype-selective affinity and absolute and/or relative subtype-selective efficacy [35].

Agonist binding to the receptor opens an intrinsic chloride ion channel, typically hyperpolarizing the cell membrane or at least opposing depolarization, thereby inhibiting neuronal transmission. Bz BS ligands are allosteric modulators, unable to induce channel openings themselves, but function to vary the frequency and not the channel opening times [37, 38]. Positive allosteric modulators at the benzodiazepine binding site (agonists) increase this frequency,

*Address correspondence to this author at the Department of Chemistry, 3210 North Cramer Street, UW-Milwaukee, Chemistry Building Milwaukee, WI 53201, UW-Milwaukee, Milwaukee, WI 53211, USA; Tel: 414-229-5856; Fax: 414-229-5530; E-mail: capncook@uwm.edu

0929-8673/07 $50.00+.00

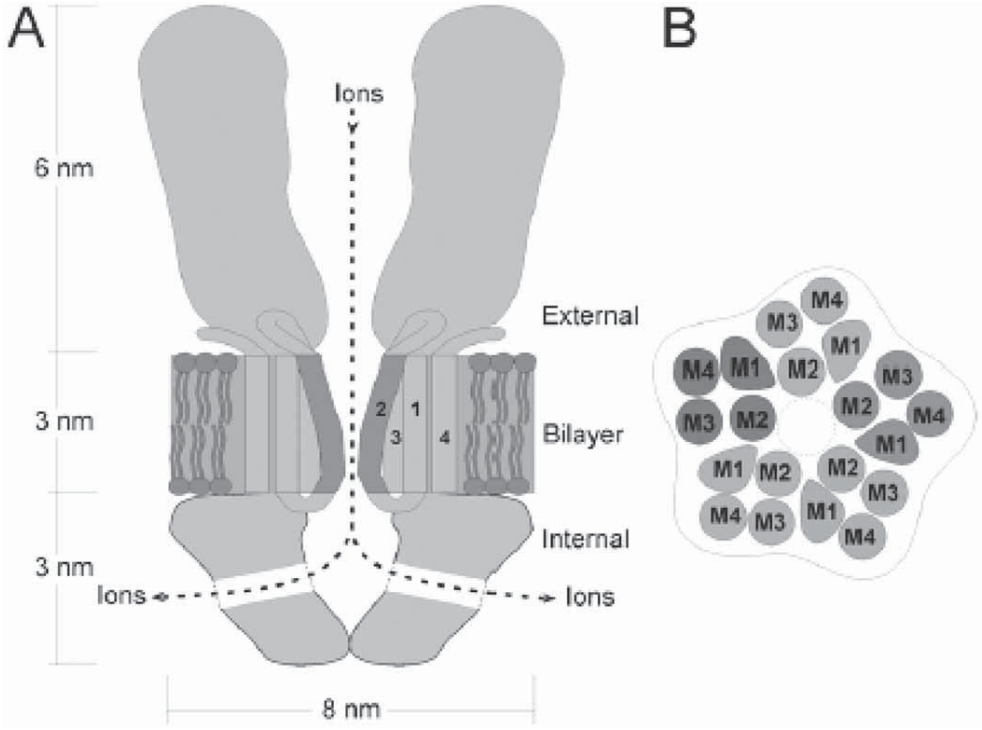

Fig. (2). Longitudinal (**A**) and cross-sectional (**B**) schematic representations of a ligand-gated ion channel. The numbers 1-4 refer to the M1-M4 segments. The M2 segment contributes to the majority of the pore lining within the membrane lipid bilayer. Figures reprinted with permission [14].

while negative allosteric modulators (inverse agonists) decrease the frequency. Currently it is not clear whether Bz BS ligands allosterically modulate GABA affinity or channel gating. Recent studies [39] support the view that high-affinity classical benzodiazepines modulate $\alpha1\beta2\gamma2$ $GABA_A$ receptors *via* allosteric coupling to channel gating [40, 41]. Further studies are needed to determine whether the mechanism of modulation varies in different receptor subtypes.

Table 1. Action of Benzodiazepines at $GABA_A$ $\alpha1-6$ $\beta3\gamma2$ Receptor Subtypes [36]

Subtype	Associated Effect
$\alpha1$	Sedation, anterograde amnesia, Some anticonvulsant action, ataxia
$\alpha2$	Anxiolytic, hypnotic (EEG), some muscle relaxation
$\alpha3$	Some anxiolytic action, some anticonvulsant action, Maybe some muscle relaxation
$\alpha4$	Diazepam-insensitive site
$\alpha5$	Cognition, temporal and spatial memory (Maybe memory component of anxiety)
$\alpha6$	Diazepam-insensitive site

In recent years a unified pharmacophore/receptor model for agonists, antagonists and inverse agonists at the Bz BS was developed, using the techniques of chemical synthesis, radioligand binding and receptor mapping [42, 43]. The overlap of these different modulators within the Bz BS has been supported by experimental data [44-46]. Using this ligand-based pharmacophore/receptor model and our $\alpha1\beta2\gamma2$ $GABA_A$ receptor models [47, 48], the experimental data of recent and past years have been evaluated, and definite trends with regard to the orientation of the regions of the protein relative to the descriptors of the pharmacophore/receptor model have been identified and are presented in this work. The need to define such an orientation has been established [49], since it permits inspection of ligand docking studies and the identification of possible roles specific residues may have within the Bz BS. These roles may then be explored in future studies involving covalent labeling, site-directed mutagenesis and structure-activity relationships, all of which contribute to the rational design of subtype-specific modulators of the Bz BS of $GABA_A$ receptors.

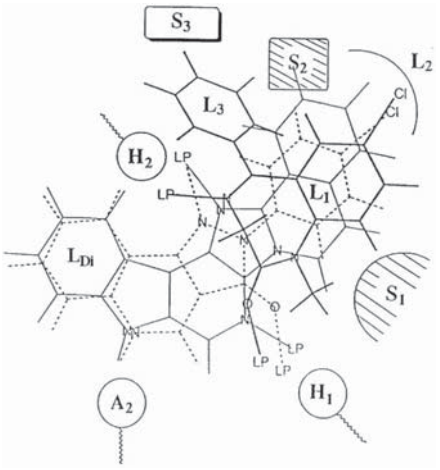

Fig. (3). Relative locations of the descriptors and regions of the unified pharmacophore/ receptor model. The pyrazolo[*3,4-c*] quinolin-3-one CGS-9896 (dotted line), a diazadiindole (thin line), and diazepam (thick line) aligned within the unified pharmacophore/receptor model for the Bz BS. H_1 and H_2 represent hydrogen bond donor sites within the Bz BS while A_2 represents a hydrogen bond acceptor site necessary for potent inverse agonist activity *in vivo*. L_1, L_2, L_3 and L_{Di} are four lipophilic regions and S_1, S_2, and S_3 are regions of negative steric repulsion. LP = lone pair of electrons on the ligands.

THE UNIFIED PHARMACOPHORE/RECEPTOR MODEL

More than 150 agonists, antagonists and inverse agonists at the Bz BS [42, 43] which encompassed 15 structural families were used for generating the unified pharmacophore/receptor model. Although the relative affinities, efficacies and functional effects displayed by various ligands from the same structural class at the diazepam-sensitive and diazepam-insensitive benzodiazepine binding sites were taken into account, the approximate locations of descriptors (hydrogen bond donor sites, hydrogen bond acceptor sites, lipophilic regions, and regions of steric repulsion) were based primarily on *in vitro* binding affinities. Ligands from different structural classes were then superposed on each other to satisfy the same descriptors, resulting in the unified pharmacophore model.

Briefly, the pharmacophore/receptor model consists of two hydrogen bond donating descriptors (H_1 and H_2), one hydrogen bond accepting descriptor (A_2) and one lipophilic descriptor (L_1). In addition to these descriptors, there are lipophilic regions of interaction (L_2, L_3 and L_{Di}) as well as regions of negative steric repulsion (S_1, S_2 and S_3). While occupation of L_2 and/or L_3 as well as interactions at H_1, H_2, and L_1 are important for positive allosteric modulation, inverse agonists only require interactions with the H_1, L_1, and A_2 descriptors of the pharmacophore/receptor model for potent activity *in vivo*. [42, 50-53] The L_{Di} descriptor is a region of lipophilic interaction, for which the difference between the diazepam sensitive (DS) and the diazepam insensitive (DI) sub-pharmacophore models is most pronounced. Depicted in Fig. (**3**) are the relative locations of the different descriptors and regions of the model.

The structures of ligands frequently referred to in this paper are shown in Fig. (**4**).

The alignments of several Bz BS ligands within this model are shown in Fig. (**5**).

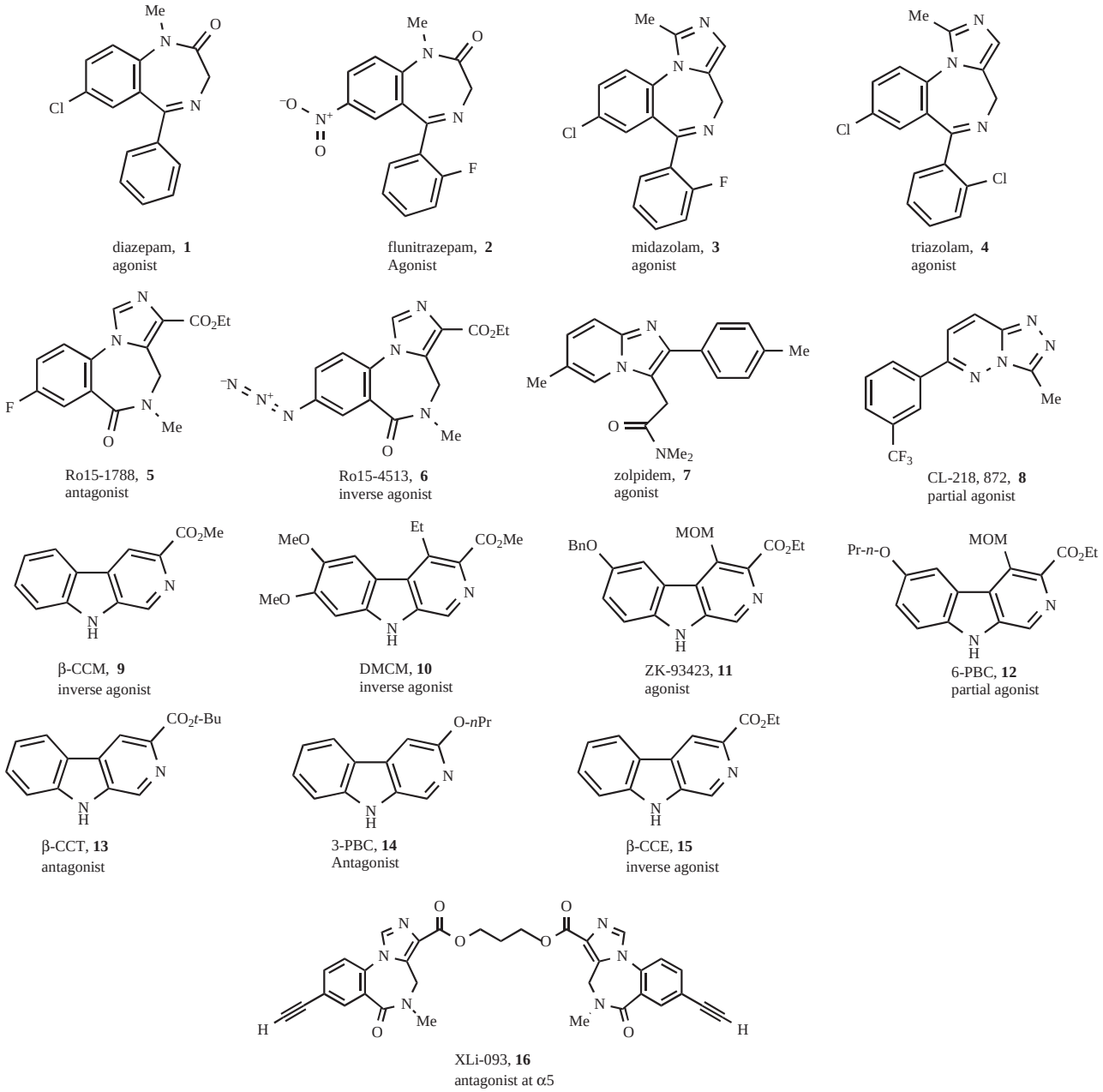

Fig. (4). Structures of ligands and their modulation at the α1 subtype.

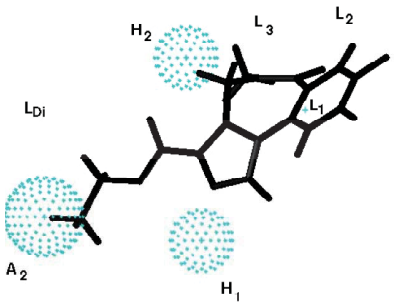

Ro 15-1788, **5**

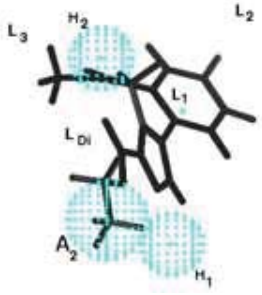

Ro 15-1788 rotated 90º

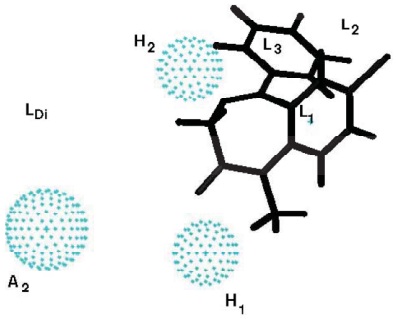

Diazepam, **1**

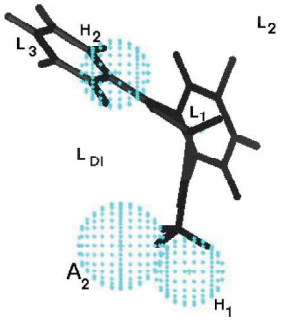

Diazepam rotated 90º

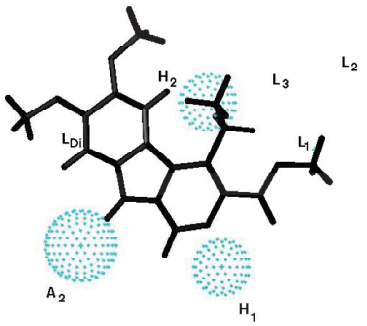

DMCM, **10**

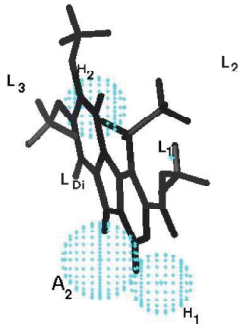

DMCM rotated 90º

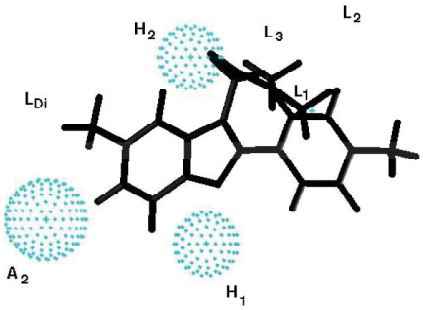

zolpidem, **7**

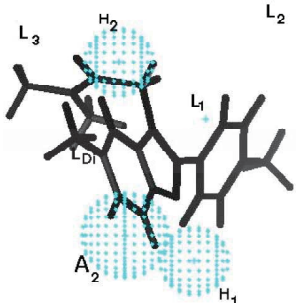

zolpidem rotated 90º

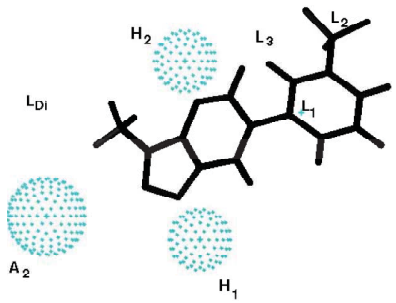

CL-218,872, **8**

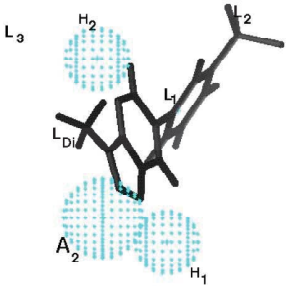

CL-218, 872 rotated 90º

Fig. (5). Alignments of several Bz BS ligands within the pharmacophore model.

INCLUDED VOLUME ANALYSIS OF LIGANDS BINDING TO RECEPTORS CONTAINING DIFFERENT ALPHA SUBUNITS

The benzodiazepine binding site of αβγ2 $GABA_A$ receptors is strongly influenced by the type of α subunit present in these receptors as indicated by the existence of ligands exhibiting certain selectivity for receptors containing the respective α subunits [1, 20, 54]. If subtype selective ligands are then aligned within the pharmacophore model according to the resulting alignment rules [55], their included volumes can be constructed and used to compare the topologies of benzodiazepine binding pockets of different receptor subtypes [55, 56]. Ligands employed in the included volume for each receptor subtype exhibited potent affinity ($K_i \leq 20$ nM) at the respective receptor subtype. CL-218,872 **5** (K_i = 57 nM at α1) and zolpidem **4** (K_i = 26.7 nM at α1) were added to the included volume of the α1β3γ2 subtype since they are both α1-subtype selective ligands. The major differences with regard to volume and affinity are shown below and are important for interpreting experimental data.

The included volume requirements show some trends that are useful to explain subtype preferences of ligands and that have already guided substance development:

1. *The included volumes of the α1, α2, and α3 subtypes are similar both in size and topology*. This is consistent with the similar affinity profiles these subtypes displayed for classical benzodiazepine agonists, pyrazoloquinolinones and imidazobenzodiazepines (*i*-BZDs) [57-59]. The included volume of the α1 subtype is slightly different from that of α2 and α3 subtype as indicated by the selective affinities of zolpidem, CL-218,872, 6-substituted β-carbolines (e.g. 6-methylbenzyl amino betacarboline) and pyridodiindoles for this subtype and the space needed for accommodating these structures (Fig. **6a**,**b**) [59]. Results from both the SAR studies and the included volume analysis imply that the α2 and α3 subtypes are very similar in shape, polarity and lipophilicity.

2. *The included volumes of the α1 and α4 or α6 subtypes are very different*. Looking at Fig. (**6d**), it is evident that the included volume of the α6 subtype is significantly smaller

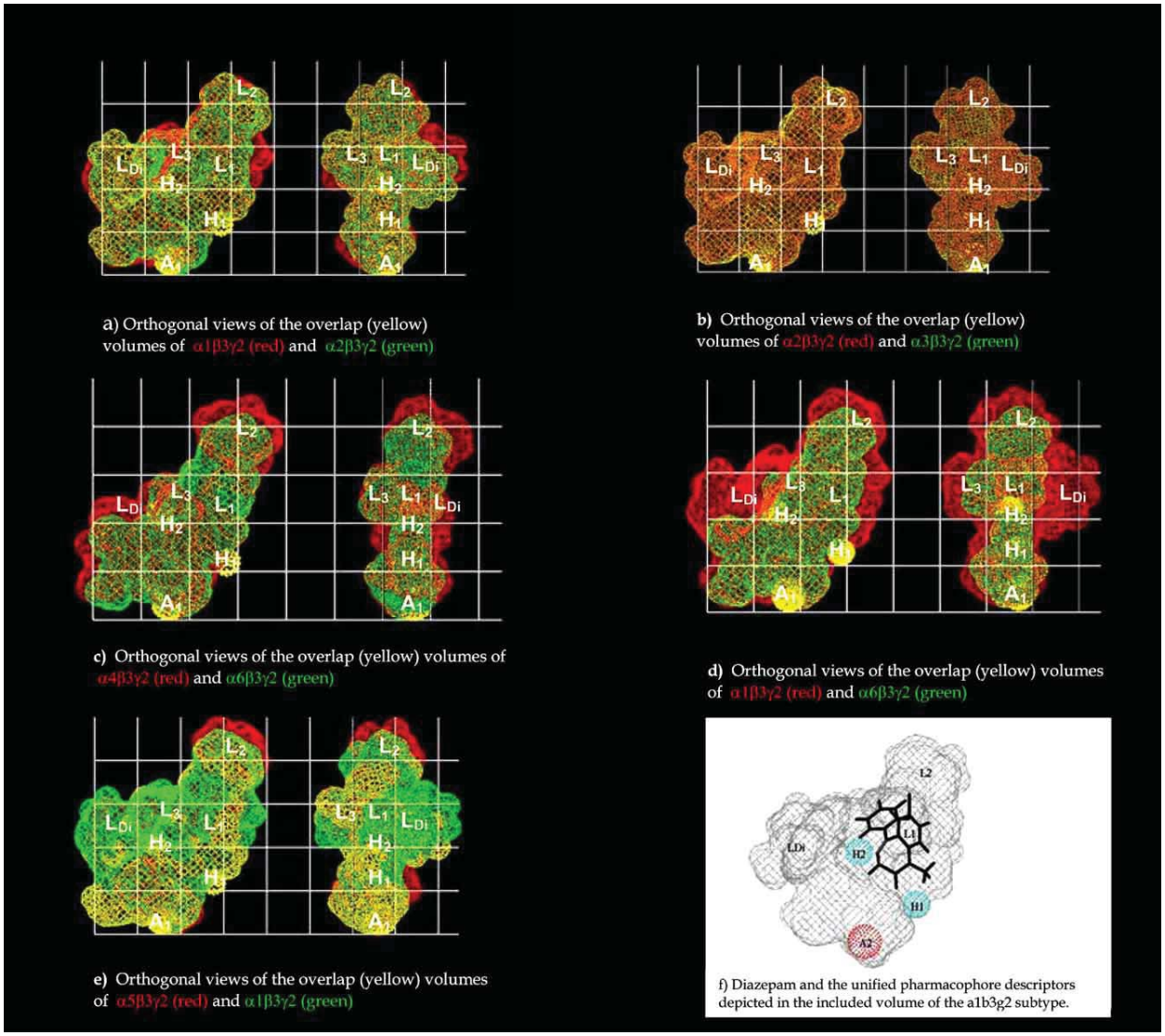

Fig. (6). Overlap between pairs of included volumes derived from receptor subtype selective ligands: a) α1 and α2, b) α2 and α3, c) α4 and α6, d) α1 and α6, e) α1 and α5. Yellow color indicates overlapping regions and each grid measures 4 Å in width and height. In order to provide the connection between this figure and other figures, f) shows diazepam and the descriptors of the unified pharmacophore model depicted in the included volume requirement of the α1 subtype.

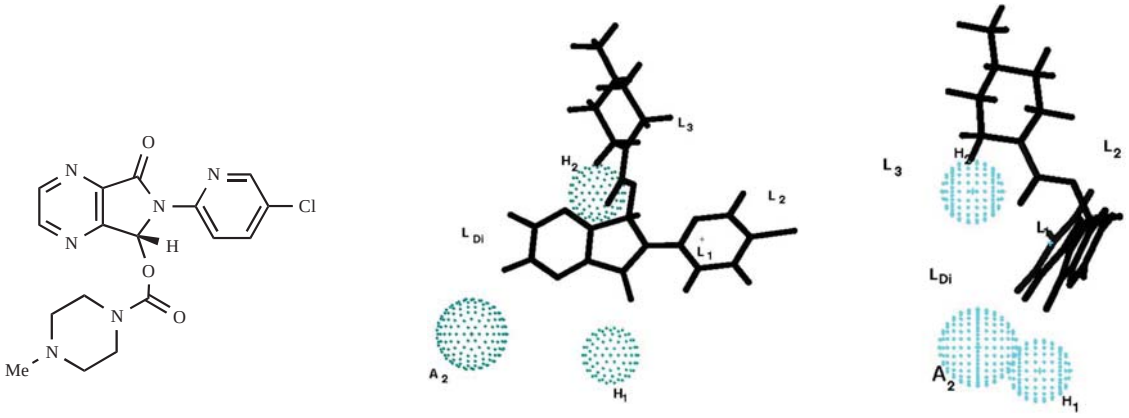

Fig. (7). Structure of zopiclone **17**, its alignment within the pharmacophore/receptor model and rotated 90 degrees.

than that of the α1 subtype. Especially the L_{Di} region is much larger in α1 receptors. Contributions to the L_{Di} region are derived in a large measure from 6-substituted β-carbolines and ring-A substituted pyrazoloquinolines, thus implying that occupation of the L_{Di} region may be critical for ligand selectivity at the α1 subtype. This is supported by the finding that the L_{Di} region was also larger for the α1β3γ2 subtype when compared with the α5β3γ2 subtype (Fig. **6e**).

3. *L_3 region is very small or non-existent for the α4 and α6 DI subtypes*. Based on the inability to bind 1,4-benzodiazepines, the lack of region L_3 was believed to be responsible for the diazepam-insensitivity of these receptor subtypes (Fig. **6c**, **d**) [42, 51]. With a few exceptions, β-carbolines also do not bind to the α6β3γ2 receptor subtype, while *i*-BZDs and pyrazoloquinolinones (CGS series) represent the primary ligands that bind to this subtype.

4. *The L_2 and L_{Di} regions are slightly smaller for the α6 versus the α4 subtype*. The sequence of the α4 subunit is most homologous to the α6 subunit and it was determined that the pharmacological profiles of these DI sites toward classical benzodiazepines are very similar [60]. Differences in the included volume of these DI sites are shown in Fig. (**6c**).

5. *The L_2 region contributes to α2 and α5 selectivity*. It has been observed that ligands with α2 and/or α5 selectivity are generally *i*-BZDs and have a lipophilic C(8)-substituent that occupies the L_2 pocket. Based on ligands from various studies, examination of data in Fig. (**6**) illustrates that the L_2 region is deeper and larger for the α2 and α5 subtypes, respectively, than for the corresponding α1 or α6 subtypes [42, 43, 51, 61]. This L_2 region seems to account for the selective affinity of ligands at the α5 subtype, as clearly illustrated in Fig. (**6e**), whereas the same region may account for the selective efficacy observed at the α2 subtype.

RECENT ALIGNMENT OF NON-CLASSICAL BZ BS LIGANDS SUPPORT THE UNIFIED PHARMACOPHORE/RECEPTOR MODEL

Besides the major classes of Bz ligands used to define the model, several non-Bz ligands also fit within the pharmacophore/receptor model very well. Examples include zopiclone **(17)** and its active enantiomer, the flavonoid **25** and the 8-chloropyrazolo[5,1-c][1,2,4]-benzotriazine 5-oxide analog **38**, as illustrated in (Figs. **7** and **8**) and (Figs. **11** and **13**).

Zopiclone and its Active Enantiomer

Since the sedative-hypnotic zopiclone **17** was first reviewed in *Drugs* in 1986 [62], a much larger body of clinical data has become available to permit a more detailed comparison of the non-benzodiazepine zopiclone with classical benzodiazepines. Results have shown that, regardless of the duration of action, zopiclone was

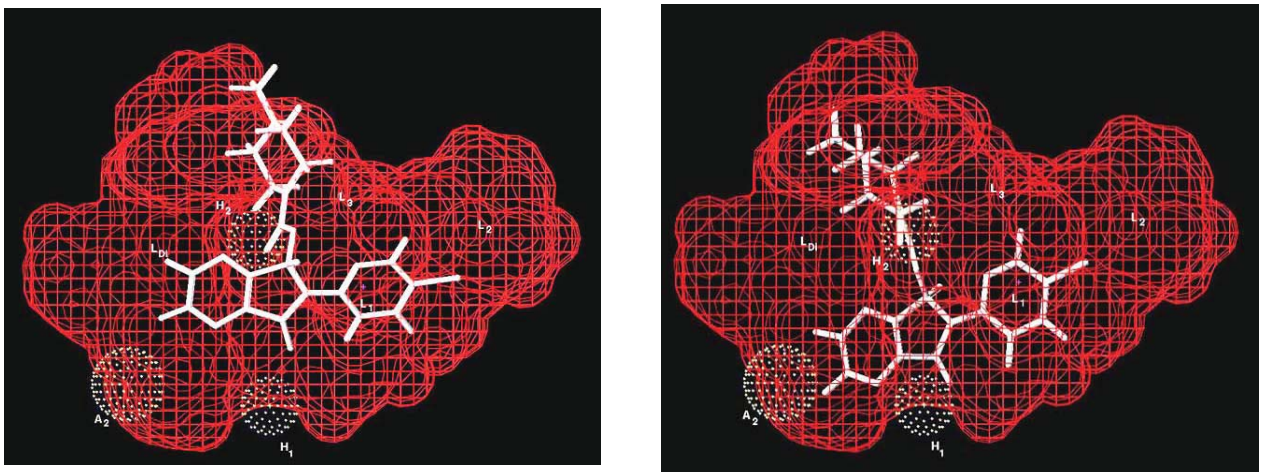

Fig. (8). Alignment of zopiclone **17** (left) and its active enantiomer (right) in the included volume of the pharmacophore/receptor model for the α1β3γ2 subtype.

generally at least as effective as benzodiazepines in the treatment of insomnia, although comparisons between zopiclone and flurazepam have produced inconsistent results. It was observed that zopiclone had a relatively low propensity to elicit residual clinical effects, such as difficulty in waking or reduced morning concentration. While tolerance to the effects of zopiclone was not noticed in short term clinical trials (≥ 4 weeks), the results from longer term studies were conflicting and, therefore, the potential for tolerance during long term administration of zopiclone was unclear. Rebound insomnia to a level above that at baseline can occur after withdrawal of zopiclone. However, on the basis of data from short term studies, this does not appear to be common. Evaluation of prescriptions filled has indicated that zopiclone does not have a high dependence potential, at least in those who are not regular drug abusers/addicts. Zopiclone was well-tolerated in both the elderly and younger patients with insomnia. A bitter after-taste was usually the most common adverse event, but was relatively infrequent at 3.6 % in the largest available post-marketing study. Thus, zopiclone has now been firmly established as an effective and well-tolerated sleep agent [63].

The structure and alignment of zopiclone within the unified pharmacophore/receptor model is shown in Fig. (**7**). The centroid of the pyridine moiety of zopiclone overlapped with region L_1 of the receptor, while the lone pair of electrons of the carbonyl oxygen (O) atom interacted with H_1 of the receptor to form a hydrogen bond between the ligand and the receptor. A second hydrogen bond was formed between the amide carbonyl oxygen atom (LP) and H_2 of the receptor protein (Fig. **7**).

However, a recent study by Sepracor [64] indicated that one of the enantiomers of zopiclone was much more active than zopiclone itself. This may be the result of receptor subtype-selective efficacy or simply a pharmacokinetic effect, but the pharmacophore/receptor model developed here revealed that the active enantiomer fits better into the included volume of the $\alpha1\beta3\gamma2$ subtype than zopiclone **17** itself (Fig. **8**). This enantiomer has just been approved by the FDA for treatment of insomnia.

SH-053BZ Enantiomers

In pursuing this approach using BZ enantiomers, the behavioral activity of three newly-synthesized compounds [65], functionally selective for α_2, α_3 and α_5-containing subtypes of $GABA_A$ receptors (SH-053-S-CH3 and SH-053-S-CH3-2'F), or essentially selective for α_5 subtypes (SH-053-R-CH3) were examined. Motor influence was tested in the elevated plus maze, spontaneous locomotor activity and rotarod test, which are considered primarily predictive of the anxiolytic, sedative and ataxic influence of BZs, respectively. There was substantially diminished ataxic potential of BZ site agonists devoid of α_1 subunit-mediated effects, with preserved anti-anxiety effects at 30 mg/kg of SH-053-S-CH3 and SH-053-S-CH3-2'F. However, all three ligands, dosed at 30 mg/kg, decreased spontaneous locomotor activity, suggesting that sedation may be partly dependent on activity mediated by α_5-containing $GABA_A$ receptors. Such an effect could not have been observed previously, because to date, all apparently non-sedating BZ receptor ligands, which are devoid of activity at α_1-containing $GABA_A$ receptors, engendered essentially antagonist [66] or only partial agonist efficacy at α_5-containing $GABA_A$ receptors [67]. Therefore, it cannot be ruled out that substantial efficacy at α5-containing $GABA_A$ receptors may contribute to sedative effects besides the effects on learning and memory processes [68, 69]. This is supported by two sets of data

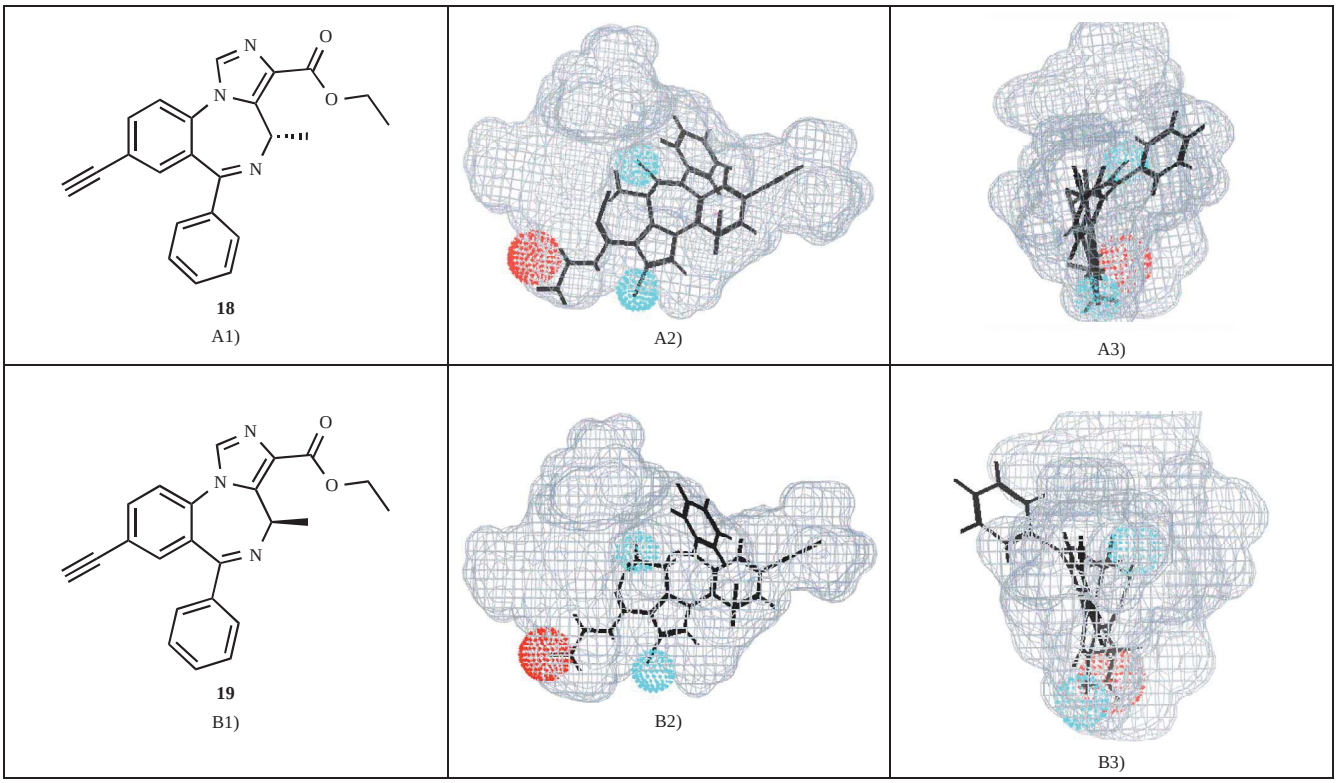

Fig. (9). Structures and conformations of SH-053-S-CH3 (A1-A3) and SH-053-R-CH3 (B1-B3). The molecular modeling was carried out as described in Zhang *et al.* 1995 and He *et al.* 2000. SH-053-S-CH_3 fits to the pharmacophore within the included volume of the $\alpha2$ subtype (A2); A3) is the same image rotated 90 degrees. It can be clearly seen that this conformer fits within the included volume. SH-053-R-CH_3 fit to the pharmacophore in the included volume of the $\alpha2$ subtype (B2); B3) is the same image rotated 90 degrees. The R-CH_3 at the prochiral center C4 changes the conformation of the molecule causing the pendant 6-phenyl to stick outside the included volume, consequently this ligand is not efficacious at the $\alpha2$ subtype. It simply does not interact strongly with $\alpha1$, $\alpha2$ or $\alpha3$ subtypes.

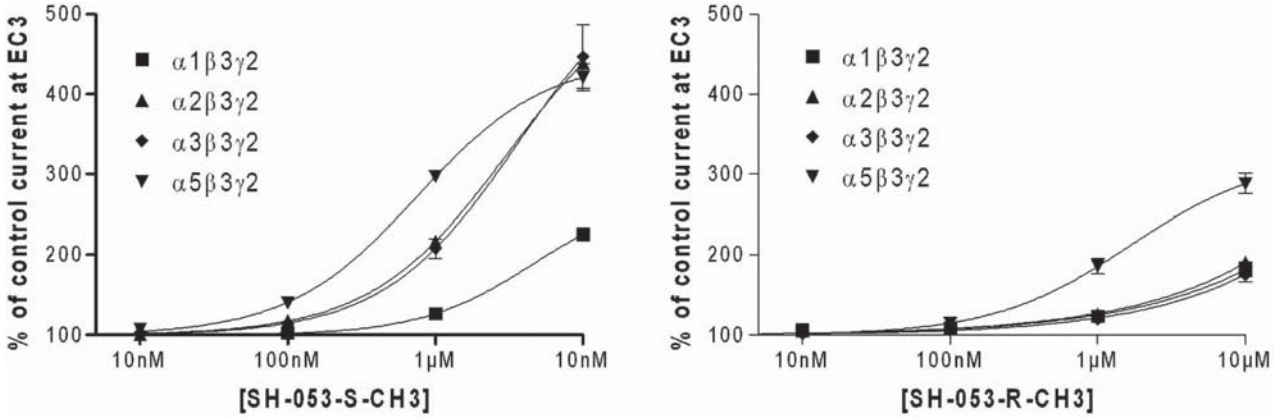

Fig. (10). Concentration-effect curves for SH-053-S-CH3 and SH-053-R-CH3 on $\alpha_1\beta_3\gamma_2$, $\alpha_2\beta_3\gamma_2$, $\alpha_3\beta_3\gamma_2$, and $\alpha_5\beta_3\gamma_2$ $GABA_A$ receptors. Data points represent means ± SEM from at least 4 oocytes from ≥ 2 batches.

which indicate the possibility of substantial motor influence *via* α5-$GABA_A$ receptor modulation: In the spinal cord, somatic and preganglionic motoneurons (lamina IX and lateral cell column) exhibited a moderate to strong staining for the α5 subunit, suggesting a possible influence of receptors containing these subunits in motor behavior [70]. In addition, the knock-in mice harboring the α5 subunit insensitive to diazepam are refractory to development of tolerance to the sedative effect of diazepam dosed subchronically. Such a tolerance development might have been caused by a down-regulation of receptors containing α5 subunits in the appropriate brain regions of wild-type mice [71]. These two sets of evidence indicate that the motor influence of α5-$GABA_A$ receptor modulation is not necessarily an indirect consequence of the established effects on learning and memory processes [68, 69]. Hence, it has been hypothesized [65] that locomotor activity changes induced by ligands possessing a substantial α5-efficacy may be, at least partly, contributed by modulation at $GABA_A$ receptors containing the α5 subunit. It therefore could be of importance to avoid substantial agonist potentiation of α_5-subunits by candidate anxioselective anxiolytics, if clinical sedation is to be avoided. Nevertheless, as a caveat to all studies examining sedation, it should be remembered that a decrease in automatically measured locomotor activity can be due to a variety of causes other than sedation, including the occurrence of stereotyped behavior, motor impairments or pain [72]. To dissect these overlaps in activity und uncertainties, much is expected from screening of even more selective BZ site ligands in the future.

Flavonoids

Flavonoids represent a class of non-Bz ligands that fit extremely well within the unified pharmacophore/receptor model. These compounds are a class of natural products isolated from a variety of herbal plants and employed as tranquilizers in folk medicine. They exhibit a wide range of biological activity, such as antiviral, anti-inflammatory, antithrombotic, antioxidant and estrogenic effects [73, 74]. Flavonoids also displayed potent anxiolytic effects and appeared devoid of myorelaxant, amnesic or sedative actions. Haberlein *et al*. has shown that the steric orientation of the substituents which lie coplanar to the aromatic ring was crucial for ligand affinity to the Bz BS [75]. This was especially true for the C(5) and C(6) positions. Furthermore, the recent work of Huang *et al*. indicated that 6,3'-dinitroflavone **25** exhibited a K_i value of 12 nM at the Bz BS (Table **2**) and was an extremely potent anxiolytic devoid of muscle relaxant effects. The 6-Br-3'-nitroflavone **26** also demonstrated increased binding affinity, however, the anxiolytic effect was lower than the dinitroanalog **25** [76].

Table 2. Affinities of a Series of Flavonoid Ligands for Benzodiazepine Receptors [76]

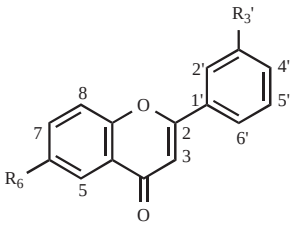

Compound	R_6	R_3'	K_i (nM)
20	F	NO_2	182
21	Cl	NO_2	8.0
22	Br	Cl	17.0
23	Cl	Br	23.0
24	Br	Br	19.1
25	NO_2	NO_2	12.0
26	Br	NO_2	1.0

The flavonoids **21**, **25** and **26** fit very well within the unified pharmacophore/receptor model. The alignment of 6,3'-dinitroflavone **25** within the α2β3γ2 subtype is shown in Fig. (**11**). The centroid of the phenyl moiety overlapped with the L_1 region

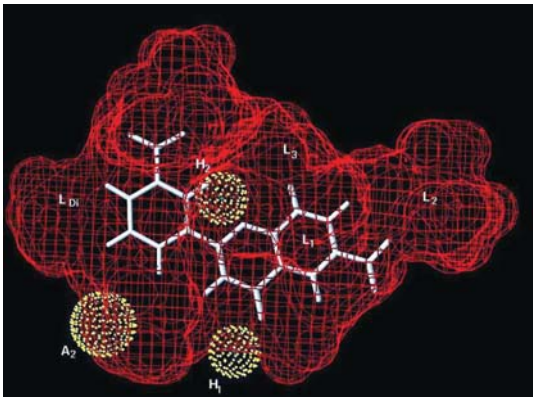

Fig. (11). Alignment of **25** within the included volume of the α2β3γ2 subtype.

and the 3'-nitro group occupied region L_2, while the lone pair of electrons of the carbonyl oxygen (O) atom interacted with H_1 to form a hydrogen bond between the ligand and the receptor. A second hydrogen bond was formed between the oxygen lone pair and H_2 of the receptor protein. This alignment essentially agrees with what has been discussed by Marder [77].

Recently, some flavone-related analogs were prepared (Fig. **12**) [78] however, these flexible ligands with additional lipophilic groups did not bind to any $GABA_A$ receptor subtype. It is believed that more planar ligands are required for affinity to these subtypes, as the twist chair of the dihydropyran unit may have prevented the fit required for high affinity at the Bz BS. Together these data, combined with the work of others, indicate the phenyl ring, the carbonyl group and the double bond between C(2) and C(3) of the flavone are the key structural features that contribute to the binding affinity of flavonoids to the Bz BS.

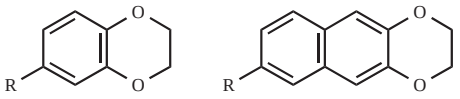

R = H, Et, $COCH_3$ or acetylene

Fig. (12). A series of flavone-related analogs that was inactive at the Bz BS.

Analogs of 8-chloropyrazolo[5,1-c][1,2,4]-benzotriazine 5-oxide

It has been recognized that small structural modifications in the same chemical family could lead to ligands which display different intrinsic activity. Costanzo *et al*. reported that small structural modifications in analogs of 8-chloropyrazolo[5,1-c][1,2,4]-benzotriazine 5-oxide produced ligands that displayed different intrinsic activity (Table **3**) [79]. When an aryl ester function occupied position-3, this class of ligands exhibited high affinity at the Bz BS (Table **3**, K_i = 11 – 35 nM). It was proposed the methoxy group of ligand **38**, which bound with an affinity of 1.0 nM, acted as an electron donor group to enhance the π–π stacking interactions between the phenyl ring of this ligand and the receptor protein. However, it may also be that the methoxy group enhanced lipophilic interactions within the L_1 region. Costanzo *et al*. proposed that net inductive and resonance effects as well as the electron donating properties (σ = - 0.27) and suitable lipophilic features (- π) of the ligand facilitated this interaction.

Table 3. Affinities of a Series of 8-Chloropyrazolo[5,1-c][1,2,4] benzotriazine 5-oxide Ligands at the Bz BS of $GABA_A$ Receptors [79]

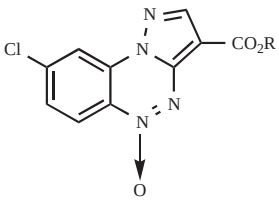

Ligand	R	K_i (nM)
27	Ph	47.5
28	4-F-Ph	146.0
29	2-F-Ph	14.0
30	4-Cl-Ph	49.2
31	2-Cl-Ph	14.4
32	4-Me-Ph	51.9
33	2-Me-Ph	38.3
34	4-NO_2-Ph	41.8
35	2-NO_2-Ph	106.0
36	4-MeO-Ph	11.6
37	3-MeO-Ph	41.1
38	2-MeO-Ph	1.0

Alignment of **38** overlaid with diazepam is shown in Fig. (**13**), wherein the N(1) and N(4) functions hydrogen bonded to the H_2 and H_1 donor receptor sites, respectively. It was felt that the 3-ester function fits into a limited dimension lipophilic pocket in the L_1/ L_2 region. Moreover, the orientation of the lone pair of electrons of the carbonyl oxygen atom of the ester function reinforced the receptor binding by means of a 3-centered hydrogen bond (N(4)/ CO/ H_1). This hydrogen bond, which is similar to that described for the C(3) ester substituent in β-carbolines, is also strengthened by the interaction between the 5-oxide group and the nitrogen atom with H_1.

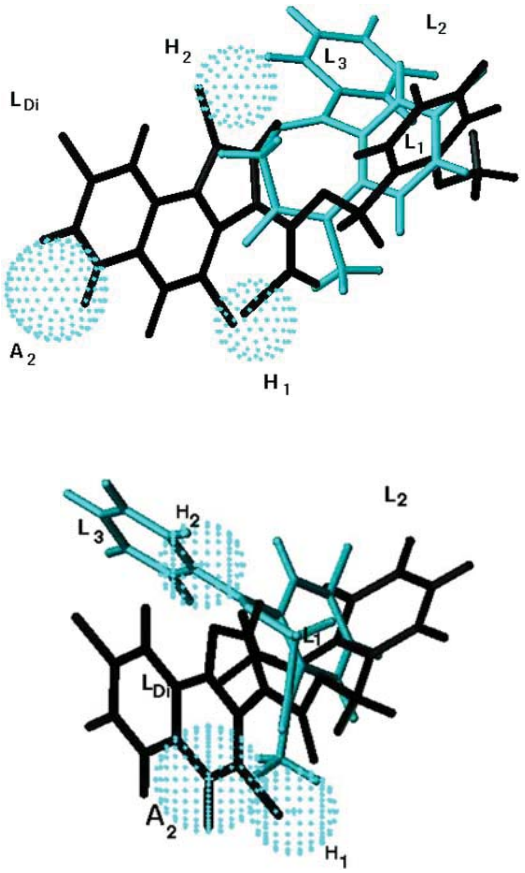

Fig. (13). Alignment of ligand **38** (black) overlayed with diazepam (cyan) within the unified pharmacophore/ receptor model and rotated 90 degrees.

Dimer Affinity for the Binding Site

Some studies which involved monomeric *i*-BZDs indicated that there might be a limit on the size of 3'-imidazo substituents the receptor may accommodate [53]; However, studies that involved bivalent ligands suggested otherwise (Table **4**) [80, 81]. It is thus possible that the spacer for *i*-BZDs dimers threaded the second portion of the bivalent ligand through and/or around the L_{Di}/A_2 region that presented steric hindrance for the monomers.

Design of the bivalent ligand XLi-093 **16** was based on the modeling of the α5–selective monomer RY-80 **52** in the α5 pharmacophore model. The ability of this ligand to bind (Table **4**) and

Table 4. Structures and Affinities at the αxβ3γ2 Subtype [53]. NR = not reported; ANT = antagonist; IA = inverse agonist; ND = not determined yet. Activity is Defined for Receptor Subtype Listed in Bold

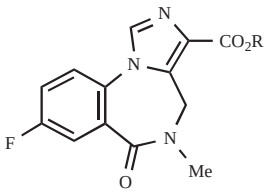

Ro15-1788, **5** (R = Et)

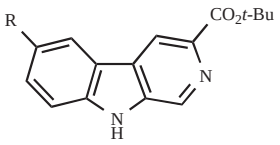

β-CCT, **13** (R = H)
WY-S-8, **39** (R = ≡—H)
WY-B-14, **40** (R = ≡—TMS)

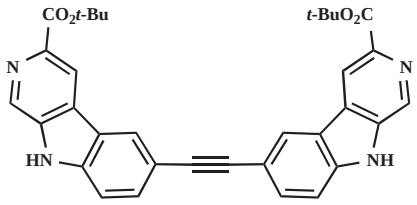

WY-S-2, **41**

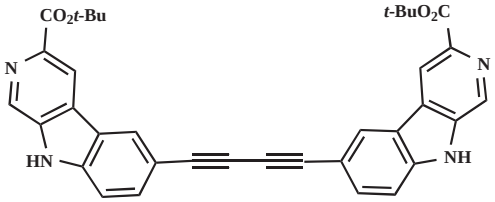

WY-S-6, **42**

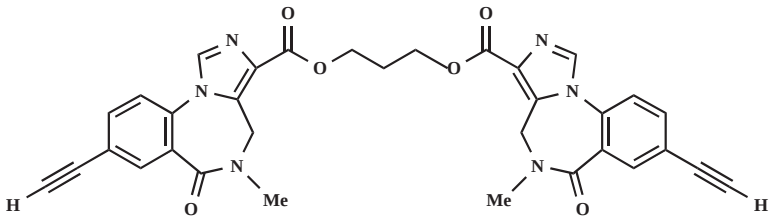

XLi-093, **16**

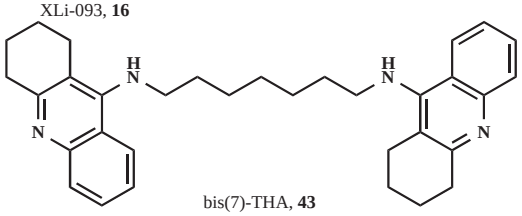

bis(7)-THA, **43**

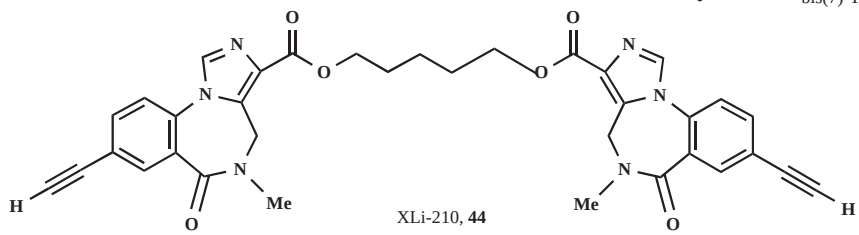

XLi-210, **44**

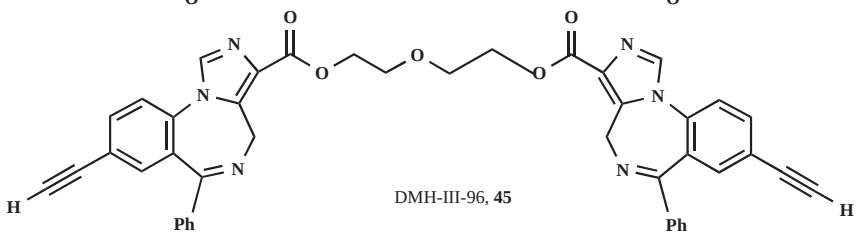

DMH-III-96, **45**

	K_i (nM)						
Ligand	**α1**	**α2**	**α3**	**α4**	**α5**	**α6**	**Activity**
5, Ro15-1788	0.8	0.9	1.05	NR	0.6	148	ANT
13, β-CCT	0.72	15	18.9	NR	110.8	5000	IA
39, WY-S-8	0.97	111	102	NR	208	1980	ND
40, WY-B-14	6.8	30	36	2000	108	1000	ND
41, WY-S-2	30	124	100	300	300	4000	ND
42, WY-S-6	120	1059	3942	NR	5000	5000	ND
16, XLi-093	1000	1000	858	1550	15	2000	ANT
43, bis(7)-THA	NR	NR	NR	NR	NR	NR	ANT
44, XLi-210	231	661	2666	NR	5.4	54.2	ND
45, DMH-III-96	460	5000	NR	NR	5000	5000	ND

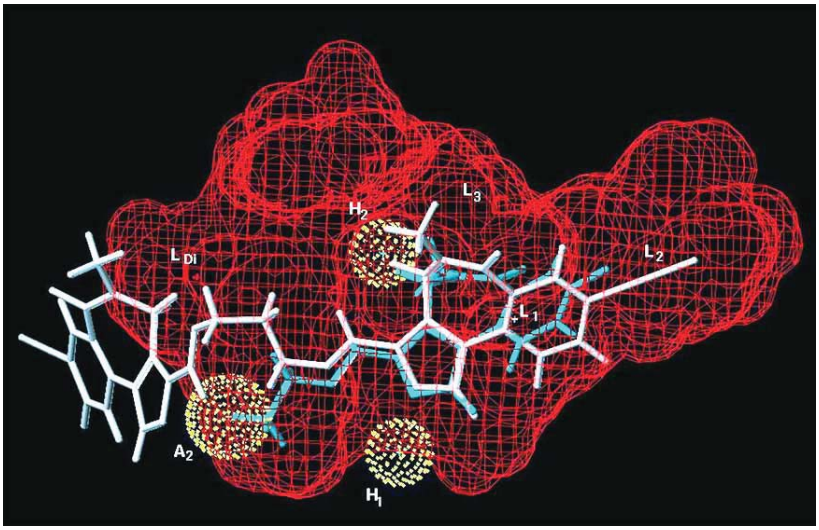

Fig. (14). Alignments of XLi-093 **16** (white) and Ro15-1788 **5** (cyan) within the included volume of the α5β3γ2 subtype.

fit well within the pharmacophore (Fig. **14**) requires the 3-carbon linker to be in a linear (*versus* folded) conformation. This linear conformation of XLi-093 has been confirmed both in the solid phase and in solution (Fig. **14**) [82]. The *J* values calculated from the dihedral angles (*J* = 5.38) were in excellent agreement with those determined from the solution NMR spectrum (*J* = 6.39). Because this bivalent ligand is the most α5-selective ligand reported, the enriched selectivity of this dimer and those similar to it, was presumably entropic in nature, as the loss of affinity at the other subtypes was profound [81, 82].

It has been shown *via* crystallographic and solution NMR studies that modification of the aliphatic spacer to a $–CH_2OCH_2–$ or a $-(CH_2)_2O(CH_2)_2–$ group, provided the bivalent ligand with a folded conformation (Fig. **15**) [82]. Modeling of this type of ligand (*e.g.* DMH-III-96 **45**, Fig. **16**) within the α5 pharmacophore model illustrated the inability of bivalent ligands in the folded conformation to bind presumably because they are too hindered to access the Bz BS. Current data displaying these trends is shown in Table **5**, while further studies are underway to evaluate the length the lipophilic spacers may contribute toward the selectivity of both the benzodiazepine and β-carboline bivalent ligands (*e.g.* XLi-210 **44** and WY-S-6 **42**).

Success of XLi-093 and earlier *in vitro* data on WY-S-8 **39** and WY-B-14 **40** (Table **4**) indicated the C(6)-substituent of β-carbolines lies in the L_{Di} region of the pharmacophore model or in the extracellular domain of Bz BS. For this reason, the β-CCT dimer, WY-S-2 **41** was designed and synthesized. Although the α1 subtype selectivity was not amplified with this particular β-carboline dimer, the ligand does bind. It was proposed that the two-carbon linker was not long enough and that crowding between the second β-CCT unit and the receptor protein decreased the binding affinity at α1 subtype, thereby negating potential selectivity [80]. Further evaluation of the β-CCT bivalent ligand with a bis-acetylene linker (WY-S-6 **42**, Fig. **17**) should shed light on this hypothesis.

Similar to XLi-093, the dimer bis-(7)-THA **43** of Wang *et al*. was determined to be a competitive antagonist at the Bz BS in both electrophysiological experiments and receptor binding assays (Table **4**) [73]. Although additional experimental data is needed, inspection of the alignment of XLi-093 (Fig. **14**) and our receptor model (see below) indicated the aliphatic linker of these bivalent ligands would thread the second half of the dimer through the L_{Di}/A_2 regions and toward the solvent accessible space outside of the pocket.

Beta-Carbolines

The crystal structures and molecular mechanics simulations of several β-carbolines has recently been reported [83]. In general,

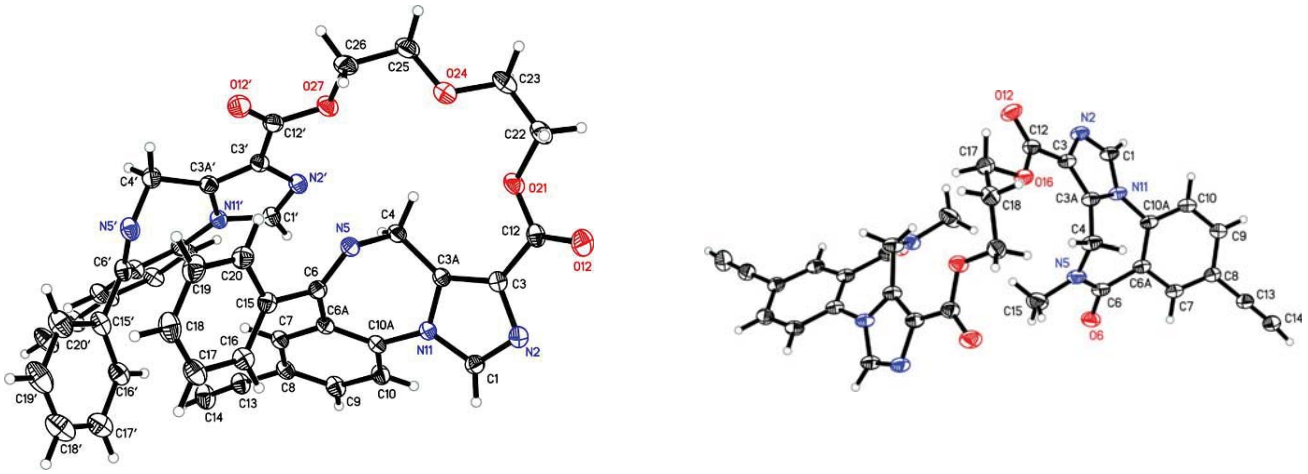

Fig. (15). Crystal structures of the linear XLi-093 **16** (left) and the folded DMH-III-96 **45** (right). Figures reprinted with permission [81, 82].

Table 5. The Molecular Composition and Stable Conformation of Various Bz BS Bivalent Ligands. ND = not determined yet

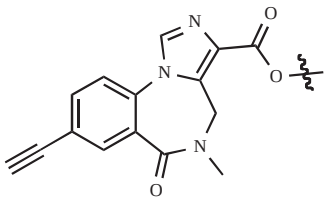

A

Ligand	Monounit 1	Monounit 2	Spacer	Conformation in solution	Crystal structure
16, XLi-093	A	A	$(CH_2)_3$	linear	linear
44, XLi -210	A	A	$(CH_2)_5$	linear	ND
46, XLi -347	A	A	$(CH_2)_2O(CH_2)_2$	folded	ND
47, XLi-374	A	A	CH_2OCH_2	folded	ND
45, DMH-III-96	-	-	$(CH_2)_2O(CH_2)_2$	folded	folded

substitution at C(3) and C(6) had the greatest effect on affinity. Consistent with the interaction with the H_1 descriptor, high affinity ligands were always associated with groups able to interact as hydrogen bond acceptors at C(3). Furthermore, affinity was much lower for constrained β-carbolines which contained the carbonyl group in the *anti* conformation, in agreement with the proposed 3-centered hydrogen bond [42, 50, 52, 61] afforded by many β-carbolines in the stable *syn* conformation with the H_1 descriptor.

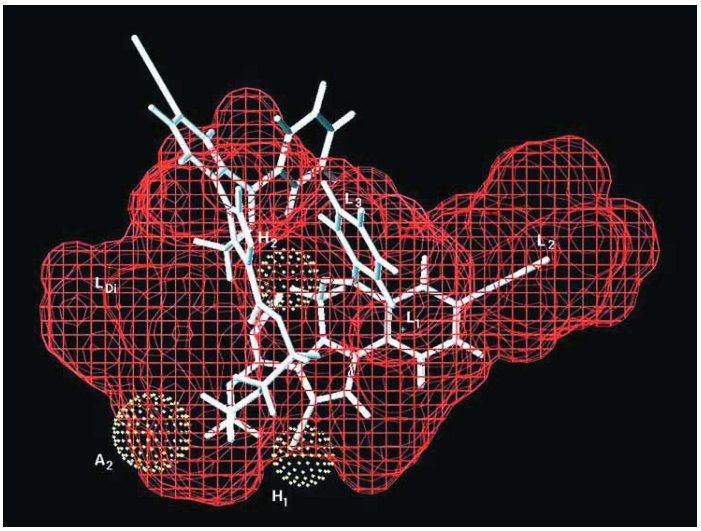

Fig. (16). Alignment of a DMH-III-96 **45** within the included volume of the α5β3γ2 subtype. It is apparent that the folded conformation prevented it from binding to this $GABA_A$ subtype.

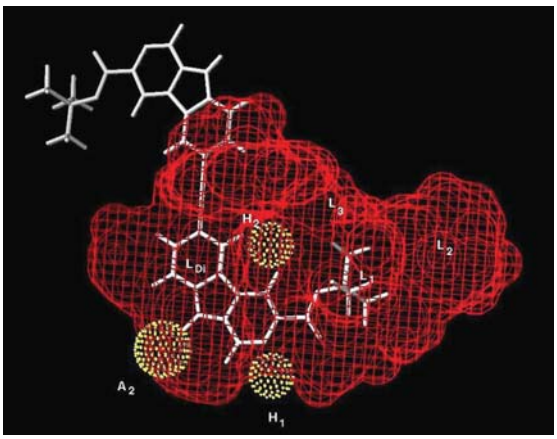

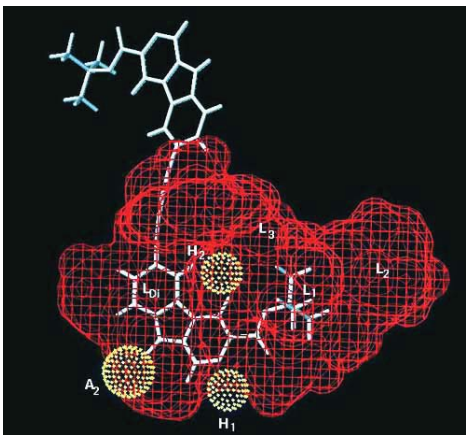

Fig. (17). Alignment of WY-S-2 **41** (left) and WY-S-6 **42** (right) within the included volume of the α1β3γ2 subtype.

Table 6. Structures and Affinities at αxβ2γ2 Recombinant Receptors and Modulation by β-Carbolines. pAg = partial agonist; Ag = agonist [84]

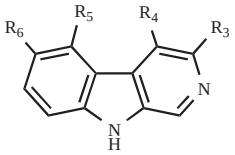

	K_i (nM)										
Ligand	**R_6**	**R_5**	**R_4**	**R_3**	**α1**	**α2**	**α3**	**α4**	**α5**	**α6**	**Activity**
12, 6-PBC	O*n*-Pr	H	MOM	CO_2Et	0.49	1.21	2.2	NR	2.39	1343	pAg
11, ZK-93423	OCH_2Ph	H	MOM	CO_2Et	4.1	4.2	6	NR	4.5	1000	Ag
48, ZK-91296	H	OCH_2Ph	MOM	CO_2Et	NR	NR	NR	NR	NR	NR	pAg
49, Abecarnil	OCH_2Ph	H	MOM	CO_2-*i*-Pr	12.4	15.3	7.5	NR	6	1000	pAg

As previously stated, the C(6)-substituent of β-carbolines lies in the L_{Di} region of the unified pharmacophore/ receptor model for inverse agonists and antagonists. However, based on the CoMFA studies of Huang *et al.* [78] β-carboline agonists have been proposed to take on a vertical alignment with respect to the horizontal alignment of inverse agonists and antagonists. While only four β-carbolines have been reported to display agonistic activity, each of these compounds had a 4-methylmethoxy group that permitted interaction with the H_2 descriptor and partial interaction with the region near the entrance to the L_3 pocket (Table **6**). It was postulated that 6-PBC **12** should display agonistic activity, and indeed, since partial occupation of a lipophilic region near the C(6)-substituent is probable (relative to ZK-93423 **11**), 6-PBC is a partial agonist [42, 84]. However, it is likely that the type of activity displayed by 6-PBC may be receptor subtype-dependent, because when evaluated *in vivo*, it inhibited PTZ-induced seizures in a dose-dependent fashion and exhibited anxiolytic activity when evaluated in the elevated plus-maze paradigm. Yet, unlike typical 1,4-benzodiazepines, 6-PBC **12** was devoid of muscle relaxant activity and even antagonized the muscle relaxant/ataxic activity of diazepam [85, 86]. Further studies are needed to fully address this issue.

LIGANDS THAT OCCUPY THE L_2 REGION AND ARE SELECTIVE FOR α5 CONTAINING RECEPTORS

RY-24 and Related Analogs

Continued interest in the development of α5 selective ligands goes forward in the CNS area for many reasons. One of these involves the localization of these receptors and their presumed importance in developmental biology. Over 30 % of $GABA_A$ receptors in neonatal rat pups are comprised of α5β3γ2 subtypes, whereas they only comprise about 5 % in adult rats [87]. In addition, these α5 subtypes are primarily found in the hippocampus [88], which prompted interest in memory and learning [25]. From the evaluation of K_i values, it was found that many 8-substituted *i*-BZDs, such as RY-24 **50** and RY-80 **52** and their trimethylsilyl precursors **51** and **53** (Table **7**), exhibited a significant degree of binding selectivity at the α5 subtype *in vitro*. This observation was in agreement with the previous hypothesis that correct occupation of the L_2 region can promote α5 selectivity of a ligand [29, 51]. Therefore, the efficacy of the α5-subtype selective ligand RY-24 **50** was evaluated *in vitro*. Recently, it was determined that this ligand was a potent inverse agonist at the α5 subtype with a much weaker efficacy at the other subtypes (Fig. **18**). These results confirmed previous binding data, which indicated that this ligand was α5-selective due to the lipophilic C(8)-substituent which fully occupied the L_2 pocket [28, 29]. The data were also in agreement with previous studies *in vivo*, which indicated that some of these ligands enhanced cognition while other Bz BS ligands were not as effective [25, 89]. Furthermore, ligands devoid of a lipophilic substituent at the C(8) position showed no selectivity for the α5 subtype (Table **7**).

Inspection of Table **7** revealed some observations worth noting. While the lipophilic substituent at R_8 of RY-24 **50** and RY-80 **52** decreased the affinity for α1, α2 and α3, it retained affinity for α5 and actually increased affinity for the α6 subtype. Furthermore, selective affinity of *i*-BZDs at the α5 subtype was independent of the occupation of the L_3 pocket, as illustrated by the *in vitro* data of DM-I-81 **55** (Table **7**). This data again supports the importance of the occupation of the lipophilic pocket L_2 for potent selectivity at α5 subtype.

June *et al*. recently reported the neurobehavioral results of RY-23 and RY-24 in rats. In agreement with previous studies [28], these α5 selective ligands were highly selective in suppressing ethanol-maintained responding (Fig. **19**) [91]. As previously stated, the hippocampus contains the greatest concentration of α5-containing receptors in the CNS [88, 92], and it is possible that these hippocampal α5 receptors may regulate alcohol-motivated responding following systemic administration of an α5-selective agent. Furthermore, RY-24 also antagonized the motor-impairing and sedative effects of ethanol in Long-Evans rats. Combined with additional studies within the ventral pallidum (VP), it has been proposed that the GABAergic systems within the VP and hippocampal pathways may represent new extensions of the mesolimbic ethanol reward circuitry. Although these data do not strongly support a direct role for the modulatory influences of intrinsic efficacy in the behaviors examined, the synthesis of α5 subtype selective ligands provides researchers a unique opportunity to explore the role of this subtype in the neurobehavioral effects of alcohol [28, 93].

In studies involving the α1 subtype, β-CCT **13** and 3-PBC **14** were observed to selectively reduce alcohol-motivated behaviors for a variety of experiments [94, 95]. However, unlike the α5 selective inverse agonist RY-23, both the β-carboline antagonists β-CCT and 3-PBC displayed mixed agonist-antagonist profiles *in vivo* in alcohol P and HAD rats. Therefore, in addition to being able to study the molecular basis of alcohol reinforcement, α1 Bz BS ligands which display mixed agonist-antagonist pharmacology in alcohol P and HAD rats may be capable of reducing alcohol intake while eliminating or greatly reducing the anxiety associated with habitual alcohol, abstinence or detoxification. Thus, these types of ligands may be ideal clinical agents for the treatment of alcohol-dependent individuals [94, 95].

Additional behavioral studies of RY-24 were performed by Helmstetter *et al*. and provided further support for the role of the

Table 7. Structures and Affinities of Some α5β3γ2-Subtype Selective Ligands

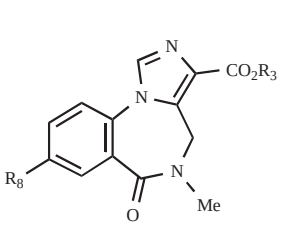

56

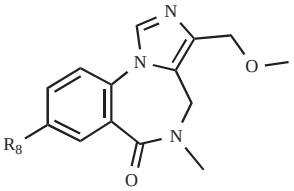

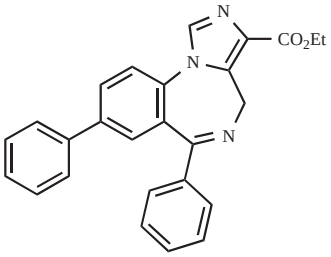

DM-I-81, **55**

Ligand	R_8	R_3	K_i (nM)				
			α1	α2	α3	α5	α6
50, RY-24	H	*t*-Bu	26.9	26.3	18.7	0.4	5.1
51, RY-23	TMS	*t*-Bu	197	143	255	2.61	58.6
52, RY-80	H	Et	28.4	21.4	25.8	0.49	28.8
53, RY-79	TMS	Et	121	142	198	5.0	114
54	H	Et	1.2	2.0	1.1	0.4	> 300
55, DM-I-81	Ph	NA	> 2000	> 2000	> 2000	176	> 2000
56, PWZ-029[90]	Cl	NA	>300	>300	>300	38.8	>300

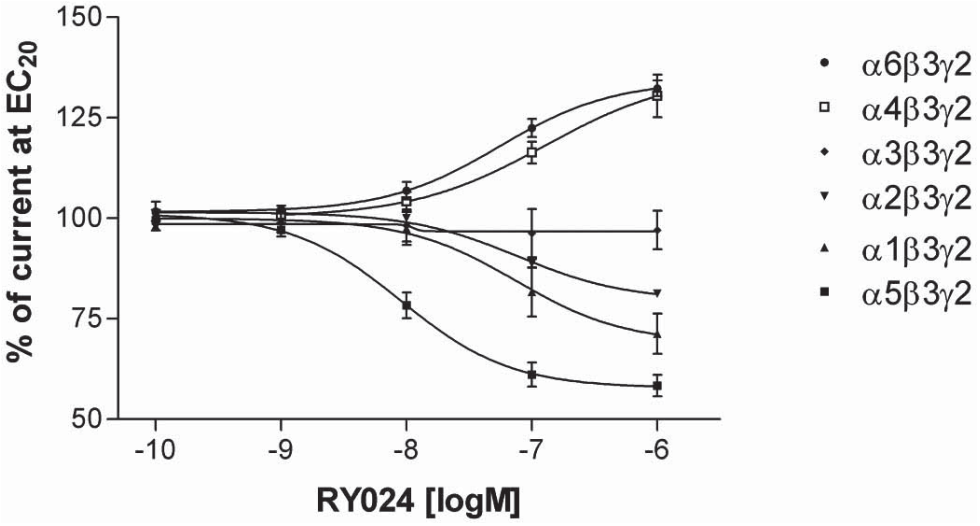

Fig. (18). Subtype efficacy of RY-24 50. Dose response curves for RY-24 in oocytes expressing different subunit combinations of $GABA_A$ receptors. Subtype combinations are indicated in legends. cRNA–injected Xenopus oocytes were held at –60 mV under two-electrode voltage clamp. Increasing concentrations of RY-24 were superfused together with a GABA concentration eliciting ~ 20% of the maximal current amplitude. RY-24 was pre-applied for 30 sec before the addition of GABA, which was co-applied with the drugs until a peak response was observed. Data were normalized for each curve assuming 100% for the response in the absence of RY-24. RY-24 was made up and diluted as stock solution in DMSO. Final DMSO concentrations perfusing the oocyte were 0.1%. Values are presented as mean ± SD of at least 4 oocytes from at least 2 batches.

hippocampus in anxiety and learning [25]. Moreover, the data suggested that Bz BSs within the hippocampus are important for the acquisition of fear conditioning. Although this subtype selective ligand has been shown to be an inverse agonist at the α5 subtype [29, 96], this study suggested that RY-24 may act as an agonist at other alpha subtypes because larger doses of RY-24 were not as anxiogenic as the smaller doses and resulted in decreased learning. Consistent with the studies of Stephens *et al*. using α5 knock-out mice [97] and the efficacy studies of Lüddens, June and Cook *et al.* [98] these findings support the concept that the pharmacology observed depends upon the dose, behavioral paradigm employed and subunit composition activated. Ligands such as RY-24 have proven to be valuable in the study of the biochemical and pharmacological properties of $GABA_A$ receptors and have permitted insight into the role this protein plays in anxiety and learning.

QH-ii-066

Due to the pharmacological profile RY-24 exhibited *in vivo*, the development of additional α5 subtype selective ligands was pursued. Thus, the 7-acetyleno analog of diazepam, QH-ii-066 **57**, was synthesized and was determined to also exhibit a binding and functional selectivity at the α5 subtype over the α1 subtype (Table **8**) [27]. This was due to the full occupation of the L_2 pocket, relative to diazepam (Fig. **20**). To our knowledge, this was the first agonist ligand to display some α5 selectivity from the 1,4-benzodiazepine

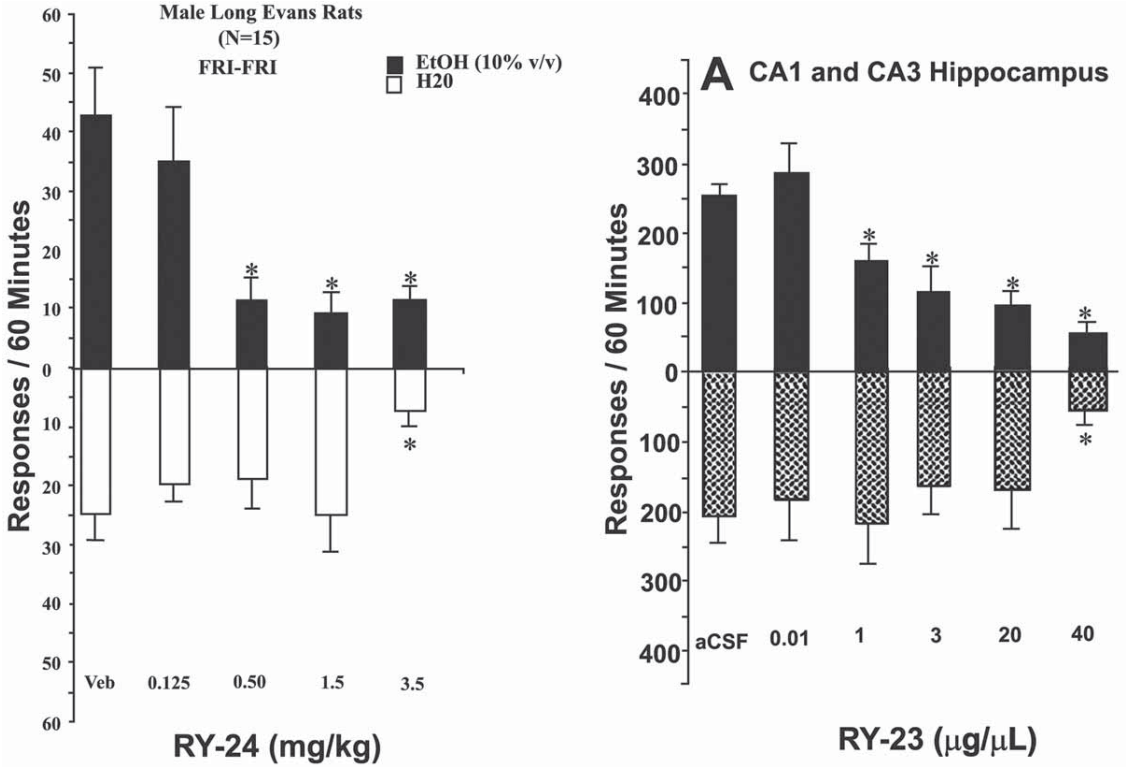

Fig. (19). Suppression of alcohol-motivated responding by RY-24 **50** and RY-23 **51** [93, 96]. Left: Dose-response of IP RY-24 (0.0–3.5 mg/ kg) and vehicle on responding maintained by ethanol (10 % v/v) (*top panel*) and water (*bottom panel*) in male Long-Evans rats. Right: Dose-response of unilateral infusions of RY-23 (0.0-40 μg) in the hippocampus on a concurrent fixed-ratio (FR4) schedule for ethanol (10 % v/v) (*top panel*) and saccharin-maintained (0.025 % v/v) (*bottom panel*). For both studies, $*p \leq 0.05$ *versus* control condition values was determined using ANOVA and *post hoc* Newman-Keuls test. Each bar represents the mean (± SEM) (n = 15 for RY-24 and n = 7 for RY-23). Figures reprinted with permission of the authors [93, 96].

family. Importantly, the 7-cyano congener **58** (Table **8**) did not potently bind to recombinant receptors of the α5 subtype, which is in agreement with earlier work of Haefely and Fryer *et al*. on the SAR of 1,4-benzodiazepines [99, 100]. This cyano ligand also did not exhibit any subtype selectivity, re-emphasizing that occupation of the L_2 region with lipophilic groups is important for α5 selectivity as well as for high affinity. The selective efficacy of this QH-ii-066 ligand over the α1 subtype was demonstrated by reversing the convulsant actions of RY-24 **50**, an α5-selective inverse agonist, in NIH mice [87]. This ability was not observed at comparable doses for the α1-selective agonist zolpidem **7**.

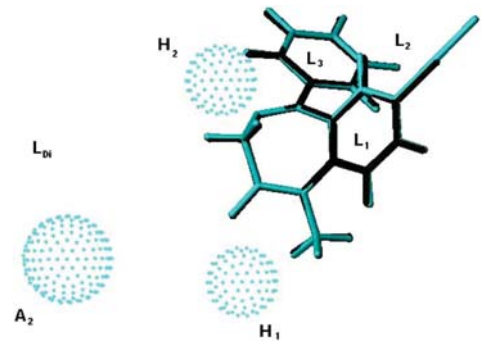

Fig. (20). Comparison of non-selective diazepam (black) with the α5-selective QH-ii-066 (cyan) when aligned within the unified pharmacophore/ receptor model. The acetylene group of QH-ii-066 increased the occupation of the L_2 region relative to that of diazepam.

Furthermore, Lelas and Cook *et al*. have recently determined that although QH-ii-066 had similar affinity for the DS subtypes in rats, it displayed functional selectivity *in vivo*, with diazepam-like efficacy at the α5 subtype and partial efficacy at the α1 subtype [27]. The study also indicated that this 7-acetyleno substituted diazepam analog exhibited less potency in protection against ECS-induced seizures relative to diazepam than against PTZ-induced seizures. Hence, the α1 subtype may play a more prominent role in ECS-induced seizures than in PTZ-induced seizures [27].

COMPARATIVE MODEL OF THE BENZODIAZEPINE BINDING SITE

Crystallization of $GABA_A$ receptors thus far has not been accomplished, but the successful structure determination of the water-soluble acetylcholine binding protein (AChBP) [101] has generated much interest in the $GABA_A$ receptor community. Although this protein shares only ~ 18 % sequence homology with the extracellular domain of the $GABA_A$ receptor [101], the structural resemblance has been estimated to be relatively high (60 – 75 %) [48]. Several comparative modeling studies have used the AChBP structure to derive models of the extracellular domain of $GABA_A$ receptors [47, 48]. Following the cryo-EM determination of the extracellular and transmembrane domain structure of the nACh receptors, these structures also were used as templates for modeling $GABA_A$ receptors [102]. Sequence homology is so low however, that detailed features of the models are highly uncertain, and the proposed dockings of Bz BS ligands [103-105] have a qualitative character and do not sufficiently explain the observed differential effects of

Table 8. Structures and Affinities of 1,4-Benzodiazepines

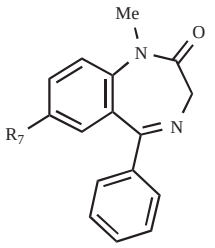

Ligand	R_7	K_i (nM)				
		α1	α2	α3	α5	α6
1, diazepam	Cl	14	20	15	11	> 3000
57, QH-ii-066		76.3	42.1	47.4	6.8	> 3000
58		320	310	350	265	> 3000

ligands interacting with different receptor subtypes. The experimental structure of the nAChR [106] has provided first data on how much the fold can vary between members of a family [106]. From this data the extent to which $GABA_A$ receptor subunits differ from each other in structure can be qualitatively extrapolated, but not predicted in detail.

As mentioned before, the majority of $GABA_A$ receptors are composed of 1γ, 2α and 2β subunits. Each subunit has per convention a "plus" and a "minus" side (Fig. **21**). The subunit interfaces consequently consist of the plus and minus sides of neighboring subunits. The modulatory Bz BS is located at the $\alpha^+\gamma^-$ subunit interface and is larger than, but homologous to the two agonist (GABA) binding sites, which are located at the $\beta^+\alpha^-$ subunit interfaces [49, 107, 108]. The absolute subunit configuration for the α1β2γ2 $GABA_A$ receptor appears to be γβαβα, when viewed counter clockwise (from + to - , Fig. **21**) [48, 109-111].

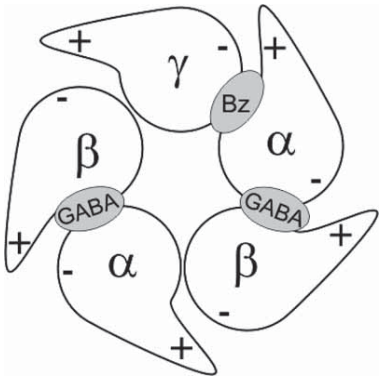

Fig. (21). Absolute subunit arrangement of the α1β2γ2 $GABA_A$ receptor when viewed from the synaptic cleft. The GABA binding sites are located at the $\beta^+\alpha^-$ subunit interfaces and the modulatory Bz binding site is located at the $\alpha^+\gamma^-$ subunit interface. The part of the schematically drawn subunits marked by the + indicates loop C of the respective subunits.

While the γ2 subunit is required for recognition and binding of benzodiazepines as well as many other substance classes that act *via* the Bz BS [112, 113], it is now clear that sequence variations between different α and γ subunits determine subtype selectivity and efficacy of Bz BS ligands [20, 112-114]. The Bz BS has been proposed to consist of three segments provided by the α^+ side, the so-called "loops A, B and C" and by three segments of the γ^-, the so-called "loops D, E and F" [112, 113]. These segments were then confirmed by X-ray crystallographic and EM-structures of AChBP [101] and the nAChR [106] to form a groove-like pocket at the interface boundary between subunits that appears to be conserved in the entire superfamily.

Even later than the nAChR structure, a series of AChBP crystal structures with co-crystallized ligands appeared [115]. These structures revealed how ligand binding can alter the local conformation of the binding site. Particularly loop C has been found to be a highly mobile subdomain, additional more subtle changes are seen along the entire subunit boundary [115]. These findings are consistent with the hypothesis that many receptor conformations exist, that are separated by low energy barriers, and can be stabilized by different ligands. Unfortunately it cannot be decided a priori which of the experimental structures is the "best" template to model a particular receptor/ligand complex. Depending on template and alignment choice, model Bz pockets differ in total volume by as much as 40% and can vary by several Angstrom in the distances between key residues in the binding site loops.

Although changes in protein conformation may be minor, it has been demonstrated that they can profoundly affect the efficacy of Bz BS ligands [116]. Furthermore, efficacy can vary for the same ligand at different $GABA_A$ receptor subtypes [27, 31, 35]. As proteins are inherently dynamic and able to sample many conformations, and the stabilization of the active state relative to the inactive state has been calculated to be less than 1 kcal/mol [117], it is impossible to provide absolute assignments of specific side chains to specific descriptors for any particular conformation. This conformational flexibility may imply that residues which satisfy certain pharmacophoric descriptors can vary, resulting in a "soft" orientation of the pharmacophore in the receptor. Thus, a unified view of a pharmacophore model and a homology derived receptor model will assign large areas of lipophilic interaction to specific regions in the protein, but allow a flexible assignment of specific interactions such as H-bridges or π- π stacking.

RELATIVE ORIENTATION OF THE PHARMACOPHORE WITHIN THE COMPARATIVE MODEL

Prior to structure determination of the AChBP, we published a review which evaluated results of site-directed mutagenesis and provided insights as to where certain side chains in the Bz BS might be located relative to the pharmacophoric descriptors [118]. However, with the knowledge gained from recent experimental data and with the aid of our $GABA_A$ receptor models, built by homology to lymnea AChBP [47], aplysia AChBP and the nAChR [102] an update of the orientation is provided here. We now propose an orientation which is favored by experimental evidence, allows some degree of conformational flexibility which can lead to variable as-

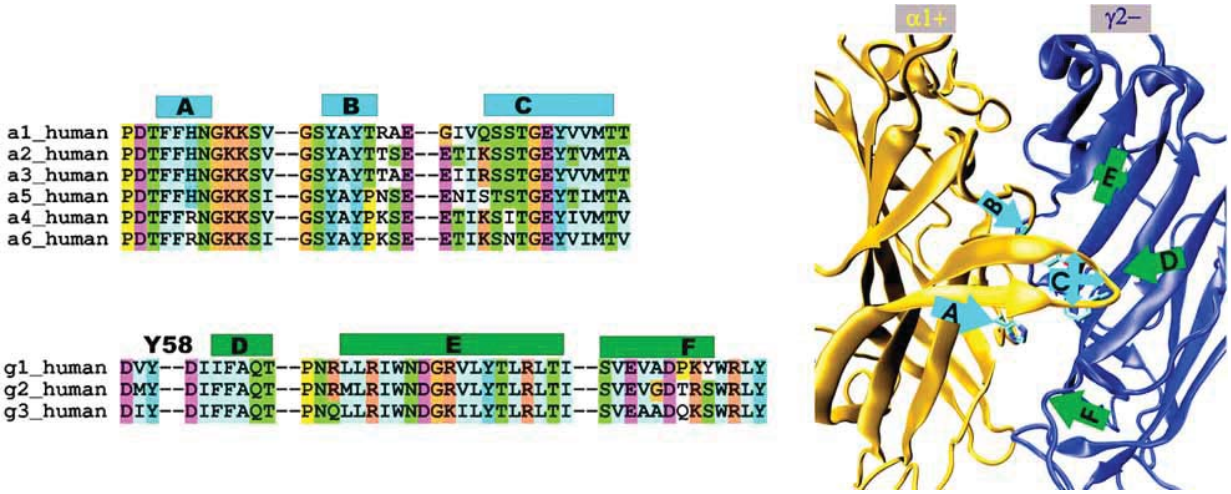

Fig. (22). Alignment and homology model depiction of the so called "loops A-F" and flanking regions of the human sequences of the Bz recognition site in different subunits. The homology model is as seen from "outside" of the channel mouth, the membrane would be parallel to the lower edge of the image. Key residues are shown in stick representation: Loop A His102, loop B Tyr 160 and loop D Phe77.

signments for H-bridge interactions, but is based on specific areas of lipophilic interactions that are determined by binding site geometry.

Evidence from Covalently Reactive Ligands Allows to Position the L2 Lipophilic Pocket

Covalent labeling studies contributed significantly to the determination of residues that are located within the Bz BS [104, 119-124].

Table 9. Ligands Used for Affinity Labeling Studies [104, 121-124]

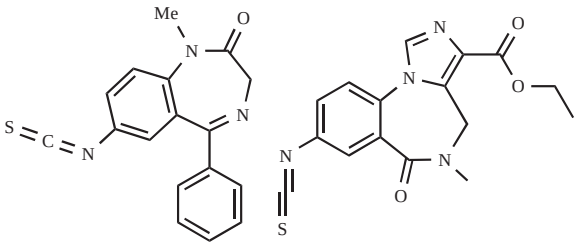

59 **60**

7-isothiocyano-1,4-benzodiazepine

Ligand	Activity	Site of Interaction
2, [^{3}H]flunitrazepam	Agonist	α1H102
6, [^{3}H]Ro15-4513	inverse agonist	α1Y210
59	Agonist	α1H101C (rat)
60	part. Agonist	α1H101C, α1G157C α1V202, α1V211C (rat)

Photoincorporation studies with the agonist [^{3}H]flunitrazepam identified α1H102 of the human sequence as the primary site of incorporation [123]. Although it is possible that flunitrazepam is coupling *via* the nitro group at the 7-position, the coupling group of flunitrazepam is currently not known. Studies with the inverse agonist [^{3}H]Ro15-4513 indicated α1Y210 as the primary site of incorporation [104]. Thus, the azido group at the 7-position of Ro15-4513 should be in close apposition to α_1Y210, assuming no rearrangement of the photo-activated intermediate. Further information comes from recent studies reporting the covalent coupling of 7-isothiocyano- derivatives of a 1,4-benzodiazepine, (substance **59** [122]) and of Ro15-1788 (substance **60** [124]) to $GABA_A$ receptors in which individual amino acid residues had been mutated to cysteines. Primary site of reaction of both substances is the rat α1H101C mutant that is homologous to α_1H102 of the human subunit. Thus, the 7-substituent both of 1,4-benzodiazepines and of imidazodiazepines appears to be in apposition to α1H102. The imidazobenzodiazepine **60** reacts with additional cysteines in positions corresponding in the human sequence to positions α_1V203C and α_1V212C in the loop C stem, and with α_1G158C in loop B (see alignment in Fig. **22**). Thus, the 7-substituent of this compound, in agreement with the data from photolabeling H102 with flunitrazepam and Y210 with Ro15-4513, is in apposition to loop A, the loop C base, and additionally loop B.

Thus, all the findings from covalently incorporated ligands given above can be reconciled by placing the 7-substituent, and thus the L2 descriptor of the unified pharmacophore model, between the loop C base near α_1V203/α_1V212/α_1Y210 and loop A α_1H102. The homology models reveal that this is not only topologically possible, but also provides the additional apposition to loop B that is suggested by the reaction of **60** with rat α1G157C. Thus, the L2 lipophilic pocket is most likely formed by the base of loop C, together with parts of loop A.

THE A2 DESCRIPTOR AND THE L_{DI} REGION

Experimental data yields some very convincing evidence for assigning the A2 descriptor and the L_{DI} region of lipophilic interaction next to A2 to protein segments close to residues γ2A79 and γ2T81 at loop D. Certain imidazobenzodiazepines, which occupy the pharmacophore volume close to A2 (see Fig. **5**), are more sensitive toγ2A79 mutations than classical benzodiazepines or benzodiazepines that lack a 3'-imidazo substituent. This was shown in a study where mutations of γ2A79 and γ2T81 had little effect on the binding of the agonists diazepam and flunitrazepam, but in a roughly size dependent fashion decreased the affinities of antagonist Ro15-1788 and inverse agonists Ro15-4513 [125, 126]. In agreement with other studies, midazolam, which lacks a 3' substituent, behaved more closely to classical benzodiazepines than *i*-BZDs [44, 125, 127,128]. This trend is enhanced by rigid and bulky 3'-imidazo substituents, altogether suggesting that γ2A79 and γ2T81 are located close to the region of the Bz BS surrounding the 3' substituent of *i*-BZDs [125]. The localization of the 3'-imidazo substituents in the unified pharmacophore model, see Fig. (5), thus positions the A_2 and L_{DI} descriptors near residues γ2A79 and

γ2T81. Further support for this localization comes from the observation that DMCM also looses affinity upon mutagenesis in positions γ2A79 and γ2T81, [125, 126] consistent with the alignment of this substance in the pharmacophore. Fig. (**5**) shows that changes to the protein near the A_2 descriptor would in all likelihood not be tolerated by DMCM.

COMBINING HOMOLOGY MODEL AND EXPERIMENTAL EVIDENCE

If the two assignments discussed above are correct, they should be reflected in results of computational ligand docking to homology models of the binding site. Thus, computational docking of diazepam and flumazenil was performed in multiple different models based on different templates [101, 106, 115] and the best 100 docking poses per model were collected in a database. A database query was then formulated to search among the (unrefined) docking poses for those with the following properties: The seven membered ring of diazepam or flumazenil is in the conformation that is assumed to be the active one; [99] the 7-substituents are near residues α1H102/α1V203/ and α1Y210/α1V212 in order to be consistent with the covalent labeling data; the 3' ester group of flumazenil is near residues γ2A79 and γ2T81. Such a query yields docking poses that are consistent with all covalent labeling studies on one hand, and with the steric requirements that were found for 3' substituted imidazobenzodiazepines [125] on the other hand. Such poses were indeed present in our database, and one representative diazepam pose is shown in Fig. (**23**): To be consistent with the presentation of the pharmacophore and its descriptors so far, the orientation of the benzodiazepine binding pocket had to be turned upside down and slightly tilted.

This and similar docking poses not only satisfy the two assignments for L2 and A2 that are discussed in the sections above, but at the same time position the remaining descriptors as follows: H1 can be satisfied by appropriate side chains near the tip of loop C, the L_{DI} region is near the subunit interface, essentially between α1 loop B (Y160) and the γ2 region spanned by the interface forming sheet involving M130, T142 and F77; A2 can be satisfied by H-bridge

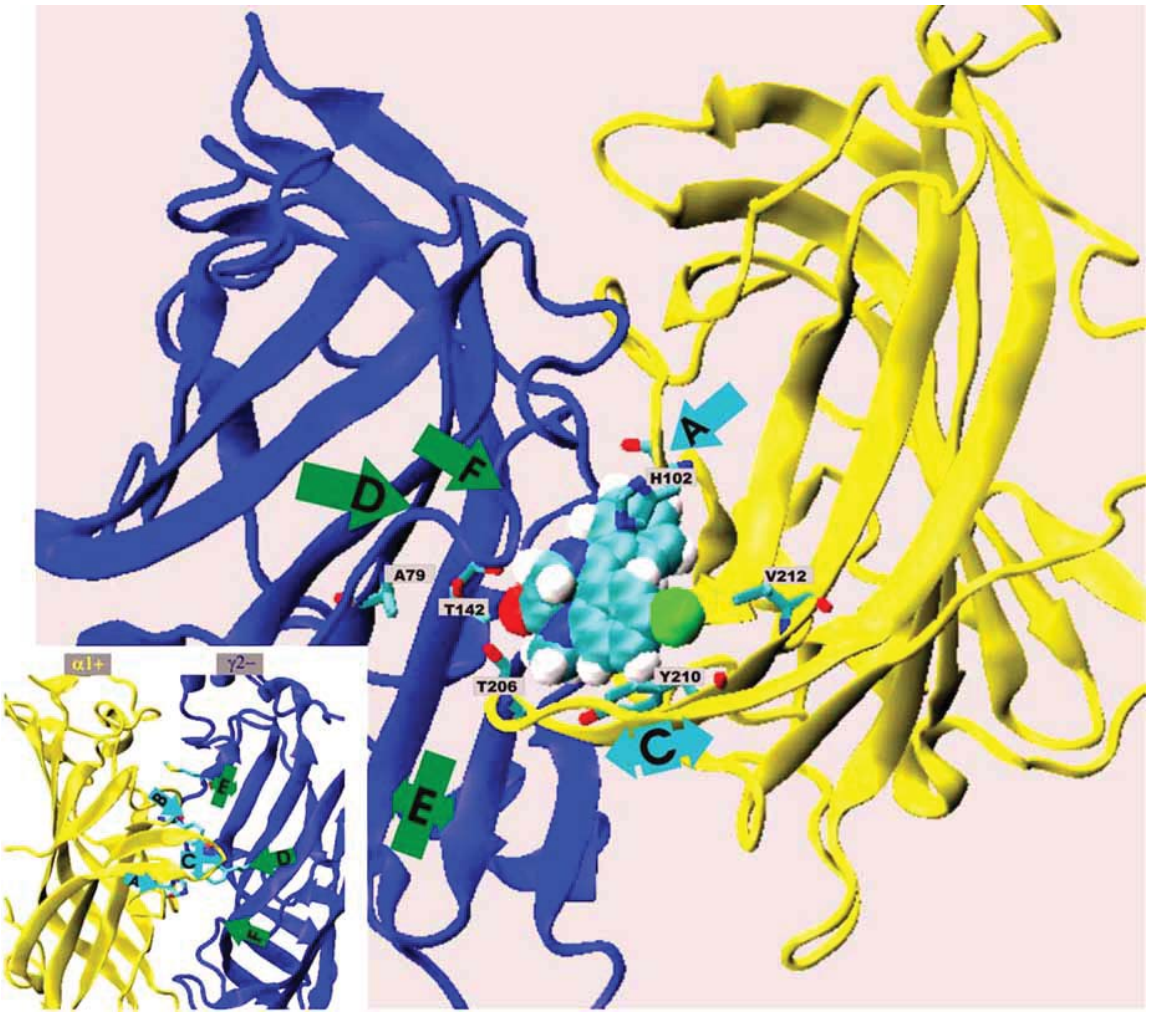

Fig. (23). The main figure shows a diazepam docking pose in an α1γ2 pocket matching the orientation proposed in the text. Diazepam is rendered space filling, (turquoise: carbon, white: hydrogen, green: halogen, red: oxygen, blue: nitrogen), the protein as ribbon, and key amino acids in stick representation. The insert figure shows the empty pocket in the "upright" position to facilitate orientation in the main figure, where the model has been turned and tilted to bring diazepam approximately into the orientation depicted in the unified pharmacophore model, Fig. (**3**). In this particular docking pose, His102 and Thr206 could satisfy H2 and H1, respectively, and His 102, Val 212 and Tyr 210 would be part of the L2 hydrophobic pocket. This positions 7-substituted reactive analogues such as compound **59** into a position where the reactive groups find free access to His102, Tyr 210, Val 212, Val 203. It should be noted that due to high uncertainties in model backbone position and side chain rotamers, high accuracy docking that correctly reflects all ligand-protein interactions is not feasible, this image is one representative of a big cluster of similar docking poses.

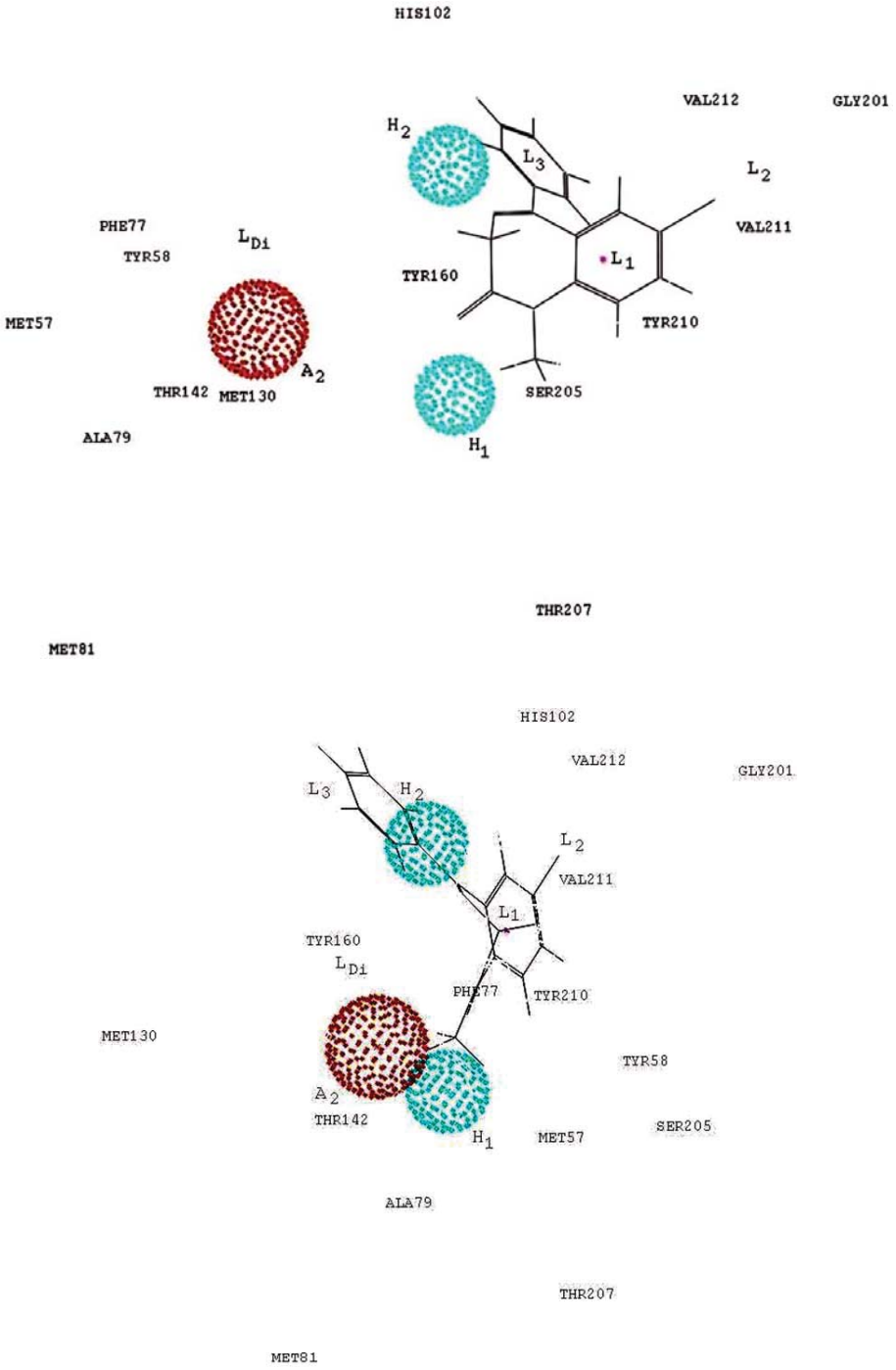

Fig. (24). Location of important Bz BS residues relative to the pharmacophoric descriptors in two views that correspond to a 90 rotation about L_1, with A_2 in front, as determined by evaluation of experimental data and the comparative model of the $\alpha1\beta2\gamma2$ $GABA_A$ receptor. The ligand shown is diazepam. Since inverse agonists stabilize protein conformations that vary from the conformations preferred by agonists, it seems plausible that more than one side chain could satisfy the same descriptor.

accepting sites near α1Y160, γ2A79, γ2T81, γ2M130 and γ2T142. If these proximity relations that are found in the docking poses are transferred to the unified pharmacophore model, the following picture emerges:

Within the different poses that exhibit this orientation, there is still some degree of variation in structural details. There are several sources for this variability in the computationally derived structures: template and alignment choice, model construction and refinement, as well as docking algorithms contribute to the variability of the poses that are found.

This orientation is also strongly supported by the observation that XLi-093, as aligned in Fig. (**14**) with the docked diazepam shown above, will be able to thread the portion of the molecule not inside the included volume towards the solvent accessible space through the subunit boundary.

Agreement between this orientation of the pharmacophore model inside the structural model of the protein with single ligand dockings that have been proposed in the past [103-105] will have to be examined in detail. The overall picture appears to be pointing towards a satisfactory orientation of the pharmacophore model in the pocket, and for those instances where there could be a discrepancy, further experiments will clarify.

Refinement of the predicted protein-ligand complexes with the aid of the unified pharmacophore model appears to be a very promising approach to arrive at 3D structures that are of sufficient accuracy to be used for structure guided drug design. Studies that combine advanced protein modeling techniques with the classical pharmacophore approach are currently underway.

CONCLUSION

A unified pharmacophore model incorporating many substance classes that act at the DS and DI benzodiazepine binding sites of $GABA_A$ receptors has been updated to include new substance classes. Compound development guided by this pharmacophore model has led to new agents with interesting pharmacological profiles, particularly enhanced preference for $\alpha2$ or $\alpha5$ containing $GABA_A$ receptor subtype. Based on the evaluation of experimental data and comparative models of the $\alpha1\beta2\gamma2$ $GABA_A$ receptor, the location of several residues relative to the descriptors of the pharmacophore/receptor model has been proposed. Although no absolute assignments were made regarding which amino acids satisfy the pharmacophoric descriptors, experimental data strongly indicated definite trends with regard to how ligands of varying pharmacological activity are oriented within the receptor. Because the unified pharmacophore/receptor model accounts for the binding and activity profiles at the six $GABA_A$ receptor subtypes containing any one of the different alpha subunits, the proposed orientation should also be similar within the different models [110] of the various receptor subtypes. Information to be immediately gained from this proposed orientation can have far reaching benefits, not only for the rational design of selective ligands and the interpretation of ligand docking results, but also for the identification and evaluation of possible roles certain residues may have within the pocket. As structure determination of the $GABA_A$ receptor is eagerly awaited, it is hoped that this proposed orientation may be used by others to gain additional insight into the potential mechanisms underlying binding and modulation at the Bz site, all of which will lead to a better understanding of the structure and function of $GABA_A$ receptors.

ACKNOWLEDGEMENTS

We wish to thank Qi Huang for helpful discussions. We wish to acknowledge support by the Research Growth Initiative of the University of Wisconsin-Milwaukee and the NIMH (MH 46851) as well as by grants of the Austrian Science Fund (P15165 and P16397).

REFERENCES

[1] Sieghart, W.; Ernst, M. *Curr. Med. Chem. Central Nervous Syst. Agents* **2005**, *5*, 217-242.
[2] Bowser, D. N.; Wagner, D. A.; Czajkowski, C.; Cromer, B. A.; Parker, M. W.; Wallace, R. H.; Harkin, L. A.; Mulley, J. C.; Marini, C.; Berkovic, S. F.; Williams, D. A.; Jones, M. V.; Petrou, S. *Proc. Natl. Acad. Sci. USA* **2002**, *99*, 15170-15175.
[3] Bateson, A. N. *Sleep Med.* **2004**, *5*, S9-S15.
[4] Otani, K.; Ujike, H.; Tanaka, Y.; Morita, Y.; Katsu, T.; Nomura, A.; Uchida, N.; Hamamura, T.; Fujiwara, Y.; Kuroda, S. *Neurosci. Lett.* **2005**, *381*, 108-113.
[5] Dean, B.; Scarr, E.; McLeod, M. *Brain Res. Mol. Brain Res.* **2005**, *138*, 145-155.
[6] Guidotti, A.; Auta, J.; Davis, J. M.; Dong, E. B.; Grayson, D. R.; Veldic, M.; Zhang, X. Q.; Costa, E. *Psychopharmacology* **2005**, *180*, 191-205.
[7] Maubach, K. *Drug Targets-CNS Neuro Disorders* **2003**, *2*, 233-239.
[8] Barrett, A. C.; Negus, S. S.; Mello, N. K.; Caine, S. B. *J. Pharmacol. Exp. Ther.* **2005**, *315*, 858-871.
[9] Anthenelli, R.; Schuckit, M. A. *Int. J. Addict.* **1990/1991**, *25*, 81-94.
[10] Schuckit, M. A. *Alcohol Clin. Exp. Res.* **1988**, *12*, 465-470.
[11] Barnard, E. A.; Skolnick, P.; Olsen, R. W.; Möhler, H.; Sieghart, W.; Biggio, G.; Braestrup, C.; Bateson, A. N.; Langer, S. Z. *Pharmacol. Rev.* **1998**, *50*, 291-313.
[12] Simon, J.; Wakimoto, H.; Fujita, N.; Lalande, M.; Barnard, E. A. *J. Biol. Chem.* **2004**, *279*, 41422-41435.
[13] Burt, D. R.; Kamatchi, G. L. *FASEB J.* **1991**, *5*, 2916-2923.
[14] Keramidas, A.; Moorhouse, A.; Schofield, P. C.; Barry, P. *Prog. Biophys. Mol. Biol.* **2004**, *86*, 161-204.
[15] Sieghart, W.; Sperk, G. *Curr. Top. Med. Chem.* **2002**, *2*, 795-816.
[16] Mossier, B.; Togel, M.; Fuchs, K.; Sieghart, W. *J. Biol. Chem.* **1994**, *269*, 25777-25782.
[17] Togel, M.; Mossier, B.; Fuchs, K.; Sieghart, W. *J. Biol. Chem.* **1994**, *269*, 12993-12998.
[18] Pirker, S.; Schwarzer, C.; Wieselthaler, A.; Sieghart, W.; Sperk, G. *Neuroscience* **2000**, *101*, 815-850.
[19] Doble, A.; Martin, I. L. *Trends Pharmacol. Sci.* **1992**, *13*, 76-81.
[20] Sieghart, W. *Pharmacol. Rev.* **1995**, *47*, 181-234.
[21] Kralic, J. E.; Korpi, E. R.; O'Buckley, T. K.; Homanics, G. E.; Morrow, A. L. *J. Pharmacol. Exp. Ther.* **2002**, *302*, 1037-1045.
[22] Crestani, F.; Assandri, R.; Tauber, M.; Martin, J.; Rudolph, U. *Neuropharmacology* **2002**, *43*, 679-684.
[23] Rudolph, U.; Crestani, F.; Benke, D.; Brunig, I.; Benson, J. A.; Fritschy, J. M.; Martin, J. R.; Bluethmann, H.; Möhler, H. *Nature* **1999**, *401*, 796-800.
[24] Collinson, N.; Cothliff, R.; Rosahl, T.; Sur, C.; Kuenzi, F. M.; Howell, O.; Seabrook, G.; Atack, J.; McKernan, R.; Dawson, G. R.; Whiting, P. *Eur. J. Neurosci.* **2000**, *12*, 171.
[25] Bailey, D. J.; Tetzlaff, J. E.; Cook, J. M.; He, X. H.; Helmstetter, F. J. *Neurobiol. Learn. Mem.* **2002**, *78*, 1-10.
[26] DeLorey, T. M.; Lin, R. C.; McBrad, B.; He, X. H.; Cook, J. M.; Lameh, J.; Loew, G. H. *Eur. J. Pharmacol.* **2001**, *426*, 45-54.
[27] Lelas, S.; Rohrbach, K.; Glick, S. D.; Zeller, K.; Bourin, C.; Sieracki, K.; Bertekap, R.; Chen, J.; Cook, C. M.; Helmstetter, F. J.; Li, X. H.; Westphal, R.; Lindner, M.; Tertyshnikova, S.; Cook, J.; McElroy, J. F. *Manuscript in preparation*.
[28] Liu, R. Y.; Zhang, P. W.; McKernan, R. M.; Wafford, K.; Cook, J. M. *Med. Chem. Res.* **1995**, *5*, 700-709.
[29] Liu, R. Y.; Hu, R. J.; Zhang, P. W.; Skolnick, P.; Cook, J. M. *J. Med. Chem.* **1996**, *39*, 1928-1934.
[30] Griebel, G.; Perrault, G.; Simiand, J.; Cohen, C.; Granger, P.; Decobert, M.; Francon, D.; Avenet, P.; Depoortere, H.; Tan, S.; Oblin, A.; Schoemaker, H.; Evanno, Y.; Sevrin, M.; George, P.; Scatton, B. *J. Pharmacol. Exp. Ther.* **2001**, *298*, 753-768.
[31] Minier, F.; Sigel, E. *Proc. Natl. Acad. Sci. USA* **2004**, *101*, 7769-7774.
[32] Wafford, K. A.; Macaulay, A. J.; Fradley, R.; O'Meara, G. F.; Reynolds, D. S.; Rosahl, T. W. *Biochem. Soc. Trans.* **2004**, *32*, 553-556.
[33] Casula, M. A.; Bromidge, F. A.; Pillai, G. V.; Wingrove, P. B.; Martin, K.; Maubach, K.; Seabrook, G. R.; Whiting, P. J.; Hadingham, K. L. *J. Neurochem.* **2001**, *77*, 445-451.
[34] Wafford, K. A.; Whiting, P. J.; Kemp, J. A. *Mol. Pharmacol.* **1993**, *43*, 240-244.
[35] Atack, J. R. *Expert Opin. Invest. Drugs* **2005**, *14*, 601-618.
[36] Möhler, H.; Rudolph, U.; McKernan, R. In ACNP, December 20, **2004**.
[37] Study, R. E. B. J.L. *Proc. Natl. Acad. Sci. USA* **1981**, *78*, 7180-7184.
[38] Rogers, C.; Twyman, R. E.; MacDonald, R. L. *J. Physiol. (London)* **1994**, *475*, 69-82.
[39] Kash, T. L.; Jenkins, A.; Kelley, J. C.; Trudell, J.; Harrison, N. L. *Nature* **2003**, *421*, 272-275.
[40] Rüsch, D.; Forman, S. A. *Anesthesiology* **2005**, *102*, 783-792.
[41] Baur, R.; Sigel, E. *Mol. Pharmacol.* **2005**, *67*, 1005-1008.
[42] Zhang, W.; Koehler, K. F.; Zhang, P.; Cook, J. M. *Drug Des. Discov.* **1995**, *12*, 193-248.
[43] Zhang, W.; Diaz-Arauzo, H.; Allen, M. S.; Koehler, K. F.; Cook, J. M. *Chemical and Computer Assisted Development of the Inclusive Pharmacophore of Benzodiazepine Receptors, in Studies in Medicinal Chemistry, M.I. Choudhary, Editor.* Harwood Academic Publishers: **1996**; pp. 303.
[44] Sigel, E.; Schaerer, M. T.; Buhr, A.; Baur, R. *Mol. Pharmacol.* **1998**, *54*, 1097-1105.
[45] Dunn, S. M. J.; Davies, M.; Muntoni, A. L.; Lambert, J. J. *Mol. Pharmacol.* **1999**, *56*, 768-774.
[46] Davies, M.; Bateson, A. N.; Dunn, S. M. J. *J. Neurochem.* **1998**, *70*, 2188-2194.
[47] Cromer, B.; Morton, C.; Parker, M. W. *Trends Biochem. Sci.* **2002**, *27*, 280-287.
[48] Ernst, M.; Brauchart, D.; Boresch, S.; Sieghart, W. *Neuroscience* **2003**, *119*, 933-943.
[49] Sigel, E. *Curr. Top. Med. Chem.* **2002**, *2*, 833-840.
[50] Allen, M. S.; Tan, Y. C.; Trudell, M. L.; Narayanan, K.; Schindler, L.; Martin, M. J.; Schultz, C. A.; Hagen, T. J.; Koehler, K. F.; Codding, P.; Skolnick, P.; Cook, J. *J. Med. Chem.* **1990**, *33*, 2343-2357.
[51] Zhang, P. W.; Zhang, W. J.; Liu, R. Y.; Harris, B.; Skolnick, P.; Cook, J. M. *J. Med. Chem.* **1995**, *38*, 1679-1688.

[52] Allen, M. S.; Laloggia, A. J.; Dorn, L. J.; Martin, M. J.; Constantino, G.; Hagen, T. J.; Koehler, K. F.; Skolnick, P.; Cook, J. *J. Med. Chem.* **1992**, *35*, 4001-4010.

[53] Wong, G.; Koehler, K. F.; Skolnick, P.; Gu, Z. Q.; Ananthan, S.; Schönholzer, P.; Hunkeler, W.; Zhang, W. J.; Cook, J. M. *J. Med. Chem.* **1993**, *36*, 1820-1830.

[54] Hevers, W.; Luddens, H. *Mol. Neurobiol.* **1998**, *18*, 35-86.

[55] He, X. B.; Huang, Q.; Ma, C. R.; Yu, S.; McKernan, R.; Cook, J. *Drug Des. Discov.* **2000**, *17*, 131-171.

[56] Huang, Q.; He, X. H.; Ma, C. R.; Liu, R. Y.; Yu, S.; Dayer, C. A.; Wenger, G. R.; McKernan, R.; Cook, J. M. *J. Med. Chem.* **2000**, *43*, 71-95.

[57] Hadingham, K. L.; Wingrove, P. B.; Wafford, K. A.; Bain, C.; Kemp, J. A.; Palmer, K. J.; Wilson, A. W.; Wilcox, A. S.; Sikela, J. M.; Ragan, C. I.; Whiting, P. J. *Mol. Pharmacol.* **1993**, *44*, 1211-1218.

[58] Barnard, E. A. *Trends Biochem. Sci.* **1992**, *17*, 368-374.

[59] Huang, Q.; Liu, R. Y.; Zhang, P. W.; He, X. H.; McKernan, R.; Gan, T.; Bennett, D. W.; Cook, J. M. *J. Med. Chem.* **1998**, *41*, 4130-4142.

[60] Wafford, K. A.; Thompson, S. A.; Thomas, D.; Sikela, J.; Wilcox, A. S.; Whiting, P. J. *Mol. Pharmacol.* **1996**, *50*, 670-678.

[61] Huang, Q.; Cox, E.; Gan, T.; Ma, C. R.; Bennett, D. A.; McKernan, R.; Cook, J. *Drug Des. Discov.* **1999**, *16*, 55-76.

[62] Drover, D. R. *Clin. Pharmacokinet.* **2004**, *43*, 227-238.

[63] Noble, S.; Langtry, H. D.; Lamb, H. M. *Drugs* **1998**, *55*, 277-302.

[64] Jerussic, T. **2006**, unpublished results.

[65] Savic, M. M.; Huang, S.; Furtmuller, R.; Clayton, T.; Huck, S.; Obradovic, D. I.; Ugresic, N. D.; Sieghart, W.; Bokonjic, D. R.; Cook, J. M. *Neuropsychopharmacology* **2007**.

[66] Dias, R.; Sheppard, W. F. A.; Fradley, R. L.; Garrett, E. M.; Stanley, J. L.; Tye, S. J.; Goodacre, S.; Lincoln, R. J.; Cook, S. M.; Conley, R.; Hallett, D.; Humphries, A. C.; Thompson, S. A.; Wafford, K. A.; Street, L. J.; Castro, J. L.; Whiting, P. J.; Rosahl, T. W.; Atack, J. R.; McKernan, R. M.; Dawson, G. R.; Reynolds, D. S. *J. Neurosci.* **2005**, *25*, 10682-10688.

[67] McKernan, R. M.; Rosahl, T. W.; Reynolds, D. S.; Sur, C.; Wafford, K. A.; Atack, J. R.; Farrar, S.; Myers, J.; Cook, G.; Ferris, P.; Garrett, L.; Bristow, L.; Marshall, G.; Macaulay, A.; Brown, N.; Howell, O.; Moore, K. W.; Carling, R. W.; Street, L. J.; Castro, J. L.; Ragan, C. I.; Dawson, G. R.; Whiting, P. J. *Nat. Neurosci.* **2000**, *3*, 587-592.

[68] Collinson, N.; Kuenzi, F. M.; Jarolimek, W.; Maubach, K. A.; Cothliff, R.; Sur, C.; Smith, A.; Otu, F. M.; Howell, O.; Atack, J. R.; McKernan, R. M.; Seabrook, G. R.; Dawson, G. R.; Whiting, P. J.; Rosahl, T. W. *J. Neurosci.* **2002**, *22*, 5572-5580.

[69] Crestani, F.; Keist, R.; Fritschi, J.; Benke, D.; Vogt, K. E.; Prut, L. *Proc. Natl. Acad. Sci. USA* **2002**, *99*, 8980-8985.

[70] Bohlhalter, S.; Weinmann, O.; Möhler, H.; Fritschy, J. M. *J. Neurosci.* **1996**, *16*, 283-297.

[71] van Rijnsoever, C.; Tauber, M.; Choulli, M. K.; Keist, R.; Rudolph, U.; Möhler, H.; Fritschy, J. M.; Crestani, F. *J. Neurosci.* **2004**, *24*, 6785-6790.

[72] Porsolt, R. D.; McArthur, R. A.; Lenegre, A. *Psychotropic Screening Procedures*. Elsevier: **1993**; pp. 23-51.

[73] Wang, Q.; Han, Y.; Xue, H. *CNS Drug Rev.* **1999**, *5*, 125-144.

[74] Miksieck, R. *Mol. Pharmacol.* **1993**, *44*, 37-43.

[75] Häberlein, H.; Tschiersch, K. P.; Schäfer, H. L. *Pharmazie* **1994**, *49*, 912-922.

[76] Huang, X. Q.; Liu, T.; Gu, J. D.; Luo, X. M.; Ji, R. Y.; Cao, Y.; Xue, H.; Wong, J. T. F.; Wong, B. L.; Pei, G.; Jiang, H. L.; Chen, K. X. *J. Med. Chem.* **2001**, *44*, 1883-1891.

[77] Marder, M.; Estiu, G.; Blanch, L. B.; Viola, H.; Wasowski, C.; Medina, J. H.; Paladini, A. C. *Bioorg. Med. Chem.* **2001**, *9*, 323-335.

[78] Yu, J.; Cook, J. **1999**, unpublished results.

[79] Costanzo, A.; Guerrini, G.; Ciciani, G.; Bruni, F.; Costagli, C.; Selleri, S.; Besnard, F.; Costa, B.; Martini, C.; Malmberg-Aiello, P. *J. Med. Chem.* **2002**, *45*, 5710-5720.

[80] Yin, W. Y.; Sarma, P.; Han, J.; Chen, J. L.; Cook, J. M. *Tetrahedron Lett.* **2005**, *46*, 6363-6368.

[81] Li, X. Y.; Cao, H.; Zhang, C. C.; Furtmueller, R.; Fuchs, K.; Huck, S.; Sieghart, W.; Deschamps, J.; Cook, J. M. *J. Med. Chem.* **2003**, *46*, 5567-5570.

[82] Han, D. M.; Forsterling, F. H.; Li, X. Y.; Deschamps, J. R.; Cao, H.; Cook, J. M. *Bioorg. Med. Chem. Lett.* **2004**, *14*, 1465-1469.

[83] Ferretti, V.; Gilli, P.; Borea, P. A. *Acta Crystalogr. Sect. B Struct. Sci.* **2004**, *60*, 481-489.

[84] Cox, E. D.; Diaz-Arauzo, H.; Huang, Q.; Reddy, M. S.; Ma, C. R.; Harris, B.; McKernan, R.; Skolnick, P.; Cook, J. M. *J. Med. Chem.* **1998**, *41*, 2537-2552.

[85] Diaz-Arauzo, H.; Evoniuk, G.; Skolnick, P.; Cook, J. *J. Med. Chem.* **1991**, *34*, 1754-1756.

[86] Diaz-Arauzo, H.; Koehler, K. F.; Hagen, T. J.; Cook, J. M. *Life Sci.* **1991**, *49*, 207-216.

[87] Skolnick, P.; Hu, R. J.; Cook, C. M.; Hurt, S. D.; Trometer, J. D.; Lu, R. Y.; Huang, Q.; Cook, J. M. *J. Pharmacol. Exp. Ther.* **1997**, *283*, 488-493.

[88] Wisden, W.; Laurie, D. J.; Monyer, H.; Seeburg, P. H. *J. Neurosci.* **1992**, *12*, 1040-1062.

[89] Harris, D. L.; DeLorey, T. M.; He, X. H.; Cook, J. M.; Loew, G. H. *Eur. J. Pharmacol.* **2000**, *401*, 271-287.

[90] Roth, B. **2006**, unpublished results.

[91] Kelly, M. D.; Smith, A.; Banks, G.; Wingrove, P.; Whiting, P. W.; Atack, J.; Seabrook, G. R.; Maubach, K. A. *Br. J. Pharmacol.* **2002**, *135*, 248-256.

[92] Turner, D.; Sapp, D.; Olsen, R. W. *J. Pharmacol. Exp. Ther.* **1991**, *257*, 1236-1242.

[93] McKay, P. F.; Foster, K. L.; Mason, D.; Cummings, R.; Garcia, M.; Williams, L. S.; Grey, C.; McCane, S.; He, X. H.; Cook, J. M.; June, H. L. *Psychopharmacology* **2004**, *172*, 455-462.

[94] Harvey, S. C.; Foster, K. L.; McKay, P. F.; Carroll, M. R.; Seyoum, R.; Woods, J. E.; Grey, C.; Jones, C. M.; McCane, S.; Cummings, R.; Mason, D.; Ma, C. R.; Cook, J. M.; June, H. L. *J. Neurosci.* **2002**, *22*, 3765-3775.

[95] Rowlett, J. K.; Spealman, R. D.; Lelas, S.; Cook, J. M.; Yin, W. Y. *Psychopharmacology* **2003**, *165*, 209-215.

[96] June, H. L.; Harvey, S. C.; Foster, K. L.; McKay, P. F.; Cummings, R.; Garcia, M.; Mason, D.; Grey, C.; McCane, S.; Williams, L. S.; Johnson, T. B.; He, X. H.; Rock, S.; Cook, J. M. *J. Neurosci.* **2001**, *21*, 2166-2177.

[97] Stephens, D. N.; Pistovcakova, J.; Worthing, L.; Atack, J. R.; Dawson, G. R. *Eur. J. Pharmacol.* **2005**, *526*, 240-250.

[98] Lüddens, H.; June, H. L.; Cook, J. (In preparation).

[99] Haefely, W.; Kyburz, E.; Gerecke, M.; and Mohler, H. *Recent Advances in the Molecular Pharmacology of Benzodiazepine Receptors and in the Structure-Activity Relationships of their Agonists and Antagonists.* Academic Press: **1985**; pp. 165-322.

[100] Fryer, R. I. *Comprehensive Medicinal Chemistry*. Pergamon Press: **1989**; pp. 539-566.

[101] Brejc, K.; van Dijk, W.; Klassen, R.; Schuurmans, M.; van Der Oost, J.; Smit, A. B.; Sixma, T. *Nature* **2001**, *411*, 269-276.

[102] Ernst, M.; Bruckner, S.; Boresch, S.; Sieghart, W. *Mol. Pharmacol.* **2005**, *68*, 1291-1300.

[103] Kucken, A. M.; Wagner, D. A.; Ward, P. R.; Teissere, J. A.; Boileau, A. J.; Czajkowski, C. *Mol. Pharmacol.* **2000**, *57*, 932-939.

[104] Sawyer, G. W.; Chiara, D. C.; Olsen, R. W.; Cohen, J. B. *J. Biol. Chem.* **2002**, *277*, 50036-50045.

[105] Sancar, F.; Ericksen, S. S.; Kucken, A. M.; Teissere, J. A.; Czajkowski, C. *Mol. Pharmacol.* **2007**, *71*, 38-46.

[106] Unwin, N. *J. Mol. Biol.* **2005**, *346*, 967-89.

[107] Sigel, E.; Buhr, A. *Trends Pharmacol. Sci.* **1997**, *18*, 425-429.

[108] Baumann, S. W.; Baur, R.; Sigel, E. *J. Biol. Chem.* **2002**, *277*, 46020-46025.

[109] Neish, C. S.; Martin, I. L.; Davies, M.; Henderson, R. M.; Edwardson, J. M. *Nanotechnol.* **2003**, *14*, 864-872.

[110] Chou, K. C. *Biochem. Biophys. Res. Commun.* **2004**, *316*, 636-642.

[111] Trudell, J. R. *Biochim. Biophys. Acta* **2002**, *1565*, 91-96.

[112] Buhr, A.; Baur, R.; Malherbe, P.; Sigel, E. *Mol. Pharmacol.* **1996**, *49*, 1080-1084.

[113] Sigel, E.; Baur, R.; Trube, G.; Möhler, H.; Malherbe, P. *Neuron* **1990**, *5*, 703-711.

[114] Khom, S.; Baburin, I.; Timin, E. N.; Hohaus, A.; Sieghart, W.; Hering, S. *Mol. Pharmacol.* **2006**, *69*, 640-649.

[115] Hansen, S. B.; Sulzenbacher, G.; Huxford, T.; Marchot, P.; Taylor, P.; Bourne, Y. *EMBO J.* **2005**, *24*, 3635-46.

[116] Mihic, S. J.; Whiting, P.; Klein, R. L.; Wafford, K.; Harris, R. A. *J. Biol. Chem.* **1994**, *269*, 32768-32773.

[117] Downing, S.; Lee, Y. F.; Farb, D. H.; Gibbs, T. T. *Br. J. Pharmacol.* **2005**, *145*, 894-906.

[118] He, X. H.; Zhang, C. C.; Cook, J. M. *Med. Chem. Res.* **2001**, *10*, 269-308.

[119] Colquhoun, D. *Br. J. Pharmacol.* **1998**, *125*, 923-947.

[120] Smith, G. B.; Olsen, R. W. *Neuropharmacology* **2000**, *39*, 55-64.

[121] McKernan, R.; Farrar, S.; Collins, I.; Emms, F.; Asuni, A.; Quirk, K.; Broughton, H. B. *Mol. Pharmacol.* **1998**, *54*, 33-43.

[122] Berezhnoy, D.; Nyfeler, Y.; Gonthier, A.; Schwob, H.; Goeldner, M.; Sigel, E. *J. Biol. Chem.* **2004**, *279*, 3160-3168.

[123] Duncalfe, L.; Carpenter, M.; Smillie, L.; Martin, I. L.; Dunn, S. L. *J. Biol. Chem.* **1996**, *271*, 9209-9214.

[124] Tan, K. R.; Baur, R.; Gonthier, A.; Goeldner, M.; Sigel, E. Structure of the benzodiazepine binding pocket in GABAA receptors: proximity-accelerated chemical reaction. In Abstract D32-527.7 SFN **2006**.

[125] Kucken, A. M.; Teissere, J. A.; Seffinga-Clark, J.; Wagner, D. A.; Czajkowski, C. *Mol. Pharmacol.* **2003**, *63*, 289-296.

[126] Teissere, J. A.; Czajkowski, C. *J. Neurosci.* **2001**, *21*, 4977-4986.

[127] Buhr, A.; Baur, R.; Sigel, E. *J. Biol. Chem.* **1997**, *272*, 11799-11804.

[128] Ogris, W.; Poltl, A.; Hauer, B.; Ernst, M.; Oberto, A.; Wulff, P.; Hoger, H.; Wisden, W.; Sieghart, W. *Biochem. Pharmacol.* **2004**, *68*, 1621-1629.

Received: May 08, 2007 **Revised: August 09, 2007** **Accepted: August 10, 2007**

III. Computational Background

1 Homology Modeling

Introduction

In the field of drug discovery, we aim to comprehend the three-dimensional structure of a protein binding site as it uncovers the proteins' interaction properties in molecular detail. These detailed structural insights provide the basis for the rational design of future drugs. Experimental procedures like X-ray and NMR spectroscopy lead to the structural resolution of about 31000 non-homologous (<=95% sequence identity) protein structures until April 2012 (Ref[1]). However, this number sounds small in comparison to the approximately 15000000 protein sequences which are deposited in the UniProt knowledge database[2].

Based on this abundance of sequence information and on the general observation that proteins with similar sequence have similar structures the methodology of homology modeling evolved. Homology modeling generates three dimensional models of a protein necessitating only its amino-acid sequence[3]. In this process the target amino-acid sequence is first compared against sequences of known structures. If a similar sequence of a known structure (template) could have been found, the protein backbone of this template works as a structural frame for the target sequence.

In the field of drug discovery, homology modeling for membrane proteins is of special interest because of two facts. First, membrane proteins account for around 60% of todays' approved drug targets[4]. And second, the structural resolution of membrane proteins is difficult, especially for human membrane proteins. Of the about 31000 resolved non-homologous proteins in the RCSB PDB[1], only around 2000 are membrane proteins (GO[5] ID:16020) and approximately 500 are humane membrane proteins.

1.1 Homology modeling workflow

In general the homology modeling procedure can be divided into four steps as described in the following[6] (**Fig. 1**):

(i) Identification of evolutionarily related proteins with experimentally determined structures

(ii) Sequence alignment between target and template sequence

(iii) building the three dimensional model based on the alignment of template structure

(iv) validation/refinement/evaluation of the models

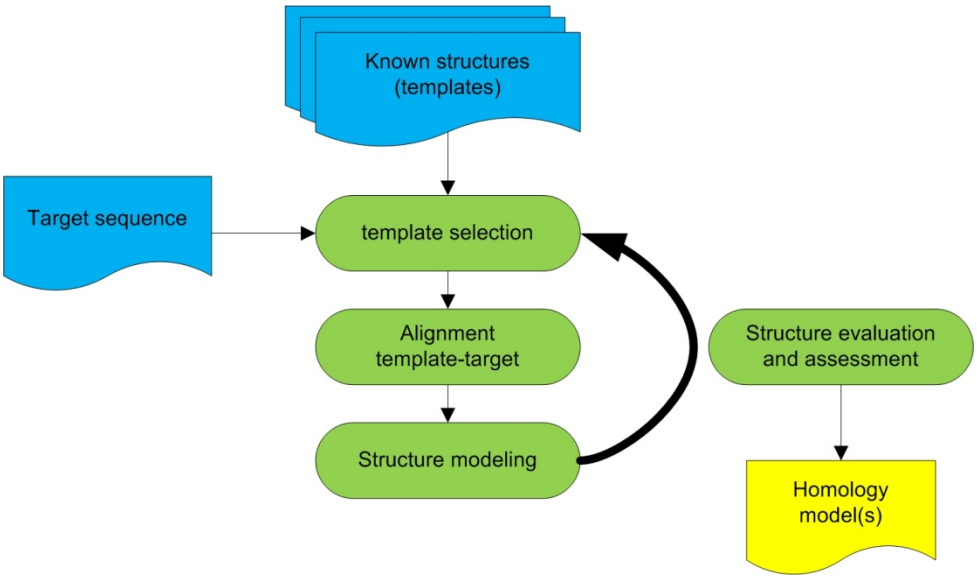

Figure 1 – The four main steps of comparative protein structure modeling: template selection, target-template alignment, model building and model quality evaluation. Figure adapted from Ref[6].

1.2 Homology modeling accuracy

As the name already implies, models are, by definition, an abstraction and thus contain errors. It has been shown that there is a clear correlation between target-template sequence identity and homology model accuracy[7].

Table 1 - Correlation between target-template sequence identity and homology model accuracy. Data and Table from Ref[7].

	sequence identity	root mean square error for main-chain	frequent type of errors
high-accuracy homology models	> 50%	1Å	side-chain packing
medium-accuracy homology models	30 - 50 %	1.5Å (~90% of main-chain atoms)	frequently side-chain packing errors, mainchain distortions
low-accuracy homology models	< 30%	>1.5Å	alignment error, sidechain packing errors, mainchain distortions

In the field of drug discovery, the following rule for homology model accuracy emerged: Models built with over 50% sequence identities are good enough for drug discovery purposes (elucidation of binding mode, hit discovery). In case the sequence identities are between 30 and 50%, derived models can be used for estimation of target drugability, and for the design of mutagenesis experiments. Finally, models that are built with a sequence identity between 15 and 30% are only suitable for the assignment of protein function and for compilation of mutagenesis experiments[8].

But next to the sequence identity also other features have to be considered in the estimation of model accuracy. For example in GPCRs, low sequence identity within the family is partly compensated by the common heptahelical transmembrane domain. This also holds true for the extracellular domain of Cys-loop pentameric ligand gated ion channels[9] (LGIC).

2 Molecular Docking

Introduction

In the past decades the number of structurally determined protein structures has increased from one structure in 1972 to approximately 75 000 protein structures in 2012 (Ref[1]). This trend clearly promotes the application of computational methods that can exploit knowledge from structurally determined protein binding sites in hit identification and lead optimization[10].

Such a methodology, docking of small molecules into protein binding sites was introduced in 1980 with the introduction of DOCK[11]. In principle, molecular docking aims to predict the binding mode and the affinity of the docked molecules against a target protein. The whole docking process can be subdivided into two steps, 1) posing and 2) scoring[12]. In the first step, the posing step, the program samples the ligands' translational, rotational and conformational degrees of freedom within the binding site. This results in a multitude of computationally generated "ligand-receptor complexes", called poses. Then, in the second step, the scoring step, the poses are evaluated by a "scoring function" which applies algorithms that approximate the underlying enthalpic and entropic contributions to binding free energy. Finally, the poses are ranked according to their scoring values, assuming the best ranked pose to be correct and its scoring value representing the ligands' binding affinity.

Nowadays dozens of docking software are available (**Fig. 2**). They mainly differ in either their posing algorithms or in their evaluative scoring functions. The next paragraphs should give a structured overview about the most important algorithms and functions applied in docking.

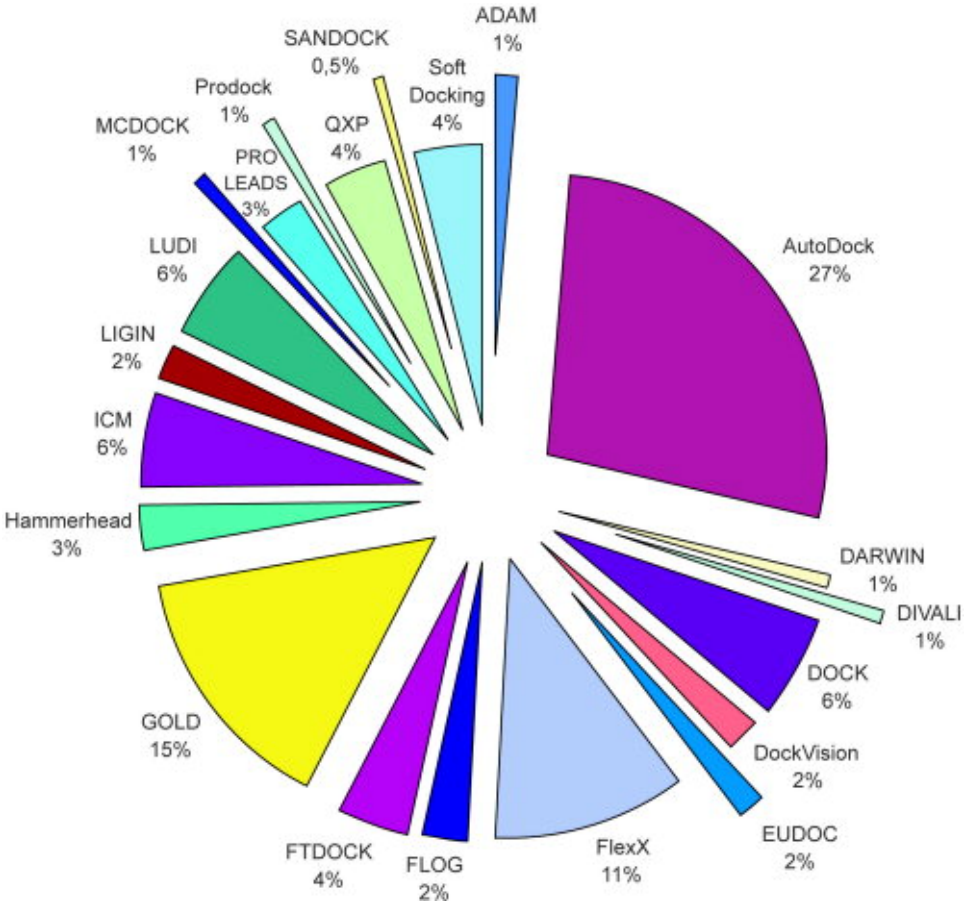

Figure 2 - Chart presentation for the most common docking software based on number of citations taken from ISI Web of Science (2005). Figure and data taken from Ref[13].

2.1 Posing

As already mentioned, posing algorithms aim to sample the ligands' translational (Tx, Ty, Tz), rotational (Rx, Ry, Rz) and conformational (N) degrees of freedom within the constraints of the binding site. During this sampling process a coarse and fast evaluation function omits poses that show severe protein clashes.

In general three groups of search methods are used for the sampling purpose and thus are implemented in docking software[12]:

- Systematic search methods **2.1.1**
- Stochastic/ random search methods **2.1.2**
- Simulation methods **2.1.3**

These three methods are described in more detail in the following paragraphs.

2.1.1 Systematic search

Systematic search algorithms aim to systematically sample all degrees of freedom during docking (**Fig. 3**). In dependence of the desired sampling resolution, sampling parameters like torsion angle increment ($\Delta\alpha$ = 10°, 30°, ... for sigma bonds) can be adjusted for ligand flexibility. As for larger molecules (high number of rotatable bonds) one will inevitably face the problem of combinatorial explosion[14], certain adaptations have been developed. Here the most prominent approach is the incremental ligand growth within the active site. In this procedure the ligand is first separated into rigid (core fragment) and flexible parts (side chains). Once the rigid cores are docked, the flexible parts are incrementally added[15,16]. Incremental growth algorithms are implemented in popular software packages such as DOCK[11], FlexX[15], Glide[17] and Hammerhead[18].

Next to incremental growth another popular method is the use of libraries of pre-generated ligand conformations. Here, the ligands' internal degrees of freedom are sampled once and then stored as a conformational library. In the subsequent step each conformation is then rigidly translated and rotated within the pocket.

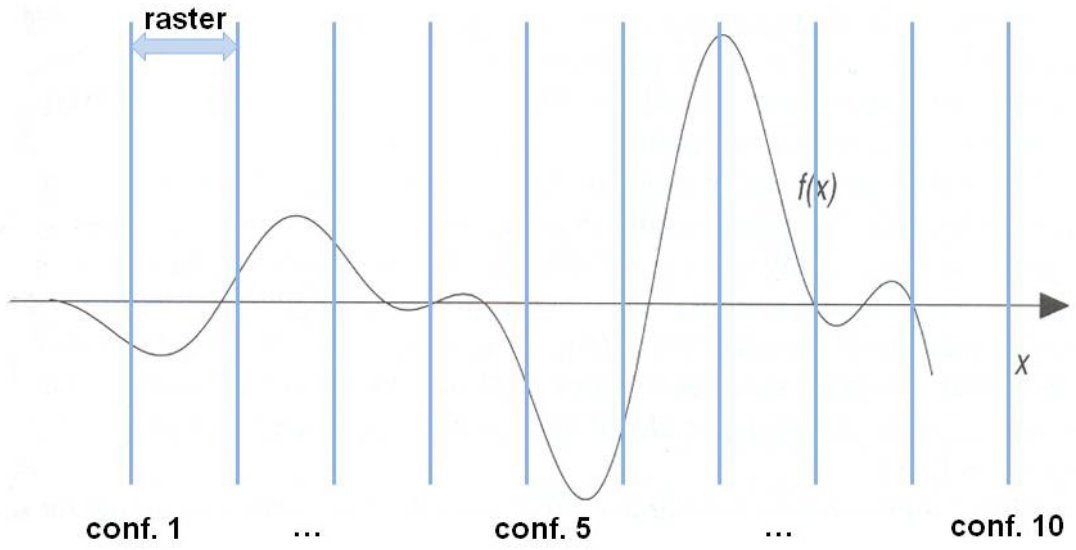

Figure 3 - Visual scheme for the systematic search approach. Here represented for ligand conformation sampling. In the scheme, the x-axis represents possible ligand conformations while the y-axis resemble the conformations' corresponding energy level. The aim of the search algorithms is the seek for the global minimum conformation. In the systematic algorithms the torsional angles of the ligand are systematically rotated by a pre-defined raster ($\Delta\alpha$ = 10°, 30°, ...) aiming to find one conformation near to the global energetic minimum.

2.1.2 Random search

In total contrast to the systematic search algorithms, the stochastic search methods aim to discover the global minimum configuration of an intermolecular complex by randomly sampling the ligands' degrees of freedom within a binding site (**Fig. 4**). Monte Carlo[19] and genetic algorithms[20] are here the most popular among the random search methods. The advantageous progress of tabu search[21] is that it takes into consideration already sampled degrees of freedom. Stochastic search algorithms are often combined with energy minimization algorithms that optimize the intermolecular complex towards the next minimum. The very prominent docking programs, AutoDock[22] and GOLD[23] use stochastic algorithms as search algorithms. The genetic algorithm in GOLD represents a pose as a chromosome consisting of a set of genes. The genes correspond to the ligands' translational, rotational and conformational degrees of freedom and are altered randomly. In the very beginning the starting population is created by randomly generating thousands of chromosomes (poses). During the docking procedure a fitness function then represses improper genes during evolution.

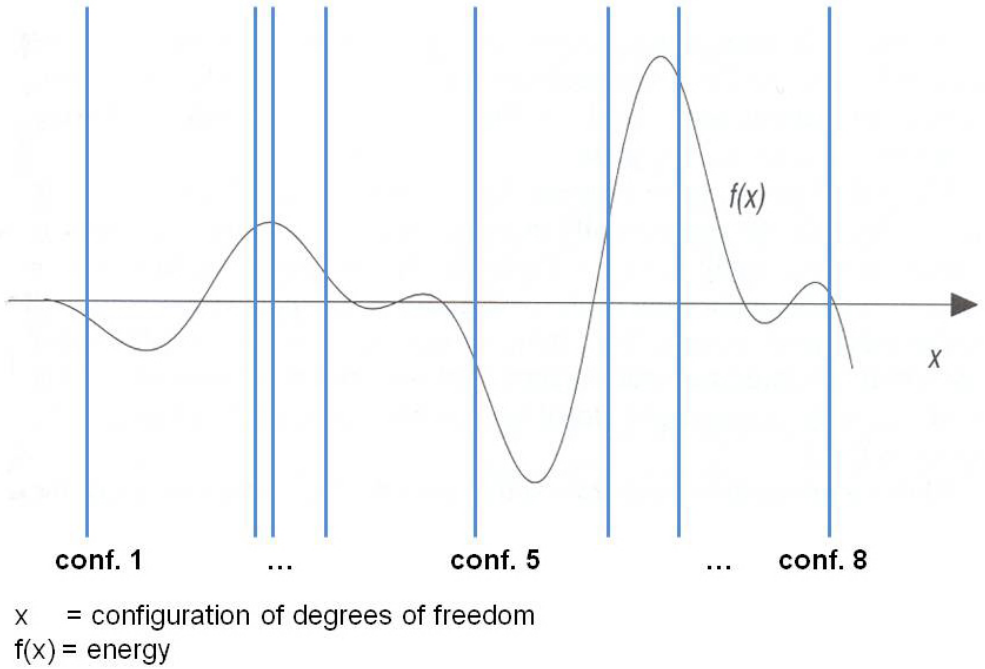

Figure 4 - Visual scheme of a stochastic search. The x-axis resemble the pose space while the y-axis correspond to the energy level. Stochastic search algorithms aim to detect the global minimum by implementation of random algorithms. Variations of rotational, translational and conformational states are introduced in a random manner. The generated poses are then frequently taken as starting point for energy minimization tools that optimize the intermolecular complex to the nearest minimum.

2.1.3 Simulation methods

The most popular method among the simulation methods is molecular dynamics. The thorough sampling of the ligands' degrees of freedom is the key advantage of these algorithms. On the other hand the drawback of molecular dynamics simulations is that they often fail to rise above high-energy barriers[24]. So if the starting configuration is chosen unfavorably (as shown in **Fig. 5**), one ends up only in local minima of the energy surface. One approach to address this drawback is to start molecular dynamics calculations from different ligand positions.

Another simulation method, energy minimization, is hardly used alone as a search algorithm due to its limitation to reach only the nearest local minima. But it is often combined with other search methods to optimize the geometry of an intermolecular complex. DOCK for example conducts a minimization after each fragment addition. Glide, DOCK and AutoDock all use simulation methods as a complementary tool in posing.

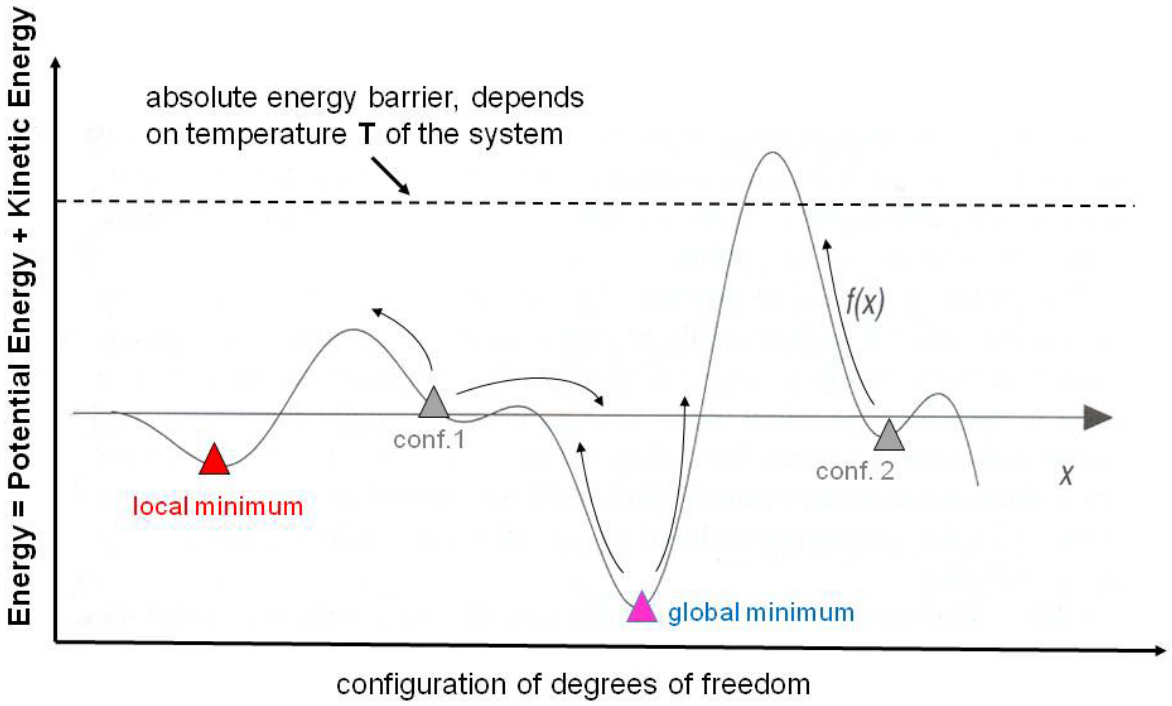

Figure 5 - Visual scheme of a molecular simulation run. Molecular simulation methods enable a high-resolution sampling but lack to overcome high-energy barriers. The starting orientation plays a critical role in the simulation output. If the starting orientation is trapped by a high-energy barrier (**conf. 2**) the molecule cannot reach the targeted global minimum. In another constellation (**conf. 1**) it is capable. One can circumvent this problem by taking multiple starting orientations, but will have to accept an increase of computational resources needed.

2.1.4 Protein flexibility

The importance of protein flexibility during ligand binding is demonstrated by the structural changes of holo and apo X-ray structures and between holo structures harboring different ligands. The mutual adaption of ligand and receptor is termed "induced fit" phenomenon. The necessity for sampling protein flexibility is even more important in case no experimental structure is available and thus ambiguous homology models are used in the docking procedure.

However, considering protein flexibility also opens a new order of complexity for posing algorithms, as the proteins' degrees of freedom have to be additionally sampled. The search algorithms for protein flexibility are less advanced than those designed for ligand flexibility. Nonetheless one has to notify that great advances have been made in the recent years.

Several methods have emerged that should account for protein flexibility in the docking process. In general, they can be grouped into four categories[25] (a) soft docking, (b) rotamer exploration, (c) molecular relaxation and (d) docking into multiple protein structures.

(a) Soft docking

The earliest and simplest attempt to account for protein flexibility was rigid receptor docking with a softened scoring function. Softened scoring functions tolerate some clash between ligand and receptor atoms thus resembling some receptor plasticity[26,27]. The big advantage of soft docking is its computationally economy (only some parameters have to be lowered). But on the other hand soft docking can only consider small conformational changes from the receptor side.

(b) Rotamer exploration

In these methods, side-chain flexibility of the receptor is sampled during the docking procedure while keeping the backbone fixed. One easy implementation was pioneered by Leach et al.[28] using a rotamer library resembling discrete site-chain flexibility. Newer more sophisticated algorithms like those implemented in the software package GOLD[23], offer in addition to rotamer libraries also continuous side-chain flexibility during docking. However, only ten amino acids at maximum can be treated flexible during docking with GOLD. Interestingly, also some minor variations in the backbone can be sampled within GOLD by enabling the "improper" option for a flexibilized amino acid. Next to these, further methodologies emerged[29].

(c) Molecular relaxation

This procedure can be divided into two steps. In the first step the ligand is docked into a rigid receptor using a softened potential. In the subsequent second step a relaxation of the binding site backbone and side-chain atoms is conducted. The relaxation or minimization is performed by Molecular Dynamics or other methods[30].

In comparison to rotamer exploration or soft docking, the molecular relaxation method is computationally more expensive because next to side-chain conformational changes also backbone flexibility has to be taken into account.

One prominent docking tool that uses this molecular relaxation algorithm is "Induced-Fit Docking" within the Schrödinger Suite[31]. Here in a sophisticated manner GLIDE docking and minimization protocols are combined to thoroughly sample protein space and induced fit phenomena.

(d) Docking into multiple protein structures

The most frequent method for taking protein flexibility into account is to dock into an ensemble of conformationally different protein structures. Knetgel et al.[32] was one of the pioneers in this field by constructing an averaged energy grid derived from experimentally-determined protein structures using a weighting scheme. Claussen et al.[33] implemented a fast and economic search algorithm that calculates protein flexibility based on an internal analysis of input structures. These input structures can consist of a set of molecular dynamics snapshots or are a series of holo X-ray structures. The detected variability between the input structures is then considered in the docking procedure in a combinatorial manner.

As the additional degrees of freedom also enhance the chance to generate false positives, the knowledge of the user is decisive. Only those parts of the protein should be kept flexible that are justifiable.

2.2 Scoring

The output of the posing process is a list of possible ligand orientations within the binding site, which is also referred to as pose list. In order to discriminate between artificially generated and the correct ligand orientation, scoring functions for pose evaluation are applied.

These scoring functions are algorithmic approximations of the underlying biophysical and biochemical events that contribute to the free energy release which occurs upon ligand binding. While enthalpic contributions like H-bonding, van der Waals interactions, charge-charge interactions, etc. can be modeled quite fast and accurate, entropic contributions like solvation and reduced conformational flexibility in the bound-state, still remain inaccurate and/or time-consuming.

However, the scoring function is used to rank the pose list, assuming the best scored pose to be correct. Ideally, this pose represents the bioactive ligand orientation and its scoring value correlate with the ligands' affinity.

In total, three different classes of scoring functions are implemented in todays' docking programs[12]:

- Force-field based scoring functions **2.2.1**
- Empirical scoring functions **2.2.2**
- Knowledge-based scoring functions **2.2.3**

and will be described in more detail in the following:

2.2.1 Force-field-based-scoring

In principal force-field-based scoring functions can be viewed as the sum of two energies, the 1) ligand-receptor interaction energy (nonbonded energy) and the 2) internal ligand energy (bonded energy). The calculation of the ligand-receptor interactions, again can be subdivided into two terms, the van der Waals term represented by a Lennard-Jones potential and the electrostatic term represented by a Coulombic formulation. On the other hand, internal ligand energy sums up strain resulting from bond stretching/ bending/ torsional distortions. The force-field parameters for energy calculation derive from AMBER[34] (AutoDock[35]), CHARMM[36], or other packages For the representation of Hydrogen-bonding different terms have evolved within different programs.

Initially the force-field parameter sets were determined to model enthalpic gas-phase contributions and thus do not inherently consider solvation and entropic effects. The most sophisticated method to account for solvents is to treat water molecules explicitly as implemented in Free Energy Perturbation (FEP) and Thermodynamic Integration (TI)[37]. However, these functions are computationally very expensive and would make virtual screening of large libraries nearly impossible. Thus methods like generalized-Born/surface area (GB/SA) models[37] and the Poisson-Boltzmann/surface (PB/SA) models[38] that have implicit solvent models, are normally preferred. Next to these, even faster methods exist that try to cover the entropic effects by the addition of a simple torsional entropy term as implemented in G-Score[39].

Well-known force-field-based scoring functions are: GOLD, AutoDock, DOCK, G-Score.

2.2.2 Empirical scoring functions

Empirical scoring functions are based on experimentally determined ligand binding energies and their structural X-ray information. These scoring functions are represented as a sum of parameterized functions as exemplified in the FlexX scoring function[15] (**Fig. 6**). Each individual function covers a certain type of free energy contribution, such as an entropic term, an H-bond term, an ionic interaction term, a hydrophobic term and an aromatic interaction term. The coefficients for the individual functions derive from regression analysis using a database of experimentally determined binding energies in connection with the corresponding structural complexes.

$$\Delta G = \Delta G_0 + \Delta G_{rot} \times N_{rot}$$

$$+ \Delta G_{hb} \sum_{neutral\ H\text{-}bonds} f(\Delta R, \Delta\alpha)$$

$$+ \Delta G_{io} \sum_{ionic\ int.} f(\Delta R, \Delta\alpha)$$

$$+ \Delta G_{aro} \sum_{aro\ int.} f(\Delta R, \Delta\alpha)$$

$$+ \Delta G_{lipo} \sum_{lipo.\ cont.} f^*(\Delta R)$$

Figure 6 - Structure of the FlexX Scoring function as a sum of parameterized functions. Each function accounts for a certain type of binding free energy contribution. The parameters (ΔR, $\Delta\alpha$) derive from regression analysis of experimental data sets.

In the representation of hydrogen bonds a great diversity of algorithms exists among empirical scoring functions. For example, in LUDI[40], two hydrogen bonds (a neutral hydrogen bond and an ionic hydrogen bond) are distinguished, whereas ChemScore[41] does not have this differentiation. In a similar manner the calculation of hydrophobic terms is manifold. In LUDI, hydrophobic contributions are calculated on basis of the molecular surface area, whereas ChemScore considers distances between hydrophobic atom pairs.

One disadvantage of empirical scoring functions is their great variability in their coefficients depending on which dataset of experimentally binding energies was used to parameterize the scoring function.

Terms for entropy and desolvation have been introduced into several empirical scoring functions like ChemScore and FlexX Score. However, these terms can only approximate this complex part in protein-ligand binding.

Well-known empirical scoring functions are: GlideScore[17], PLP[42], X-Score[43], ChemScore[41] and LUDI[40].

2.2.3 Knowledge-based scoring functions

As opposed to the other scoring functions, knowledge-based scoring functions are developed to primarily reproduce experimentally determined ligand-receptor complexes rather than binding energies. The basis for knowledge-based scoring functions is described by the inverse Boltzmann relation (**Fig.7**).

$$w(r) = -k_{\mathrm{B}}T \ln[\rho(r)/\rho^*(r)]$$

Figure 7 - Inverse Boltzmann relation, where k_B is the Boltzmann constant, T stands for the absolute temperature, $\rho(r)$ is the pair density between protein-ligand atoms at a distance of r in the training set, and $\rho^*(r)$ is the density of protein-ligand atom pairs in a reference state with no interatomic interactions.

In analogy to empirical scoring functions, also knowledge-based scoring functions extract their parameters from experimental structures. They use the interatomic distances in the ligand-recptor complexes and transform them into distance-dependent interaction free energies.

In principle, the scoring value is the sum of pairs of ligand atom – receptor atom interactions which makes the calculation very fast- This is one of the big advantages of knowledge-based scoring functions and predispose them for virtual screening issues.

Prominent representatives of these scoring functions are: POTENTIAL OF MEAN FORCE (PMF)[44] and DrugScore[45].

2.3 Molecular Docking Performance

Pharmaceutical companies have a deep interest in an objective and thorough performance check for applications in drug discovery. This fact made the survey of Warren et al.[46] especially interesting as it was driven by GlaxoSmithKline Pharmaceuticals to rigorously evaluate molecular docking performance from a unbiased position. In their survey they evaluated the performance of not less than 10 widely used docking programs across seven different target types. More interestingly the ligand set for each target consisted of a large number of experimentally determined affinities with closely related structures (**Table 2**), mimicking corporate compound libraries.

For this reason the findings of Warren et al. constitute the core in the next paragraphs that describe the docking performance in the light of three tasks in structure-based drug discovery

- binding mode prediction **2.3.1**
- virtual screening **2.3.2**
- potency prediction **2.3.3**

In the study of Warren et al. for each of the 8 targets the corresponding ligand set was docked with the following docking pograms: Dock4[11], DockIt[47], FlexX[15], Glide[17], GOLD[23], Flo, Fred, LigFit, MOEdock and MVP. See **Table 2** for the composition of the data set.

Table 2 – Protein and ligand data set details used in the survey of Warren et al.[46].

protein	No. of ligands	No. of ligand classes	No. of cocrystals	Max affinity (nM)	Min affinity (nM)
Chk1	193	2	15	7	>10000
factorXa	218	4	10	<1	5000
Gyrase B	138	3	7	4	>10000
HCV polymerase	205	2	13	5.6	>10000
Met tRNA synthetase	144	2	31	1	>10000
E. coli PDF	199	3	2	1	>10000
Strep PDF	186	3	4	<2	>10000
PPARd	206	5	54	0.3	>10000

Finally the molecular docking performance against homology models will be reviewed (**2.3.4**). Here the focus was set on two studies: The study of Kairys et al.[48] which was mainly concerned with the capability of molecular docking software packages to reproduce the

experimentally determined binding mode (**2.3.4.a**), and the study of Fan et al.[49] that analyzed the virtual screening performance of docking into homology models (**2.3.4.b**).

2.3.1 Binding Mode Prediction

First, the capability of docking programs to reproduce the crystallographically determined ligand-receptor complex will be described. The test set for this evaluation contains 136 ligands (representing 21 compound classes) for which cocrystals exist (**Table 2**). Ten docking programs were used to redock these ligands into its native X-ray structure and the similarity between the docking poses and the experimentally determined ligand bound orientations was assessed by calculating the Root-Means-Square-Deviation (RMSD) of the ligands' heavy atoms. Poses with a RMSD <= 2Å to the crystallographic orientation were considered as good. And poses with a RMSD <= 4Å are considered as fairly good, roughly representing the correct global orientation. Each docking program produced multiple docking poses for each of the 136 ligands and rmsd values for all generated poses were calculated. The performance of the 10 docking programs against the 8 targets is summarized in **Figure 8**.

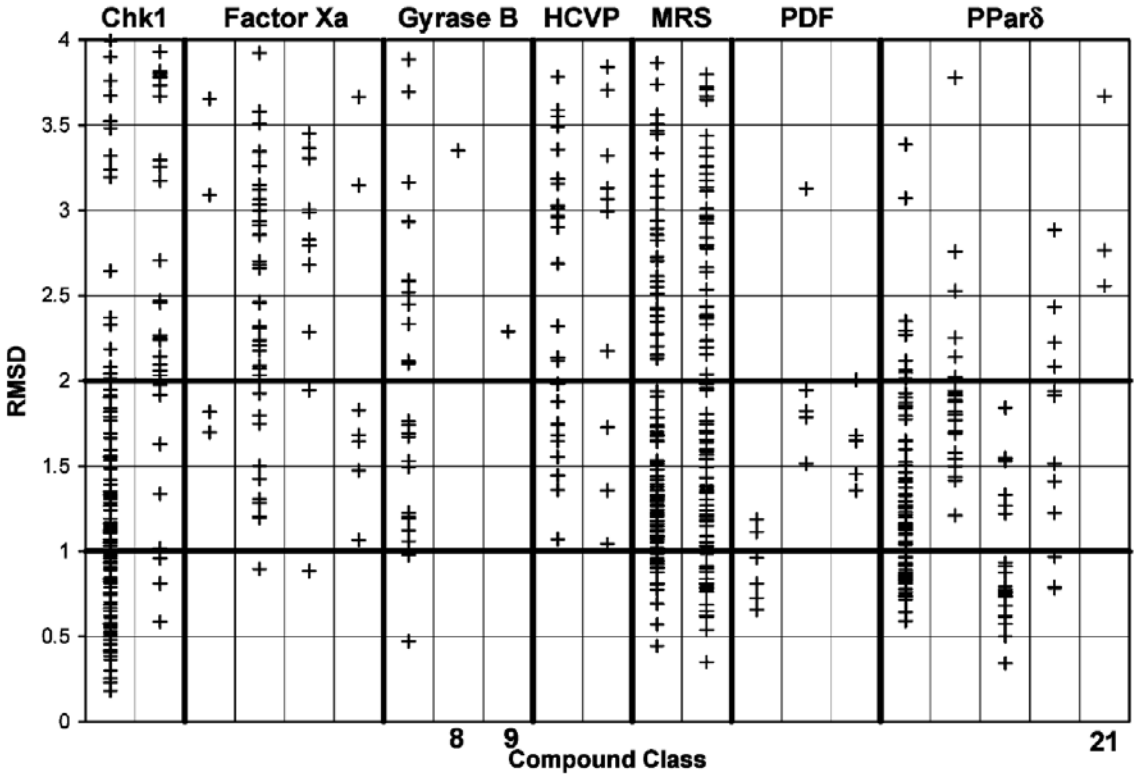

Figure 8 - Representation of docking performance in binding mode prediction from the study of Warren et al.[46]. Plot of docking poses with rmsd value of <= 4Å generated with all ten docking programs, against the 21 compound classes used in the binding mode prediction survey. Only for three compound classes no pose was generated that had a rmsd of <= 2Å to the crystal structure. Figure taken from Ref[46].

The results of this study showed that in general docking programs are capable of correctly predicting the experimentally determined binding mode, but with the important limitation that scoring functions were less successful at identifying the pose which was closest to the crystal structure from the pose list. Finally it was stated that among the ten docking programs tested not a single one performed well against all protein targets.

2.3.2 Virtual Screening

In the field of drug discovery the virtual screening performance of molecular docking is of special interest. It evaluates the crucial ability of this methodology to select active chemotypes out of a pool of decoy molecules.

For this purpose all ligand sets (**Table 2**), compromising 1303 ligands, were docked into its corresponding target keeping only the best scored pose for each ligand. The resulting eight docking libraries are then ranked according to their scoring value, resulting in eight score-sorted libraries. For each of the libraries the enrichment factor for the top 10% of the score-sorted library were calculated. This procedure was undertaken with all ten docking programs and the results are presented in **Table 3**.

Table 3 – Enrichment Factor for actives (<= 1µM) found at 10% of the score-sorted library found in the study of Warren et al.[46].

program	Chk1	FXa	gyrase B	HCVP	MRS	E. coli PDF	Strep PDF	PPARδ
ideal	10.0	9.8	10.0	9.5	10.0	7.6	8.3	8.6
Dock4	1.4	4.1	1.7	1.8	4.2	0.9	0.8	1.7
DockIt	4.2	2.0	2.0	1.0	1.0	0.2	0.0	3.2
FlexX	7.0	2.2	5.8	0.9	3.9	0.8	0.8	5.2
Flo+	5.6	2.7	2.3	3.4	1.7	1.5	0.8	3.6
Fred	2.9	4.1	1.9	2.0	0.6	3.2	1.2	1.1
Glide	6.3	3.4	1.0	1.0	5.3	0.6	0.4	4.8
Gold	0.1	4.1	4.0	0.0	0.8	1.0	0.1	5.5
LigandFit	3.3	1.9	2.8	1.8	2.9	2.9	1.7	1.2
MOEDock	3.9	0.6	0.0	0.0	1.0	2.1	0.6	0.0
MVP	7.2	5.8	5.3	3.6	6.4	6.7	6.9	3.9

In essence the study of Warren et al. showed that virtual screening was capable in enriching actives out of a population of decoy molecules. But it has to be noted that the performance across diverse targets was inhomogeneous.

Another important study in this field was undertaken by Huang et al.[50] presenting for the first time the directory of useful decoys (DUD). The DUD is actually developed to test docking algorithms by providing challenging decoys together with a broad target set. In total it

contains 2950 known active ligands for 40 structurally determined targets. And for each active ligand, 36 “decoys” with dissimilar structural topology but similar physicochemical properties (e.g. number of H-bond donors, number of H-bond acceptors, molecular weight, calculated logP, …) were selected summing up to 95316 decoy compounds (**Table 4**). Ligands and decoys are then docked into their corresponding target using DOCK[11] and enrichment factors for actives were calculated for the top 1% and top 20% of the score-sorted library, respectively (**Table 4**). The average enrichment for the top 1% and top 20% across all 40 proteins was 17.3 and 2.6, respectively.

Table 4 - DUD benchmark set consisting of 40 targets, 2950 unique ligands and 95316 decoys, described in Huang et al.[50]. Each set was docked into its corresponding target and EF1% and EF20% for actives was calculated.

protein	PDB-code	resolution (A)	no ligands	no decoys	EF 1%	EF20%
AR	1xq2	1.9	74	2630	33.5	3.8
ERagonist	1l2i	1.9	67	2361	19.2	4.5
ERantagonist	3ert	1.9	39	1399	12.7	1.3
GR	1m2z	2.5	78	2804	8.9	1.4
MR	2aa2	1.9	15	535	46.2	3.7
PPARg	1fm9	2.1	81	2910	0	0
PR	1sr7	1.9	27	967	0	2
RXRa	1mvc	1.9	20	708	24.8	2.2
CDK2	1ckp	2.1	50	1780	13.9	1.4
EGFr	1m17	2.6	416	14914	2.1	2.4
FGFr1	1agw	2.4	118	4216	0	0.2
HSP90	1uy6	1.9	24	861	8.6	2
P38 MAP	1kv2	2.8	234	8399	2.1	2.4
PDGFrb	model	n/a	157	5625	0	0.6
SRC	2src	1.5	162	5801	1.2	1.5
TK	1kim	2.1	22	785	54	5
VEGFr2	1vr2	2.4	74	2647	1.3	1.4
FXa	1f0r	2.7	142	5102	14.6	3.8
thrombin	1ba8	1.8	65	2294	13.7	2.9
trypsin	1bju	1.8	43	1545	22.5	2.6
ACE	1o86	2	49	1728	40.4	3.7
ADA	1stw	2	23	822	12.9	2.4
COMT	1h1d	2	12	430	0	3.3
PDE5	1xp0	1.8	51	1810	11.8	2.3
DHFR	3dfr	1.7	201	7150	21.7	3.5
GART	1c2t	2.1	21	753	42.4	3.3
AChE	1eve	2.5	105	3732	1.9	2
ALR2	1ah3	2.3	26	920	38.1	2.3
AmpC	1xgj	2	21	734	17.1	4.7
COX-1	1p4g	2.1	25	850	4	1.6
COX-2	1cx2	3	349	12491	20.1	3.3
GPB	1a8i	1.8	52	1851	22.8	4.1
HIVPR	1hpx	2	53	1888	3.7	2.2
HIVRT	1rt1	2.6	40	1439	5	3
HMGR	1hw8	2.1	35	1242	33.9	2.1
InhA	1p44	2.7	85	3043	0	0.3
NA	1a4g	2.2	49	1745	20.2	3.3
PARP	1efy	2.2	33	1178	6	3.6
PNP	1b8o	1.5	25	884	31.7	4.4
SAHH	1a7a	2.8	33	1159	78	5

An overviewof successfully experimentally validated hits derived from docking-based virtual screening is presented in Kolb et al.[51] for the time range 2007 to mid-2009 (see **Table 5**). These results are in line with the good screening performance reported in the survey of Warren et al.[46] and Huang et al.[50].

Table 5 - Docking predictions subsequently confirmed by experiments: 2007 to mid-2009. Data and table taken from Ref[51]

Target	Docking program	Lead inhibitor IC_{50} (μm)
AdoMetDC	Glide	12
AHAS	DOCK 4/AutoDock	15.2
Aldose reductase	N/A	0.53
CDC25 phosphatase	FRED/Surflex/LigandFit	13
DNA gyrase	DOCK 5	50
EphB4	DAIM-SEED-FFLD	1.5
FFAR	Glide	3.6
Histamine H4	FlexX	95.8
Human pregnane X	Surflex	0.049
MCH-R1	ICM	7.5
Pim-1 kinase	Glide	0.091
PNP	GOLD	18.9
PPAR-γ	Glide/IFD	2.9
Tm0936	DOCK 3.5	10^5 m^{-1} S^{-1} (K_{cat}/K_m)
TRH-R1/TRH-R2	FlexX	0.29
β_2-Adrenergic receptor	DOCK 3.5.54	0.009
β-Lactamase	DOCK 3.5.54	140
SHP2	DOCK	100
Al-2 quorum sensing	DOCK 5	35
Anthrax edema factor	HINT/AutoDock	1.7
hPRMT1	GOLD	12

2.3.3 Affinity Prediction Tool

Scoring functions try to estimate the free energy of binding and thus the assigned scoring values for docking poses should correlate with the ligands' affinity.

Warren et al. showed for their dataset (**Table 2**) that there was no strong correlation found for any scoring function-protein target pair. **Table 6** presents the correlation coefficients between compound affinity and docking score.

Table 6 – Best Correlation Coefficient r between –log Affinity and Docking Score for all Programs across All Targets in the study of Warren et al.[46].

program	Chk1	FXa	gyrase B	HCVP	MRS	E. coli PDF	Strep PDF	PPARδ
Dock4	-0.33	-0.31	-0.39	0.00	-0.13	-0.38	-0.34	0.07
DockIt	-0.49	-0.19	-0.37	0.04	-0.28	-0.13	-0.30	-0.34
FlexX	-0.57	-0.31	-0.39	-0.12	-0.01	-0.42	-0.25	-0.36
Flo+	-0.44	-0.38	-0.36	-0.09	0.05	-0.27	-0.39	-0.42
Fred	-0.14	0.01	-0.13	-0.07	0.13	0.07	-0.24	0.06
Glide	-0.47	-0.08	-0.21	-0.04	0.08	-0.13	-0.12	-0.35
Gold	-0.42	-0.05	-0.14	-0.09	0.04	-0.12	-0.11	-0.43
LigandFit	-0.45	-0.13	-0.39	-0.06	-0.15	-0.21	-0.49	-0.10
MOEDock	-0.29	0.00	0.07	-0.01	-0.13	0.08	0.20	0.17
MVP	-0.26	0.10	-0.33	-0.01	-0.18	-0.17	-0.16	-0.18

2.3.4 Docking into Homology Models

(a) Binding mode prediction

Kairys et al.[48] analyzed the capability of molecular docking into homology models in binding mode prediction. For this purpose, homology models for four experimentally determined protein structures (carboxypeptidase A, factor Xa, CDK2 and AChE) were generated, whereby the target-to-template sequence identity ranged from 30.9 to 66.6. These models were then used for molecular docking and the resulting poses were then compared to the experimentally observed ligand orientation, using RMSD as a similarity measure.

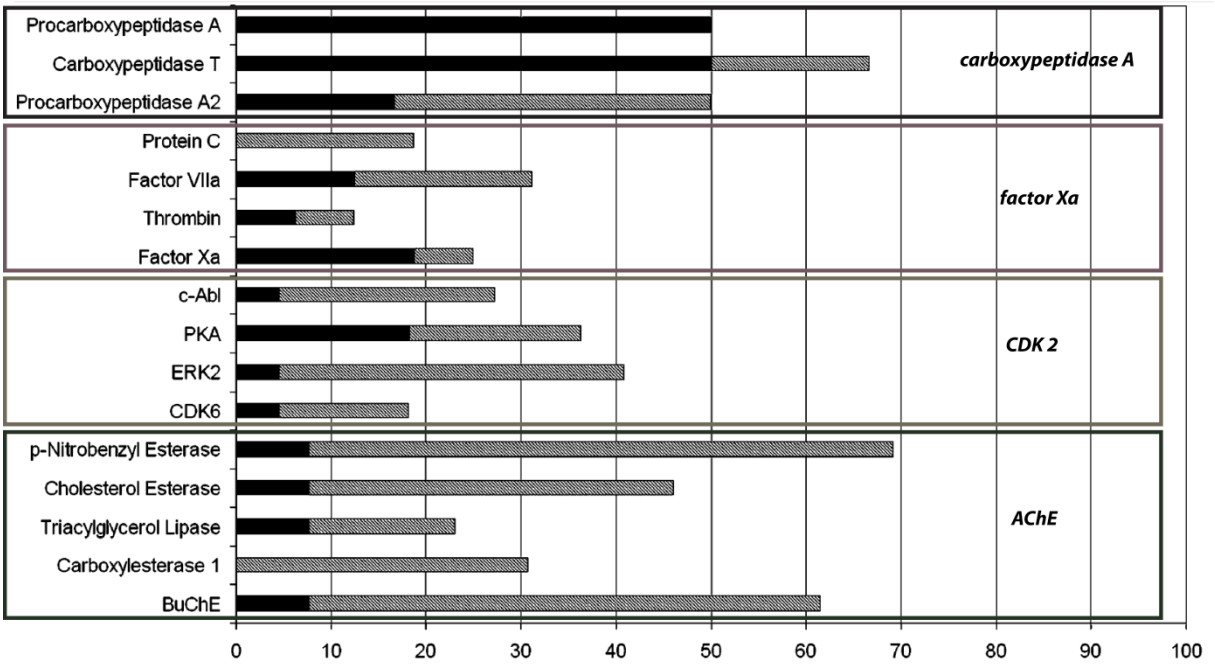

Figure 9 – Representation of the findings of Kairys et al.[48] in examining the performance of molecular docking into homology models in binding mode prediction. For the four experimentally determined ligand-target complexes (carboxypeptidase A, factor Xa, CDK2 and AChE), a total of 16 homology models was created. These models were based on 16 templates (**Table 7**) listed on the left hand side of the Figure. Bars show the percentage of ligand-target complexes with available crystal structures for which top scoring pose has a RMSD < 2Å (black) and < 4Å (black + gray). Figure edited from Ref[48].

Table 7 - Templates and associated template-to-target sequence identity for proteins analyzed in Kairys et al.[48].

target	template	sequence identity
carboxypeptidase A	Procarboxypeptidase A	30.9
	Carboxypeptidase T	31.8
	Procarboxypeptidase A2	66.6
factor Xa	Protein C	34.9
	Factor VIIa	38.8
	Thrombin	40.7
	Factor Xa	100
CDK2	c-Abl	28.6
	PKA	31.2
	ERK2	37.0
	CDK6	48.2
AChE	para-nitrobenzyl esterase	31.4
	Cholesterol Esterase	32.8
	Triacylglycerol Lipase	32.8
	Carboxylesterase 1	36.2
	BuChE	53.3

These findings clearly demonstrate that molecular docking into homology models is capable to regenerate the experimentally observed ligand-protein complex for proteins with a sequence identity greater than 30%.

(b) Virtual screening

The first exhaustive virtual screening performance comparison between experimentally determined structures and homology models thereof was assessed by Fan et al.[49]. They used the widely applied docking benchmark set of the "directory of useful decoys" (DUD) for performance evaluation[50].

In the study of Fan et al. 38 of the 40 subsets described in DUD were used to compare the virtual screening performance using homology models or crystal structures. For each of the 38 targets, template structures were selected (1-12 per target) with varying sequence identity (ranging from 20% to 99%), resulting in a total set of 222 templates and 222 homology models (5 models per target on average). Finally DUD ligands and decoys (38 of the 40 subsets in **Table 4**) were docked with DOCK against the 38 X-ray structures and against the 222 homology models. Subsequently, enrichment factors expressed as logAUC were calculated and the results were compared (**Table 8**).

Table 8 - Ligand enrichments found in Fan et al. for molecular docking into homology models and X-ray structures. Table taken from Fan et al.[49].

	most enriching model		*best model by SI*		consensus	holo X-ray
protein target	SI	enrichment	SI	enrichment	enrichment	enrichment
ACE	44.1	50.2	54.8	37.9	48.9	40.6
ADA	26.5	40.3	84.8	38.8	41.1	22.7
COMT	20.1	0	20.1	0	0.0	27.6
PDE5	30.4	22.1	95.5	20.5	18.6	12.1
DHFR	27.9	34.6	37.3	13.1	20.3	18.9
GART	40.4	27.5	41.5	0.6	27.4	35.3
FXa	30.4	52.1	63.8	27.2	49.6	41.8
thrombin	30	43.4	39.5	36.9	42.4	29.4
Trypsin	78.8	38	78.8	38	32.3	29.3
AChE	38	35.7	92.7	17.3	29.1	38.5
ALR2	68.7	41.9	86.6	39.5	37.1	39.7
AmpC	76.6	46.6	76.6	37.2	40.3	47.4
COX-1	63.4	26.2	63.4	26.2	25.3	28.3
COX-2	64.4	13.3	64.7	8.2	12.4	40.8
GPB	41.8	8.9	80.7	6.5	6.8	17.1
HIVPR	49	30.5	96.9	4.8	23.7	11.9
HIVRT	97.7	12.9	98.9	0	12.9	25.8
HMGR	100	43.2	100	43.2	41.5	40.9
InhA	29	14.6	29	14.6	11.8	8.2
NA	28.8	51.2	34.2	20.4	42.6	47.6
PARP	46.4	9.2	86.8	6.4	6.3	8.2
PNP	36.9	33.5	93.1	19.3	23.9	49.1
SAHH	84.7	82.4	84.7	82.4	78.4	82.8
CDK2	27.6	13.5	94.9	10.1	11.7	11.3
EGFr	37.7	13.2	38.1	12.3	10.7	21.5
FGFr1	41.3	12.3	51	6.2	11.9	6.7
HSP90	62.4	18.7	70.4	14.5	11.5	24.6
P38 MAP	29.4	31.4	62.2	21.2	15.6	12.5
SRC	68.8	13.8	82	13.4	12.3	9.5
TK	20.7	13.4	40.4	3	2.9	63.5
AR	56	31.7	84.3	31.5	14.5	48.2
ERagonist	93.1	41	93.1	41	19.6	55.4
ERantagonist	21	19.2	93	9	14.7	23.2
GR	27.4	18.8	56.6	15.2	16.7	20.5
MR	56.8	30.5	56.8	30.5	29.5	57
PPARg	20.2	13.2	65	9.2	8.8	4.4
PR	53.5	35.9	53.5	35.9	11.8	23.2
RXRa	87	26.9	88.8	2	11.2	37.9

Enrichment, the ligand enrichment is represented by logAUC. SI, stands for the target to template sequence identity.

Taking only the most enriching model for each target, the averaged enrichment (logAUC) for the holo X-ray structures was 30.6 which was only slightly higher than the average enrichment (logAUC) of the most enriching homology models (28.7). However, this difference was not statistically significant.

Subsequently they analyzed model properties (template resolution, binding-site sequence identity, overall sequence identity, N-DOPE score) which could correlate with enrichment performance, in the hope to identify parameters that can predict model performance. However none of the parameters showed a strong correlation with model enrichment performance.

But on the other hand they noticed that homology models performed significantly better if models were left out which derive from orthologous templates and template-model pairs where the sequence identity is lower than 25%. This indicates that models below a sequence identity of 25% show a significant weaker performance.

References:

1. Berman, H.M. et al. The Protein Data Bank. *Nucleic Acids Res* **28**, 235-42 (2000).
2. UniProtConsortium. Reorganizing the protein space at the Universal Protein Resource (UniProt). *Nucleic Acids Res* **40**, D71-5 (2012).
3. Sali, A. & Blundell, T.L. Comparative protein modelling by satisfaction of spatial restraints. *J Mol Biol* **234**, 779-815 (1993).
4. Yildirim, M.A., Goh, K.I., Cusick, M.E., Barabasi, A.L. & Vidal, M. Drug-target network. *Nat Biotechnol* **25**, 1119-26 (2007).
5. Ashburner, M. et al. Gene ontology: tool for the unification of biology. The Gene Ontology Consortium. *Nat Genet* **25**, 25-9 (2000).
6. Bordoli, L. et al. Protein structure homology modeling using SWISS-MODEL workspace. *Nat Protoc* **4**, 1-13 (2009).
7. Baker, D. & Sali, A. Protein structure prediction and structural genomics. *Science* **294**, 93-6 (2001).
8. Hillisch, A., Pineda, L.F. & Hilgenfeld, R. Utility of homology models in the drug discovery process. *Drug Discov Today* **9**, 659-69 (2004).
9. Cavasotto, C.N. & Phatak, S.S. Homology modeling in drug discovery: current trends and applications. *Drug Discov Today* **14**, 676-83 (2009).
10. Bajorath, J. Integration of virtual and high-throughput screening. *Nat Rev Drug Discov* **1**, 882-94 (2002).
11. Kuntz, I.D., Blaney, J.M., Oatley, S.J., Langridge, R. & Ferrin, T.E. A geometric approach to macromolecule-ligand interactions. *J Mol Biol* **161**, 269-88 (1982).
12. Kitchen, D.B., Decornez, H., Furr, J.R. & Bajorath, J. Docking and scoring in virtual screening for drug discovery: methods and applications. *Nat Rev Drug Discov* **3**, 935-49 (2004).
13. Sousa, S.F., Fernandes, P.A. & Ramos, M.J. Protein-ligand docking: current status and future challenges. *Proteins* **65**, 15-26 (2006).
14. Leach, A.R. Molecular Modelling: Principles and Applications. *Addison Wesley Longman Limited* (1996).

15. Rarey, M., Kramer, B., Lengauer, T. & Klebe, G. A fast flexible docking method using an incremental construction algorithm. *J Mol Biol* **261**, 470-89 (1996).
16. DesJarlais, R.L., Sheridan, R.P., Dixon, J.S., Kuntz, I.D. & Venkataraghavan, R. Docking flexible ligands to macromolecular receptors by molecular shape. *J Med Chem* **29**, 2149-53 (1986).
17. Friesner, R.A. et al. Glide: a new approach for rapid, accurate docking and scoring. 1. Method and assessment of docking accuracy. *J Med Chem* **47**, 1739-49 (2004).
18. Welch, W., Ruppert, J. & Jain, A.N. Hammerhead: fast, fully automated docking of flexible ligands to protein binding sites. *Chem Biol* **3**, 449-62 (1996).
19. Hart, T.N. & Read, R.J. A multiple-start Monte Carlo docking method. *Proteins* **13**, 206-22 (1992).
20. Oshiro, C.M., Kuntz, I.D. & Dixon, J.S. Flexible ligand docking using a genetic algorithm. *J Comput Aided Mol Des* **9**, 113-30 (1995).
21. Westhead, D.R., Clark, D.E. & Murray, C.W. A comparison of heuristic search algorithms for molecular docking. *J Comput Aided Mol Des* **11**, 209-28 (1997).
22. Goodsell, D.S., Lauble, H., Stout, C.D. & Olson, A.J. Automated docking in crystallography: analysis of the substrates of aconitase. *Proteins* **17**, 1-10 (1993).
23. Jones, G., Willett, P. & Glen, R.C. Molecular recognition of receptor sites using a genetic algorithm with a description of desolvation. *J Mol Biol* **245**, 43-53 (1995).
24. Brooijmans, N. & Kuntz, I.D. Molecular recognition and docking algorithms. *Annu Rev Biophys Biomol Struct* **32**, 335-73 (2003).
25. Huang, S.Y. & Zou, X. Advances and challenges in protein-ligand docking. *Int J Mol Sci* **11**, 3016-34 (2010).
26. Jiang, F. & Kim, S.H. "Soft docking": matching of molecular surface cubes. *J Mol Biol* **219**, 79-102 (1991).
27. Ferrari, A.M., Wei, B.Q., Costantino, L. & Shoichet, B.K. Soft docking and multiple receptor conformations in virtual screening. *J Med Chem* **47**, 5076-84 (2004).
28. Leach, A.R. Ligand docking to proteins with discrete side-chain flexibility. *J Mol Biol* **235**, 345-56 (1994).
29. Desmet, J., Wilson, I.A., Joniau, M., De Maeyer, M. & Lasters, I. Computation of the binding of fully flexible peptides to proteins with flexible side chains. *FASEB J* **11**, 164-72 (1997).
30. Davis, I.W. & Baker, D. RosettaLigand docking with full ligand and receptor flexibility. *J Mol Biol* **385**, 381-92 (2009).
31. Sherman, W., Day, T., Jacobson, M.P., Friesner, R.A. & Farid, R. Novel procedure for modeling ligand/receptor induced fit effects. *J Med Chem* **49**, 534-53 (2006).
32. Knegtel, R.M., Kuntz, I.D. & Oshiro, C.M. Molecular docking to ensembles of protein structures. *J Mol Biol* **266**, 424-40 (1997).
33. Claussen, H., Buning, C., Rarey, M. & Lengauer, T. FlexE: efficient molecular docking considering protein structure variations. *J Mol Biol* **308**, 377-95 (2001).
34. Ponder, J.W. & Case, D.A. Force fields for protein simulations. *Adv Protein Chem* **66**, 27-85 (2003).
35. Morris, G.M. et al. Automated Docking Using a Lamarckian Genetic Algorithm and and Empirical Binding Free Energy Function. *J Computational Chemistry* **19**, 1639-1662 (1998).
36. Brooks, B.R. et al. CHARMM - a programm for macromolecular energy minimization, and dynamics calculations. *J Computational Chemistry* **4**, 187 (1983).
37. Wang, W., Donini, O., Reyes, C.M. & Kollman, P.A. Biomolecular simulations: recent developments in force fields, simulations of enzyme catalysis, protein-ligand, protein-protein, and protein-nucleic acid noncovalent interactions. *Annu Rev Biophys Biomol Struct* **30**, 211-43 (2001).
38. Guimaraes, C.R. & Cardozo, M. MM-GB/SA rescoring of docking poses in structure-based lead optimization. *J Chem Inf Model* **48**, 958-70 (2008).
39. Kramer, B., Rarey, M. & Lengauer, T. Evaluation of the FLEXX incremental construction algorithm for protein-ligand docking. *Proteins* **37**, 228-41 (1999).
40. Bohm, H.J. LUDI: rule-based automatic design of new substituents for enzyme inhibitor leads. *J Comput Aided Mol Des* **6**, 593-606 (1992).
41. Eldridge, M.D., Murray, C.W., Auton, T.R., Paolini, G.V. & Mee, R.P. Empirical scoring functions: I. The development of a fast empirical scoring function to estimate the binding affinity of ligands in receptor complexes. *J Comput Aided Mol Des* **11**, 425-45 (1997).

42. Gehlhaar, D.K. et al. Molecular recognition of the inhibitor AG-1343 by HIV-1 protease: conformationally flexible docking by evolutionary programming. *Chem Biol* **2**, 317-24 (1995).
43. Wang, R., Lai, L. & Wang, S. Further development and validation of empirical scoring functions for structure-based binding affinity prediction. *J Comput Aided Mol Des* **16**, 11-26 (2002).
44. Muegge, I. & Martin, Y.C. A general and fast scoring function for protein-ligand interactions: a simplified potential approach. *J Med Chem* **42**, 791-804 (1999).
45. Gohlke, H., Hendlich, M. & Klebe, G. Knowledge-based scoring function to predict protein-ligand interactions. *J Mol Biol* **295**, 337-56 (2000).
46. Warren, G.L. et al. A critical assessment of docking programs and scoring functions. *J Med Chem* **49**, 5912-31 (2006).
47. Blaney, J.M. & Dixon, J.S. DockIt, version 1.0. *Metaphorics, LLC: Mission Viejo; CA; www.metaphorics.com/products/dockit.html*.
48. Kairys, V., Fernandes, M.X. & Gilson, M.K. Screening drug-like compounds by docking to homology models: a systematic study. *J Chem Inf Model* **46**, 365-79 (2006).
49. Fan, H. et al. Molecular docking screens using comparative models of proteins. *J Chem Inf Model* **49**, 2512-27 (2009).
50. Huang, N., Shoichet, B.K. & Irwin, J.J. Benchmarking sets for molecular docking. *J Med Chem* **49**, 6789-801 (2006).
51. Kolb, P., Ferreira, R.S., Irwin, J.J. & Shoichet, B.K. Docking and chemoinformatic screens for new ligands and targets. *Curr Opin Biotechnol* **20**, 429-36 (2009).

IV. Aim of the study

1,4-benzodiazepines exert their anxiolytic, anticonvulsant, muscle relaxant, and sedative-hypnotic properties by allosterically enhancing the action of GABA at $GABA_A$ receptors via their benzodiazepine binding site[1]. After 50 years of clinical use, the molecular basis of this interaction still is not known. The primary aim of this thesis is the elucidation of the binding mode of 1,4-benzodiazepines in the benzodiazepine binding site of $\alpha1\beta2\gamma2$ $GABA_A$-receptors with the computational means of homology modeling and molecular docking. The identified binding mode should be in accordance with existing experimental data, and ultimately the gained structural knowledge should predict novel ligand classes acting at the benzodiazepine binding site. Furthermore the derived structural models will also improve the current mechanistic understanding from modulator binding (at the benzodiazepine binding site) to alterations in channel gating. This can be achieved by the analysis of intra-molecular protein-protein interactions in proximity to the benzodiazepine binding site that may mediate $GABA_A$ receptor modulation.

But let's face the facts:

- ➔ No crystal structures for $GABA_A$ receptors available
- ➔ Target to template sequence identities of around 18% at the time the thesis was conducted
- ➔ A highly flexible loop shaping the benzodiazepine binding site
- ➔ And finally, major difficulties of scoring functions to rank the correctly computed ligand orientation on the top position even in redocking experiments

Honestly spoken the aim to uncover the binding mode of 1,4-benzodiazepines in the $GABA_A$-receptor seems at least challenging. In principle there are two problems associated with the development of accurate models of ligand bound benzodiazepine binding sites. First, the homology models that could be built at the time of the study are quite uncertain as the sequence identity between templates and target is only around 18%. Second, although standard docking tools are capable of reproducing the correct binding mode, they normally fail to rank these on top of the pose list.

In the workflow of the thesis these problems will be tackled in a two step approach. In the first step, the *explorative step*, we want to face the high ambiguity in the input data by broadly sampling the pose space. **This will inevitably result in an enormous amount of poses, but with a high likelihood of generating a plausible ligand-receptor complex.**

Consequently, the aim of the subsequent step, the *selection step*, will be the selection of the most plausible ligand-receptor complex(es) out of an ocean of poses. Exhaustive implementation of various sources of information (experimental, computational, structural) in

an orchestrated and integrative manner will be the key factor for this evaluative process that should finally narrow down the gigantic pose space to one single coherent solution.

Once the plausible binding mode has been identified the predictive power of the identified ligand-receptor complex should be tested in the field of drug discovery by the conduction of structure-based virtual screening runs.

In the following a short description of the steps is provided.

Step 1, *exploration step*. In this step, homology modeling and molecular docking will be used in order to produce binding hypotheses for 1,4-benzodiazepines at the benzodiazepine binding site. The sampling during the docking has to be broad as the input data is highly ambiguous (low target-template sequence identity, flexible loop in binding site, low resolution of templates).

In detail multiple homology models will be built deriving from different templates and varying sequence alignments. Additionally, flexible side-chains will be used during the docking procedure, once more adding degrees of freedom. And finally the first 100 poses per ligand per model will be kept for further evaluation. **This all will result in an enormous amount of poses, but with a high likelihood of generating the correct ligand-receptor complex.**

Step 2, *selection step*. The aim of this step will be the selection of the most plausible binding mode out of the thousands of docking poses, generated in the exploration step. A large array of evaluation criteria (comparison with experimental data, docking scores, structure activity relationships and others) will be used in this sensible selection step.

In this process the emphasis will be on the integration of existing experimental data as binding mode quality criteria. Plenty information about the spatial arrangement between ligand and binding site has already been accumulated in the last 50 years of research[2,3]. They are encoded as labeling data, mutagenesis data or can be found as structure-activity relationships. But as the experiments were compiled with various ligands we face a challenging situation: The plethora of information is dispersed through either i) different ligands within a compound class or ii) through ligands that belong to different classes.

In this thesis the **common binding mode (CBM)** hypothesis will be applied as an adequate integrative platform that connects these seemingly dispersed informative pieces. The **CBM** provides an assumption about the **ligand alignment** of ligands acting at the same binding site. Hence the CBM can be used to incorporate information from ligands that derive from a common ligand class (*narrow definition*) or beyond that, also implements information that derive from other ligands classes (*extended definition*).

In the *narrow definition*, the **CBM** hypothesis is based on the general assumption that the scaffold of ligands belonging to the same class (here: 1,4-benzodiazepines, **Fig. 10a**) bind in the same mode in the binding site, thus providing a hypothesis for the **mutual spatial alignment** of these ligands.

In the *more extended view* of the **CBM** hypothesis, which will be used as supplementary validation, information from further ligand classes (e.g. imidazobenzodiazepines, **Fig. 10b**) will be used in validating the binding mode of 1,4-benzodiazepines (**Fig. 10a**).

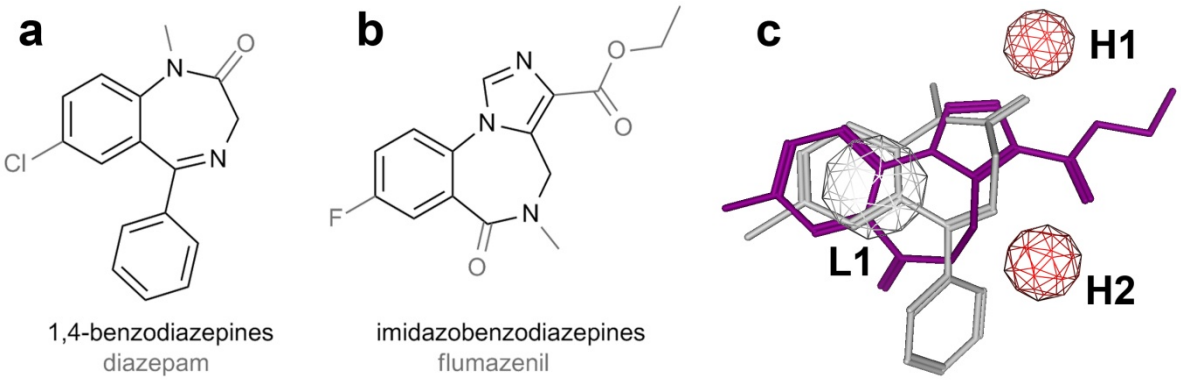

Figure 10 - Representation of the structures of 1,4-benzodiazepines (**a**), imidazobenzodiazepines (**b**) and their mutual alignment in a widely accepted pharmacophore model (**c**). (**a**) The common scaffold of 1,4-benzodiazepines is depicted in black colour. For the most prominent representative of this ligand class (diazepam) additional structural elements are shown in grey colour. (**b**) The common scaffold of imidazobenzodiazepines is depicted in black colour. For the most prominent representative of this ligand class (flumazenil) additional structural elements are shown in grey colour. (**c**) Representation of the mutual spatial alignment of diazepam (grey stick representation) and flumazenil (violet stick representation) in the ligand based pharmacophore model of Cook et al.[4] These aligned ligands share one common hydrophobic feature (**L1**, white meshed sphere) and two H-bond acceptor features (**H1** and **H2**, red meshed spheres).

The spatial link from 1,4-benzodiazepines to accessory ligand classes (e.g. imidazo-benzodiazepines) will be taken from the **ligand alignment** described in a widely accepted pharmacophore model[4] (**Fig. 10c**). This alignment will be the connective platform that facilitates cross evaluation among various compound classes. Consequently a diazepam (**Fig. 10a**) pose can then be additionally validated by experimental evidence deriving from other ligand classes, for example by a flumazenil (**Fig. 10b**) docking pose that is found to spatially align (according to the pharmacophore model alignment, **Fig. 10c**) with the mentioned diazepam pose. So the pharmacophore model should enable the combination of information deriving from different ligand classes.

Once the binding mode of 1,4-benzodiazepines has been identified, the ligand-receptor complex will be used in structure-based virtual screening runs taking the information encoded in the ligand-receptor complex to identify novel benzodiazepine binding site ligands.

References:

1. Sieghart, W. Structure and pharmacology of gamma-aminobutyric acidA receptor subtypes. *Pharmacol Rev* **47**, 181-234 (1995).
2. Sigel, E. Mapping of the benzodiazepine recognition site on GABA(A) receptors. *Curr Top Med Chem* **2**, 833-9 (2002).
3. Clayton, T. et al. An updated unified pharmacophore model of the benzodiazepine binding site on gamma-aminobutyric acid(a) receptors: correlation with comparative models. *Curr. Med. Chem.* **14**, 2755-2775 (2007).
4. Zhang, W., Koehler, K.F., Zhang, P. & Cook, J.M. Development of a comprehensive pharmacophore model for the benzodiazepine receptor. *Drug. Des. Discov.* **12**, 193-248 (1995).

B. Results and Discussion

I. Diazepam-bound $GABA_A$ receptor models identify new benzodiazepine binding-site ligands

nature chemical biology

ARTICLE

PUBLISHED ONLINE: 25 MARCH 2012 | DOI: 10.1038/NCHEMBIO.917

Diazepam-bound $GABA_A$ receptor models identify new benzodiazepine binding-site ligands

Lars Richter[1], Chris de Graaf[2], Werner Sieghart[3], Zdravko Varagic[3], Martina Mörzinger[3], Iwan J P de Esch[2], Gerhard F Ecker[1] & Margot Ernst[3]*

Contribution of the thesis author to this article:

For the presentation of the thesis authors' contribution to this publication the **Author contributions** section of the article is presented:

Author contributions

L.R., W.S., G.F.E., I.J.P.d.E., C.d.G. and M.E. contributed to the design and evaluation of experiments. Docking and virtual screening experiments were performed by L.R. (supervised by G.F.E.) and C.d.G. $GABA_AR$ models were generated and evaluated by M.E. and M.M. Radioligand and electrophysiological experiments were performed by Z.V. The manuscript was written by W.S., L.R., G.F.E., I.J.P.d.E., C.d.G. and M.E., and all authors commented on and helped to revise the text.

nature chemical biology

ARTICLE

PUBLISHED ONLINE: 25 MARCH 2012 | DOI: 10.1038/NCHEMBIO.917

Diazepam-bound $GABA_A$ receptor models identify new benzodiazepine binding-site ligands

Lars Richter[1], Chris de Graaf[2], Werner Sieghart[3], Zdravko Varagic[3], Martina Mörzinger[3], Iwan J P de Esch[2], Gerhard F Ecker[1] & Margot Ernst[3]*

Benzodiazepines exert their anxiolytic, anticonvulsant, muscle-relaxant and sedative-hypnotic properties by allosterically enhancing the action of GABA at $GABA_A$ receptors via their benzodiazepine-binding site. Although these drugs have been used clinically since 1960, the molecular basis of this interaction is still not known. By using multiple homology models and an unbiased docking protocol, we identified a binding hypothesis for the diazepam-bound structure of the benzodiazepine site, which was confirmed by experimental evidence. Moreover, two independent virtual screening approaches based on this structure identified known benzodiazepine-site ligands from different structural classes and predicted potential new ligands for this site. Receptor-binding assays and electrophysiological studies on recombinant receptors confirmed these predictions and thus identified new chemotypes for the benzodiazepine-binding site. Our results support the validity of the diazepam-bound structure of the benzodiazepine-binding pocket, demonstrate its suitability for drug discovery and pave the way for structure-based drug design.

$GABA_A$ receptors ($GABA_A$Rs) are the major inhibitory transmitter receptors in the brain and the site of action of a variety of pharmacologically and clinically important drugs, such as benzodiazepines, barbiturates, neuroactive steroids, anesthetics and convulsants[1]. These receptors are chloride ion channels composed of five subunits that can belong to different subunit classes. A total of 19 $GABA_A$ receptor subunits (α1–6, β1–3, γ1–3, δ, ε, π, θ, ρ1–3) have been identified in mammalian brain. The majority of $GABA_A$Rs are composed of one γ-, two β- and two α-subunits. The two GABA-binding sites of these receptors are located extracellularly at β-α interfaces (**Fig. 1a**). Classical benzodiazepines, such as diazepam, predominantly exert their action via $GABA_A$Rs composed of α1βγ2, α2βγ2, α3βγ2 and α5βγ2 subunits and are known to bind at the extracellular α-γ interface[2] (**Fig. 1b**). Owing to the lack of high-resolution structural data for this important drug-binding site, however, a consensus binding-mode hypothesis explaining all of the experimental data is still lacking.

$GABA_A$Rs, together with nicotinic acetylcholine receptors (nAChRs), glycine receptors and serotonin type 3 receptors, are members of the cysteine-loop receptor superfamily. Although so far no crystal structure of a $GABA_A$R is available, a variety of crystal structures from a functional and structural homolog of the ligand-binding domain of cysteine-loop receptors, the acetylcholine-binding protein (AChBP), and more recently from the nAChR and bacterial homologs thereof, is available[3] and demonstrates a high structural conservation within this receptor superfamily. Some of these structures have served as templates for protein homology models and docking studies that have yielded controversial binding-mode hypotheses for various benzodiazepines[4–8]. However, because of their low sequence identity of <20%, different members of the superfamily have appreciable variability in local interface and pocket structure[3]. To overcome this problem, we constructed multiple homology models of the $GABA_A$R from a variety of structural templates to broadly sample the benzodiazepine-pocket geometry. We then developed a workflow that, in contrast to automated ligand-supported modeling approaches[9], did not rely on energetic scoring functions. This workflow allowed unbiased selection and refinement of those models best suited to describe a diazepam-bound state as well as evaluation of several thousand docking poses of diazepam and its close structural analogs. The procedure yielded a binding mode for diazepam and analogs that is convincingly supported by experimental evidence. Using this binding hypothesis in a virtual screening of a large compound library, we identified new allosteric modulators of $GABA_A$Rs acting via the benzodiazepine site, thus confirming their suitability for drug discovery and structure-based drug design.

RESULTS

Computational modeling and docking

To account for the substantial variability in local interface and pocket structures[10] of cysteine-loop receptor family members, we constructed a total of 37 homology models of the $GABA_A$R derived from eight distinct structural templates (**Supplementary Methods**, **Supplementary Table 1**), multiple sequence alignments (**Supplementary Fig. 1**) and variations in degrees of protein flexibility (**Supplementary Schemes 1** and **2**). We then docked diazepam in its bioactive conformation (M conformation; **Supplementary Fig. 2** and **Supplementary Table 2**) into all initial models (**Supplementary Results**, **Supplementary Tables 3** and **4** and **Supplementary Fig. 3**) using the software package FlexX[11]. FlexX and other docking algorithms are able to explore the conformational space sufficiently well to generate correctly docked poses, but they often fail in ranking the correct poses on top. Furthermore, the binding-mode prediction accuracy of scoring functions is target dependent[12]. We therefore evaluated the 100 top-scoring poses (FlexX score), thus ensuring that correct poses were retained. We then eliminated homology models that predominantly provided poses with poor lipophilic interaction for ligand features L1 and L3 (**Fig. 1c**) of the diazepam structure or featured no simultaneous ligand contacts with α1 and γ2 subunits. For the remaining 14 models, we extended docking to multiple ligands (**1**, **3**–**5**, **8**, **9**; in M conformation in **Fig. 1c**) and used the docking protocol FlexE[13] to enable the flexibility of those

[1]Department of Medicinal Chemistry, University of Vienna, Vienna, Austria. [2]Leiden–Amsterdam Center for Drug Research, Division of Medicinal Chemistry, Faculty of Sciences, VU University Amsterdam, Amsterdam, The Netherlands. [3]Department of Biochemistry and Molecular Biology, Center for Brain Research, Medical University of Vienna, Vienna, Austria. *e-mail: margot.ernst@meduniwien.ac.at

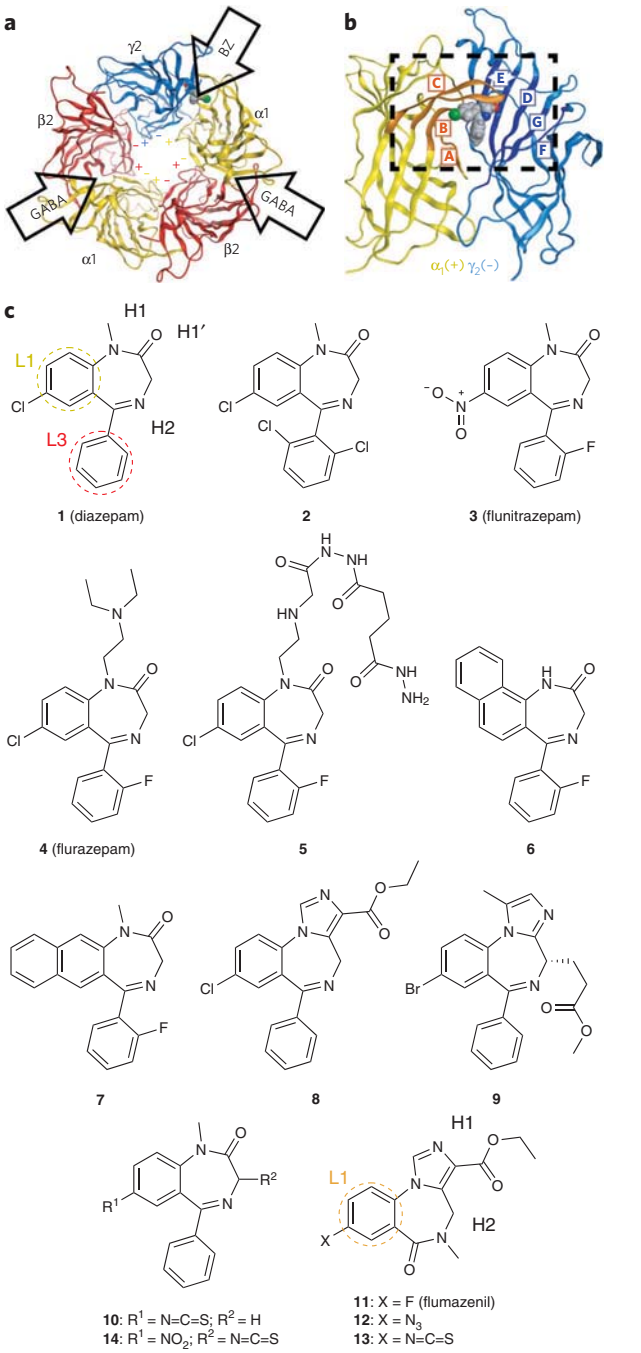

Figure 1 | Structure of diazepam-sensitive $GABA_AR$s and of benzodiazepine ligands. (**a**) Top view of the extracellular domain of the pentameric α1β2γ2 $GABA_AR$ in ribbon mode. The benzodiazepine-binding site (BZ) and the two GABA-binding sites are indicated by arrows. Diazepam in the benzodiazepine-binding site is depicted in space-filling mode. (**b**) View from a perspective nearly parallel with the lipid bilayer of the α1γ2 extracellular interface in ribbon mode with a diazepam-bound pose of CBM I in space-filling mode. The dashed window indicates the section shown in **Figures 2**–**5**. Segments (loops) A, B, C, D, E, F and G are labeled, and the corresponding protein segment is rendered in a darker shade. In both panels the plus (+) and minus (−) sides of the subunits are indicated. (**c**) Chemical structures of compounds used in this study. **1**–**9** were used for docking and **10**–**14** were used for validation. The pharmacophoric features L1, L3, H1 and H2 (ref. 48) are superimposed on two-dimensional structures of diazepam and flumazenil (**11**). As an additional feature we introduce H1′ to denote the interaction with the second lone pair of the carbonyl oxygen. More detailed information on the compounds can be found in **Supplementary Table 5**.

amino acid side chains that have been shown to be important for ligand recognition[2] and/or constitute the main steric determinants of the binding site. By applying the above-mentioned criteria for each ligand docked, we further reduced the number of homology models. The three best-performing models were based on Protein Data Bank (PDB) entries 2BYQ[3] (*Aplysia californica* AChBP, epibatidine bound), 1UW6 (ref. 3) (*Lymnea stagnalis* AChBP, nicotine bound) and 2QC1 (ref. 3) (mouse nAChR, α1 subunit, α-bungarotoxin bound). To improve conformational sampling, we further increased the flexibility of these three models by considering additional rotamers of amino acid side chains in direct contact with pocket-defining residues, especially at the crowded subunit interface between loops A and B. This resulted in three additional models (**Supplementary Scheme 2**).

Subsequently, we docked ligands **1**–**9** (**Fig. 1c**) into the six final models (**Supplementary Table 3**) using the FlexE protocol. We then performed an energy minimization of all poses and calculated the L1 and L3 interaction strengths. Of the 4,997 energy-minimized poses, we retained 1,463 with L1 and L3 interaction strengths above the median value. These poses still sampled a wide variety of putative binding geometries for smaller ligands such as diazepam and flunitrazepam. Ligands with bulky substituents (**Fig. 1c**; **4**–**9**) assumed more restricted poses. Thus, by using only lipophilic interaction strength as our selection criterion, we retrieved a set of poses in which all of the binding modes compatible with the sampled pocket topologies were still present.

Binding-mode search

To compare binding modes in different templates, we three-dimensionally aligned the ligand-protein complexes on the basis of the conserved domains of the α- and γ-subunits of their benzodiazepine-binding pocket. Then, we identified similar binding modes through cluster analysis (**Supplementary Scheme 3**) after computing the r.m.s. deviation values of the ligands' common atom positions[14] between each pair of poses and storing them as a matrix. Cluster analysis then produced groups of poses with small differences in r.m.s. deviation. By allowing 2-Å scatter around each centroid pose, thirty clusters, each comprising a group of similar binding modes, emerged (**Supplementary Figs. 4** and **5**).

Common binding-mode screen

To define candidate geometries representing a common binding mode (CBM), we split the docked ligands (**Fig. 1c** and **Supplementary Table 5**) into mandatory 'core ligands' (**Fig. 1c**; **1**–**5**), and 'accessory ligands' (**Fig. 1c**; **6**–**9**). Core ligands have very similar chemical structures, affinities, efficacies and patterns in their response to mutation, suggesting tightly overlapping bound-state geometries. Although this assumption is not necessarily true in each case, it is the basis of all rational hit-optimization efforts and (quantitative) structure-activity studies. Additionally, we also considered compound **5** 'core', not as a ligand but as affinity chromatography bait (**Supplementary Fig. 6**). Accessory ligands should also bind in a similar binding mode as the core ligands, but they either do not share all pharmacophore features with diazepam or, because of steric requirements, may induce somewhat different conformations of the binding site. Only three of the clusters contained all of the mandatory core ligands and were thus further considered as CBMs (**Supplementary Scheme 3**).

For these three clusters, we extended the measure of 'binding-mode similarity' to include not only the orientation of the ligand's common substructure but also the pocket atoms interacting with this substructure. The resulting 'bound-complex r.m.s. deviation' value describes the similarity of ligand-pocket interaction patterns. By clustering the bound-complex r.m.s. deviation values, we finally extracted the most homogenous subsets of poses from each parent cluster, resulting in CBM candidates CBM I, CBM II and CBM III (**Fig. 2** and **Supplementary Tables 6**–**8**).

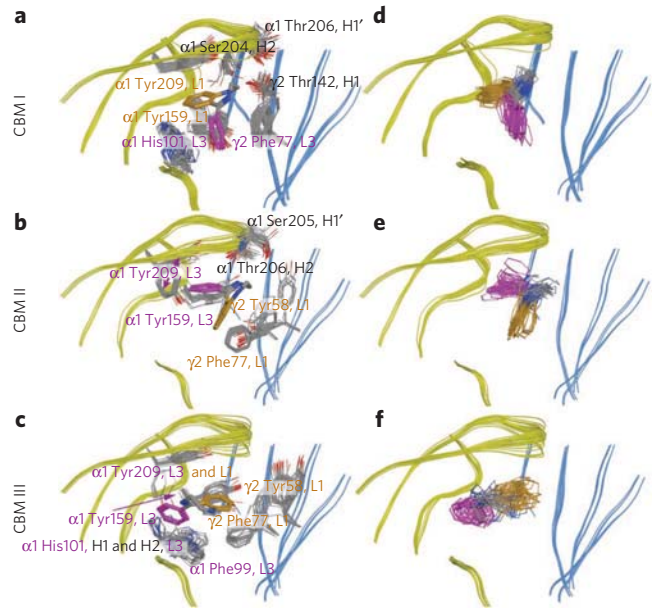

Figure 2 | CBM candidates. View of the benzodiazepine-binding pockets of the CBM pose pools as depicted in the dashed window of **Figure 1b**. (**a**–**f**) In all panels, the L1-forming annealed benzene group is depicted in orange and the L3-forming pendant phenyl group in purple. The α-subunits are shown in yellow fine-line representation, and the γ-subunits are shown in blue. Color codes used for the seven-membered ring and the side chains: gray for carbon, blue for nitrogen and red for oxygen. All labels are color-matched to the interaction partner. All side chains providing major interactions (H1, H1′, H2, L1 and L3 as defined in **Fig. 1c**) in a given CBM are indicated in panels **a**–**c** to show the variability. The scatter of core ligand poses (**Supplementary Table 9**) is depicted for each CBM in panels **d**–**f**.

Evaluation of the CBM candidates

CBM I (**Figs. 2** and **3** and **Supplementary Fig. 7**) contains the highest number of poses of core and accessory ligands and is more homogeneous in terms of ligand overlap (small average r.m.s. deviation distance to centroid) than the other putative binding modes (**Fig. 2** and **Supplementary Table 9**).

Analysis of all types of ligand interactions with pocket residues indicated that not all of the poses of a given CBM feature all interactions. Whereas in particular the highly rotamer-sensitive hydrogen bonds fluctuate considerably, major lipophilic interactions are present in most poses and are CBM defining. CBM I is the only pose pool in which both of the lipophilic L-features (**Fig. 1c**) and hydrogen bonds of all of the core ligands are matched. CBM II fails to provide a consensus H1 hydrogen bond (**Fig. 1c**), and CBM III has a very heterogeneous L-feature pattern (**Supplementary Tables 6** and **9**).

A comparison of the crystal structures of ligand-bound members of the cysteine-loop receptor family indicated that the positions of large side chains within the binding pocket seem to be well conserved. Notably, the positions of CBM I α1 Tyr159 and α1 Tyr209, the key residues defining its L1 pocket (**Fig. 2**), are similar to those of homologous residues of the ligand-bound complexes of both AChBP and nAChR, even though we kept all large side chains in the pocket flexible during docking (**Supplementary Fig. 8**).

Subjecting all poses from the five core ligands used for the CBM screen to two scoring functions[15,16] indicated that 13 of the 50 top ten scoring poses were located in CBM I, none were in CBM II and one was in CBM III. The remaining top-scoring poses were distributed randomly across the other 27 clusters (**Supplementary Table 9**).

Validation of binding modes by experimental evidence

The correct binding mode must be supported by experimental evidence. When flunitrazepam was used as a photolabel for the benzodiazepine-binding pocket, covalent modification of α1 His101 (loop A) was observed[17]. Similarly, when covalent labeling of various cysteines engineered into the benzodiazepine pocket was investigated with compound **10** (**Fig. 1c**), which carries a cysteine-reactive isothiocyanate at a position equivalent to that of the nitro group in flunitrazepam, irreversible labeling and permanent modulation of receptors containing the α1 H101C mutation was reported, suggesting that the active state was captured[18]. CBM I (**Fig. 4**) and CBM II allow such covalent labeling, whereas CBM III does not (**Table 1**).

Receptors that contain the α1 H101R mutation have a drastically reduced affinity for classical benzodiazepines such as flunitrazepam. Compounds lacking the pendant phenyl ring, such as flumazenil, tolerate this mutation[19], possibly suggesting an interaction of α1 His101 with the pendant phenyl ring. Alternatively, the loss of flunitrazepam binding in the α1 H101R mutant could reflect an unfavorable steric interaction with arginine[7]. However, having a cysteine in this position[20] results in a loss of affinity for flunitrazepam by a factor of 200, whereas glutamine leads to a loss of affinity by a factor of only 15. These findings were interpreted as evidence for a strong aromatic or hydrophobic interaction between the pendant phenyl ring (L3) of flunitrazepam and α1 His101 (ref. 20). Such an interaction is present in CBM I (**Figs. 2** and **3**), in which α1 His101 is an essential part of the pocket accommodating L3, and to a lesser degree in CBM III but not in CBM II.

The loop C mutation α1 Y209A, though producing a near wild-type GABA response, leads to a decrease in binding affinity both for diazepam (by a factor of 40) and the imidazobenzodiazepine flumazenil (by a factor of 41) (**Fig. 1c**; **11**)[21]. This suggests that α1 Tyr209, in contrast to α1 His101, provides an essential interaction with a structure common to diazepam and flumazenil. In CBM I, the L1 pharmacophoric feature common to both compounds forms a strong aromatic interaction with α1 Tyr209 (**Fig. 4a**,**b**). Notably, the imidazobenzodiazepine Ro15-4513 (**Fig. 1c**; **12**), which is structurally similar to flumazenil, photolabels α1 Tyr209 (ref. 22) (**Fig. 4b**). More recently, a derivative of Ro15-4513, in which the azido group has been replaced by an isothiocyanate group (**Fig. 1c**; **13**), has also been shown to react with several engineered cysteines in the α-subunit[23]. Only CBM I is fully consistent with the reaction patterns of both studies (**Fig. 4b**) and with the additional reaction of compound **13** with the α1 H101C mutant, which was interpreted as strong evidence for an overlapping binding mode of

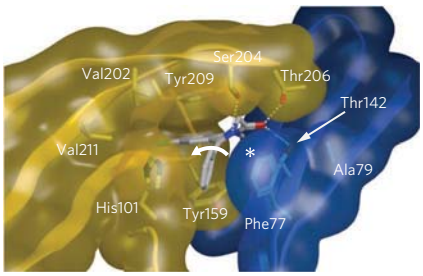

Figure 3 | Representation of a CBM I pose of diazepam. The L1 hydrophobic feature (**Fig. 1c**) shows strong interactions with α1 Tyr159 and α1 Tyr209 (ref. 26). The L3 hydrophobic feature (**Fig. 1c**) shows strong interactions with α1 His101 and γ2 Phe77. The asterisk on γ2 Phe77 indicates the position of the hydroxyl group in the ligand-bound F77Y mutants[24] (**Supplementary Fig. 9a**). The arrow indicates rotational freedom of the pendant phenyl ring. The imine nitrogen forms a hydrogen bond with α1 Ser204. The carboxyl oxygen of diazepam with its two lone pairs interacts with γ2 Thr142 and α1 Thr206. The α1 subunit is in yellow, and the γ2 subunit is in blue.

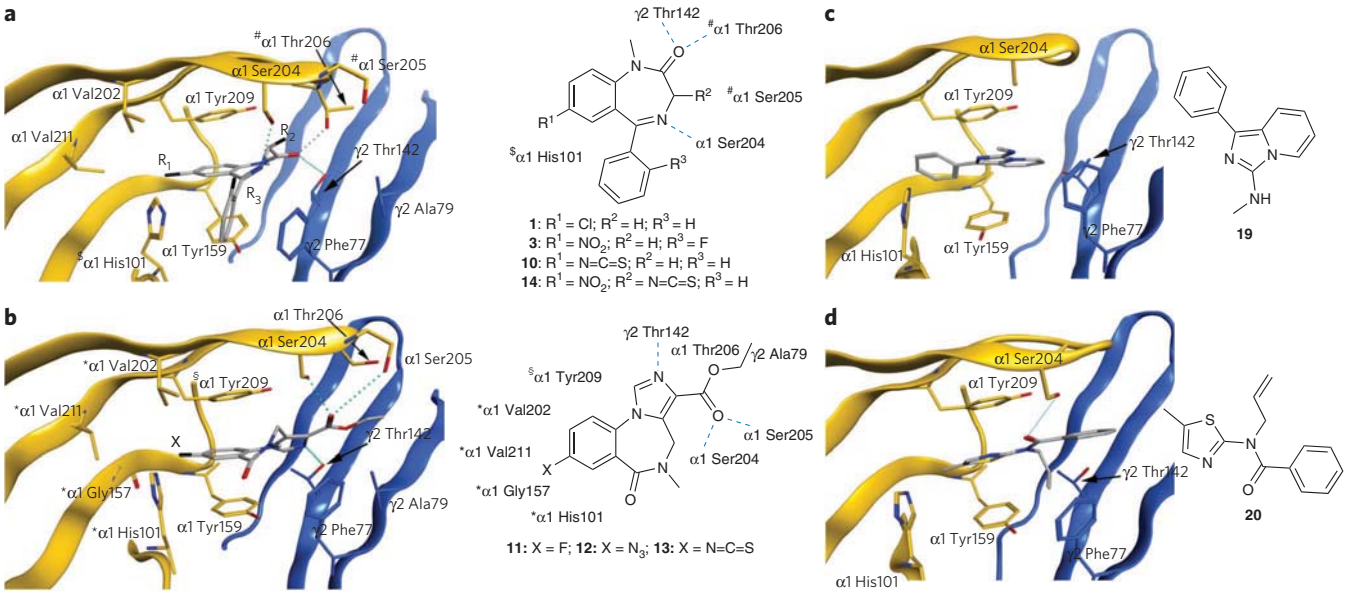

Figure 4 | CBM I reference binding modes of diazepam and flumazenil compared to docking poses of virtual screening hits 19 and 20, selected by IFP scoring. Representation shows the α-subunit (yellow) and γ-subunit (blue). Ligand and key residues are rendered in stick representation, and hydrogen-bond interactions are indicated by cyan dotted lines. (**a**) Two-dimensional scheme shows diazepam **1** and analogs **3**, **10** and **14** in CBM I. Position of covalent incorporation of 7-NCS[18] is indicated by ($), and the sites of 3-NCS[28] reactivity are indicated by (#). (**b**) Two-dimensional scheme shows flumazenil (**11**) and analogs **12** and **13** in CBM I. Residues whose respective cysteine mutants react with the imid **13** (ref. 23) are marked (*), and the α1 Tyr209 whose bovine homolog is photolabeled by **12** (ref. 22) is marked (§). The ester group is localized between loops C and D. (**c**,**d**) **19** (**c**) and **20** (**d**) place their phenyl and thiazol groups in the same tight aromatic binding pocket between α1 His101, α1 Tyr159 and α1 Tyr209 as that occupied by the L1 ring of **1** in **a** and **11** in **b**, and they stack with the same γ2 Phe77 as the reference ligands.

diazepam and flumazenil[23]. Together, these results suggest that only CBM I can provide a single structural hypothesis for all of these covalently incorporated derivatives of diazepam, flunitrazepam and flumazenil.

Compounds with a pendant phenyl ring suffer an affinity loss in the loop D γ2 F77Y mutant, which is relatively less pronounced (by a factor of 250) for diazepam but is much stronger in diazepam analogs with chlorine substituents (monochlorodiazepam, by a factor of 530; dichlorodiazepam (**Fig. 1c**), by a factor of 700 (ref. 24)) that decrease the flexibility of the pendant phenyl ring. Thus, γ2 Phe77 has been proposed to interact with the pendant phenyl ring of diazepam and its analogs[24]. CBM I features precisely this interaction and has a sufficiently narrow L3 pocket, defined mostly by γ2 Phe77 and α1 His101, to possibly cause steric problems when phenylalanine is replaced by tyrosine. Diazepam might be able to accommodate to the loss of space by its pendant phenyl ring adapting another rotational state (**Fig. 3**) that is probably not possible for its more rigid analogs. Neither CBM II nor CBM III offer interactions consistent with these findings.

Other mutations in γ2 Phe77 have subtle effects on the affinities of diazepam and flumazenil. The point mutation γ2 F77L is tolerated well by both ligands, whereas γ2 F77I leads to a loss of affinity for flumazenil by a factor of 2,000 but to a loss of affinity for diazepam[25] or Ro15-8670 by a factor of only 4–5 (**Supplementary Fig. 9a**,**b**). Docking of flumazenil into the final models indicated that flumazenil, much like Ro15-8670, can be accommodated in all three CBM geometries, thus supporting the postulated CBM between diazepam and flumazenil[23] by direct docking. The CBM I pose (**Fig. 4b**) features a strong hydrophobic interaction between γ2 Phe77 and flumazenil. After replacement of phenylalanine with leucine in our flumazenil-bound wild-type CBM I structures, both the hydrophobic interaction and local ligand burial of flumazenil are reduced, although the pocket structure tolerates the point mutation without detectable unfavorable interactions. When isoleucine replaces phenylalanine, the loss of hydrophobic interaction and ligand burial are much more pronounced. In addition, steric clashes are observed and thus suggest that this mutation would induce local rearrangements in the pocket involving both subunits. CBM I structures are thus fully compatible with experimental data on the F77X mutants.

Several other experimental findings, such as the importance of α1 Tyr159 (loop B) for the action of diazepam, flunitrazepam and flumazenil[23,26] or of subtle effects of the α1 T206V substitution in loop C for the potency of diazepam and Ro15-8670 (ref. 24), together can only be explained by CBM I and suggest a close approximation between the ester group of Ro15-8670 (**8**) and α1 Thr206 (**Table 1** and **Supplementary Fig. 9a**,**c**). This conclusion is supported by the effects of α1 S205N substitutions on compounds with or without this ester group[27] as well as by covalent labeling of α1 S205C and α1 T206C mutants by a nitrazepam derivative carrying a reactive isothiocyanate in the seven-membered ring's 3C position[28] (**Fig. 1c**; **14**; also **Fig. 4b**). Finally, other experiments indicated that the ester group of 3′-ester–substituted imidazobenzodiazepines must be located close to γ2 Ala79 (ref. 29) (**Fig. 4b** and **Supplementary Fig. 9c**). All of these results are consistent with CBM I poses of these ligands (**Table 1**) and thus again support an overlapping orientation of benzodiazepines and imidazobenzodiazepines within the benzodiazepine binding pocket.

Alternative workflow leads to the same binding mode

To avoid the assumption of a common binding mode, we also subjected the initial pool of 30 pose clusters to an alternative workflow (**Supplementary Scheme 3**) and evaluated all poses by geometric restraints (distance between a pocket residue and a ligand atom) derived from experiments 2, 3, 7, 8, 10 and 11 cited in **Table 1**. Only two clusters met all criteria at different cutoff levels for the

Table 1 | CBM candidates in light of experimental data

	Ligands[a]	CBM I		CBM II		CBM III	
α1 His101							
(1) Flunitrazepam photolabeling[17]	3	All	++	All	++	None	–
(2) 7-NCS covalent labeling[18]	10	All	++	All	++	None	–
(3) α1 His101 interacts with L3 (ref. 20)[b]	3	13/16[c]	++	None	–	3/6[c]	+
α1 Tyr209							
(4) α1 Tyr209 interacts with L1 (ref. 21)	1	All	++	None	–	All	++
(5) Ro15-4513 photolabeling[22]	12	All	++	None	–	All	++
α1 His101, α1 Gly157, α1 Val202 and α1 Val211							
(6) 'Imid-NCS' compound covalent labeling[23]	13	All	++	None	–	None	–
γ2 Phe77							
(7) γ2 Phe77 interacts with L3 (ref. 24)[b]	1-3	All	++	3/8[c]	+	7/12[c]	+
α1 Thr206							
(8) α1 Thr206 hydrogen bonding[24]	1,3	34/37[c]	++	3/7[c]	+	None	–
(9) α1 Thr206 contacts ester[24]	8	All	++	1/3[c]	+	None	–
α1 Ser205 and α1 Thr206							
(10) 3-NCS covalent labeling[28]	14	All	++	All	++	None	–
γ2 Ala79							
(11) γ2 Ala79 near ester[29]	8	All	++	All	++	None	–

[a]Only poses of the defined ligands (**Fig. 1c**) were used for evaluation. [b]Interactions were calculated using SCORING.SVL. [c]Number of poses fulfilling the respective criterion in relation to number of total poses in a CBM (**Supplementary Table 7** lists the total number of poses per ligand within a CBM).

selected distances. These two clusters are the parent clusters of CBM I and CBM II. When all poses were scored by two scoring functions as above, the group of poses containing CBM I once again emerged as a strong candidate.

Neither of the two approaches led to a single bound-state model. The bound-state hypotheses derived in this work represent groups of poses with some uncertainty associated with atomic positions and protein-ligand interactions. The pose groups derived from the CBM analysis are smaller and more homogeneous, as we used their interaction pattern in defining the binding mode (**Supplementary Tables 6–8**).

Retrospective validation of CBM I by virtual screening

If CBM I structures are indeed binding competent, they should be suitable for enriching other benzodiazepine-site ligands from different structural classes out of a library of decoy molecules. To investigate this possibility, we generated a 'validation' library in analogy to the directory of useful decoys (DUD) database[30] (**Supplementary Scheme 4**) by extracting 41 benzodiazepine-binding-site ligands from different structural classes from the literature (**Supplementary Table 10**). We property-matched decoys on the basis of the five terms used to construct the DUD database, plus net formal charge[31]. Thus, for each of the 41 ligands, we generated all protonation states near pH 7.0, resulting in 48 unique ligand protomers. For each of them, we created 50 decoy molecules that are physically similar but topologically distinct and thus should not bind the benzodiazepine site, resulting in a library of 2,400 decoys. After seeding the 48 unique ligand protomers into the decoy library, the resulting validation library was used for virtual screening using structure-based pharmacophore models. These we generated using the software program LigandScout[32] using bound-state complexes from all three CBM pools as our basis (**Supplementary Fig. 10**). We sorted the compounds in the validation library for those that best matched these pharmacophore models . In the sorted libraries, we computed[33] the enrichment of known binders in the top 0.5%, 1%, 2%, 5% and 10% for each CBM. CBM I performed much better than CBM II and CBM III (**Supplementary Table 9**), resulting in an enrichment over random selection of 24.8 when the top 0.5% was analyzed. With the exception of purely two-dimensional similarity searching, this screen outperforms those conducted with a ligand-based pharmacophore model and shape-based similarity search (**Supplementary Table 11**). Such enrichment factors are comparable to the average enrichment factors obtained for the 40 crystal structures of the original DUD database[30], clearly indicating that CBM I complexes are sufficiently binding competent to identify known benzodiazepine-site ligands from different structural classes.

CBM I binding hypotheses predict new ligands

We then investigated whether CBM I–derived pharmacophore models (**Supplementary Fig. 10**) can be used for the discovery of new ligands (**Supplementary Scheme 5**). As a screening library we used the large DUD databank[30], which contains 95,357 compounds and covers a large chemical space. After the screening run, we grouped the top 0.5% of compounds in the DUD screen according to their chemical scaffolds. Some of the compound classes in the top 0.5% were found to have anticonvulsive activity in animal models but were never investigated for a possible interaction with $GABA_A$Rs. Representatives from four of these compound classes were commercially available and were tested for displacement of [^{3}H]flunitrazepam binding from mouse cerebellum membrane preparations (**Table 2**).

In contrast to compounds **16**–**18**, the 3-hydroxyoxindole **15** at a 10-μM concentration was able to inhibit [^{3}H]flunitrazepam binding to 18 ± 7% of the control values, indicating that it interacts with the benzodiazepine-binding site of $GABA_A$Rs. This compound at 1-μM and 10-μM concentrations also significantly ($P < 0.001$) stimulated GABA-induced currents in recombinant α1β3γ2 receptors expressed in *Xenopus laevis* oocytes (**Table 2**). Notably, the ligand-based screening approaches would have missed this new hit compound (**Supplementary Table 12**).

A subsequent similarity search revealed that other 3-hydroxyoxindoles were also present in the top 0.5%, four of which (**15a**–**15d**) were commercially available. To further increase the number of compounds for the follow-up study, we bought five additional analogs

Table 2 | Effects of top 0.5% compounds on [^{3}H]flunitrazepam binding to cerebellar membranes and on GABA-stimulated currents in recombinant α1β3γ2 receptors

Cmpd. 15, 15a–15i

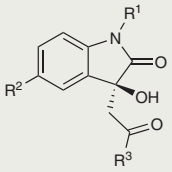

Cmpd.	ZINC code	R^1	R^2	R^3	Percentage of flunitrazepam binding left at 10 μM	Percentage of GABA EC_3 stimulation at α1β3γ2 receptors	
						1 μM	10 μM
15	ZINC00657218[a,b]	H	Ethyl	*p*-Bromophenyl	18 ± 7	130 ± 4	300 ± 28
15a	ZINC00106837[b]	H	Methyl		69 ± 7	124 ± 9	140 ± 5
15b	ZINC01320283[b]	H	Methyl	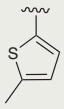	34 ± 5	118 ± 3	168 ± 9
15c	ZINC02854078[b]	H	Bromo	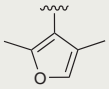	77 ± 6	134 ± 9	165 ± 16
15d	ZINC01108532[b]	2-Ethinyl	Bromo	4-Pyridyl	Inactive	n.d.	n.d.
15e	ZINC17744128[c]	H	H	Methyl	Inactive	n.d.	n.d.
15f	ZINC00037760[c]	Methyl	H	Phenyl	Inactive	n.d.	n.d.
15g	ZINC00299974[c]	Isopropyl	H	Phenyl	Inactive	n.d.	n.d.
15h	ZINC00089290[c]	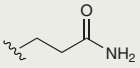	H	Phenyl	Inactive	n.d.	n.d.
15i	ZINC00299984[c]	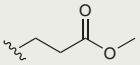	H	Phenyl	Inactive	n.d.	n.d.
16	ZINC00421595[a]	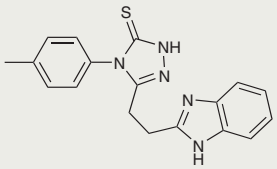			Inactive	n.d.	n.d.
17	ZINC00627050[a]	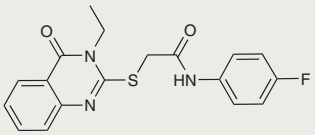			Inactive	n.d.	n.d.
18	ZINC00099714[a]	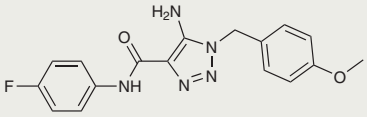			Inactive	n.d.	n.d.
19	IOTA0004[d]	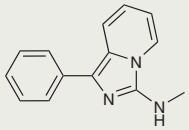			25.6 ± 9.6 μM[e]		
20	IOTA0431[d]	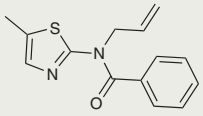			34.7 ± 2.6 μM[e]		

[a]Compounds ranked within the top 0.5% in score-sorted DUD decoys database that belong to a compound class in which anticonvulsive activity was shown in literature. [b]Compounds ranked within top 0.5% in score-sorted DUD decoys database that belong to the 3-hydroxyoxindole class. [c]3-hydroxyoxindoles not contained in DUD decoys database. [d]Compounds ranked within the top 30 of the IFP score-sorted fragment library capable of displacing [^{3}H]flunitrazepam in radioligand assays. [e]IC_{50} values were measured by the competition for [^{3}H]flunitrazepam binding to mouse brain membranes. Data are means ± s.d. from three independent [^{3}H]flunitrazepam binding assays performed in triplicate. n.d., not determined.

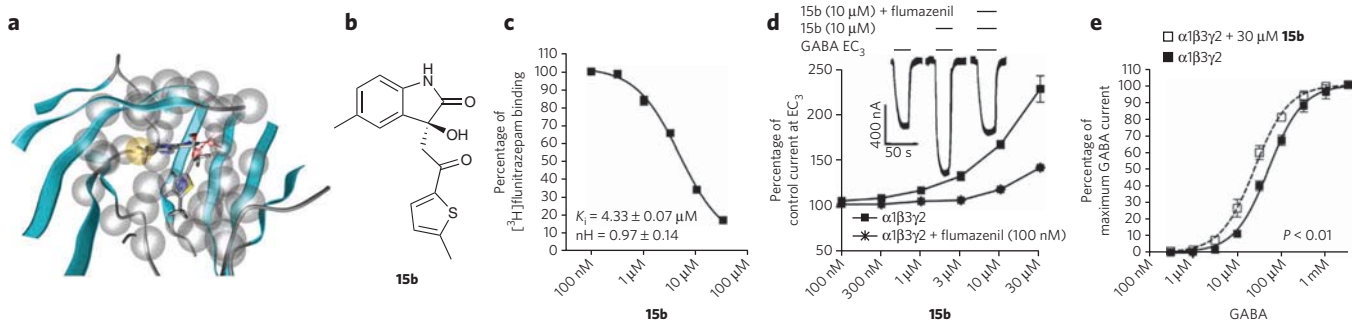

Figure 5 | 3-hydroxyoxindoles as a new class of benzodiazepine-binding-site ligands of $GABA_ARs$. (**a**) The CBM I–derived pharmacophore model (**Supplementary Fig. 10a**) based on the diazepam-bound structure and its match with **15b** is depicted. Both dark blue aromatic features match, as do the red hydrogen bond and the yellow lipophilic feature. The steric exclusion volumes are depicted in an overlay with a ribbon structure to provide orientation in the model. (**b**) Two-dimensional structure of **15b**. (**c**) Inhibition of 2 nM [^{3}H]flunitrazepam binding to mouse cerebellar membranes by **15b**. Data represent means ± s.d. from three experiments performed in triplicate. nH, Hill coefficient. (**d**) Electrophysiological traces and dose-response curve of **15b** on GABA EC_3 (3% of maximum GABA current) currents in the absence (squares) or presence of 100 nM flumazenil (asterisks), obtained from *X. laevis* oocytes expressing recombinant $GABA_ARs$ composed of α1β3γ2 subunits. Data represent means ± s.d. from three separate experiments performed in different oocytes from two different batches. (**e**) GABA dose-response curves in α1β3γ2 receptors expressed in *X. laevis* oocytes with (open squares) and without (filled squares) 30 μM **15b**. Data represent means ± s.d. from three separate experiments performed in different oocytes from two different batches. In **c**, **d** and **e**, *x*-axis scale is logarithmic.

(**15e**–**15i**) not present in the DUD database. We then tested all nine additional 3-hydroxyoxindoles, as shown in **Table 2.** Displacement of [^{3}H]flunitrazepam binding at 10-μM compound concentrations revealed that, in addition to compound **15**, the compound **15b** at 10 μM was able to inhibit [^{3}H]flunitrazepam binding to about 34 ± 5% of control binding (P <0.001), whereas compounds **15a** and **15c** inhibited this binding to approximately 70% (P < 0.01). The other 3-hydroxyoxindoles investigated did not significantly (P < 0.5) inhibit [^{3}H]flunitrazepam binding at this concentration. All four compounds able to displace [^{3}H]flunitrazepam binding were also able to significantly (P < 0.001) enhance GABA-elicited currents in α1β3γ2 recombinant receptors expressed in *X. laevis* oocytes at 10-μM concentration (**Table 2**). We then characterized compounds **15b** and **15**, which had the highest potency for inhibition of [^{3}H] flunitrazepam binding (half-maximum inhibitory concentration (IC_{50}) values of 4.9 ± 1.5 μM and 3.8 ± 0.8 μM, respectively; **Fig. 5** and **Supplementary Fig. 11**). Both compounds showed a dose-dependent stimulation of GABA-induced currents and shifted the GABA dose-response curve to the left. In addition, the effect of these compounds could be reduced by coapplication of 100 nM of the benzodiazepine-site antagonist flumazenil, indicating that the effect was at least partially generated by interaction with the benzodiazepine-binding site of these receptors. Flumazenil inhibited the effects of **15b** more strongly than those of **15**. The additional effect of these compounds in the presence of flumazenil might have been caused by their interaction with additional binding sites at these receptors[34].

These data clearly indicate that 3-hydroxyoxindoles are unique modulators of $GABA_ARs$ via the benzodiazepine-binding site. The structural novelty of this compound class is also reflected by the fact that the most similar known benzodiazepine-site ligand (**Supplementary Table 12**) has a Tanimoto similarity of 0.56 (based on molecular access system (MACCS) keys).

Results obtained for this small data set indicate that an aromatic ring at R3 in combination with an unsubstituted nitrogen atom seems to be beneficial for biological activity. This idea is also supported by the orientation of compound **15b** in the pharmacophore model, which shows a considerable overlap of substituent R3 with the pendant phenyl ring of diazepam and a hydrogen bond of the NH group to the backbone carbonyl of α1 Tyr159 (**Fig. 5**). However, systematic studies have to be performed to get deeper insights into the structure-activity relationship and binding mode of this unique ligand class. Finally, whether this activity accounts for some of the previously reported anticonvulsive activity of this compound class[35] has to be clarified in future experiments.

In an alternative approach, we performed docking-based virtual screening studies (**Supplementary Scheme 5**) against the diazepam-bound (**Fig. 4a**) and flumazenil-bound (**Fig. 4b**) $GABA_AR$ models (CBM I) used for generating the protein-based pharmacophore model (**Supplementary Fig. 10**)[36]. To assess the robustness of the benzodiazepine-binding-site models, we used a docking method (protein-ligand ANT system (PLANTS)[37]) different from that used to derive ligand binding modes (FlexX) for virtual screening studies. To consider protein flexibility, we performed two independent docking simulations for each of the two benzodiazepine-pocket models: a 'rigid' docking run considering no side chain flexibility and a 'flexible' docking run allowing flexibility of the side chains of γ2 Thr142 (ref. 38) and α1 Thr206 (ref. 24) (important hydrogen bond–donating residues involved in ligand binding and activation). We used the original ligand poses of diazepam and flumazenil in the respective benzodiazepine-binding-site models to define reference interaction fingerprints (IFPs) for scoring the docking poses of an in-house library of 1,010 chemically diverse fragment-like molecules, as described previously[39]. The IFP scoring method determines ligand binding mode similarity to experimentally supported ligand binding poses (**Fig. 4a**,**b**). IFPs have been used as an efficient alternative postprocessing method of docking poses[36,39] to overcome target-dependent scoring problems[12]. We used seven different interaction types (negatively charged, positively charged, hydrogen bond–accepting, hydrogen bond–donating, aromatic face-to-edge, aromatic-face-to-face and hydrophobic) to define the IFP (**Supplementary Table 13**). We used the Tanimoto coefficient measuring IFP similarity with the reference ligand pose in the benzodiazepine-binding-site receptor model to score the docking poses of known actives and decoys. Normalized IFP scores (Z values) of the docking poses in the diazepam and flumazenil binding pocket receptor models were merged and ranked with respect to the normalized IFP score. We successfully used this docking-based virtual screening procedure to identify two new benzodiazepine-binding-site ligands from the 1,010 chemically diverse fragment-like molecules (**Supplementary Scheme 5**)[40]. From the top-ranked 30 fragment-like compounds, we selected 10 fragments, chemically dissimilar from known benzodiazepine-binding-site ligands, for radioligand binding assays. Two of these *in silico* hits, **19**

and 20, inhibited [^{3}H]flunitrazepam binding (IC_{50} values of 25.6 ± 9.6 μM and 34.7 ± 2.6 μM, respectively; **Table 2**). Remarkably, the new ligands are proposed to make the same interactions with the benzodiazepine-binding-site as diazepam and flumazenil 11, but most of the functional groups (hydrogen bond acceptors and aromatic ring systems) mediating these conserved interactions are located at positions different than those of the corresponding functional groups in the reference ligands (**Fig. 4**). The newly identified chemical scaffolds (the MACCS Tanimoto similarity of 0.58 was the closest to any of the 41 benzodiazepine-binding-site ligands; **Supplementary Table 12**) illustrate the suitability of this molecular IFP approach for scaffold-hopping purposes[41].

CBM I models are similar to the GluCl structure

After submission of this study, a nematode glutamate-gated chloride channel (GluCl) structure was reported (PDB code 3RIF)[42]. This cysteine-loop receptor features 28%, 35% and 29% sequence identity in the extracellular domain with α1, β2 and γ2 subunits, respectively, and thus it is clearly the template of choice for future studies. Careful analysis of this structure and homology models derived from it (**Supplementary Table 4**) indicated that our CBM I models indeed are more similar to the structure with PDB code 3RIF than the AChBP structures used in modeling and, more importantly, much more so than the models that we rejected through our workflow. This again highlights the validity of our approach.

DISCUSSION

In the absence of a crystal structure of the ligand-bound benzodiazepine-binding-site of $GABA_A$Rs, protein homology modeling and computational ligand dockings are the only bases on which structure-based hypotheses for the interaction of benzodiazepines with their binding site can be formed. However, accurate prediction of membrane-protein structures and ligand interactions remains a challenge[43] and requires accurate modeling of structurally divergent regions and extensive use of experimental evidence, as shown recently in a community-wide G protein–coupled receptor structure-prediction assessment. Here we compensated for the local uncertainty resulting from structurally divergent regions of related cysteine-loop receptor family members by constructing a variety of homology models from different templates. We then exploited the given structure of diazepam and its derivatives to select those models best accommodating these compounds. To do so, we developed a workflow that allowed handling of multiple models and several thousand diazepam docking poses. The only selection criteria used were a reasonable lipophilic interaction with the hydrophobic parts of the diazepam structure as well as simultaneous contacts of diazepam with the α1 and the γ2 subunit of $GABA_A$Rs. With the assumption that diazepam and its close structural analogs have a CBM within the benzodiazepine-binding pocket and by clustering of ligand poses according to a similar orientation of their common structure and according to similar interactions with pocket residues, we were finally led to three CBM geometries, CBMs I–III.

CBM I binding geometry and interactions are supported by a large variety of structural, computational and experimental evidence. Furthermore, CBM I can provide a single structural hypothesis for seemingly discrepant results obtained with various covalently incorporated compounds and supports the hypothesis that diazepam and the imidazobenzodiazepines Ro15-4513 or flumazenil show a similar binding mode within the benzodiazepine pocket. Finally, CBM I can also explain subtle changes in affinity of various ligands for various amino acid substitutions. Taken together, this abundance of evidence indicates that CBM I is the correct binding mode of diazepam in the benzodiazepine-binding pocket.

Previous studies also featured docking poses of diazepam or its analogs. Overall, however, the conclusions remained contradictory. In one study[5], a flunitrazepam orientation similar to the CBM III poses was reported. Another study[6] identified a diazepam pose vaguely similar to the CBM I pose, but apparently it had a very different interaction pattern owing to a different pocket topology. A pharmacophore-derived diazepam pose[4] is in a position intermediate between that of CBM II and CBM I. Most recently, binding modes vaguely resembling our CBM II were proposed based on modeling structures from a single template and covalently incorporated ligands[7]. In a study more concerned with zolpidem[8], flunitrazepam poses featured the P conformation, which has been demonstrated to be inactive at the benzodiazepine-binding site (**Supplementary Table 2**).

A correct structure, however, should also be able to accommodate other ligands of this site from different structural classes. Thus, by using structure-based pharmacophore models derived from CBM I, we identified 5 out of 41 benzodiazepine-site ligands from different structural classes within the top 0.5% of hits of a benzodiazepine-focused set of decoy molecules (validation library), and we found five additional compounds within the top 2% and eight more in the top 10% of compounds (**Supplementary Tables 9** and **10**). Such enrichment factors, as well as the remaining false negatives (binders that are not ranked in the top range) are comparable to those obtained from docking into ligand-bound crystal structures[30].

Virtual screening with the DUD database[30] identified not only additional known benzodiazepine-site ligands present in this database but also a variety of other anticonvulsive compounds that so far have not been associated with $GABA_A$Rs. By investigating a commercially available subset for a possible interaction with the benzodiazepine-binding site of $GABA_A$Rs, we identified several 3-hydroxyoxindole derivatives that were able to modulate GABA-induced currents in recombinant receptors via the benzodiazepine-binding site. Furthermore, in a complementary approach, docking-based virtual screening studies using a molecular protein-ligand IFP scoring method identified two additional new chemical scaffolds, which were proven active in [^{3}H]flunitrazepam displacement assays. These data further support the validity of our diazepam-bound structure of the benzodiazepine-binding site and demonstrate its suitability for structure-based drug discovery.

Further exploration of our *in silico* screening results presumably will identify additional new ligand classes for the benzodiazepine-binding site. Information from docking studies with other benzodiazepine-site ligands as well as molecular dynamics studies will identify the flexible and rigid parts of the pocket and define their ligand-pocket interactions as well as the mechanism of allosteric modulation of positive, negative and neutral interactors. The present structural models can also be used for modeling of the benzodiazepine-binding sites of other $GABA_A$R subtypes, and docking of unselective and subtype-selective ligands into their binding sites will ultimately lead to appropriate structural hypotheses that allow lead optimization and fragment-based drug design. Finally, our structures can be used for the modeling of similar extracellular pockets of $GABA_A$Rs[34], again enabling lead optimization and drug discovery.

METHODS

Template characterization and preparation. Six AChBP structures (PDB codes 1I9B, 1UW6, 2BYN, 2BYQ, 2BYR and 2BYS)[3] and two nAChR structures (PDB codes 2BG9 and 2QC1)[3] were used as $GABA_A$ modeling templates (**Supplementary Table 1**) and structurally aligned with ProFit (http://www.bioinf.org.uk/software/profit/). Only the extracellular domains of the structures with PDB codes 2BG9 and 2QC1 were considered, and both complete pentamers and individual subunits, reassembled into multitemplates, were used.

Alignment and model building. A multiple-sequence alignment with all templates' extracellular domains and the $GABA_A$R α1, γ2 and β2 extracellular domains' sequences was constructed with clustalX[44] (**Supplementary Scheme 1** and **Supplementary Fig. 1**). All templates were structurally aligned with secondary-structure matching[10]. Individual pairwise sequence-to-structure alignments between the $GABA_A$R subunits and all template subunits were obtained from the

Fugue server[45]. From these data, alignment variants of variable segments were constructed[46], and homology models were built using Modeller. For the two subunits that contribute to the benzodiazepine-binding site, multiple template combinations were used to sample the structural variations in the templates.

Creation of input ligands. Seven 1,4-benzodiazepines and three 1,4-imidazobenzodiazepines were built in Molecular Operating Environment (MOE) version 2007.09 (http://www.chemcomp.com), using the M conformation of the seven-membered ring that is supported by experimental studies (**Supplementary Table 2** and **Supplementary Fig. 2**).

FlexX docking. Diazepam was docked into all models using FlexX v2.0.3 (ref. 11). RING_MODE was set to 0 (constraining the ring conformation), and all other parameters were left in their default values. The pose output limit was set to 100 for each run for extensive conformational sampling.

FlexE docking. FlexE[13] allows protein flexibility through an ensemble of superposed protein structures where similar parts of the structures are merged and dissimilar areas are treated as separate alternatives. To prepare such ensembles, we explored the rotameric states of α1 His101, α1 Tyr159, α1 Val202, α1 Ser204, α1 Ser205, α1 Thr206, α1 Tyr209, γ2 Tyr58, γ2 Phe77 and γ2 Thr142 with the MOE tool Rotamer Explorer. In cases in which more than ten rotamers were obtained for a certain side chain, the ten most diverse rotamers were retained. Each benzodiazepine-binding-site ligand was docked into the ensemble structures of the corresponding homology models, generating 100 poses for each ligand. Finally, each ligand-receptor complex of the final pose pool was refined using the MOE tool LigX energy minimize. Lipophilic interactions of L1 and L3 both in docked and energy-minimized poses were calculated with the Scientific Vector Language (SVL)-exchange tool SCORING.SVL (http://svl.chemcomp.com).

CBM candidate selection. We defined the CBM of a molecular scaffold to require common orientation of the scaffold and common binding-site topology surrounding the common scaffold. Poses were superposed on the backbone atoms of the conserved protein segments using MOE to determine ligands' common scaffold r.m.s. deviation. The SVL-exchange script MOL_RMSD.SVL (http://svl.chemcomp.com) was used for the r.m.s. deviation computation of the common ligand scaffolds. Then, the Microsoft Excel add-in XLSTAT (http://www.xlstat.com) was used for hierarchical clustering of the r.m.s. deviation dissimilarity matrix using the WARD method.

All protein heavy atoms within 4 Å of any heavy atom of the molecular scaffold in more than 90% of all poses of the cluster were considered part of the binding site of the common scaffold. The identified atoms and the common scaffold were used for the calculation of the bound-complex r.m.s. deviation, which was used to cluster the poses to candidate binding modes within their parent cluster.

Evaluating covalent incorporation and mutagenesis data. Poses were considered to fit experimental data if the smallest distance between the atoms in any of the following combinations was <6 Å: (i) any atom of the nitro group (flunitrazepam) and any atom of α1 His101 (ref. 17), (ii) the photoreactive nitrogen of the arylazido group (Ro15-4513) and α1 Tyr209 (ref. 22), (iii) any atom of the ester moiety (Ro15-8670) and side chain atoms of α1 Thr206 or the C_β of γ2 Ala79 (ref. 29) or (iv) the carbon of isothiocyanate (NCS)-substituted ligands and the sulfur of the respective cysteine mutant.

Generation and validation of pharmacophore models. Two structure-based pharmacophore models were created for each CBM, one derived from the top-scoring diazepam pose (pharmacophore D) and the other from the flumazenil pose, which showed the lowest bound-complex r.m.s. deviation from the diazepam-selected pose (pharmacophore F). Pharmacophore models were created using LigandScout 3.0 (ref. 32) (**Supplementary Methods**).

Validation library. For each of the 41 known benzodiazepine-binding-site ligands (**Supplementary Table 10**), protonation states near pH 7.0 were generated, resulting in 48 unique ligand protomers. For each of them, we created 50 decoy molecules that are physically similar but topologically distinct and thus should not bind the benzodiazepine site, resulting in a library of 2,400 decoys (**Supplementary Methods**). A conformational database was created with OMEGA v2.3.3 (http://www.eyesopen.com/omega) and screened against pharmacophore D and pharmacophore F using LigandScout 3.0. Hits of each pharmacophore model were sorted according to scoring value, and enrichment factors[33] were determined for the top 0.5%, 1%, 2%, 5% and 10% for each CBM.

Discovery library. To test the ability of the CBM I–derived pharmacophore model to identify new ligands, we generated three-dimensional conformations for the DUD[30] databank (using OMEGA v2.4.1 (http://www.eyesopen.com/omega) and screened the resulting database of 93,597 compounds against pharmacophore D and pharmacophore F using LigandScout 3.0 (ref. 32). Compounds **15**, **15a**–**15i** and **18** were bought from Ambinter, and compounds **16** and **17** were bought from Asinex.

PLANTS docking and IFP scoring. PLANTS[37] speedup settings were used twice to generate 15 poses for each compound in two independent docking runs: one run considering no side chain flexibility and another run allowing flexibility of the γ2 Thr142 and α1 Thr206 side chains. The original ligand poses in the respective $GABA_A$ models were used to define reference IFPs, as described previously[36,39]. The cavity used for the IFP analysis consisted of all of the residues within 5 Å of the reference ligand. Standard IFP scoring parameters[36] and a Tanimoto coefficient measuring IFP similarity with the reference ligand pose were used to rank the docking poses.

Experimental section: Recombinant $GABA_A$Rs were expressed in *X. laevis* oocytes, and HEK cells and compound modulatory effects were investigated using the two-electrode voltage-clamp technique at a GABA concentration eliciting 3% of the maximum current[34]. Binding of compounds was investigated by [^{3}H]flunitrazepam displacement studies[47] in mouse cerebellar membrane preparations.

Accession codes. PDB: the previously determined crystal structures for *A. californica* AChBP, *L. stagnalis* AChBP, mouse nAChR, a nematode glutamate-gated chloride channel, an nAChR structure and four AChBP structures are deposited under accession codes 2BYQ, 1UW6, 2QC1, 3RIF, 2BG9, 1I9B, 2BYN, 2BYR and 2BYS, respectively.

Received 24 March 2011; accepted 2 February 2012; published online 25 March 2012

References

1. Sieghart, W. Structure and pharmacology of γ-aminobutyric acid A receptor subtypes. *Pharmacol. Rev.* **47**, 181–234 (1995).
2. Sigel, E. Mapping of the benzodiazepine recognition site on $GABA_A$ receptors. *Curr. Top. Med. Chem.* **2**, 833–839 (2002).
3. Miller, P.S. & Smart, T.G. Binding, activation and modulation of Cys-loop receptors. *Trends Pharmacol. Sci.* **31**, 161–174 (2010).
4. Clayton, T. *et al.* An updated unified pharmacophore model of the benzodiazepine binding site on γ-aminobutyric $acid_A$ receptors: correlation with comparative models. *Curr. Med. Chem.* **14**, 2755–2775 (2007).
5. Mokrab, Y. *et al.* Exploring ligand recognition and ion flow in comparative models of the human GABA type A receptor. *J. Mol. Graph. Model.* **26**, 760–774 (2007).
6. Ci, S., Ren, T. & Su, Z. Investigating the putative binding-mode of GABA and diazepam within $GABA_A$ receptor using molecular modeling. *Protein J.* **27**, 71–78 (2008).
7. Berezhnoy, D., Gibbs, T.T. & Farb, D.H. Docking of 1,4-benzodiazepines in the α1/γ2 $GABA_A$ receptor modulator site. *Mol. Pharmacol.* **76**, 440–450 (2009).
8. Sancar, F., Ericksen, S.S., Kucken, A.M., Teissére, J.A. & Czajkowski, C. Structural determinants for high-affinity zolpidem binding to $GABA_A$ receptors. *Mol. Pharmacol.* **71**, 38–46 (2007).
9. Evers, A., Gohlke, H. & Klebe, G. Ligand-supported homology modelling of protein binding-sites using knowledge-based potentials. *J. Mol. Biol.* **334**, 327–345 (2003).
10. Krissinel, E. & Henrick, K. Secondary-structure matching (SSM), a new tool for fast protein structure alignment in three dimensions. *Acta Crystallogr. D Biol. Crystallogr.* **60**, 2256–2268 (2004).
11. Rarey, M., Kramer, B., Lengauer, T. & Klebe, G. A fast flexible docking method using an incremental construction algorithm. *J. Mol. Biol.* **261**, 470–489 (1996).
12. Moitessier, N., Englebienne, P., Lee, D., Lawandi, J. & Corbeil, C.R. Towards the development of universal, fast and highly accurate docking/scoring methods: a long way to go. *Br. J. Pharmacol.* **153** (suppl 1): S7–S26 (2008).
13. Claussen, H., Buning, C., Rarey, M. & Lengauer, T. FlexE: efficient molecular docking considering protein structure variations. *J. Mol. Biol.* **308**, 377–395 (2001).
14. Chema, D., Eren, D., Yayon, A., Goldblum, A. & Zaliani, A. Identifying the binding mode of a molecular scaffold. *J. Comput. Aided Mol. Des.* **18**, 23–40 (2004).
15. Wang, R., Lai, L. & Wang, S. Further development and validation of empirical scoring functions for structure-based binding affinity prediction. *J. Comput. Aided Mol. Des.* **16**, 11–26 (2002).
16. Labute, P. The generalized Born/volume integral implicit solvent model: estimation of the free energy of hydration using London dispersion instead of atomic surface area. *J. Comput. Chem.* **29**, 1693–1698 (2008).
17. Duncalfe, L.L., Carpenter, M.R., Smillie, L.B., Martin, I.L. & Dunn, S.M. The major site of photoaffinity labeling of the γ-aminobutyric acid type A receptor by [^{3}H]flunitrazepam is histidine 102 of the α subunit. *J. Biol. Chem.* **271**, 9209–9214 (1996).
18. Berezhnoy, D. *et al.* On the benzodiazepine binding pocket in $GABA_A$ receptors. *J. Biol. Chem.* **279**, 3160–3168 (2004).

19. Wieland, H.A., Lüddens, H. & Seeburg, P.H. A single histidine in $GABA_A$ receptors is essential for benzodiazepine agonist binding. *J. Biol. Chem.* **267**, 1426–1429 (1992).
20. Davies, M., Bateson, A.N. & Dunn, S.M. Structural requirements for ligand interactions at the benzodiazepine recognition site of the $GABA_A$ receptor. *J. Neurochem.* **70**, 2188–2194 (1998).
21. Buhr, A., Schaerer, M.T., Baur, R. & Sigel, E. Residues at positions 206 and 209 of the α1 subunit of γ-aminobutyric $acid_A$ receptors influence affinities for benzodiazepine binding site ligands. *Mol. Pharmacol.* **52**, 676–682 (1997).
22. Sawyer, G.W., Chiara, D.C., Olsen, R.W. & Cohen, J.B. Identification of the bovine γ-aminobutyric acid type A receptor α subunit residues photolabeled by the imidazobenzodiazepine [^{3}H]Ro15–4513. *J. Biol. Chem.* **277**, 50036–50045 (2002).
23. Tan, K.R. *et al.* Proximity-accelerated chemical coupling reaction in the benzodiazepine-binding site of γ-aminobutyric acid type A receptors: superposition of different allosteric modulators. *J. Biol. Chem.* **282**, 26316–26325 (2007).
24. Sigel, E., Schaerer, M.T., Buhr, A. & Baur, R. The benzodiazepine binding pocket of recombinant α1β2γ2 γ-aminobutyric $acid_A$ receptors: relative orientation of ligands and amino acid side chains. *Mol. Pharmacol.* **54**, 1097–1105 (1998).
25. Buhr, A., Baur, R. & Sigel, E. Subtle changes in residue 77 of the γ subunit of α1β2γ2 $GABA_A$ receptors drastically alter the affinity for ligands of the benzodiazepine binding site. *J. Biol. Chem.* **272**, 11799–11804 (1997).
26. Amin, J., Brooks-Kayal, A. & Weiss, D.S. Two tyrosine residues on the α subunit are crucial for benzodiazepine binding and allosteric modulation of γ-aminobutyric $acid_A$ receptors. *Mol. Pharmacol.* **51**, 833–841 (1997).
27. Derry, J.M.C., Dunn, S.M.J. & Davies, M. Identification of a residue in the γ-aminobutyric acid type A receptor α subunit that differentially affects diazepam-sensitive and -insensitive benzodiazepine site binding. *J. Neurochem.* **88**, 1431–1438 (2004).
28. Tan, K.R., Baur, R., Charon, S., Goeldner, M. & Sigel, E. Relative positioning of diazepam in the benzodiazepine-binding-pocket of $GABA_A$ receptors. *J. Neurochem.* **111**, 1264–1273 (2009).
29. Kucken, A.M., Teissére, J.A., Seffinga-Clark, J., Wagner, D.A. & Czajkowski, C. Structural requirements for imidazobenzodiazepine binding to $GABA_A$ receptors. *Mol. Pharmacol.* **63**, 289–296 (2003).
30. Huang, N., Shoichet, B.K. & Irwin, J.J. Benchmarking sets for molecular docking. *J. Med. Chem.* **49**, 6789–6801 (2006).
31. Mysinger, M.M. & Shoichet, B.K. Rapid context-dependent ligand desolvation in molecular docking. *J. Chem. Inf. Model.* **50**, 1561–1573 (2010).
32. Wolber, G. & Langer, T. LigandScout: 3-D pharmacophores derived from protein-bound ligands and their use as virtual screening filters. *J. Chem. Inf. Model.* **45**, 160–169 (2005).
33. Wei, B.Q., Baase, W.A., Weaver, L.H., Matthews, B.W. & Shoichet, B.K. A model binding site for testing scoring functions in molecular docking. *J. Mol. Biol.* **322**, 339–355 (2002).
34. Ramerstorfer, J. *et al.* The $GABA_A$ receptor α+β- interface: a novel target for subtype selective drugs. *J. Neurosci.* **31**, 870–877 (2011).
35. Popp, F.D., Parson, R. & Donigan, B.E. Synthesis of potential anticonvulsants: condensation of isatins with acetone and related ketones. *J. Pharm. Sci.* **69**, 1235–1237 (1980).
36. Marcou, G. & Rognan, D. Optimizing fragment and scaffold docking by use of molecular interaction fingerprints. *J. Chem. Inf. Model.* **47**, 195–207 (2007).
37. Korb, O., Stutzle, T. & Exner, T.E. Empirical scoring functions for advanced protein-ligand docking with PLANTS. *J. Chem. Inf. Model.* **49**, 84–96 (2009).
38. Mihic, S.J., Whiting, P.J., Klein, R.L., Wafford, K.A. & Harris, R.A. A single amino acid of the human γ-aminobutyric acid type A receptor γ2 subunit determines benzodiazepine efficacy. *J. Biol. Chem.* **269**, 32768–32773 (1994).
39. de Graaf, C. & Rognan, D. Selective structure-based virtual screening for full and partial agonists of the β2 adrenergic receptor. *J. Med. Chem.* **51**, 4978–4985 (2008).
40. Verheij, M.H. *et al.* Fragment library screening reveals remarkable similarities between the G protein-coupled receptor histamine H and the ion channel serotonin 5-HTA. *Bioorg. Med. Chem. Lett.* **21**, 5460–5464 (2011).
41. Venhorst, J., Nunez, S., Terpstra, J.W. & Kruse, C.G. Assessment of scaffold hopping efficiency by use of molecular interaction fingerprints. *J. Med. Chem.* **51**, 3222–3229 (2008).
42. Hibbs, R.E. & Gouaux, E. Principles of activation and permeation in an anion-selective Cys-loop receptor. *Nature* **474**, 54–60 (2011).
43. Michino, M. *et al.* Community-wide assessment of GPCR structure modelling and ligand docking: GPCR Dock 2008. *Nat. Rev. Drug Discov.* **8**, 455–463 (2009).
44. Larkin, M.A. *et al.* Clustal W and Clustal X version 2.0. *Bioinformatics* **23**, 2947–2948 (2007).
45. Shi, J., Blundell, T.L. & Mizuguchi, K. FUGUE: sequence-structure homology recognition using environment-specific substitution tables and structure-dependent gap penalties. *J. Mol. Biol.* **310**, 243–257 (2001).
46. Sali, A. & Blundell, T.L. Comparative protein modelling by satisfaction of spatial restraints. *J. Mol. Biol.* **234**, 779–815 (1993).
47. Sieghart, W. & Schuster, A. Affinity of various ligands for benzodiazepine receptors in rat cerebellum and hippocampus. *Biochem. Pharmacol.* **33**, 4033–4038 (1984).
48. Zhang, W., Koehler, K.F., Zhang, P. & Cook, J.M. Development of a comprehensive pharmacophore model for the benzodiazepine receptor. *Drug Des. Discov.* **12**, 193–248 (1995).

Acknowledgments

Financial support from the Doctoral Fellowship Programme of the Austrian Academy of Science (L.R.), the Austrian Science Fund grant P19653 (M.E.) and the European Commission Seventh Framework Programme grant HEALTH-F4-2008-202088 (W.S. and I.J.P.d.E.) is gratefully acknowledged. We also thank Inte:Ligand for providing us a free license for LigandScout 3.0 and Open Eye for an Omega license. We thank M. Mysinger and J. Irwin from the Shoichet laboratory for generating the focused 'benzodiazepine' decoy set. In addition we thank E. Sigel for helpful suggestions and discussions during generation of this work; M. Stojanovic for technical assistance in the binding assays; A. Chalikiopoulos and M. Verheij for assistance in fragment docking studies; and E. Urban, S. Haselmaier, J. König, H. Custers and A. van de Stolpe for providing HRMS and ^{1}H- and ^{13}C-NMR spectral data.

Author contributions

L.R., W.S., G.F.E., I.J.P.d.E., C.d.G. and M.E. contributed to the design and evaluation of experiments. Docking and virtual screening experiments were performed by L.R. (supervised by G.F.E.) and C.d.G. $GABA_AR$ models were generated and evaluated by M.E. and M.M. Radioligand and electrophysiological experiments were performed by Z.V. The manuscript was written by W.S., L.R., G.F.E., I.J.P.d.E., C.d.G. and M.E., and all authors commented on and helped to revise the text.

Competing financial interests

The authors declare no competing financial interests.

Additional information

Supplementary information and chemical compound information are available online at http://www.nature.com/naturechemicalbiology/. Reprints and permissions information is available online at http://www.nature.com/reprints/index.html. Correspondence and requests for materials should be addressed to M.E.

Supplementary Information

Diazepam-bound $GABA_A$ receptor models identify novel benzodiazepine site ligands

Lars Richter, Chris de Graaf, Werner Sieghart, Zdravko Varagic, Martina Mörzinger, Iwan J. P. de Esch, Gerhard F. Ecker, Margot Ernst

Nature Chemical Biology: doi:10.1038/nchembio.917

Supplementary Methods……..4

Nature Chemical Biology: doi:10.1038/nchembio.917

Nature Chemical Biology: doi:10.1038/nchembio.917

Supplementary Methods - Supplementary Schemes

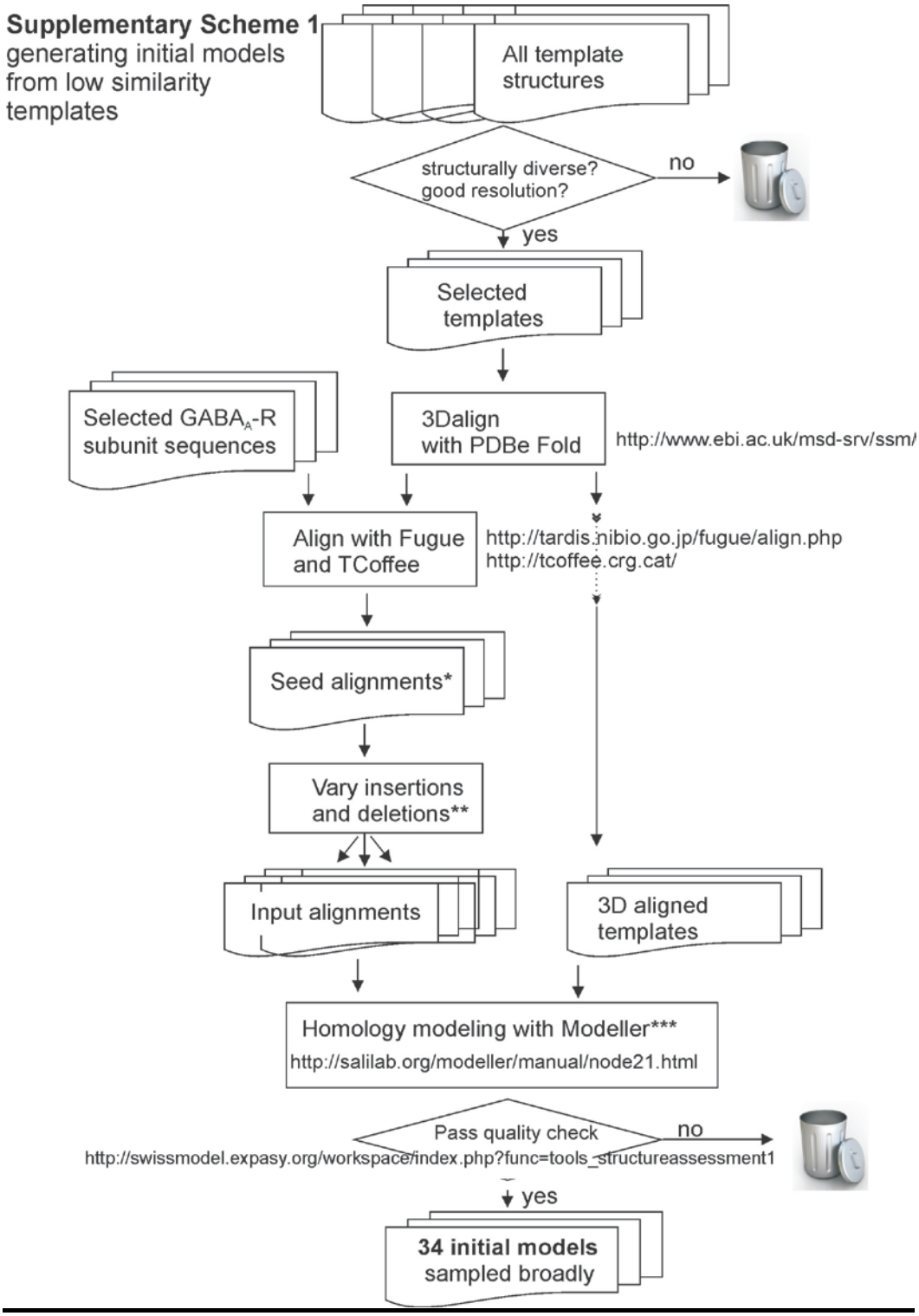

* In an initial step, the $GABA_A$ receptor sequences are aligned against each template structure with a sequence-to-structure alignment algorithm such as TCoffee[49] or FUGUE[50] yielding seed alignments.

** In the seed alignments, gap positions in variable regions are varied according to the User's Manual of Modeller[51], thus generating a variety of input alignments.

*** The standard homology modelling script supplied with the program is combined with one or more template structures and input alignments to generate the homology models.

Nature Chemical Biology: doi:10.1038/nchembio.917

Supplementary Scheme 2 – Model selection workflow

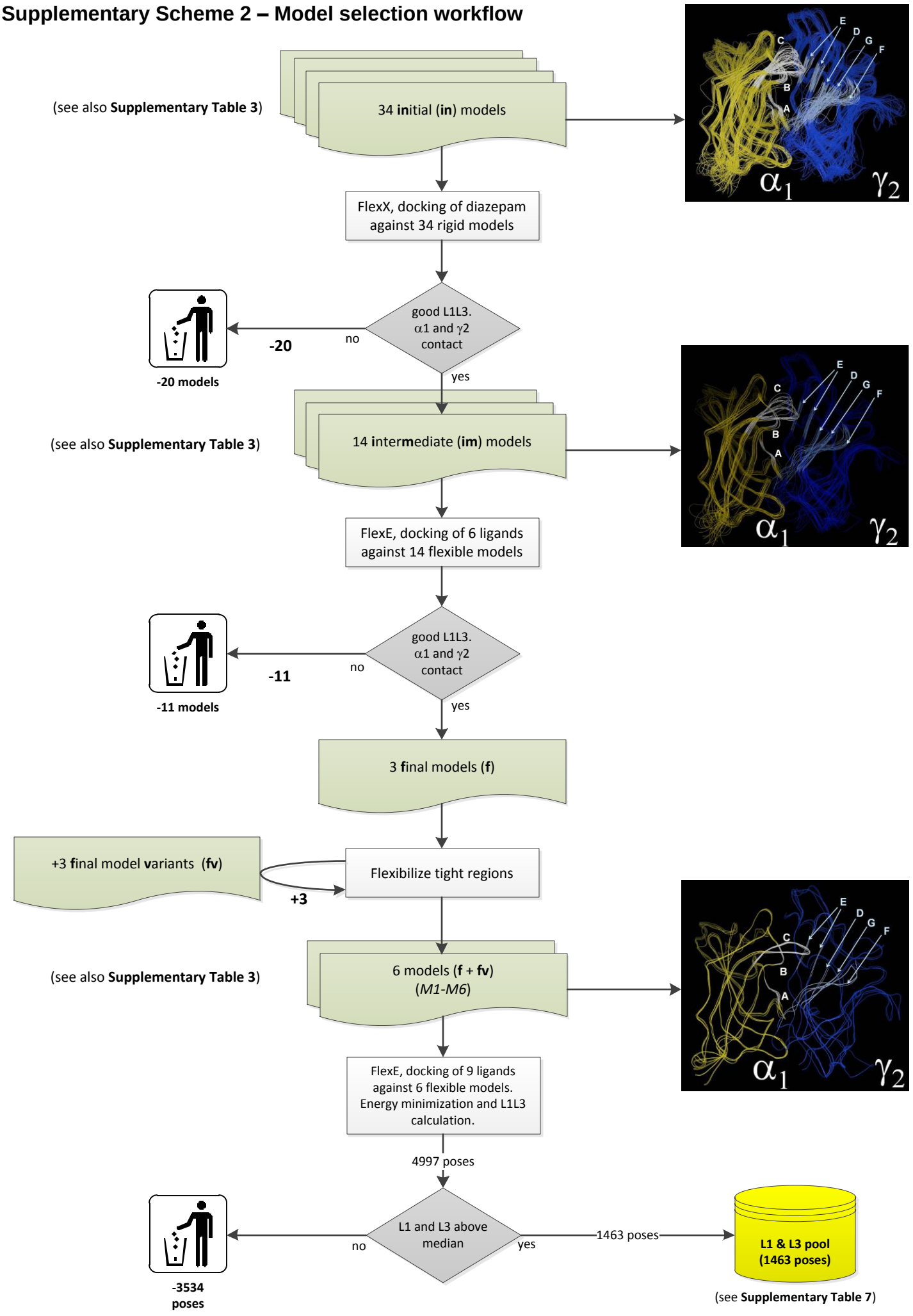

Nature Chemical Biology: doi:10.1038/nchembio.917

Supplementary Scheme 3 - Binding mode search

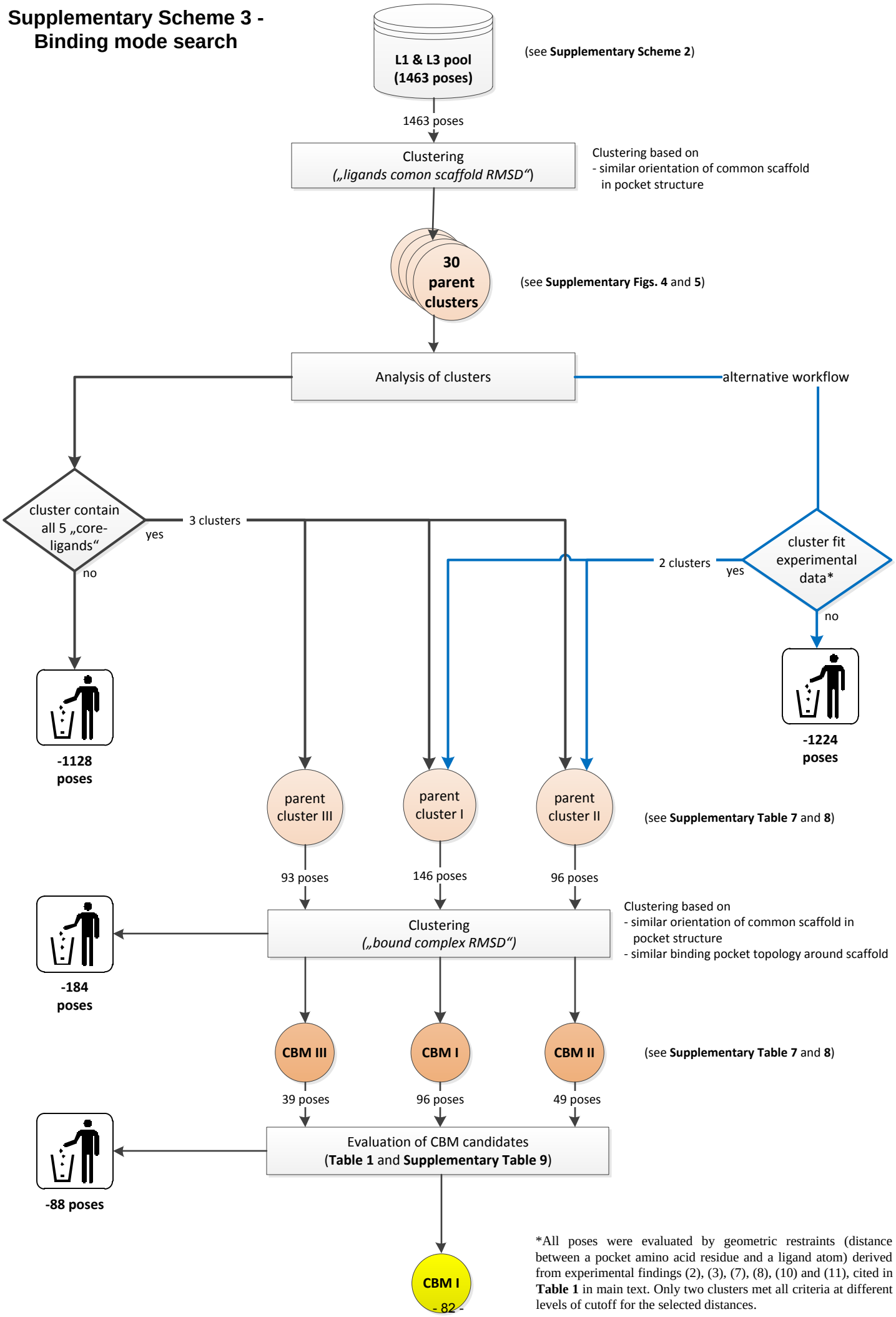

*All poses were evaluated by geometric restraints (distance between a pocket amino acid residue and a ligand atom) derived from experimental findings (2), (3), (7), (8), (10) and (11), cited in **Table 1** in main text. Only two clusters met all criteria at different levels of cutoff for the selected distances.

Nature Chemical Biology: doi:10.1038/nchembio.917

Supplementary Scheme 4 – Retrospective validation of CBMs by virtual screening

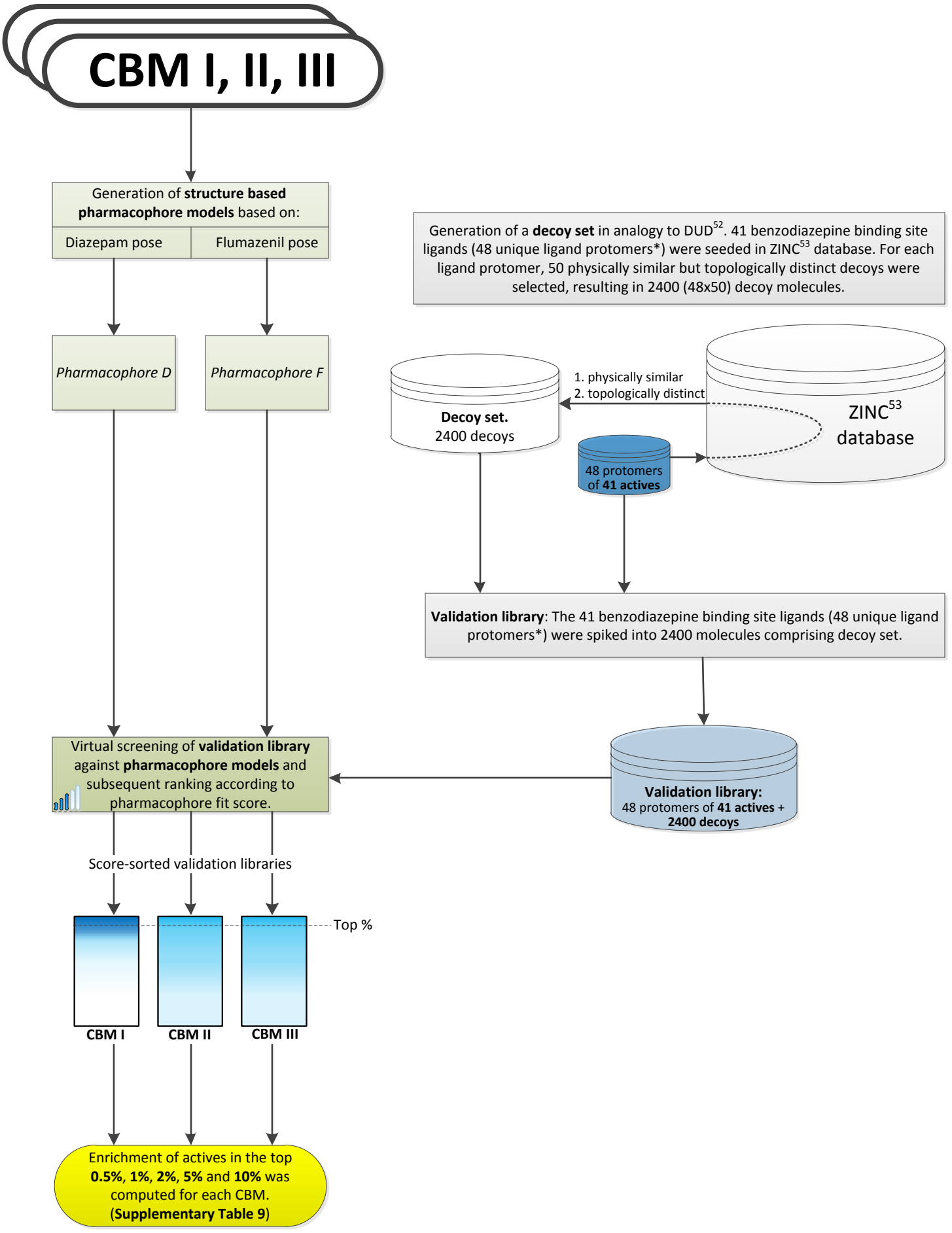

*As decoys were also property matched against net formal charge, for each of the 41 ligands all protonation states near pH 7.0 were generated, resulting in 48 unique ligand protomers. These 48 ligand protomers were seeded into the **ZINC-database** as well as into the **validation library**.

Nature Chemical Biology: doi:10.1038/nchembio.917

Supplementary Scheme 5 – CBM I binding hypotheses predict novel ligands

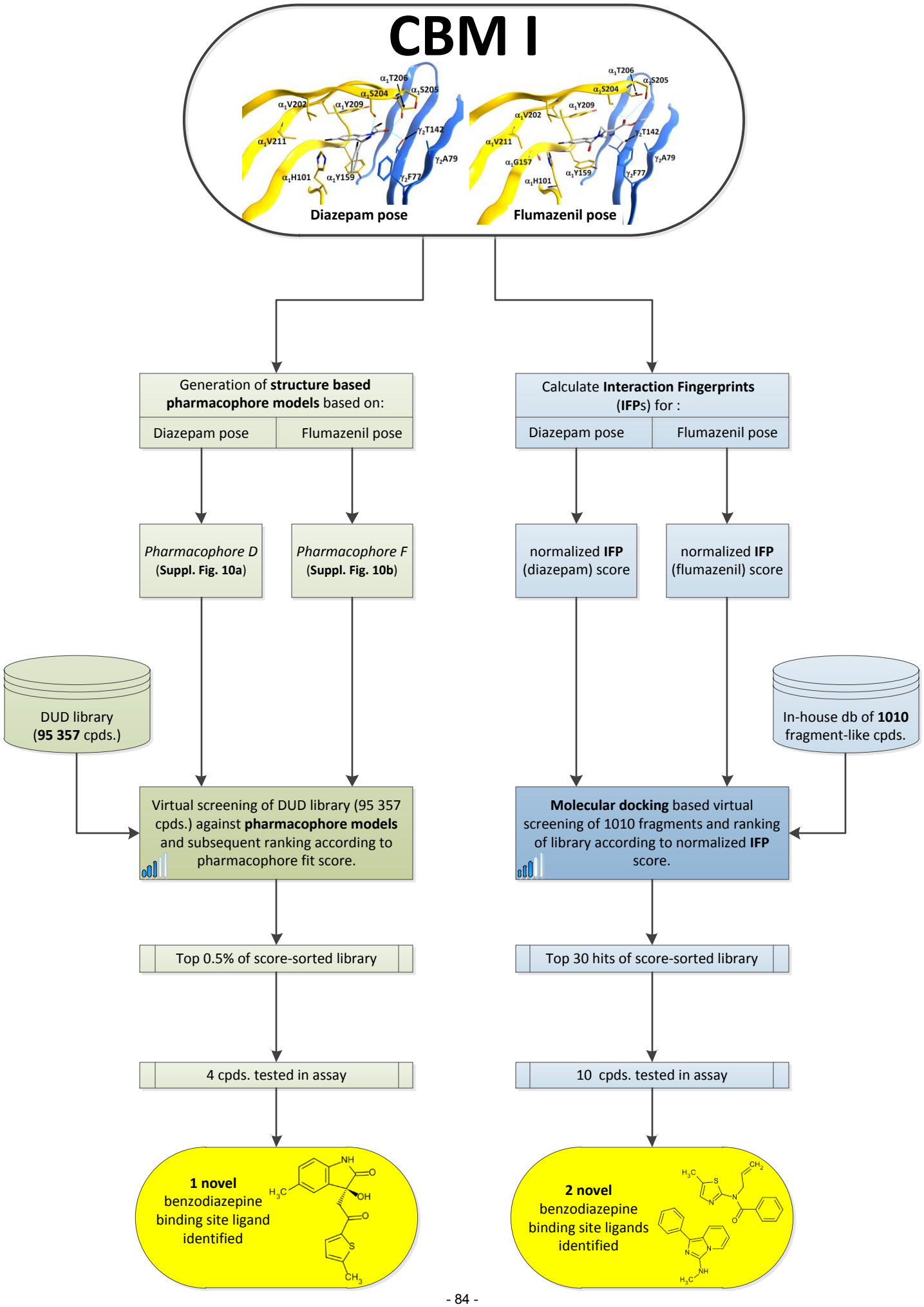

Nature Chemical Biology: doi:10.1038/nchembio.917

Supplementary Methods - Supplementary Tables

Supplementary Table 1– Templates used in model construction

PDB ID	*protein*	*ligand*
1I9B[54]	Lymnea AChBP	HEPES bound
1UW6[55]	Lymnea AChBP	nicotine bound
2BG9[56]	Torpedo nAChR	apo/ undefined
2BYN[57]	Aplysia AChBP	apo
2BYQ[57]	Aplysia AChBP	epibatidine bound
2BYR[57]	Aplysia AChBP	methyllycaconitine bound
2BYS[57]	Aplysia AChBP	lobeline bound
2QC1[58]	mouse nAChR alpha1 extracellular domain	alpha-bungarotoxin bound
3RIF[59]	Nematode glutamate gated chloride channel	glutamate

Templates up to and including 2QC1[58] were considered in the original study. The selection criteria were conformational diversity and resolution of the structures. Bacterial homologs released after 2QC1 were examined as the study progressed, and it was felt that models based on these would not alter the overall outcome. Upon revision, 3RIF[59]and related structures were also integrated in retrospect and found to be in good agreement with our model.

Nature Chemical Biology: doi:10.1038/nchembio.917

Supplementary Table 2 - Affinities of the two atropisomers/ enantiomers of 1,4-benzodiazepines at the BZ- binding site.

reference:	conformation M	conformation P
Salvadori et al. 1997[60]	annotation in ref: **cpd. 7a** affinity: 93 nM	annotation in ref: **cpd. 7b** affinity: 1750 nM
	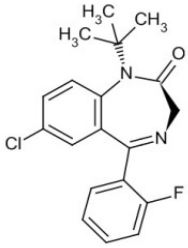	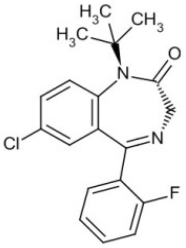
Gilman et al. 1990[61]	annotation in ref: **cpd. 11** affinity: 420 nM	annotation in ref: **cpd. 12** affinity: > 1000 nM
	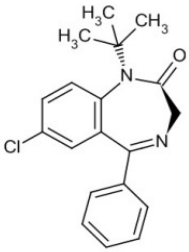	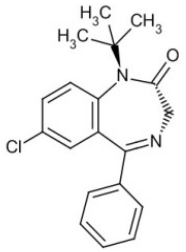
Gilman et al. 1993[62]	annotation in ref: **cpd. 31a** affinity: 26.5 nM	annotaton in ref: **cpd. 31b** affinity: 540 nM
	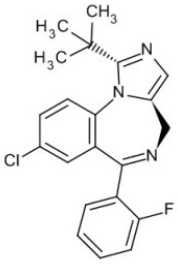	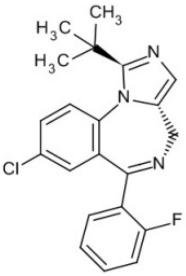
Gilman et al. 1993[62]	annotation in ref: **cpd. 25a** affinity: 7 nM	annotation in ref: **cpd. 25b** affinity: 220 nM
	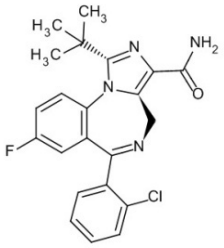	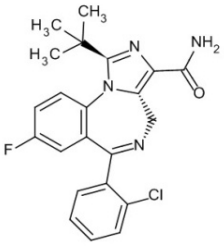
Lee at al. 2008[63]	annotation in ref: **1a-R** affinity: 46 nM	annotation in ref: **1a-S** affinity: 2320 nM
	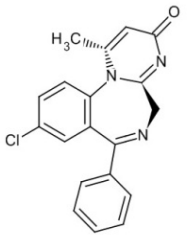	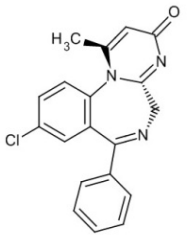

Nature Chemical Biology: doi:10.1038/nchembio.917

reference:	conformation M	conformation P
Blount et al. 1983[64]	annotation in ref: **5** affinity: 6.4 nM	annotation in ref: **6** affinity: 2320 nM
	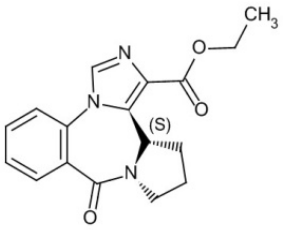	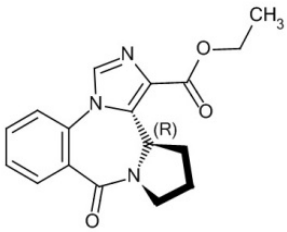

In principle two 1,4-diazepine ring conformations are energetically plausible for 1,4-benzodiazepines (**conformation M** and **conformation P,** see also **Supplementary Fig. 2**) and are hence present in small molecule crystal structures (CSD reference code: ANIXAX, FLDAZP).A literature search provides strong and coherent evidence that **conformation M** of the 7-ring is present in the high affinity bound-state complex of 1,4-benzodiazepines in the benzodiazepine binding site of $GABA_A$receptors. Gilman et al.[61,62] and Salvadori et al.[60] applied a selective synthetic procedure that leads to stable 1,4-benzodiazepines in either **conformation M** or **conformation P**. The interconversion of the synthesized molecules into the other 7-ring conformation was hindered by a bulky tert-butyl group either at N1 (1,4-benzodiazepines) or C1' (imidazobenzodiazepines). Lee et al.[63] used a different approach to isolate atropisomers of 1,4-benzodiazepines. They first synthesized pyrimido[1,2-a][1,4]-benzodiazepines that have a high interconversion energy. After synthesis, the racemat of pyrimido[1,2-a][1,4]-benzodiazepines (containing both, **conformation M** and **conformation P**) was then separated on a chiral column. Blount et al.[64] synthesized pyrroloimidazobenzodiazepines that were constrained to **conformation M** (S enantiomer) or **conformation P** (R enantiomer) by ring annelation. The isolated atropisomers/enantiomers deriving from either synthesis or chiral separation, were then tested in radio-ligand binding assays. The experiments clearly demonstrate that compounds in the **conformation M** exhibit a much higher affinity for the $GABA_A$ receptor benzodiazepine site than compounds in **conformation P**. Furthermore, studies based on 3-substituted 1,4-benzodiazepines came to the same conclusion that **conformation M** is the 1,4-diazepine conformation [64-66] in the high affinity bound-state complex.

Nature Chemical Biology: doi:10.1038/nchembio.917

Supplementary Methods - Supplementary Figures

Supplementary Fig. 1 – Variable alignment portions of the alignments used for M1-6. The alignment is based on a multi sequence alignment as presented previously[67]. The different templates were aligned using the SSM server[68], and the sequence alignment adjusted to the 3D alignment where needed. The sequence to structure alignments in the variable regions were initially made by Fugue[50], and additional variants were made as suggested in[51]. The relevant variable segments are shown here for those models, from which the final pose pool was derived. For the pre-loop E region, that has an indirect influence on pocket volume, the final alignments to 2BYQ and 2QC1 are indicated. For loop F all variants that were used in the final models are also shown. Only one loop C variant entered the final model pool. It should be noted that the alignment based restraints do not restrain the pocket geometry beyond the initial model building step, and thus do not strongly enter the final conformations seen in the energy minimized poses. M1 and M2 are based on the same choice of templates and alignment, so are M3 and M4, as well as M5 and M6.

Gamma subunit, minus side variable segments: pre-loop E and loop F:

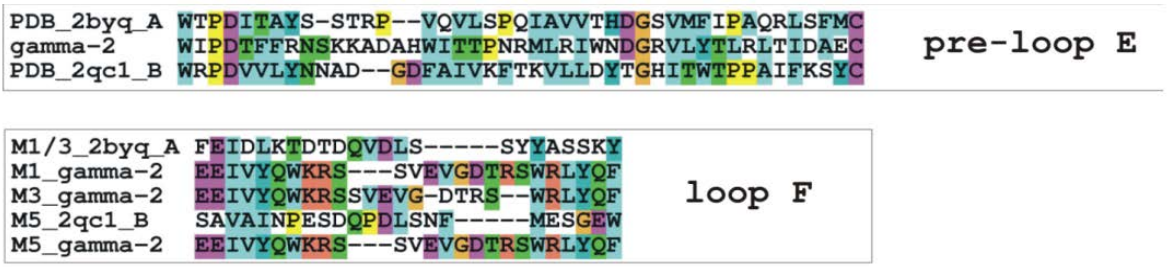

Full alignment for the gamma subunit, M1-6:

```
PDB_2byq_A      DDDD-KLHSQAN---LMRLKSDLFNR------SPMY-PGP----T--KDDPLTVTLGFTL
gamma-2         QKSDD-DYEDYASNKTWVLTPKVPEGDVTVILNNLLEGYDNKLRPDIGVKPTLIHTDMYV
PDB_2qc1_B      -KSE---HET-------RLEAKLFED----YSS-VVRPVEDH-----RE-IVQVTVGLQL


PDB_2byq_A      QDIVKADSSTNEVDLVYYEQQRWKLNSLMWDPNEYGNITDFRTSAADIWTPDITAYSSTR
gamma-2         NSIGPVNAINMEYTIDIFFAQTWYDRRLKFNSTI-KVLRLNSNMVGKIWIPDTFFRNSKK
PDB_2qc1_B      IQLINVDEVNQIVTTNVRLKQQWVDYNLKWNPDDYGGVKKIHIPSEKIWRPDVVLYNNAD


PDB_2byq_A       --PVQVL-SPQIAVVTHDGSVMFIPAQRLSFMCD---PTGVDSEEGATCAVKFGSWVYSG
gamma-2          ADAHWITTPNRMLRIWNDGRVLYTLRLTIDAECQLQLHN--FPMDEHSCPLEFSSYGYPR
PDB_2qc1_B       GDFAIVKFT--KVLLDYTGHITWTPPAIFKSYCE-IIVTH-FPFDEQNCSMKLGTRTYDG


PDB_2byq_A       FEIDLKTD--TDQV-DLSSYYASSKYEILSATQTRQVQHYSCCP-EPYIDVNLVVKFRER
gamma-2          EEIVYQWKRSSVEVGDTRSWR-LYQFSFVGLRNTTEVVKTTSG---DYVVMSVYFDLSRR
PDB_2qc1_B       SAVAINPE--SDQP-DLSNFMESGEWVIKEARGWKHWVFYSCCPTTPYLDITYHFVMQRL
```


Nature Chemical Biology: doi:10.1038/nchembio.917

Alpha subunit, plus side variable segment: loop C:

Full alignment for the alpha subunit, M1-6:

```
PDB_2byq_A      ------DDDD--KLHSQANLMRLKSDLFNR-SPMY-PGPT--KDDPLTVTLGFTLQDIVK
PDB_1uw6_A      ----EFDRAD--ILYNIRQ--TSRPDVIP----------TQRDR-PVAVSVSLKFINILE
alpha-1         QPSQ-DELKDNTTVFTR-----ILDRLLDGYDNRLR---PGLGERVTEVKTDIFVTSFGP


PDB_2byq_A      ADSSTNEVDLVYYEQQRWKLNSLMWDPNEYGNITDFRTSAADIWTPDITAYSSTR--PVQ
PDB_1uw6_A      VNEITNEVDVVFWQQTTWSDRTLAWNSS--HSPDQVSVPISSLWVPDLAAYNAIS--KPE
alpha-1         VSDHDMEYTIDVFFRQSWKDERLKFKGPM-TVLRLNNLMASKIWTPDTFFHNGKKSVAHN


PDB_2byq_A      VL-SPQIAVVTHDGSVMFIPAQRLSFMCDPTG--VDSEEGATCAVKFGSWVYSGFEIDLK
PDB_1uw6_A      VL-TPQLARVVSDGEVLYMPSIRQRFSCDVSG--VDTESGATCRIKIGSWTHHSREISVD
alpha-1         MTMPNKLLRITEDGTLLYTMRLTVRAECPMHLED-FPMDAHACPLKFGSYAYTRAEVVYE


PDB_2byq_A      TD---TDQV--DLSSYYASSKYEILSATQTRQVQHYSCCPEPYIDVNLVVKFRERR--
PDB_1uw6_A      PT---T-ENSDDSEYFSQYSRFEILDVTQKKNSVTYSCCPEAYEDVEVSLNFRKKGRS
alpha-1         WTREPARSVVVAE-DGSRLNQYDLLGQTVDSGIVQSS-TG-EYVVMTTHFHLKRKIG-
```

Below is a more up to date full alignment. The alignments used in this study can be derived by simply repositioning the gaps in the variable segments as indicated in the figure above. The full alignment is based on structural 3D alignment of the newest crystal structure[59] (PDB_3rif_A) with the templates used for this study, and the $GABA_A$ receptor subunits then aligned against the structural alignment data. Future modeling studies should consider the 3RIF and related structures when modeling $GABA_A$ receptors.

```
CLUSTAL X (1.83) multiple sequence alignment


PDB_2byq_A       -DDDD-KLHSQAN-----LMR---------LKSDLFNRSPMY--PGPTK---D-D--PLT
PDB_1uw6_A       ----------EFD-----RAD---------ILYNIRQ--TSRPDVIPTQ---R-DR-PVA
PDB_2qc1_B       ---------KSEH-----ETR---------LEAKLFED-Y-SSVVRPVE---DHRE-IVQ
PDB_3rif_A       ------------S-----DSK---------ILAHLFTSGY-DFRVRPPTD--N-GG-PVV
1uw6_A           ----------EFD-----RAD---------ILYNIRQ--TSRPDVIP----TQRDR-PVA
2byq_A           -DDDD-KLHSQAN-----LMR---------LKSDLFNR-SPMY-PGPT------KDDPLT
alpha-1          -QPSQDELKDNTT-----VFTR--------ILDRLLDG--YDNRLR-----PGLGERVTE
minu2byq_A       -DDDD-KLHSQAN-----LMR---------LKSDLFNR-SPMY-PGP----T--KDDPLT
minu2qc1_B       ---------KSE------HET--------RLEAKLFED-YSS-VVRPVEDH---RE-IVQ
gamma-2          QKSDD-DYEDYASNKTWVLTPKVPEGDVTVILNNLLEG--YDNKLR-----PDIGVKPTL
                                               :   :

PDB_2byq_A       VTLGFTLQDIVKADSSTNEVDLVYYEQQRWKLNSLMWD--PNEYGNITDFRTS---AADI
PDB_1uw6_A       VSVSLKFINILEVNEITNEVDVVFWQQTTWSDRTLAWN--SS--HSPDQVSVP---ISSL
PDB_2qc1_B       VTVGLQLIQLINVDEVNQIVTTNVRLKQQWVDYNLKWN--PDDYGGVKKIHIP---SEKI
PDB_3rif_A       VSVNMLLRTISKIDVVNMEYSAQLTLRESWIDKRLSYGVKGD--GQPDFVILTVGHQ--I
1uw6_A           VSVSLKFINILEVNEITNEVDVVFWQQTTWSDRTLAWN--SS--HSPDQVSVP---ISSL
2byq_A           VTLGFTLQDIVKADSSTNEVDLVYYEQQRWKLNSLMWD--PNEYGNITDFRTS---AADI
alpha-1          VKTDIFVTSFGPVSDHDMEYTIDVFFRQSWKDERLKFKGPM-TVLRLNNLMAS-----KI
minu2byq_A       VTLGFTLQDIVKADSSTNEVDLVYYEQQRWKLNSLMWD--PNEYGNITDFRTS---AADI
minu2qc1_B       VTVGLQLIQLINVDEVNQIVTTNVRLKQQWVDYNLKWN--PDDYGGVKKIHIP---SEKI
gamma-2          IHTDMYVNSIGPVNAINMEYTIDIFFAQTWYDRRLKFNSTI-KVLRLNSNMVG-----KI
```


Nature Chemical Biology: doi:10.1038/nchembio.917

```
                :  .: .  :   .              *    * :                    :

PDB_2byq_A      WTPDITAYSSTR--PVQVL-----SPQIAVVTHDGSVMFIPAQRLSFMCDPT------GV
PDB_1uw6_A      WVPDLAAYNAIS--KPEVL-----TPQLARVVSDGEVLYMPSIRQRFSCDVS------GV
PDB_2qc1_B      WRPDVVLYNNADGDFAIVK-----F-TKVLLDYTGHITWTPPAIFKSYCEIIVTHFPFD-
PDB_3rif_A      WMPDTFFPNEKQ--A-YKHTIDKPN-VLIRIHNDGTVLYSVRISLVLSCPMYLQYYPMD-
1uw6_A          WVPDLAAYNAIS--KPEVL-----TPQLARVVSDGEVLYMPSIRQRFSCDVSG------V
2byq_A          WTPDITAYSSTR--PVQVL-----SPQIAVVTHDGSVMFIPAQRLSFMCDPTG------V
alpha-1         WTPDTFFHNGKKSVAHNMT----MPNKLLRITEDGTLLYTMRLTVRAECPMHLED-----
minu2byq_A      WTPDITAYSSTR--PVQVL-----SPQIAVVTHDGSVMFIPAQRLSFMCDPTG------V
minu2qc1_B      WRPDVVLYNNADGDFAIVKFT------KVLLDYTGHITWTPPAIFKSYCEIIVTH-----
gamma-2         WIPDTFFRNSKKADAHWIT----TPNRMLRIWNDGRVLYTLRLTIDAECQLQLHN-----
                * **    .                    :   * : :         *

PDB_2byq_A      DSEEGATCAVKFGSWVYSGFEIDLKTD---TDQ--VDLSSYY-ASSK--YEILSATQTR-
PDB_1uw6_A      DTESGATCRIKIGSWTHHSREISVDPT---TENS-DDSEYFS-QYSR--FEILDVTQKK-
PDB_2qc1_B      ----EQNCSMKLGTRTYDGSAVAINPE---SDQ--PDLSNFM-ESGE--WVIKEARGWK-
PDB_3rif_A      ----VQQCSIDLASYAYTTKDIEYLWK---EHSP-LQL-KVGLSSSLPSFQLTNTSTTYC
1uw6_A          DTESGATCRIKIGSWTHHSREISVDPT--T-ENS-DDSEYFS-QYSR--FEILDVTQKK-
2byq_A          DSEEGATCAVKFGSWVYSGFEIDLKTD---TDQV--DLSSYY-ASSK--YEILSATQTR-
alpha-1         FPMDAHACPLKFGSYAYTRAEVVYEWT---REPARSVVVAE-DGSRLNQYDLLGQTVDS-
minu2byq_A      DSEEGATCAVKFGSWVYSGFEIDLKTD---TDQV--DLSSYY-ASSK--YEILSATQTR-
minu2qc1_B      FPFDEQNCSMKLGTRTYDGSAVAINPE---SDQP--DLSNFM-ESGE--WVIKEARGWK-
gamma-2         FPMDEHSCPLEFSSYGYPREEIVYQWKRS------SVEVG-DTRSWR-LYQFSFVGLRNT
                       * :.:.:  :    :                         : :

PDB_2byq_A      QVQHYSCC-P-EPYIDVNLVVKFRER-R--------------------------------
PDB_1uw6_A      NSVTYSCC-P-EAYEDVEVSLNFRKK-GRS------------------------------
PDB_2qc1_B      HWVFYSCCPT-TPYLDITYHFVMQRL-P--------------------------------
PDB_3rif_A      T-SVTNT----GIYSCLRTTIQLKREFSFYLLQLYIPSCMLVIVSWVSFWFDRTAIPARV
1uw6_A          NSVTYSCC-P-EAYEDVEVSLNFRKK-GRS------------------------------
2byq_A          QVQHYSCC-P-EPYIDVNLVVKFRER-R--------------------------------
alpha-1         -GIVQSS-TG--EYVVMTTHFHLKRKIG--------------------------------
minu2byq_A      QVQHYS-CCP-EPYIDVNLVVKFRER-R--------------------------------
minu2qc1_B      HWVFYS-CCPTTPYLDITYHFVMQRLP---------------------------------
gamma-2         TEVVKTT-SG--DYVVMSVYFDLSRRMG--------------------------------
                     .      *  :   . : .
```


Nature Chemical Biology: doi:10.1038/nchembio.917

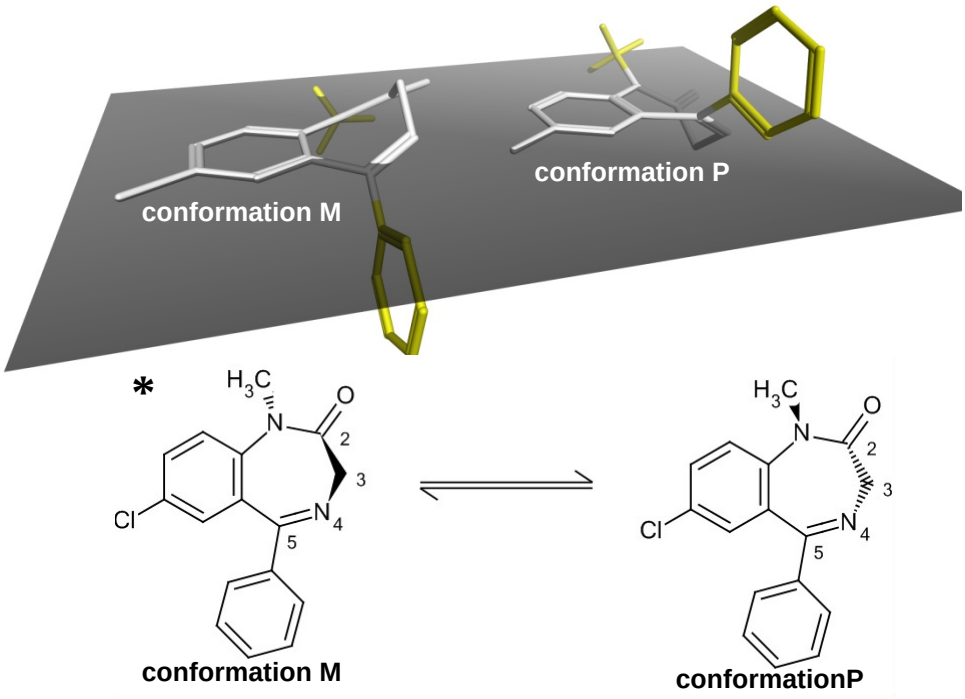

Supplementary Fig. 2 - Depiction of the two possible 1,4-diazepine conformations in 5-aryl-1,4-benzodiazepines. The two conformations can be distinguished by the dihedral angle of the atoms C2-C3-N4-C5. Conformation M (Minus) has a negative dihedral angle while conformation P (Positive) has a positive angle. A plethora of evidence summarized in **Supplementary Table 2** showed that **conformation M** of the 7-ring is present in the high affinity bound-state complex of 1,4-benzodiazepines in the benzodiazepine binding site of $GABA_A$ receptors.

***Natta projection** was used for illustrative issues and does not indicate stereochemistry. Solid or dashed wedged bonds represent bonds pointing above-the-plane or below-the-plane of the fused benzene ring of 1,4-benzodiazepines, respectively

Nature Chemical Biology: doi:10.1038/nchembio.917

Supplementary Methods - Supplementary Text

Generation of the validation library (Bz-focused decoy set). The selection of decoys was accomplished with an automated decoy generator (M.M.Mysinger and John J. Irwin, unpublished results) in an analogous manner to the DUD[52]. First, 41 benzodiazepine binding site ligands (**Supplementary Table 10**) were seeded into the ZINC database[53]. Then ZINC compounds with Tanimoto coefficient (Tc) less than 0.5 (Daylight fingerprint) to any of the 41 ligands were selected, thus resulting in a subset of ZINC compounds that are topologically dissimilar to the ligands.

Next, for each of the 41 seed compounds, all protonation states near pH 7.0 were generated, resulting in 48 unique ligand protomers. For each of them, 50 decoy molecules that property-match with the ligand protomer were selected from the subset of the ZINC library. The following six physicochemical descriptors were used for property-matching: molecular weight, number of hydrogen bond acceptors, number of hydrogen bond donors, number of rotatable bonds, logP, and the net formal charge[69].

Thus for all 41 benzodiazepine binding site ligands, compromising 48 unique ligand protomers, 2400 (48x50) decoys that are physically similar but topologically distinct to the ligands, were generated. To generate finally the validation library, the 48 ligand protomers were added to the 2400 decoys (**Supplementary Scheme 4**).

Structure-based pharmacophore models. Pharmacophore models were created using LigandScout 3.0[70]. Feature specific feature ranges were 2.2 – 4.2 Angstrom for H Bond Donor and H Bond Acceptor, respectively. Detected pharmacophoric features which are also represented in **Fig. 1c** were set to obligatory features. Exclusion volumes coats were added, using an Alpha C distance of 2-7 A and an Alpha C exclusion tolerance of 1.75 A. In case a hydrophobic and an aromatic feature were detected, only the more specific (aromatic) was kept. For the remaining parameters default values were used.

Nature Chemical Biology: doi:10.1038/nchembio.917

Ligand-based pharmacophore models. The structure of diazepam was taken and the following features were assigned using LigandScout 3.0[70]: hydrophobic to the fused benzene ring (L1), hydrophobic to the pendant phenyl ring (L3), H-bond acceptor to the carbonyl oxygen atom (H1), and H-bond acceptor to the imino nitrogen atom (H2) (see also **Fig. 1c**, main text and below). For flumazenil, the pharmacophore feature assignment was as follows: hydrophobic to the fused benzene ring (L1), H-bond acceptor to the imidazo-nitrogen (H1) and H-bond acceptor to the carbonyl-oxygen (H2) (see also **Fig. 1c**, main text and below).

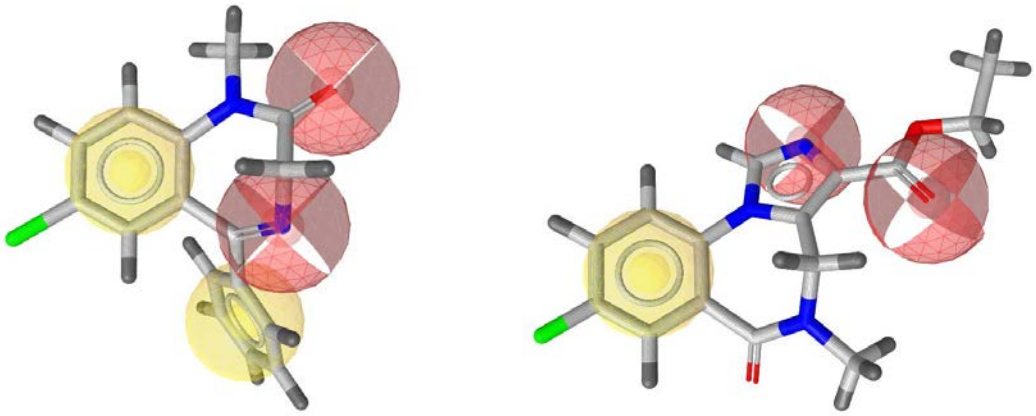

Depiction of assigned features (green = hydrophobic, red = H-bond acceptor) to the structures of diazepam (left) and flumazenil (right), respectively.

Nature Chemical Biology: doi:10.1038/nchembio.917

Compound characterization data

Characterization data for [3H]-Flunitrazepam:

[3H]-Flunitrazepam was purchased from PerkinElmer with a purity of greater than 97% as described by the vendor.

Characterization data for cpd. 8 (Ro15-8670):

High field ^{1}H NMR was performed for cpd. **8** (see p. 19), demonstrating high purity (>98%) and identity of cpd. **8**. HRMS C20H16ClN3O2: [M+1]calc: 366.8189 [M+1]found: 366.8191.

Characterization data for cpds. 15, 15a-c (active compounds)**:**

Compounds **15** and **15a-c** were ordered from Ambinter. High field ^{1}H NMR and ^{13}C NMR were performed for compounds **15** and **15a-c** (see p. 20-27), demonstrating high purity (>98%) and identity of the active compounds.

Characterization data for cpds. 15d-i, 16-18 (inactive compounds)**:**

Compounds **15d-i** and **18** were ordered from Ambinter, compounds **16** and **17** from Asinex. The inactive compounds **15d-i** and **16-18** had a purity of greater than 90% as described by the vendors.

Characterization data for cpds. 19 and 20 (active compounds)**:**

High field ^{1}H NMR and ^{13}C NMR was performed for cpd. **19** (p. 28 and 29). HRMS C14H14N3: [M+1]calc: 224.1187 [M+1]found: 224.1153. The purity of this compound was then verified in LCMS (see p. 30) analysis.

High field ^{1}H NMR and ^{13}C NMR was performed for cpd. **20** (p. 31 and 32). HRMS C14H15N2OS: [M+1]calc: 259.0905 [M+1]found: 259.0866. The purity of this compound was then verified in LCMS (see p. 33) analysis.

Nature Chemical Biology: doi:10.1038/nchembio.917

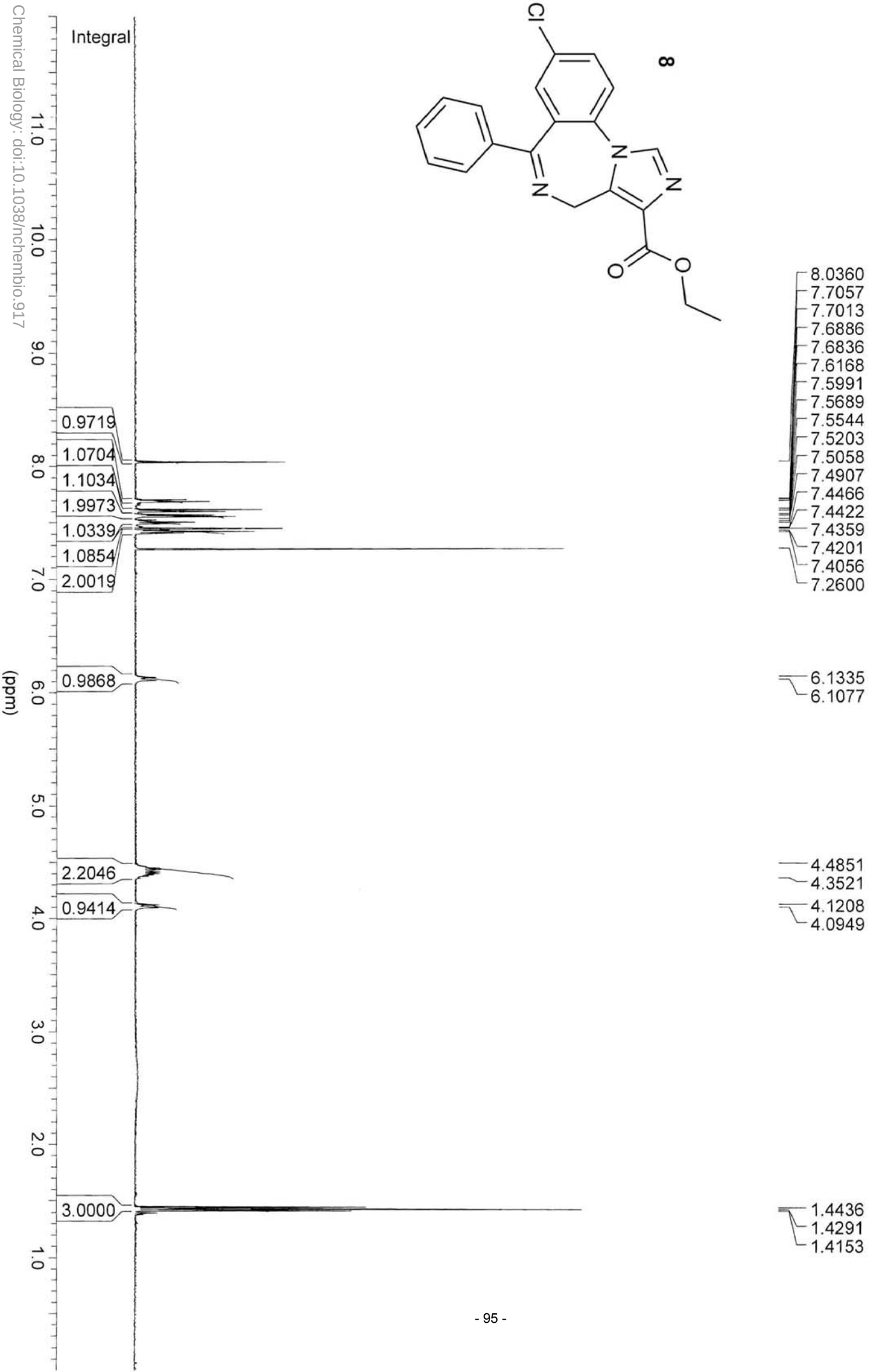

compound **15**: ^{1}H NMR (500 MHz, DMSO)

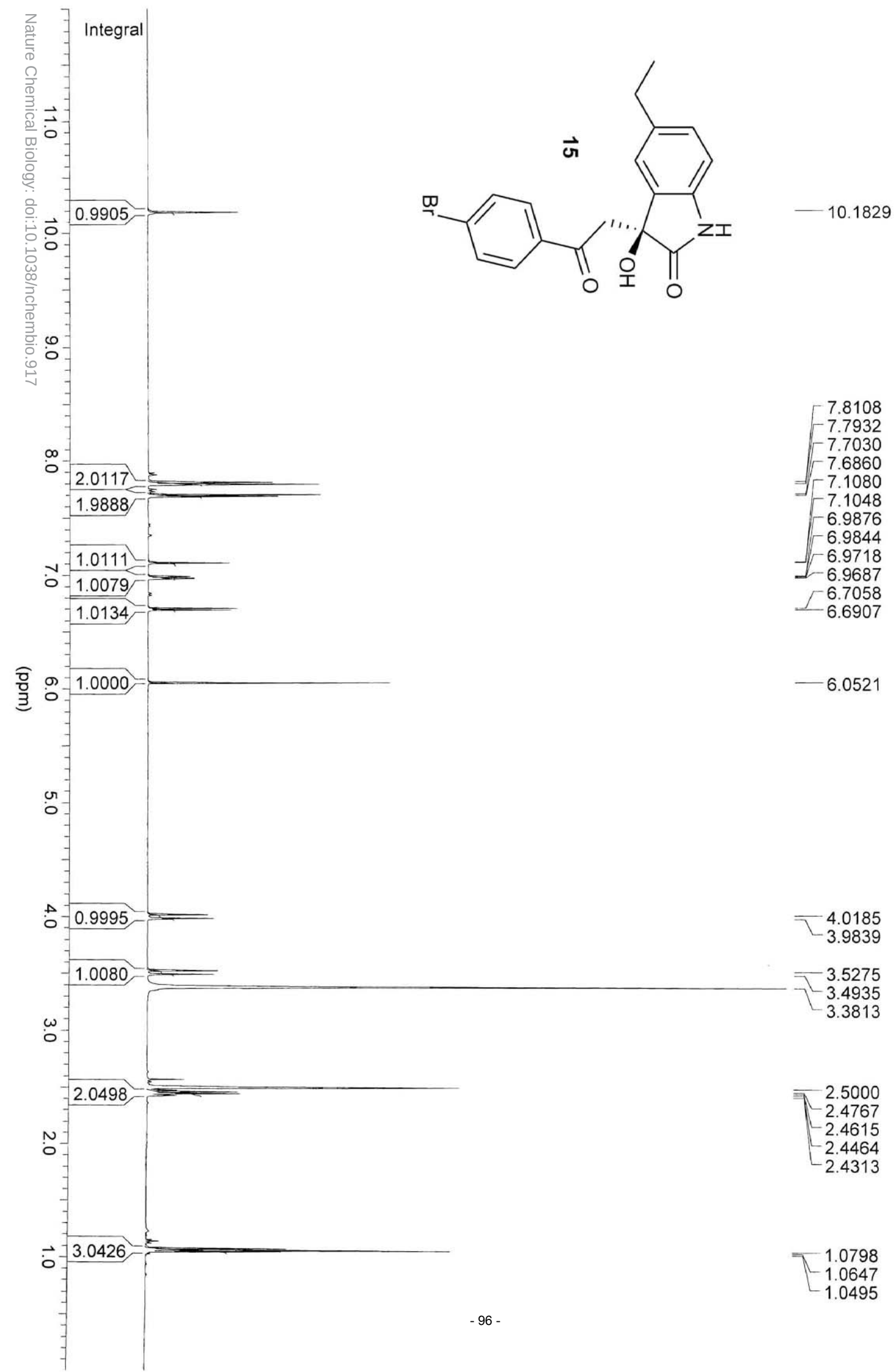

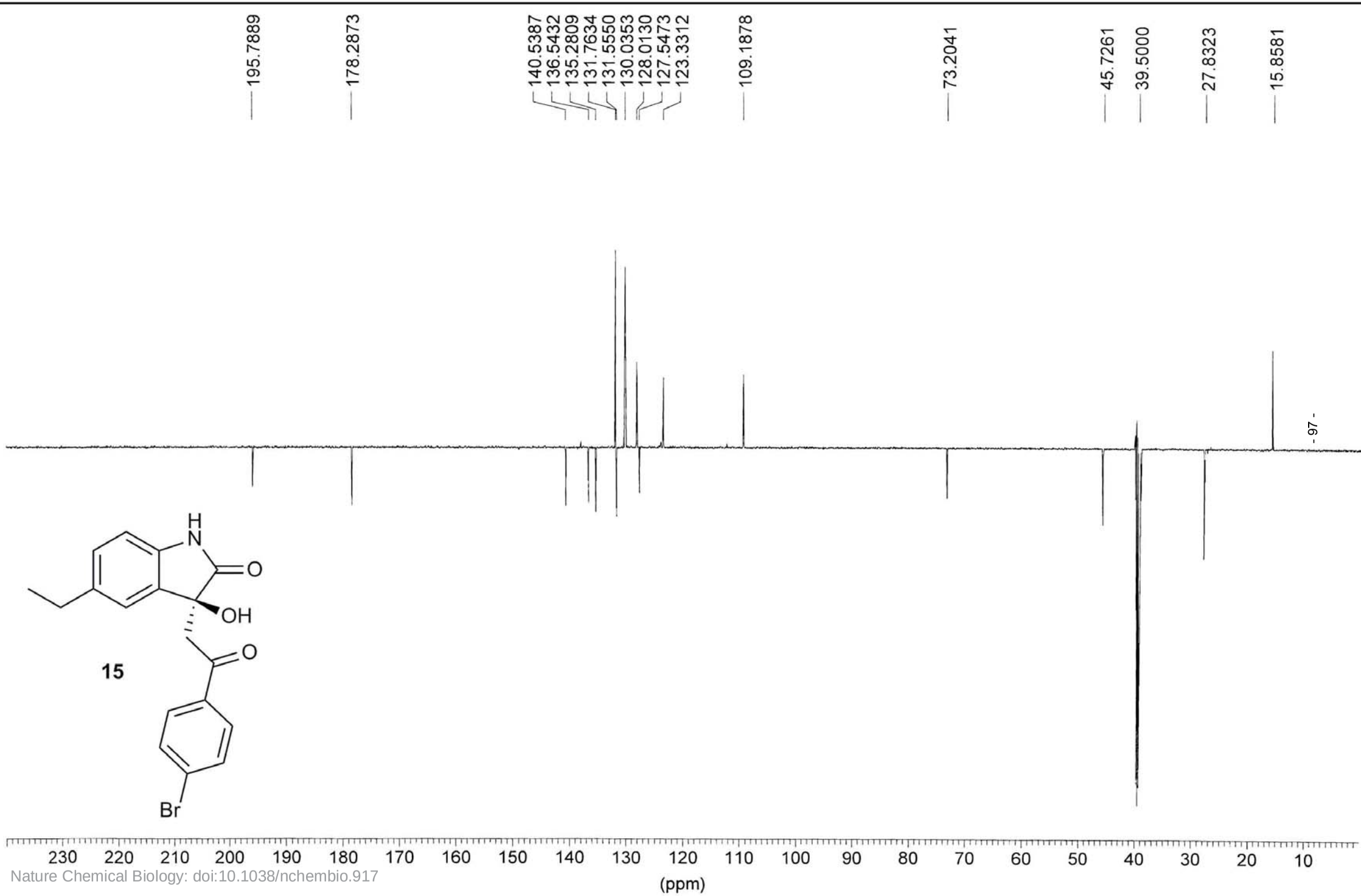

Nature Chemical Biology: doi:10.1038/nchembio.917

compound **15a**: ^{1}H NMR (500 MHz, DMSO)

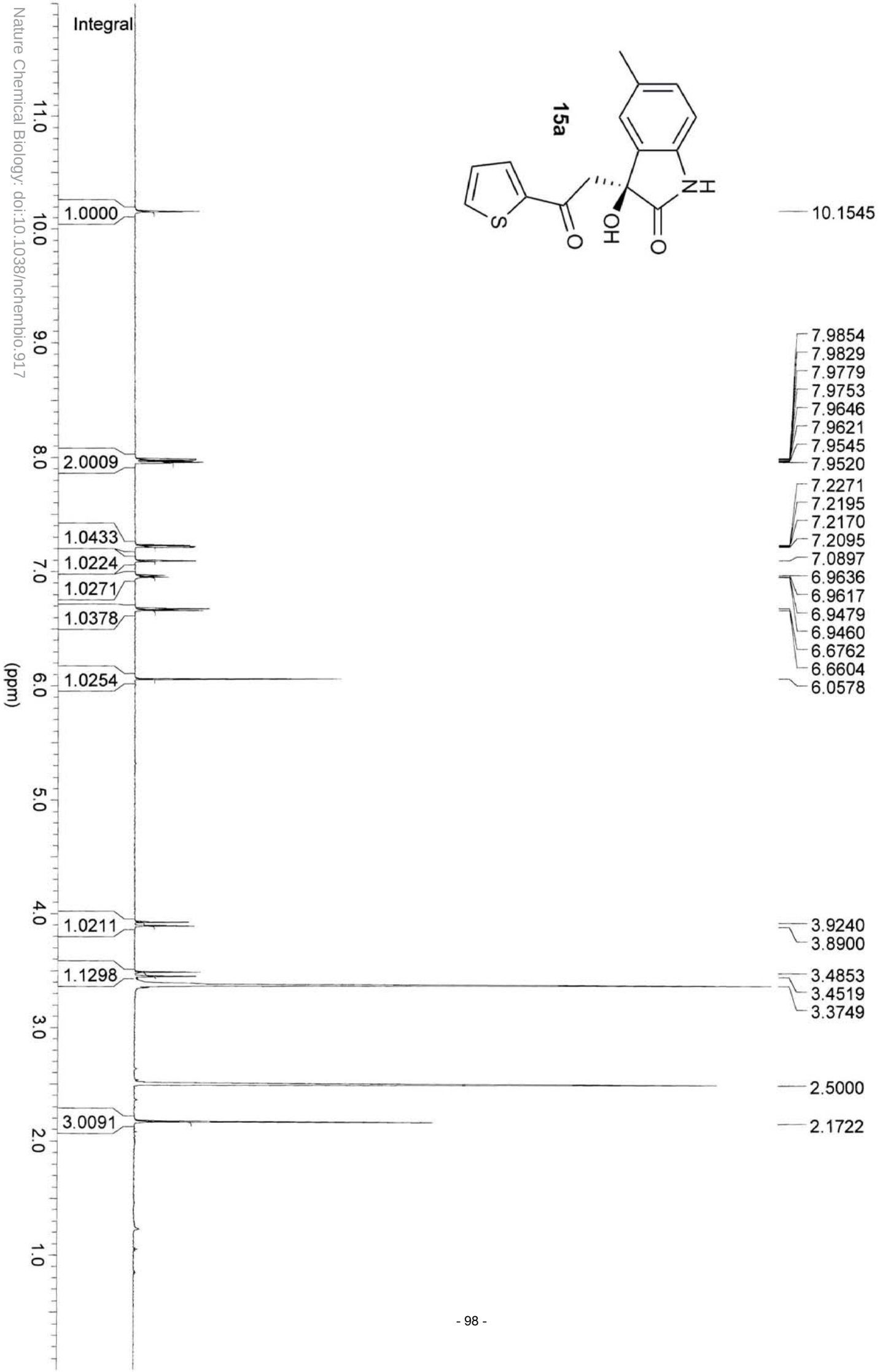

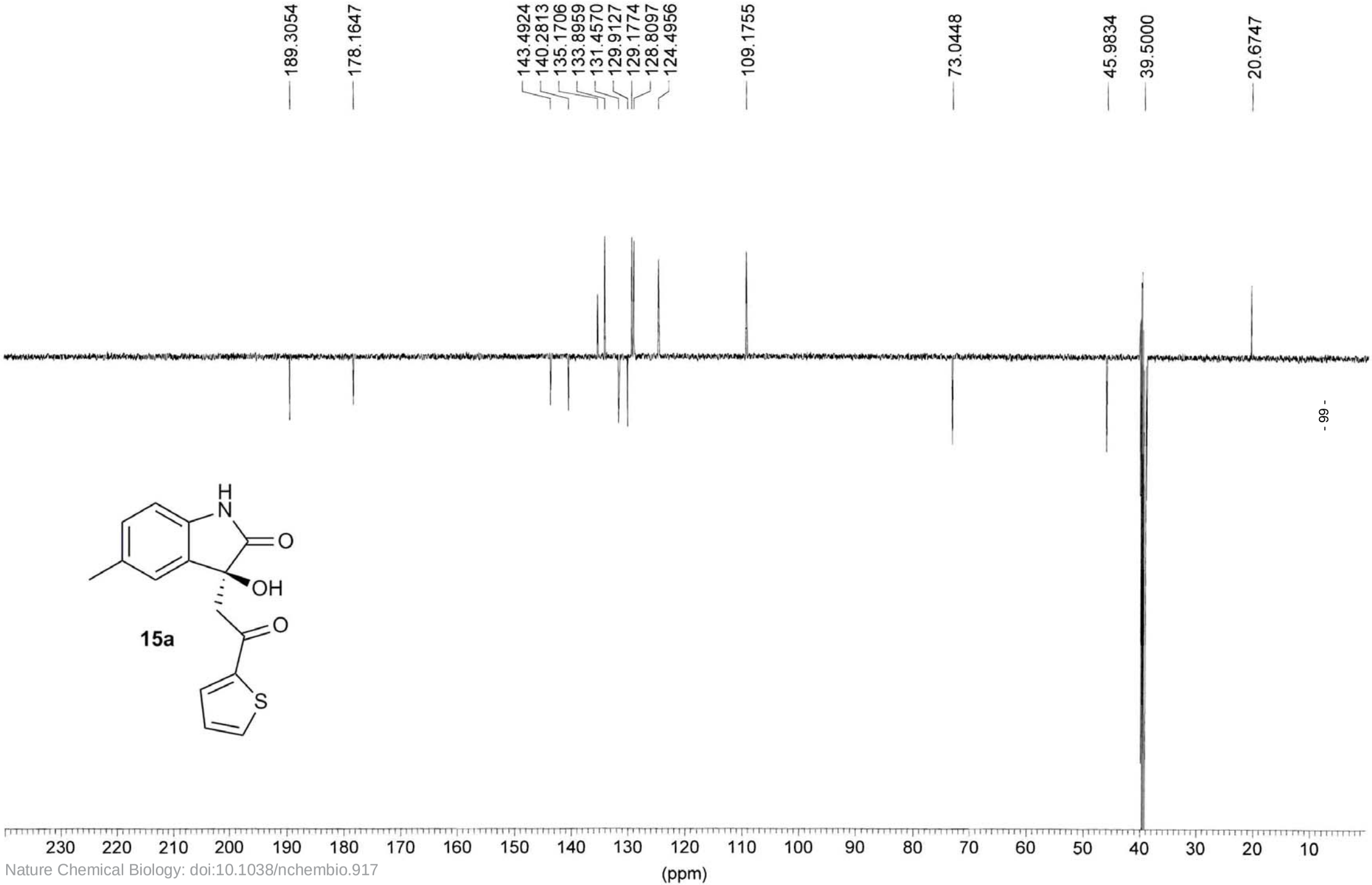

Nature Chemical Biology: doi:10.1038/nchembio.917

compound **15b**: ^{1}H NMR (500 MHz, DMSO)

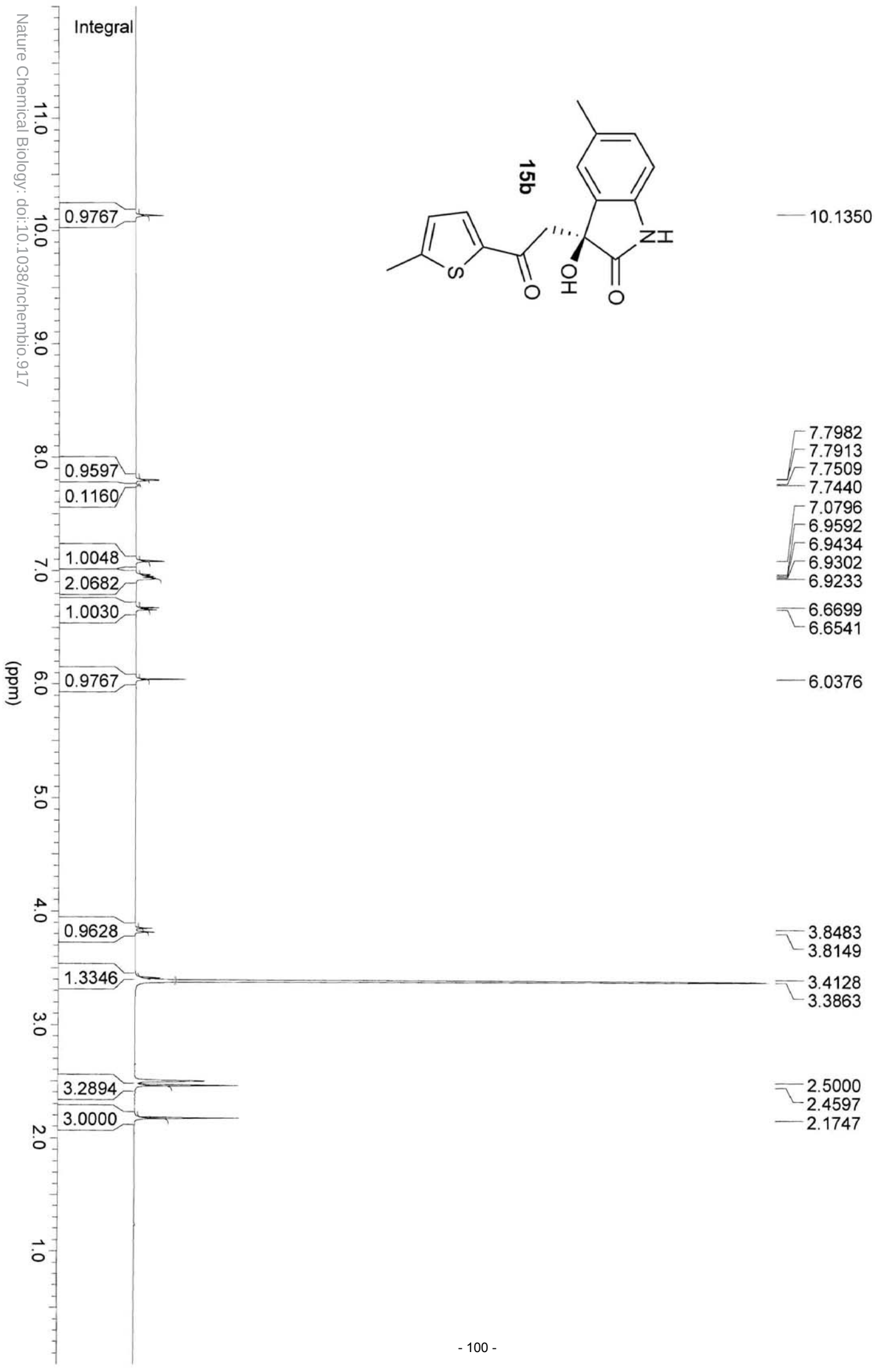

compound **15b**: ^{13}C NMR (125 MHz, DMSO)

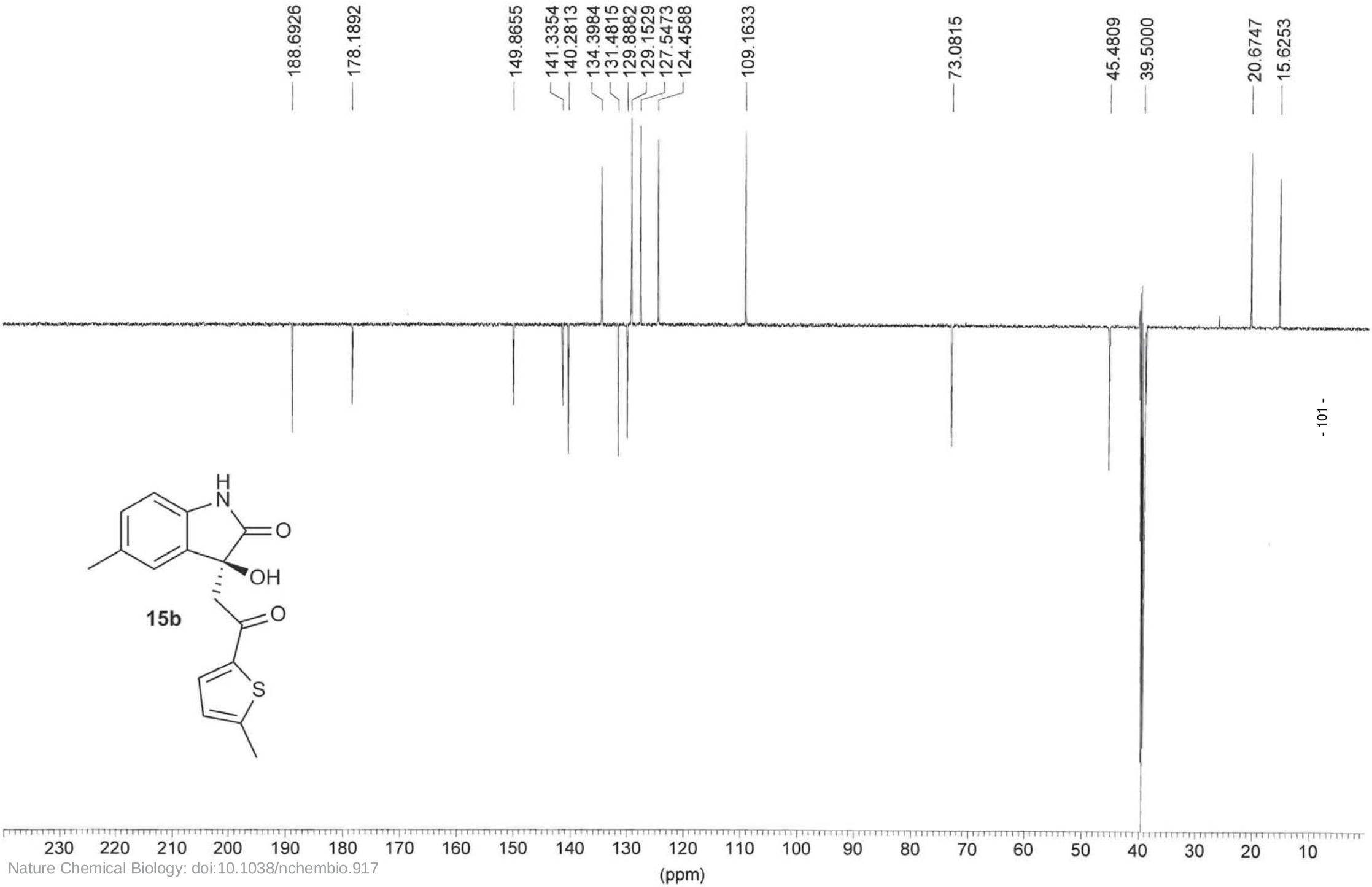

15b

Nature Chemical Biology: doi:10.1038/nchembio.917

compound **15c**: ^{1}H NMR (500 MHz, DMSO)

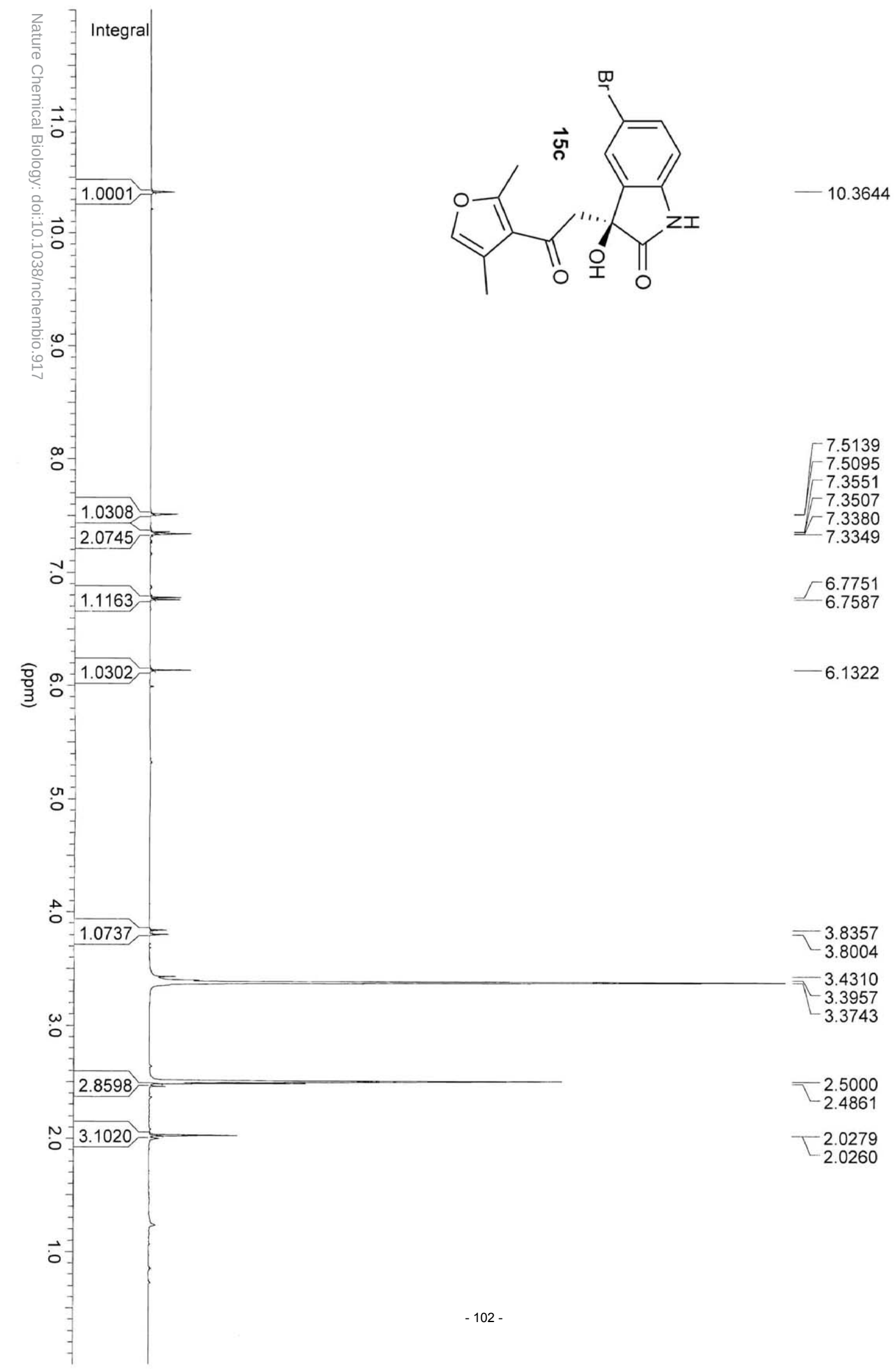

compound **15c**: ^{13}C NMR (125 MHz, DMSO)

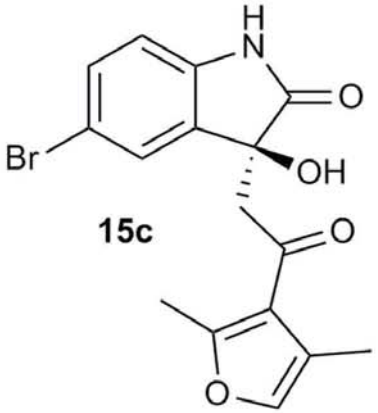

15c

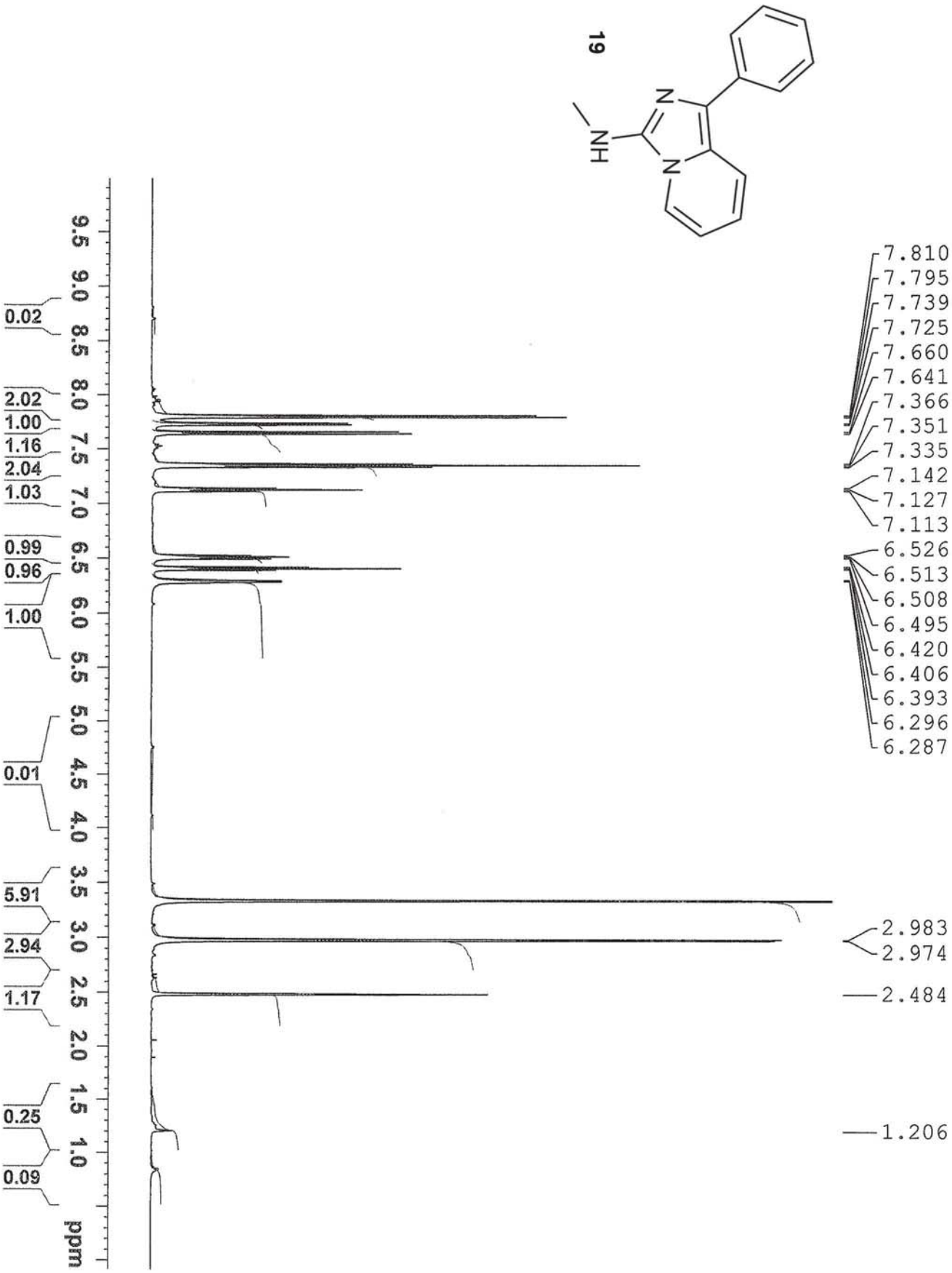

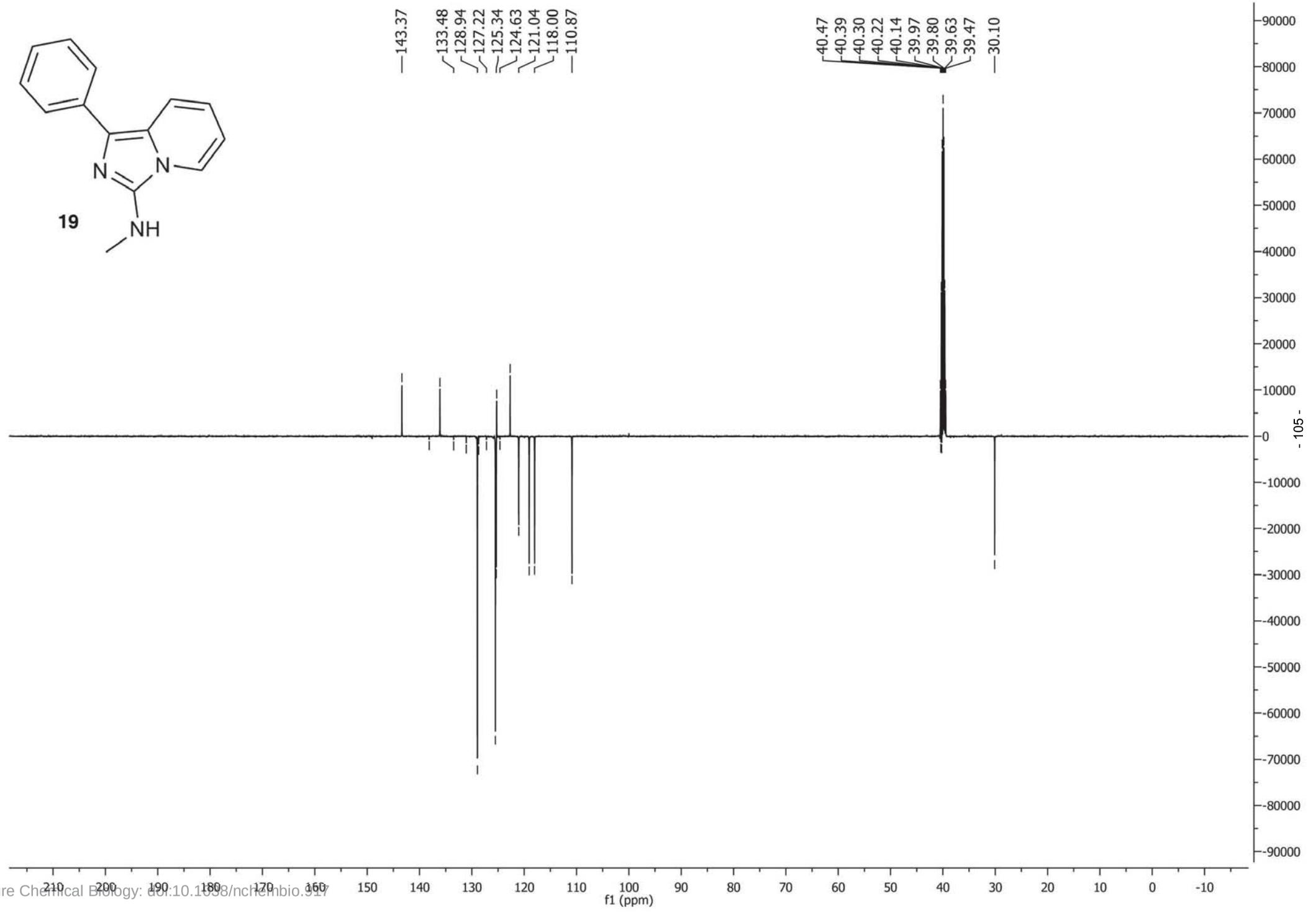

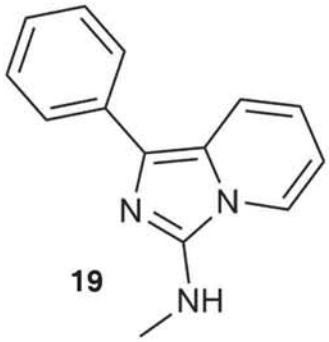

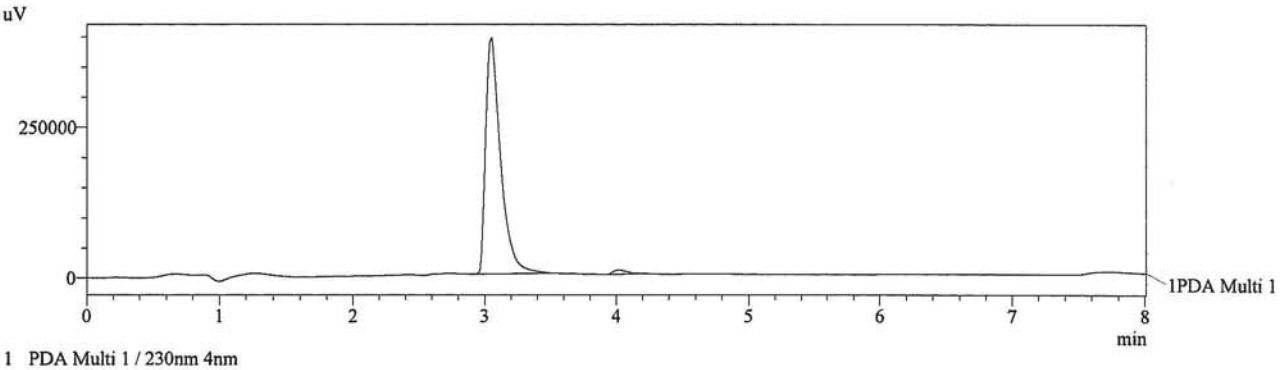

1 PDA Multi 1 / 230nm 4nm

PeakTable

PDA Ch1 230nm 4nm

Peak#	Name	Ret. Time	Area	Area %
1		3.043	3061534	98.153
2		4.015	49289	1.580
3		5.563	8310	0.266

MS Spectrum Graph

#:1 Ret.Time:Averaged 3.110-3.220(Scan#:312-323)
Mass Peaks:8 Base Peak:223.95(3964103) Polarity:Pos Segment1 - Event1

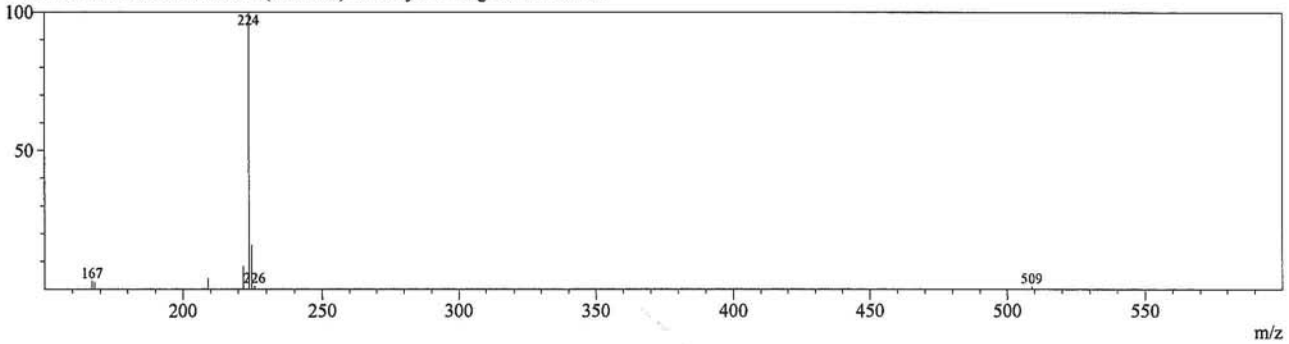

MS Spectrum Table

#:1 Ret.Time:
BG Mode:None
Mass Peaks:8 Base Peak:223.95(3964103) Polarity:Pos Segment1 - Event

#	m/z	Abs.Inten.	Rel.Inten.	Charge	Polarity	Monoisotopic	#	m/z	Abs.Inten.	Rel.Inten.	Charge	Polarity	Monoisotopic
1	166.95	119715	3.02				5	223.95	3964103	100.00			
2	167.95	106670	2.69				6	224.95	632260	15.95			
3	208.95	160513	4.05				7	225.95	49099	1.24			
4	221.95	332303	8.38				8	509.00	45440	1.15			

Nature Chemical Biology: doi:10.1038/nchembio.917

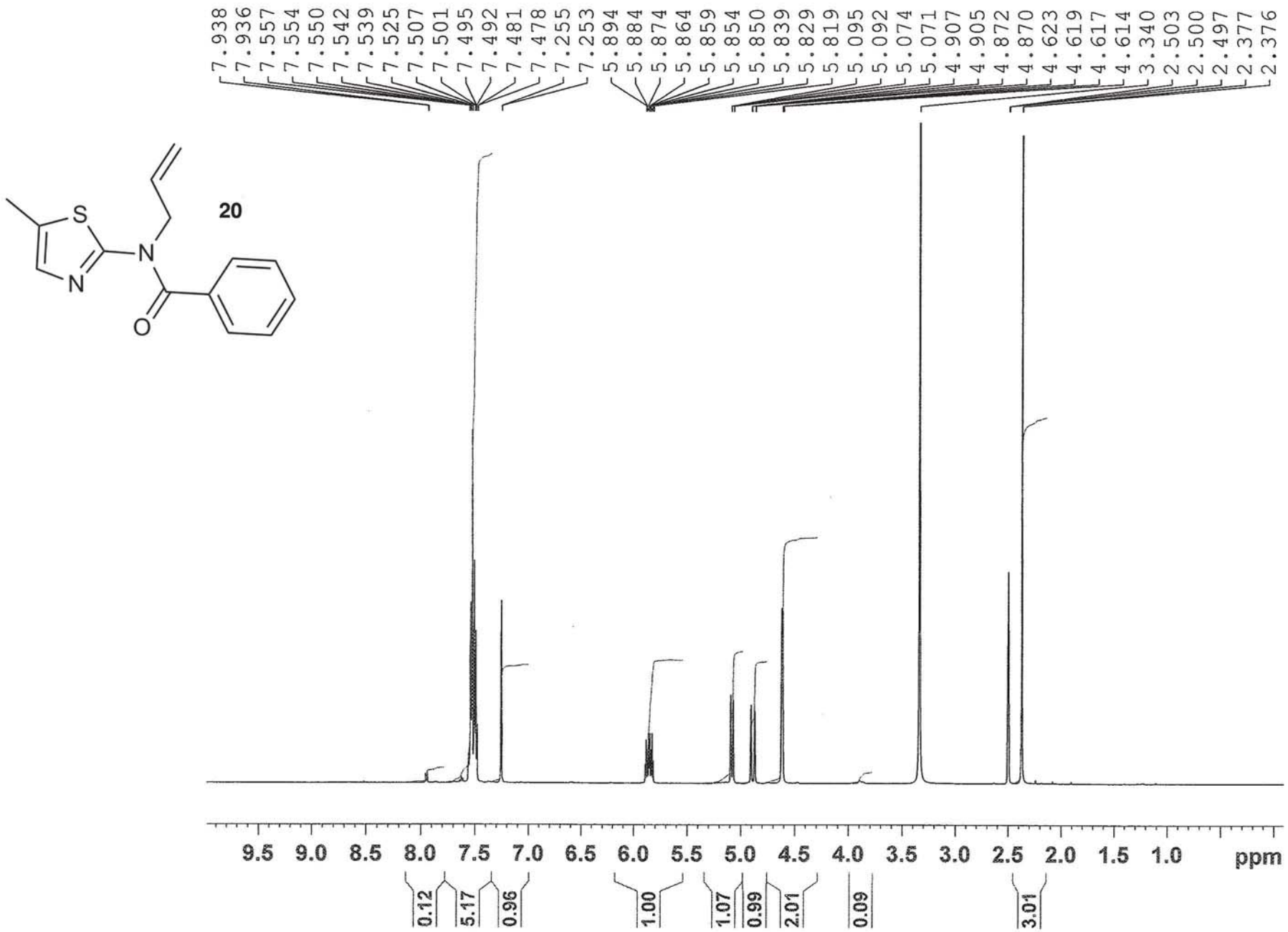

Nature Chemical Biology: doi:10.1038/nchembio.917

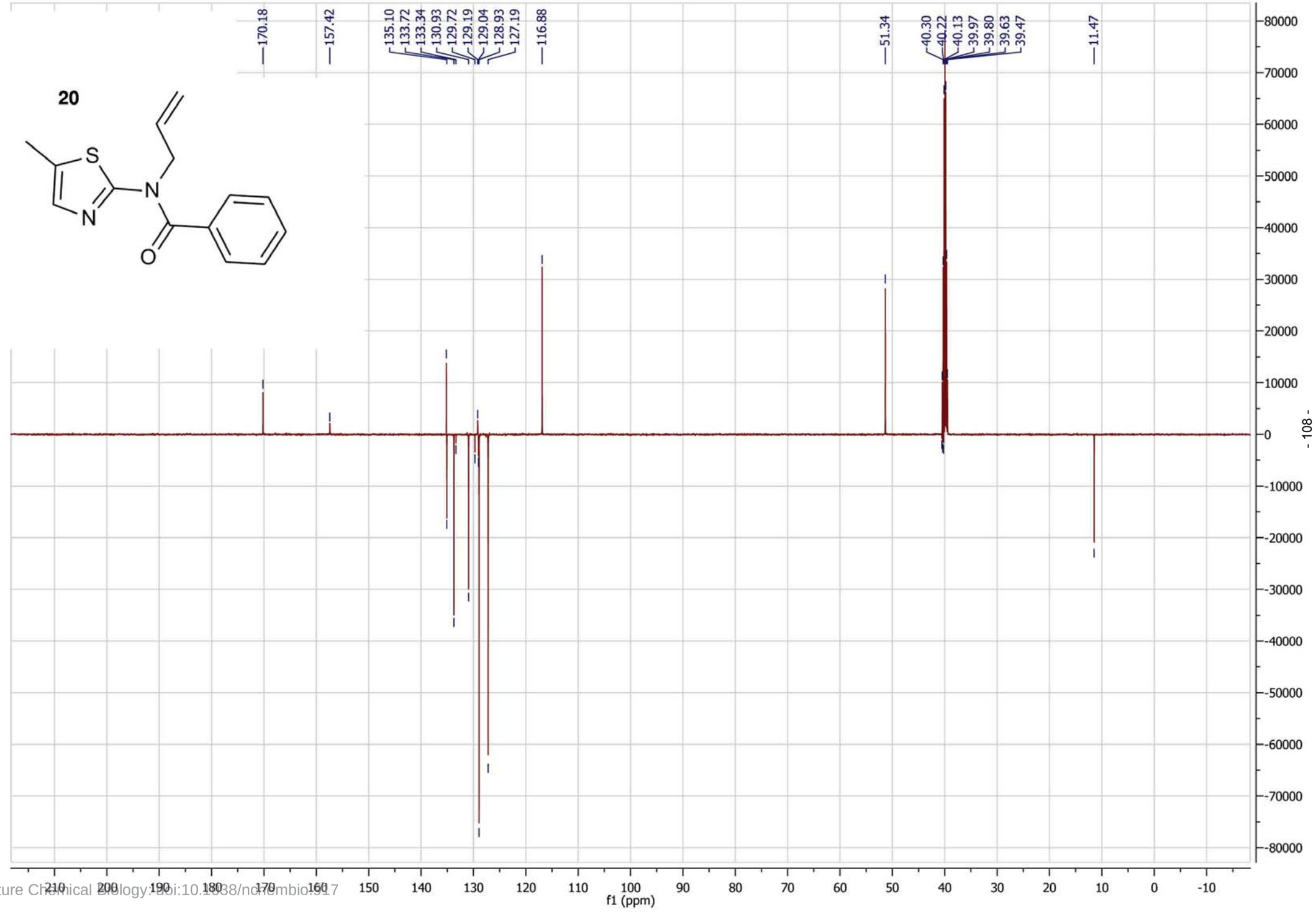
20
170.18
157.42
135.10
133.72
133.34
130.93
129.72
129.19
129.04
128.93
127.19
116.88
51.34
40.30
40.22
40.13
39.97
39.80
39.63
39.47
11.47
f1 (ppm)

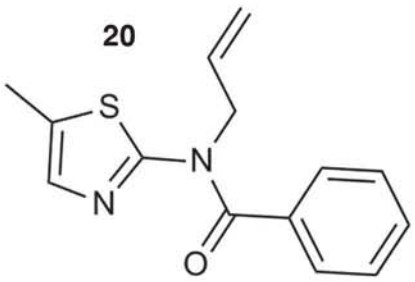

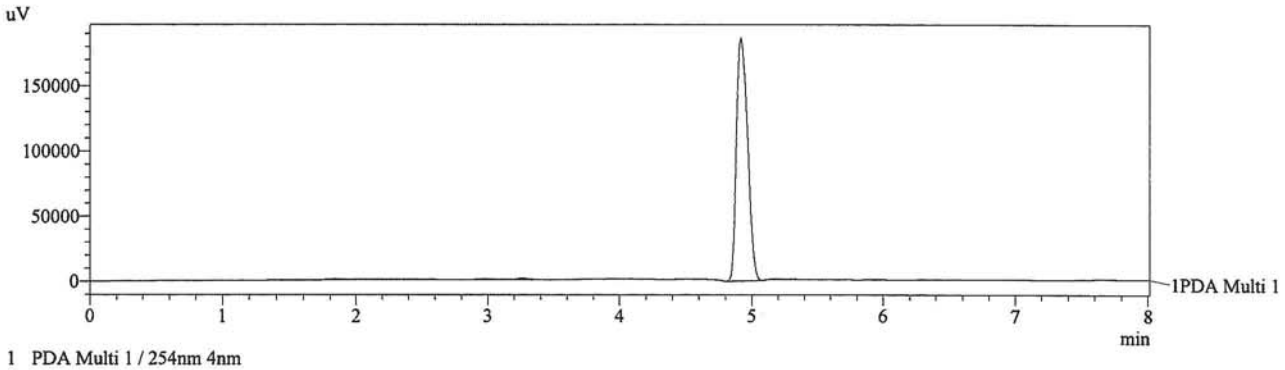

1 PDA Multi 1 / 254nm 4nm

PeakTable

PDA Ch1 254nm 4nm

Peak#	Name	Ret. Time	Area	Area %
1		1.832	5069	0.457
2		2.953	4040	0.365
3		3.246	5148	0.465
4		4.911	1093895	98.713

MS Spectrum Graph

#:1 Ret.Time:Averaged 4.980-5.060(Scan#:499-507)
Mass Peaks:3 Base Peak:259.00(1370744) Polarity:Pos Segment1 - Event1

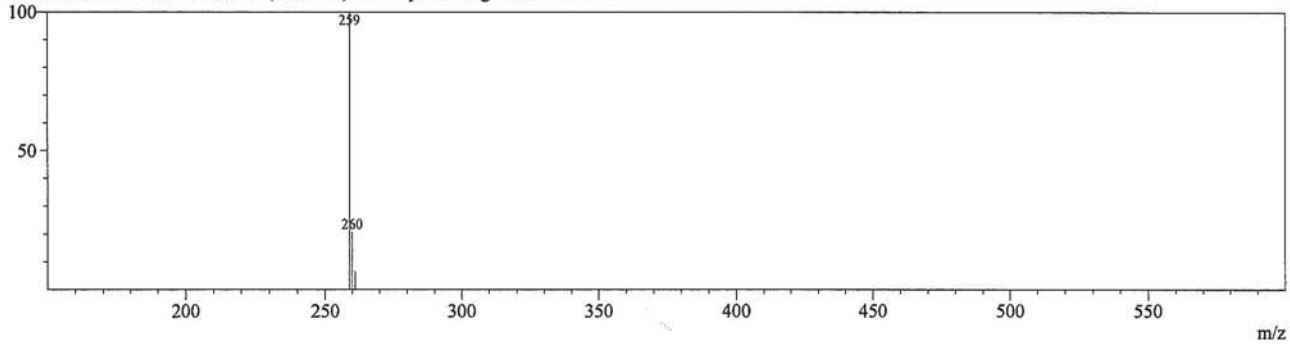

MS Spectrum Table

#:1 Ret.Time:
BG Mode:None
Mass Peaks:3 Base Peak:259.00(1370744) Polarity:Pos Segment1 - Event

#	m/z	Abs.Inten.	Rel.Inten.	Charge	Polarity	Monoisotopic	#	m/z	Abs.Inten.	Rel.Inten.	Charge	Polarity	Monoisotopic
1	259.00	1370744	100.00				3	260.95	91480	6.67			
2	259.95	284319	20.74										

Nature Chemical Biology: doi:10.1038/nchembio.917

Supplementary Results - Supplementary Tables

Supplementary Table 3 – modeling parameters

Main template(s)	Screening stages[a]				Templates for the individual subunits and the interface geometry[b]			Varied parameters
	in	**im**	**f**	**fv**	alpha	gamma	interface	
1I9B	4	3			1I9B	1I9B	1I9B	Alignment[c]
2BYN	2	1			2BYN	2BYN	2BYN	Alignment[c]
2BYS	3	2			2BYS	2BYS	2BYS	Alignment[c]
2BYQ	3	2	2[d]		2BYQ	2BYQ	2BYQ	Alignment[c]
				2[e]	2BYQ/1UW6	2BYQ	2BYQ	Loop C[f]
2BG9	1				2BG9_C	2BG9_B	2BG9_CB	
2BYQ/2BG9	5	4			2BYQ	2BYQ	2BG9_CB	Alignment[c]
2BYQ/2BG9	5				2BYQ	2BYQ	2BG9_BA	Alignment[c]
2BYQ/2QC1	1	1	1[g]		2BYQ	2QC1	2BYQ	
				1[h]	2BYQ/1UW6	2QC1	2BYQ	Loop C[f]
2BYN/2BG9	1				2BYN	2BYN	2BG9_CB	
2BYR/2BG9	5	1			2BYR	2BYR	2BG9_CB	Alignment[c]
2BYR/2BG9	4				2BYR	2BYR	2BG9_BA	Alignment[c]

[a] From each set of main template(s), one or more model variants were derived by varying additional modeling parameters. Models used in the **in**itial screen are denoted "**in**" (rigid docking of diazepam with FlexX[71]), "**im**" those that were retained for the **i**nter**m**ediate screening (flexible docking of cpds. **1,3,4,5,8,9** with FlexE[72], see text), "**f**" are the **f**inal models of the original set, and **fv** are the **v**ariants of the final models that were obtained by enhanced rotamer exploration and additional conformational sampling thus increasing the sampling density of the most promising pocket geometries (see also **Supplementary Scheme 2**).

[b] Subunit templates were 3D-aligned with the indicated template for the interface geometry, in order to sample the relative orientation of the two subunits. This was necessary for including the monomeric structure 2QC1 as template, and for investigating the interface geometries seen in the 2BG9 heteropentameric structure. The chain IDs used for the interface are indicated as 2BG9_C, etc.

[c] Alignment variants in the unconserved segments that contain "loops" C, E and F were constructed as recommended[51] (see **Supplementary Fig. 1**) with standard procedures[49,50,67,73] to generate a wide variety of initial geometries.

[d] corresponds to models M1 and M3 in **Supplementary Table 8**.

[e] corresponds to models M2 and M4 in **Supplementary Table 8**.

[f] In order to improve the sampling of the flexible C-loop tip, the alpha subunit was also modeled by local multi-template restraints based on two templates[51].

[g] corresponds to model M5 in **Supplementary Table 8**.

[h] corresponds to model M6 in **Supplementary Table 8**.

Nature Chemical Biology: doi:10.1038/nchembio.917

Models were constructed from a broad variety of templates and parameters to identify those best suited for the bound state complex of diazepam and analogues (see also **Supplementary Schemes 1 and 2**). Some models were eliminated prior to docking due to poor stereochemistry and are not included in the table. The full breadth of structural variety in the pocket was then investigated with the initial model pool, (**in**). Based on exploratory docking, models that were largely incapable of providing promising poses of diazepam with sufficient hydrophobic interaction with L1 and L3 and pocket forming residues were eliminated. To those that remained, docking was extended to multiple ligands and parameters were added to consider conformational and side chain flexibility (intermediate pool, **im**). Upon evaluation of the intermediate pool using criteria as mentioned above for each of the investigated ligands, three best performing final (**f**) models were selected. From those three models, additional final variants (**fv**) were built to increase the sampling density of the models of interest. This resulted in a total of six models providing the final pool of docking poses, the three best performing of the intermediate pool, and one variant of each of those. In the variants, a more extensive rotamer exploration at the subunit interface (see **Methods,** main text) and a more detailed exploration of loop C conformations were performed as indicated by RMSD analysis and visual inspection of “empty” patches in the sampling of pocket geometries.

Nature Chemical Biology: doi:10.1038/nchembio.917

Supplementary Table 4 – Model variability in pocket forming segments

	total	*final*	*compared to 3RIF-model*	
Segment	*37 models ave.(max)*	*6 models ave. (max)*	*37 models ave.(max)*	*6 models ave. (max)*
A-Loop (α_1F99 – α_1N102)	1.9 (3.6)	0.3 (0.4)	1.5 (2.1)	1.3 (1.7)
B-Loop (α_1Y159 – α_1Y161)	1.4 (2.5)	0.3 (0.5)	0.9 (3.0)	0.5 (0.8)
C-Loop (α_1V202 – α_1V211)	3.1 (5.4)	0.5 (0.6)	2.6 (4.9)	1.1 (1.2)
G-Loop (γ_2D56 – γ_2N60)	1.9 (3.8)	0.7 (1.0)	2.0 (3.5)	0.7 (0.7)
D-Loop (γ_2F77 – γ_2A79)	1.6 (3.4)	0.6 (0.8)	1.5 (2.9)	0.8 (0.8)
E-Loop (γ_2M130 –γ_2 I133 &γ_2L140–γ_2T142)	1.5 (2.5)	0.5 (0.7)	1.8 (2.3)	1.8 (1.8)
F-Loop ($\gamma_2$185 - $\gamma_2$194)	4.3 (11.9)	4.2 (6.1)	4.9 (8.8)	4.3 (6.1)
Loops (A-E & G)	2.2 (3.3)	0.5 (0.8)	2.1 (3.3)	1.2 (1.3)
Loops (A-F & G)	2.8 (6.0)	2.1 (3.0)		

Average and maximum backbone RMSD values of pocket forming segments. The entire model pool has much higher variability than the final pool, which has converged to optimally accommodate the ligands. Loop F is not engaged in any obvious interactions with the ligands investigated, and thus remains variable. Since loop F suffers from template uncertainty and undefined alignments, total pocket RMSD is computed with and without loop F contribution. The value without loop F contribution is a good measure for the variability obtained in the structurally conserved pocket portions. The loop C value is a measure for the observed flexibility (**Supplementary Fig. 3**).The total maximal RMSD for the final models is a measure for combined overall protein variability that cannot be reduced with the workflow used here. It contains uncertainty, possibly induced fit contributions and lack of information to narrow down further. After submission of this work, a new structure (PDB ID 3RIF) of a glutamate gated Cl^- channel, which shares ~30% PID with $GABA_A$ receptor subunits, was released. The “hindsight” validation against the models based on the new 3RIF glutamate bound structure (last columns) shows that our final models are more similar to this new structure than to some of the initial models.

Thus, our workflow successfully identified models, that are “better” in the light of this new X-ray structure over alternative models, that were equally valid in the light of the older structural data.

Nature Chemical Biology: doi:10.1038/nchembio.917

Supplementary Table 5 – Compound information

type	*cpd.*	*Name*	*affinity ($\alpha_1\beta_2\gamma_2$) nM*	*modulation*
core[a]	**1**	Diazepam[74]	12	positive modulator
core	**2**	Ro07-5220[74]	2	(not known)
core	**3**	Flunitrazepam[74]	3	positive modulator
core	**4**	Flurazepam[75]	62	positive modulator
core	**5**	Ro 7-1986/1[76]	--[b]	(not known)
accessory[c]	**6**	8,9-benzofused[77]	55	positive modulator
accessory	**7**	7,8-benzofused[77]	120	(not known)
accessory	**8**	Ro15-8670[74]	34	positive modulator
accessory	**9**	CNS7056[78]	29	positive modulator
not used for docking[d]	**10**	7-NCS[79]	3170	positive modulator
docked only in **f** and **fv** models[e]	**11**	Flumazenil[74]	0.61	null modulator
not used for docking[d]	**12**	Ro15-4513[80]	3.9	negative modulator
not used for docking[d]	**13**	„Imid compound“[81]	10	null modulator
not used for docking[d]	**14**	3-NCS[82]	340	--[f]

[a] core ligands were those for which a more strict definition of common binding mode was used: At the level of clustering by ligand RMSD, all core ligands were mandatory for a cluster of poses to be considered CBM-parent candidate. At the level of clustering with bound complex RMSD a tighter overlap (2 Å) was requested of those.

[b] This compound is coupled to chromatography beads as affinity bait.

[c] accessory ligands were those that were not considered mandatory in the first cluster analysis, and permitted larger bound complex RMSD in the second analysis (2.5 Å). If a CBM contained them, they were also used for CBM evaluation by experimental evidence, see **Table 1** in the main text.

[d] those ligands were aligned by the common atoms' coordinates with docked ligands to evaluate the resulting position in the light of experimental evidence, see **Table 1** in the main text.

[e]Flumazenil was only docked into the final models (**f**) of the original set, and into the **fv**, the variants of the final models (see **Supplementary Table 3**)

[f]data for wildtype $\alpha1\beta2\gamma2$ receptor not shown, positive allosteric modulator in $\alpha1S205C\beta2\gamma2$ and $\alpha1T206C\beta2\gamma2$.

Core ligands: In the workflow shown in **Supplementary Scheme 3**, only those clusters were retained that contained all core ligands. Core ligands are assumed to share common binding and interaction patterns due to similar structure and biological profile

Accessory ligands: were used additionally and less tight similarity was required in the **Supplementary Scheme 3** workflow to further restrict the possible binding geometries by bulkier ligands.

Nature Chemical Biology: doi:10.1038/nchembio.917

Supplementary Table 6 – bound complex defining and major interaction forming residues

	alpha1					*gamma2*		
Parent cluster[a] I	H101, Y159, S204, T206, Y209					Y58, N60, F77, T142		
Parent cluster II	H101, S158, Y159, S204, S205, T206, Y209					Y58, N60, F77, T142		
Parent cluster III	F99, H101, K155, G157, Y159, V202, Q203, S204, T206, Y209, V211					Y58, F77, T142		
	L1	*L3*		*H1*	*H1'*	*H2*	*L1*	*L3*	*H1*
CBM I	Y159 *100%* Y209 *100%*	H101	*66%*	*γ2*	T206	S204	*α1*	F77 *100%* Y58 *19%*	T142
CBM II	*γ2*	Y159 Y209	*100%* *100%*	-	S205	T206	Y58 *100%* F77 *100%*	*α1*	-
CBM III	Y209 *94%*	F99 H101 Y159 Y209	*88%* *48%* *74%* *100%*	H101	-	H101	Y58 *59%* F77 *100%*	*α1*	-

[a] Parent cluster was selected by "ligands common scaffold RMSD" clustering (**see Supplementary Scheme 3**).

For each putative common binding geometry (parent cluster), that was identified based on the clustering by ligand overlap RMSD ("ligands common scaffold RMSD"), the major bound complex forming atoms were determined. The upper three lines list those amino acid residues that were selected, based on average distance to the ligands' common scaffold in the respective cluster, to compute the cluster's individual "bound complex RMSD" values. Many, but not all of those residues are found in the final CBM poses as major interaction partners. The last three lines list the residues that were subsequently found to provide major interactions in the final CBM poses, for the lipophilic L interactions the percentage of core poses featuring the respective interaction is also indicated. This shows the heterogeneity that is present in the individual CBM pose pools. **Please note: Our structural hypotheses do feature well defined geometries and interaction pattern, but also some residual scatter. Thus, no single pose can be considered "best" or "correct", the final poses define a conformational space in which the "true structure" is assumed to be contained.**

Nature Chemical Biology: doi:10.1038/nchembio.917

Supplementary Table 7 – poses for each compound tracked through the workflow from pose pool to CBM

		Compound number								
	total	***1***	***2***	***3***	***4***	***5***	***6***	***7***	***8***	***9***
rawposepool[a]	4997	600	444	600	537	588	595	510	538	585
L1 & L3pool[b]	1463	257	156	183	210	156	181	164	123	33
Parent cluster I	146	34	13	21	11	9	21	18	16	3
Parent cluster II	96	20	12	9	17	22	4	5	4	3
Parent cluster III	93	15	4	11	13	13	9	13	15	0
CBM I	96	21	5	16	11	9	14	6	12	2
CBM II	49	5	1	2	11	22	3	1	3	1
CBM III	39	4	2	6	6	13	5	1	2	0

[a] The raw pose pool refers to the number of poses obtained with FlexE flexible docking and retaining up to 100 poses.
[b] L1& L3 pool denotes the pool of models that satisfies the lipophilic saturation requirements.

Supplementary Table 8 – distribution of poses in the final models

		Model identifier[a]					
model:	***total***	***M1***	***M2***	***M3***	***M4***	***M5***	***M6***
rawposepool	4997	886	827	843	790	856	795
L1 & L3pool	1463	114	239	237	389	236	248
Parent cluster I	146	4	23	5	48	12	54
Parent cluster II	96	8	4	8	24	48	4
Parent cluster III	93	20	14	13	3	12	31
CBM I	96	0[b]	23	0	28	0	45
CBM II	49	1	0	2	1	44	1
CBM III	39	4	7	2	0	4	22

[a]See**Supplementary Table 3** and **Supplementary Fig. 1** for the modeling parameters used in these six models.
[b] It is worth noting that the final binding mode CBM I occurs only in the models M2, M4 and M6 which were obtained by extending the rotamer flexibility (see **Methods**), and were thus able to assume an energetically more favorable loop B conformation. This table thus illustrates that a binding mode can be missed by insufficient sampling of model flexibility.

The Supplementary Tables 7 and 8 illustrate the effects of the different work steps on the poses obtained with a given ligand (**Supplementary Table 7**) or a given model (**Supplementary Table 8**). See also **Supplementary Scheme 3**.

Nature Chemical Biology: doi:10.1038/nchembio.917

Supplementary Table 9 – Characterization and computational evaluation of CBM candidates

	ligands[a]	CBM I		CBM II		CBM III	
Homogeneity of poses							
number of core poses	**1-5**	62		41		31	
average distance to centroid Å	**1-5**	1.2		1.24		1.45	
number of acc. ligands	**6-9**	*all*		*all*		3/4	
number of acc. poses	**6-9**	34		8		8	
average distance to centroid Å	**6-9**	1.55		1.81		1.14	
Major interactions[b] (see **Fig. 2***)*							
L1 – hydrophobic feature	**1-5**	α1Y159,α1Y209		γ2Y58,γ2F77		α1Y209,γ2Y58,	
L3 – hydrophobic feature	**1-5**	α1H101,γ2F77, γ2Y58		α1Y159,α1Y209		α1F99,α1H101, α1Y159,α1Y209	
H1 – H-bond donor feature	**1-5**	γ2T142		*none*		α1H101	
H1' – H-bond donor feature	**1-5**	α1T206		α1S205		*none*	
H2 – H-bond donor feature	**1-5**	α1S204		α1T206		α1H101	
Poses exhibiting side chain positions conserved in superfamily (see ***Supplementary Fig. 8****)*							
Conserved α_1Y159	**1-5**	*all*	**++**	*none*	**-**	*none*	**-**
Conserved α_1Y209	**1-5**	*all*	**++**	28/41[c]	**+**	28/31[c]	**++**
Scoring performance							
Top10 *X-Score*[83]	**1-5**	13	**++**	*none*	**-**	1	**-**
Top10 *London dG*[84]	**1-5**	13	**++**	*none*	**-**	1	**-**
Enrichment factors[85] *in Retrospective virtual screening (Number of actives in database fraction) (see* ***Supplementary Scheme 4****)*							
EF 0.5%		24.8 (5)	**++**	14.9 (3)	**+**	9.9 (2)	**+**
EF 1.0%		14.9 (6)	**++**	7.4 (3)	**+**	5.0 (2)	**+**
EF 2.0%		12.2 (10)	**++**	3.7 (3)	**-**	2.5 (2)	**-**
EF 5.0%		6.9 (14)	**++**	3.0 (6)	**-**	2.0 (4)	**-**
EF 10.0%		4.5 (18)	**++**	1.7 (7)	**-**	1.7 (7)	**-**

[a] only poses of the defined ligand(s) (**Fig. 1c**) are used for evaluation.
[b] interactions were calculated using *SCORING.SVL* (*http://svl.chemcomp.com).*
[c] number of poses fulfilling the respective criterion in relation to number of total poses in a CBM (see **Supplementary Table 7** for total number of poses per ligand within a CBM).

The slightly smaller average distance to centroid for CBM III results from the fact that this binding mode accommodates only three of the four accessory ligands.

Nature Chemical Biology: doi:10.1038/nchembio.917

Supplementary Table 10 – 41 known binders used in enrichment computation

cpd.	2D structure	annotation in reference	Screening CBMI[a]	affinity (nM)
11	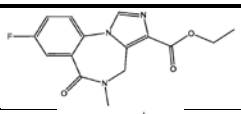	Flumazenil[86]	Top 0.5%	0.8
1	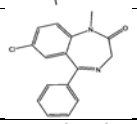	Diazepam[86]	Top 0.5%	14
21	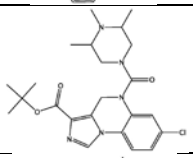	U-97775[87]	Top 0.5%	1.2
22	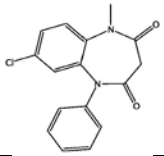	Clobazam[88]	Top 0.5%	170
23	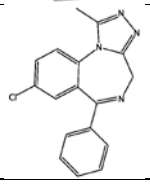	Triazolam[86]	Top 0.5%	0.8
24	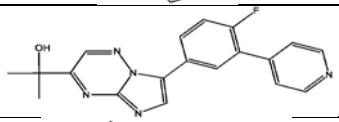	2b[89]	Top 1%	0.55
25	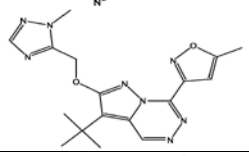	MRK-016[90]	-	0.92
26	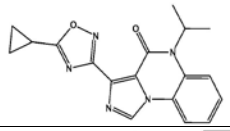	Panadiplon[91]	-	1.56
27	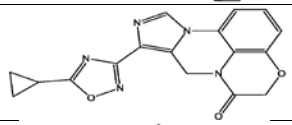	38[92]	Top 10%	2.0
28	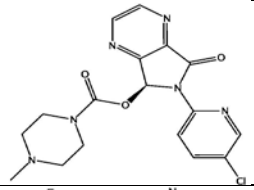	Eszopiclone[93]	Top 5%	50.1
29	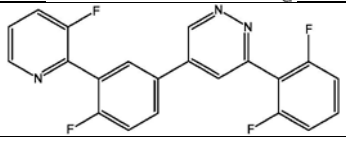	10[94]	Top 5%	0.1

Nature Chemical Biology: doi:10.1038/nchembio.917

cpd.	2D structure	annotation in reference	Screening CBMI[a]	affinity (nM)
30	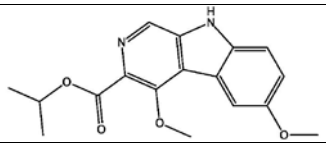	71[95]	Top 2%	0.14
31	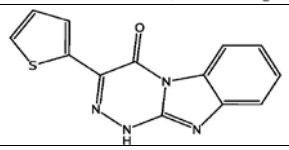	1k[96]	Top 2%	13
32	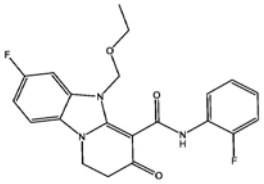	RWJ-51204[97]	-	0.37
33	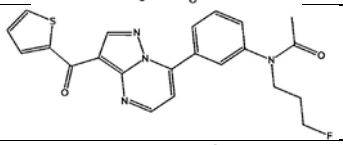	2b[98]	-	2.36
34	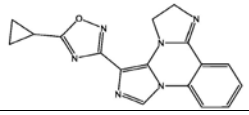	U-85575[87]	Top 2%	0.3
35	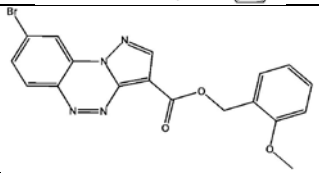	4aR[99]	Top 10%	7.5
36	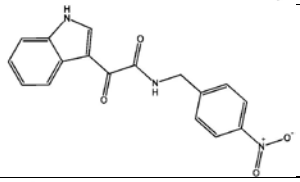	1a[100]	Top 10%	21
37	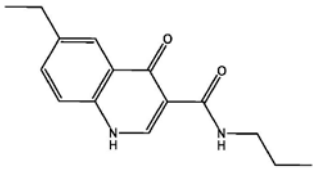	23[101]	-	0.26
38	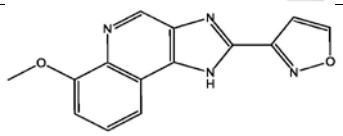	4k[102]	-	0.5
39	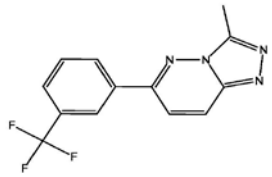	CL218,872[86]	-	57

Nature Chemical Biology: doi:10.1038/nchembio.917

cpd.	2D structure	annotation in reference	Screening CBMI[a]	affinity (nM)
40	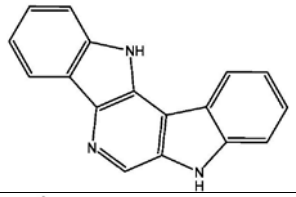	Pyridodiindole[86]	-	1.1
41	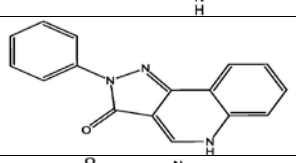	CGS-8216[86]	Top 10%	0.05
42	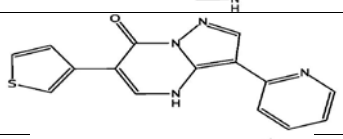	2i[103]	Top 2%	3.9
43	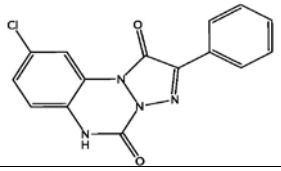	45[104]	-	2.8
44	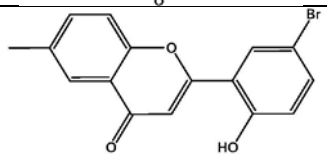	41[105]	-	0.9
45	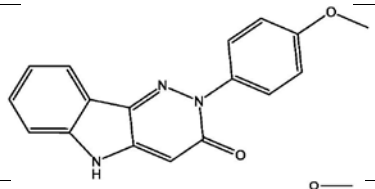	1e[106]	-	5.4
46	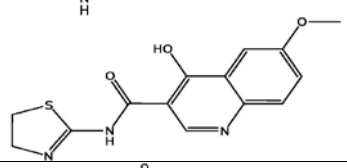	DU43028[107]	-	0.07
47	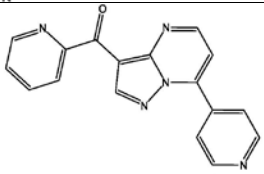	Ocinaplon[108]	Top 5%	1200
48	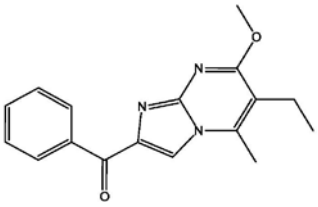	RU32698[109]	-	114

Nature Chemical Biology: doi:10.1038/nchembio.917

cpd.	2D structure	annotation in reference	Screening CBMI[a]	affinity (nM)
49	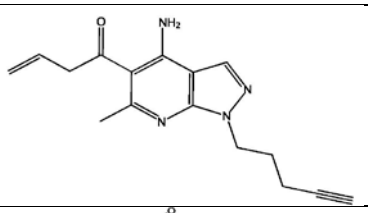	74[110]	-	5.5
50	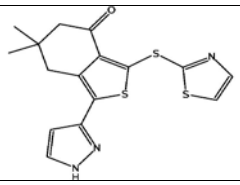	21[111]	-	2.3
51	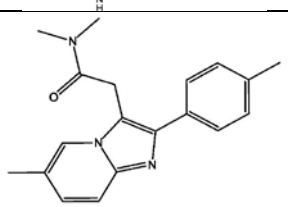	Zolpidem[86]	-	156
52	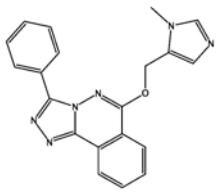	35[112]	Top 5%	0.51
53	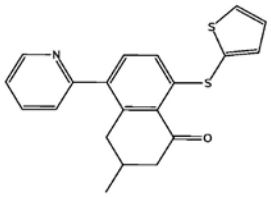	14[113]	-	4.3
54	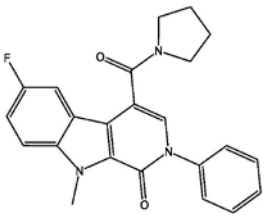	SL-651498[114]	-	6.8
55	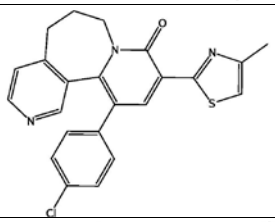	2b[115]	-	0.2
56	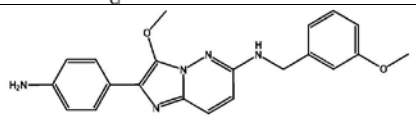	GBLD-345[116]	-	0.9

Nature Chemical Biology: doi:10.1038/nchembio.917

cpd.	2D structure	annotation in reference	Screening CBMI[a]	affinity (nM)
57	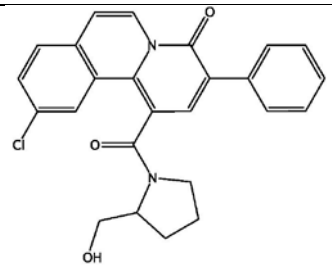	Ro19-8022[117]	-	0.38
58	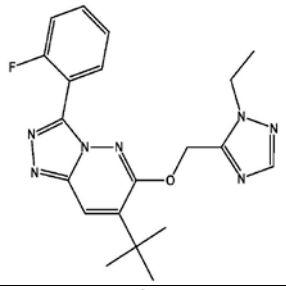	TPA023[118]	-	0.92
59	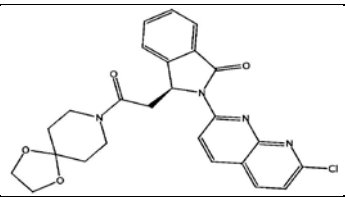	Pazinaclone[119]	-	0.7

[a]Ranking of benzodiazepine binding site ligands in the top 0.5%, 1%, 2%, 5% or 10% of the score-sorted validation library. Rankings derive from virtual screening of the validation library (see **Supplementary Methods**) against the CBM I derived pharmacophore models (**Supplementary Fig. 10**).

These 41 known benzodiazepine binding site ligands from different chemical classes were extracted from the literature. These ligands together with property-matched decoys (validation library, **Supplementary Methods**) were used in virtual screening against structure-based pharmacophore models of CBM I-III (**Supplementary Scheme 4).** For CBM I, data indicate that flumazenil, diazepam and benzodiazepine binding site ligands from 8 additional compound classes were ranked within the top 2% of the score-sorted validation library by the structure based pharmacophores. The enrichment obtained (see also **Supplementary Table 11**) is comparable to the average enrichment obtained by docking of the DUD database into the 40 crystal structures[52].

Nature Chemical Biology: doi:10.1038/nchembio.917

Supplementary Table 11 - Retrospective virtual screening results of the validation library (Bz-focused decoy set) using different methodologies

EF[a] (%)	pharmacophore models		2D fingerprint (FP) search		shape-similarity search[f]
	structure-based[b] (CBM I)	ligand-based[c]	pharmacophore FP (GpiDAPH3)[d]	substructural FP (MACCS)[e]	
0.5%	24.8 (24.4)	14.9 (14.6)	24.9 (29.3)	29.8 (29.3)	19.8 (19.5)
1%	14.9 (17.1)	7.5 (7.5)	17.4 (17.1)	14.9 (14.6)	12.4 (12.2)
2%	12.2 (12.2)	5.0 (5.0)	11.2 (12.2)	8.5 (8.5)	6.1 (6.1)
5%	6.9 (6.8)	2.0 (2.0)	6.5 (6.8)	4.0 (3.9)	2.5 (2.4)
10%	4.5 (4.4)	1.7 (1.7)	4.0 (3.9)	3.0 (2.9)	2.2 (2.2)

[a]Enrichment factors were calculated as described in Wei et al.[85]. Values in brackets represent enrichment factors calculated according to guideline of Nicholls et al.[120].

[b]Structure-based pharmacophore models were created using LigandScout 3.0[70] (see **Supplementary Methods**) based on CBM I diazepam (*pharmacophore D*, see **Supplementary Fig. 10a**) and flumazenil (*pharmacophore F*, **Supplementary Fig. 10b**) poses. Conformational database was created using default values within OMEGA toolkit release 2.3.3 (http://www.openeye.com/omega). Virtual screening was performed within LigandScout 3.0[70].

[c]Ligand-based pharmacophore models were generated based on the structures of diazepam and flumazenil (**Supplementary Methods**) using LigandScout 3.0[70]. Conformational database was created using default values within OMEGA toolkit release 2.3.3 (http://www.openeye.com/omega). Virtual screening was performed within LigandScout 3.0[70].

[d]2D-similarity search was performed with MOE (http://www.chemcomp.com) against diazepam and flumazenil, respectively, using the pharmacophore graph triangle fingerprints GpiDAPH3 and Tanimoto similarity measure.

[e]2D-similarity search was performed with MOE (http://www.chemcomp.com) against diazepam and flumazenil, respectively, using MACCS fingerprint keys and Tanimoto similarity measure.

[f]Shape-similarity search was performed with Phase (http://www.schrodinger.com) using diazepam and flumazenil as templates, respectively. Conformations were generated 'on-the-fly' within Phase.

Nature Chemical Biology: doi:10.1038/nchembio.917

Supplementary Table 12 – Prospective virtual screening ranks of novel and experimentally validated benzodiazepine site ligands and fragment hits

cpd	pharmacophore models		2D fingerprint (FP) search		shape-similarity search[e]	closest 2D-similarity to BDZ site ligand[f]
	structure-based (CBM I)[a]	ligand based[b]	pharmacophore FP (GpiDAPH3[c])	substructural FP (MACCS)[d]		
15	245	5108	53333	48446	2866	0.50 (cpd. **37**)
15b	313	3441	58873	61808	597	0.56 (cpd. **46**)
19	-[g]	-[g]	-[g]	-[g]	-[g]	0.58 (cpd. **39**)
20	-[g]	-[g]	-[g]	-[g]	-[g]	0.55 (cpd. **55**)

[a]Rank in protein-based pharmacophore screening with LigandScout 3.0[70] based on CMB I diazepam (*pharmacophore D*, **Supplementary Fig. 10a**) and flumazenil (*pharmacophore F*, **Supplementary Fig. 10b**) poses.

[b]Ligand-based pharmacophore models were generated based on the structures of diazepam and flumazenil (**Supplementary Methods**) using LigandScout 3.0[70]. Conformational database was created using default values within OMEGA toolkit release 2.3.3 (http://www.openeye.com/omega). Virtual screening was performed within LigandScout 3.0[70].

[c]Rank in 2D-similarity search of the DUD library against the template structures diazepam and flumazenil, using the pharmacophore graph triangle fingerprints GpiDAPH3 (http://www.chemcomp.com).

[d]Rank in 2D-similarity search of the DUD library against the template structures diazepam and flumazenil, based on MACCS fingerprint keys.

[e]Rank in Phase(www.schrodinger.com) shape-based similarity search based on diazepam and flumazenil structures.

[f]Highest Tanimoto similarity to any of the 41 benzodiazepine binding site ligands (**Supplementary Table 10**) based on MACCS fingerprint keys using Tanimoto similarity measure (ligand name with highest Tanimoto similarity score is give between brackets).

[g]Hits**15** and **15b** derive from screening of DUD database against protein-based pharmacophore models of CBM I, while hits **19** and **20** are identified by docking-based virtual screening of another library of 1010 fragment-like compounds using CBM I derived bound complexes.

Nature Chemical Biology: doi:10.1038/nchembio.917

Supplementary Table 13 - Interaction Finger Prints

	α1H101							α1Y159							α1S204							α1T206						
diazepam **1**	1	0	1	0	0	0	0	1	1	1	0	0	0	0	1	0	0	1	0	0	0	1	0	0	1	0	0	0
cpd **19**	1	0	1	0	0	0	0	1	1	1	0	0	0	0	1	0	0	0	0	0	0	1	0	0	0	0	0	0
flumazenil **11**	1	0	1	0	0	0	0	1	1	1	0	0	0	0	1	0	0	1	0	0	0	1	0	0	0	0	0	0
cpd **20**	1	0	1	0	0	0	0	1	1	1	0	0	0	0	1	0	0	1	0	0	0	1	0	0	0	0	0	0

	α1Y209							γ2F77							γ2T142						
diazepam **1**	1	1	0	0	0	0	0	1	0	1	0	0	0	0	1	0	0	1	0	0	0
cpd **19**	1	1	0	0	0	0	0	1	0	1	0	0	0	0	1	0	0	0	0	0	0
flumazenil **11**	1	1	0	0	0	0	0	1	0	1	0	0	0	0	1	0	0	1	0	0	0
cpd **20**	1	1	0	0	0	0	0	1	0	1	0	0	0	0	1	0	0	0	0	0	0

The interaction finger print (**IFP**) bit string of the poses of **19** and **20** are compared to the reference IFP of diazepam and flumazenil. For reasons of clarity, the bit strings of only seven residues (out of 31) are shown as an example. Compounds **19** and **20** place their phenyl and thiazol groups in the same tight aromatic binding pocket between α1H101, α1Y159, and α1Y209 as occupied by the L1 ring (**Fig. 1c**) of diazepam **1** and flumazenil **11**, and stack with the same γ2F77 residue as the reference ligands as indicated by the IFP bit-string. Interestingly, the amide carbonyl oxygen atom of cpd **20** does not align with the ether carbonyl oxygen atom of flumazenil **11** but accepts an H-bond from the same α1S204 residue. The interaction types are color coded: gray – hydrophobic, dark green – aromatic face to face, bright green – aromatic edge to face, pink – H-bond (donor- acceptor)

Nature Chemical Biology: doi:10.1038/nchembio.917

Supplementary Results - Supplementary Figures

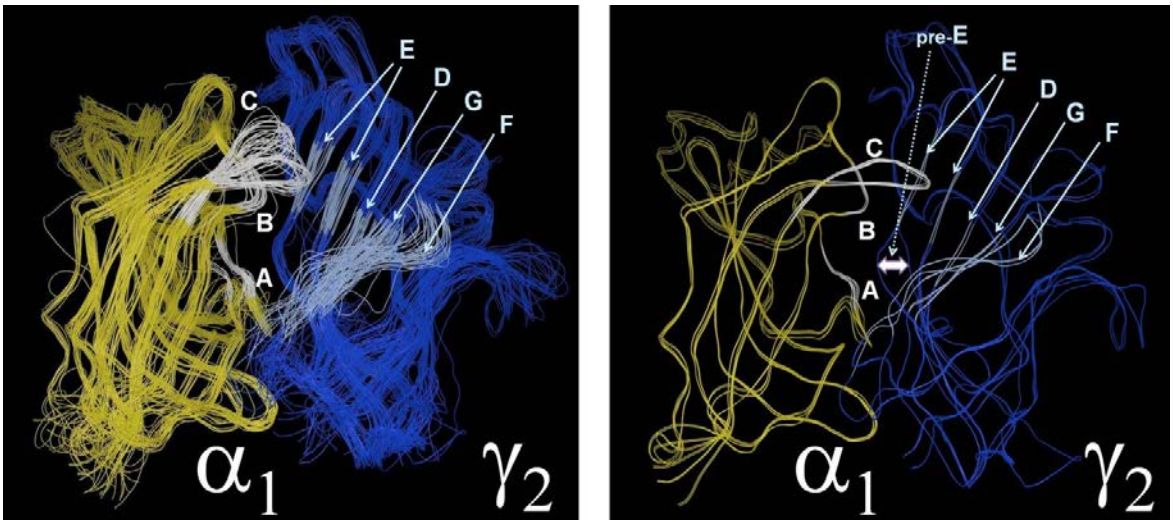

Supplementary Fig. 3 – View of the binding site from slightly below loop C to illustrate model variability. The left panel shows the entire model pool (each model in line ribbon mode), the right panel shows the final six models used in this study. By selecting models that provide docking poses with high lipophilic saturation regardless of the bound state geometry, the conformations of the loops A, B and C are reduced from a wide variety to a set of nearly identical models. Only one interface geometry (see **Supplementary Table 3**) was found to consistently feature well saturated lipophilic ligand interactions. In contrast, the minus side remains more uncertain: Segments D, E, and G are within 1 (Ångstrom) RMSD in all final models. But the region pre-E loop and the loop F region still vary significantly. This is consistent with the observation that these segments are not directly involved in diazepam binding. See **Supplementary Table 4** for more detailed information on the variability in final models.

Nature Chemical Biology: doi:10.1038/nchembio.917

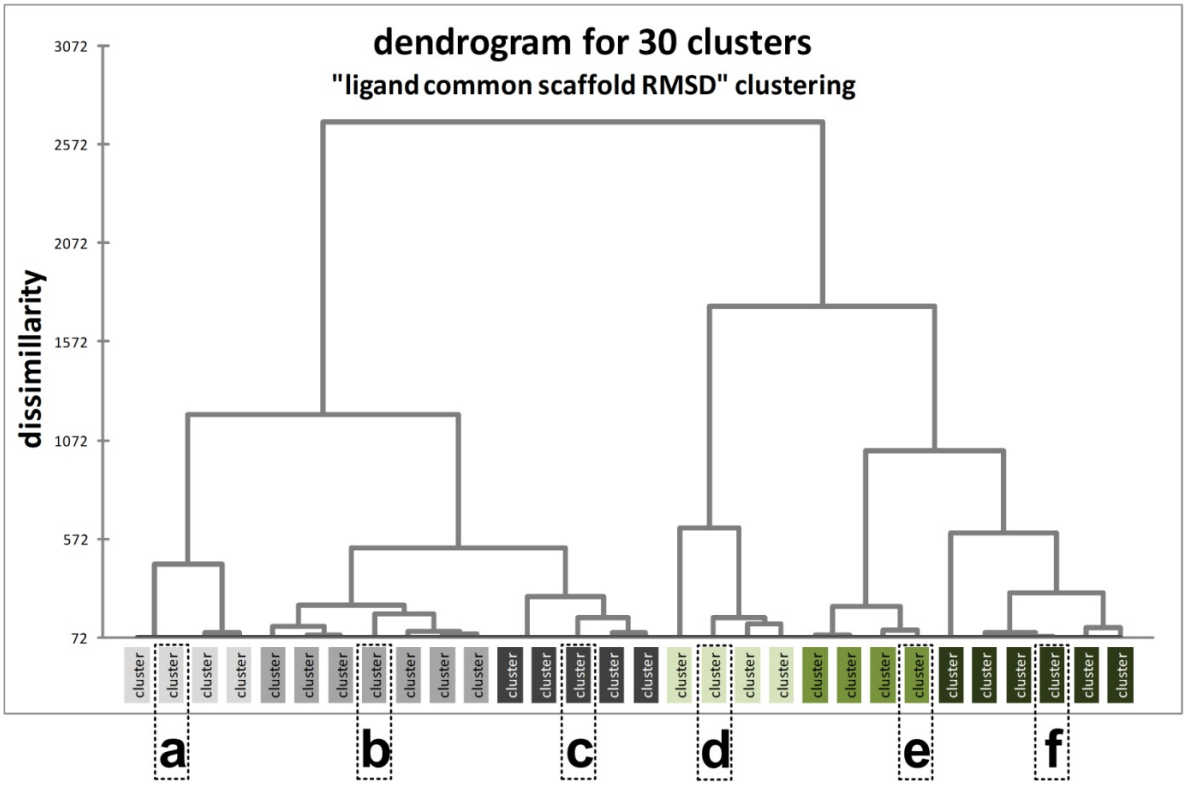

Supplementary Fig. 4 – Dendrogram of the cluster analysis by “ligands common scaffold RMSDs” (resulting in 30 parent clusters). Poses are grouped according to similar orientation of the common scaffold in the pocket structure. In order to depict the variety in ligand orientation, six dissimilar clusters were selected (**a**, **b**, **c**, **d**, **e** and **f**) and their respective centroid pose is depicted in **Supplementary Fig. 5**. Only three clusters, parent clusters I-III, fulfil the criteria for a common binding mode containing all core ligands. Parent cluster II corresponds to **a**, parent cluster I to **d** and parent cluster III to **e** in **Supplementary Figs. 4** and **5**.

Nature Chemical Biology: doi:10.1038/nchembio.917

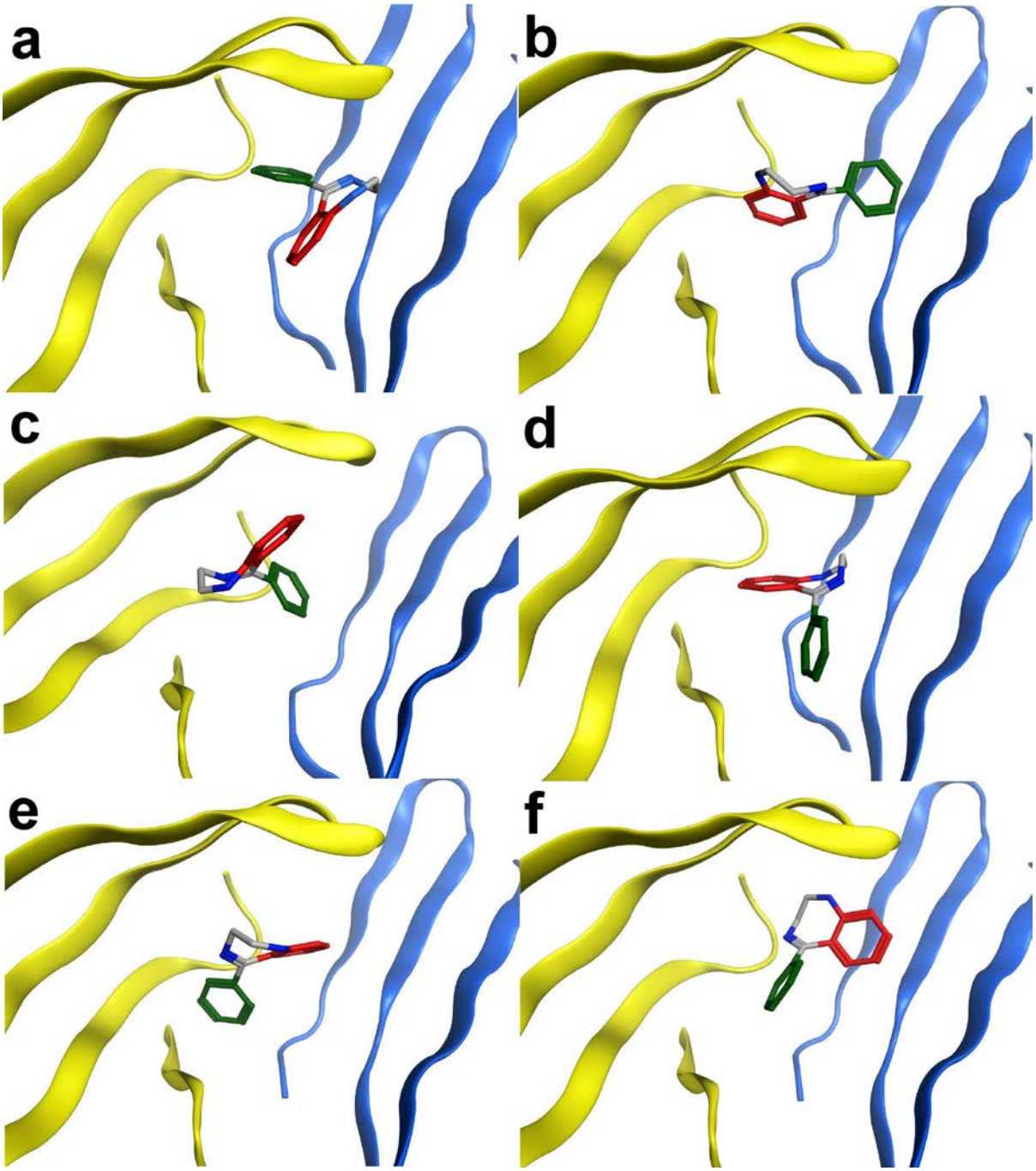

Supplementary Fig. 5 – Sampling space of the initial pose pool represented by the centroids of six dissimilar clusters (**a**-**f**) shown in **Supplementary Figure 4**. The letter on the images corresponds with that of the respective cluster. The alpha subunits are shown in yellow ribbon representation, the gamma subunits are shown in blue. In all panels, the 5-aryl-1,4-benzodizepine scaffold of the centroid pose is depicted. The L1 forming annealed benzene group is depicted in red and the L3 forming pendant phenyl group in green. Color codes used for the 7-ring: gray for C and blue for N.

Nature Chemical Biology: doi:10.1038/nchembio.917

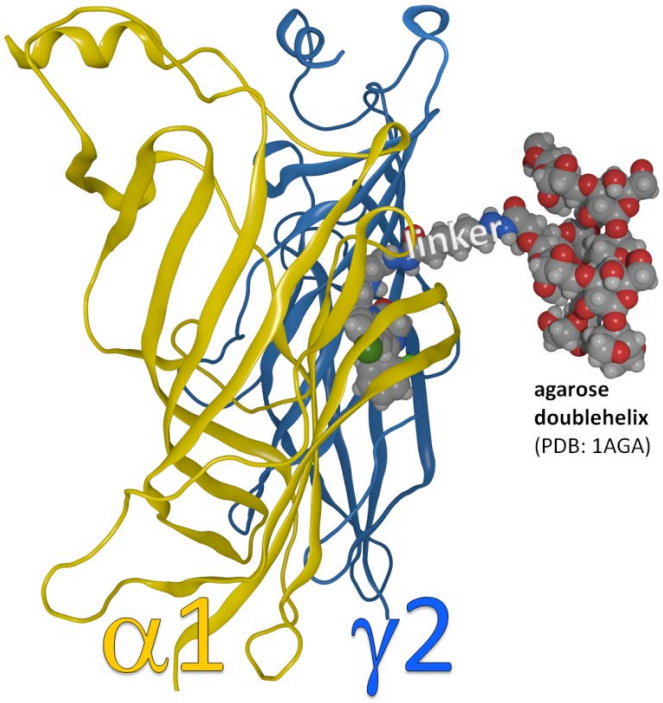

Supplementary Fig. 6 – CBM I poses of compound **5** comfortably accommodate the spacer that is linked to the N1-position of the diazepam scaffold and connecting the affinity chromatography bait with the agarose bead. However, substituents in the N1-position, such as the diethylamine of flurazepam, are fully buried in CBM I poses and correspond to the small portion of the linker that is seen in this rendering to be buried.

Nature Chemical Biology: doi:10.1038/nchembio.917

Supplementary Fig. 7 – Representative CBM I poses of cpds. **1-9**

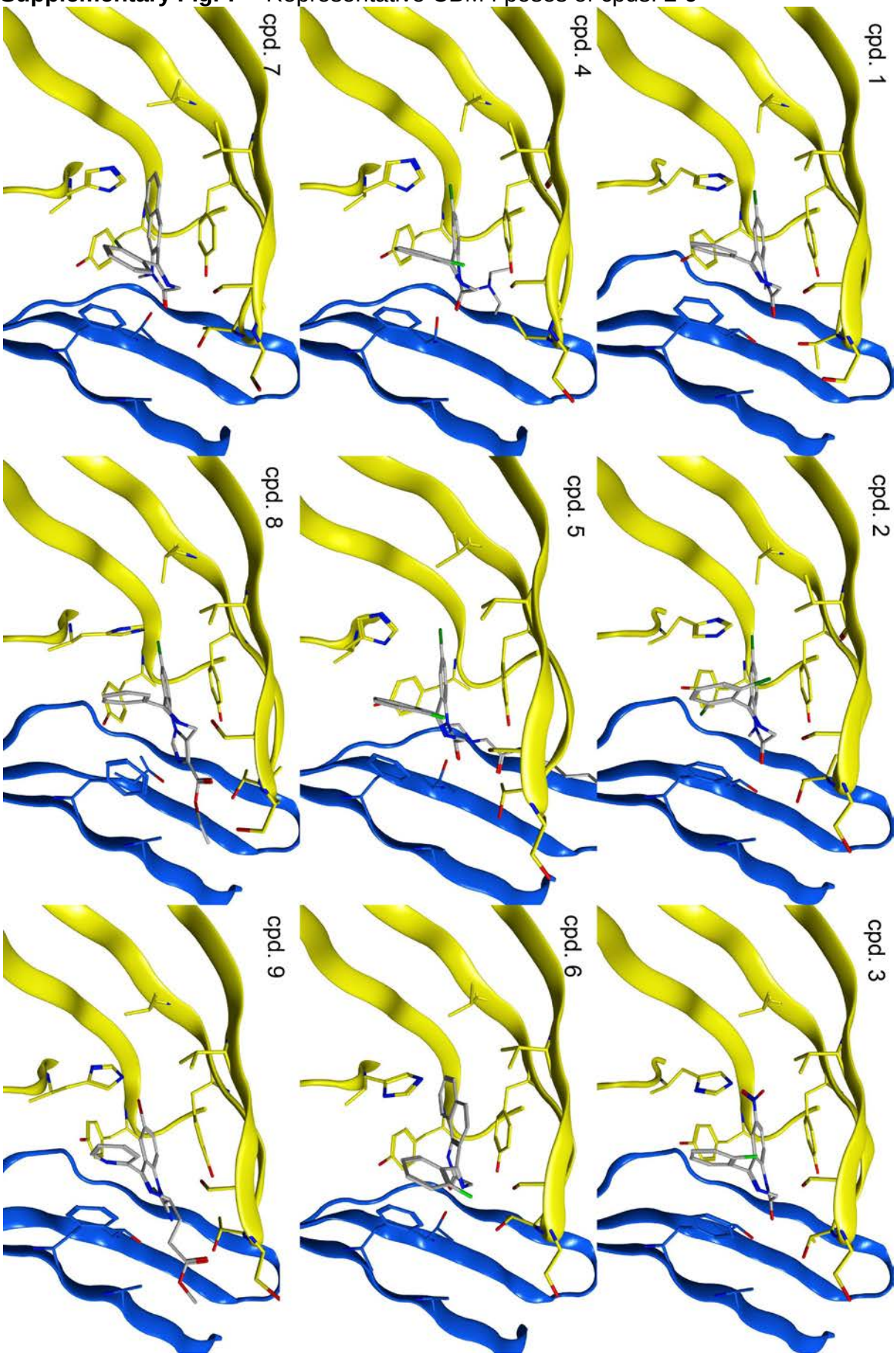

Nature Chemical Biology: doi:10.1038/nchembio.917

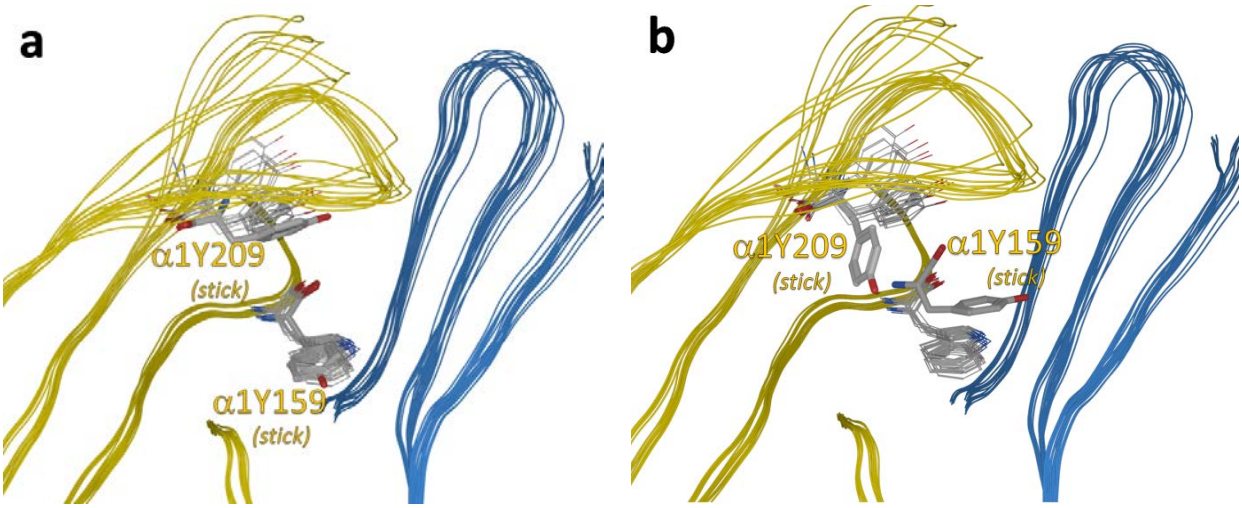

Supplementary Fig. 8 – (a) Rotamer constellation of α1Y159/Y209 (stick representation) as seen in CBM I poses,overlaid with all template structures used in this study. The templates' amino acid side chains that are homologous with α1Y159/Y209 are shown in fine line. The Trp that is homologous with $GABA_AR$ α1Y159 is seen to be in a highly conserved position. The Y on loop C appears to feature a conserved rotamer throughout the superfamily, and probably serves as transduction element for induced fit conformations in the flexible loop C tip. **(b)** Rotamer constellation of α1Y159/Y209 (stick representation) as seen in CBM II poses. The overlay shows that the pattern seen in other superfamily members is lacking, this $GABA_A$ R' model features a completely distinct topology. Quantitative analysis of the entire pose pool that was used in this study revealed that the pattern depicted in panel **(a)** is unique for CBM I poses, and not found in any other pose group.

Nature Chemical Biology: doi:10.1038/nchembio.917

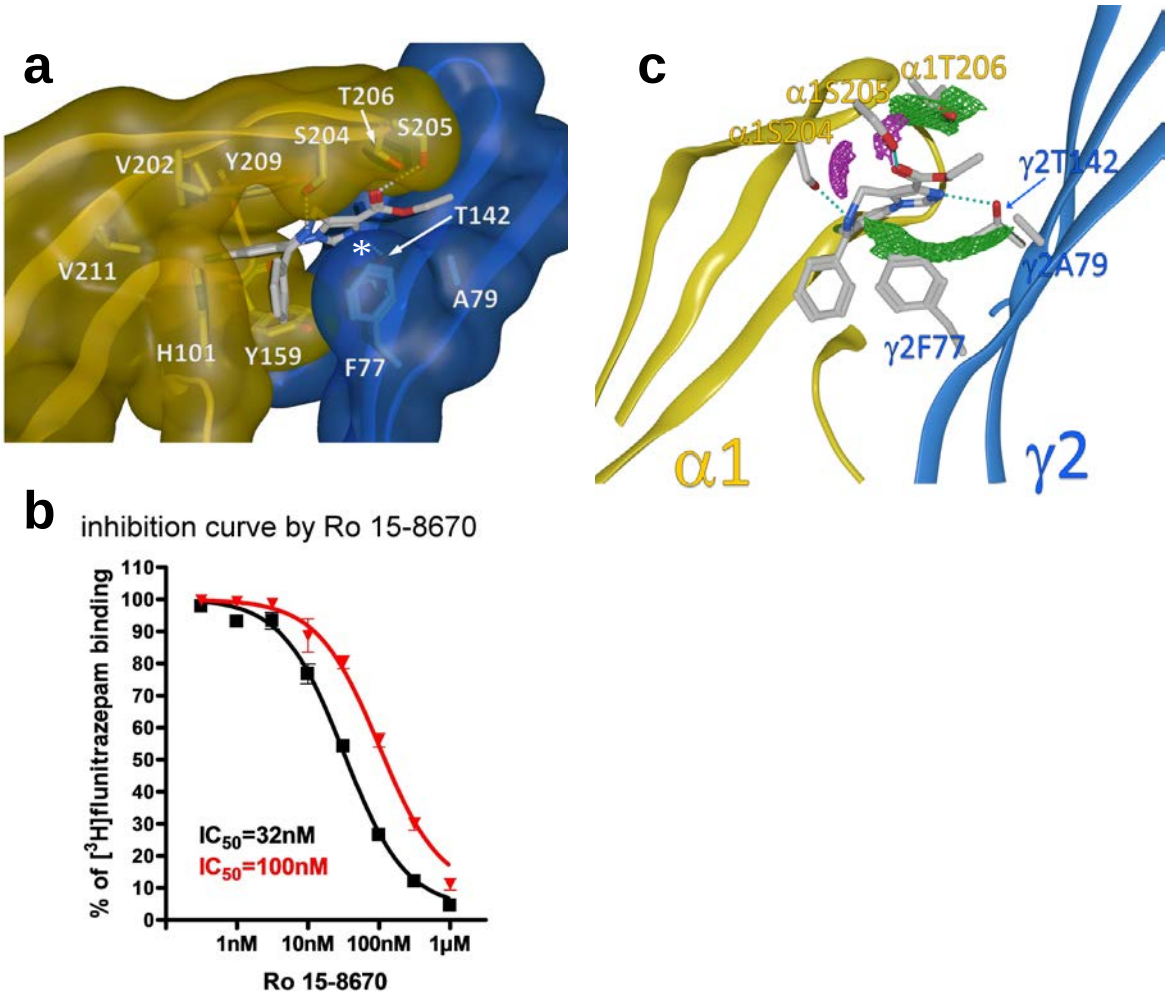

Supplementary Fig. 9 – (**a**) Representation of a CBM I Ro15-8670 pose. Interestingly, in this pose, γ2F77 adapts a rotameric state that allows the phenylalanine-ring to interact with the ester-moiety. Consequently, a γ2F77Y mutation (hydroxyl-group position is indicated by the white star) would not clash the pendant phenyl ring (compare with **Fig. 3**, main text). This observation is completely consistent with the finding that in the γ2F77Y mutant only a 6x reduction was found for Ro15-8670, while a 250x reduction in affinity was seen for diazepam[74] which lacks an ester-moiety. Thus, this structure offers a hypothesis for the observed affinity changes in F77Y by an induced fit. In contrast to the γ2F77Y mutation, the γ2F77I mutation should affect both ligands. Indeed this was shown by **(b)** inhibition of [^{3}H]flunitrazepam binding by Ro 15-8670 in wild-type α1β3γ2 (black curve) and point mutated α1β3γ2F77I (red curve) receptors. Data represent means ± SD from an experiment performed in triplicate. The affinity loss of Ro15-8670 by the mutation γ2F77I is comparable to the one published for diazepam (see text), thus again supporting similar interactions.

Nature Chemical Biology: doi:10.1038/nchembio.917

(c) The same CBM I Ro15-8670 from another perspective focusing on the position of the ester moiety. This pose contains strong structural support for several findings. A α1T206V substitution in loop C caused a 7-fold reduction in affinity of diazepam, but a 16-fold increase in affinity of Ro15-8670[74]. Assuming a common binding mode of these compounds, in CBM I the imine nitrogen of the seven membered ring of diazepam or Ro15-8670 forms a hydrogen bond with α1S204, and the imidazo-group of Ro15-8670 interacts with γ2T142. The carbonyl oxygen of diazepam with its two lone pairs interacts with α1T206, as previously proposed as well as with γ2T142 (see also main text **Fig. 3**). In receptors containing the α1T206V mutation, diazepam is losing an H-bond partner and Ro15-8670 is gaining hydrophobic interactions from the T206V mutant as the valine makes favourable contacts with the ester moiety. This is visualized by an interaction potential map created with a MOE built-in application which draws upon the work of GRID[121,122]. The map graphically illustrates where a hydrophobic probe (dashed green) or an H-bond donating probe (dashed magenta) has favourable interactions with the molecular surface, here depicted for the ester-moiety of Ro15-8670. While the areas in plane of the ester-moiety favour hydrophilic interactions, the areas above and below this moiety favour hydrophobic interactions. Based on this map, the finding that the α1T206V mutation leads to a 16fold gain in affinity is fully consistent with the pose, as the –OH group of the wt T206 “penetrates” the hydrophobic interaction surface, indicating an unfavourable interaction potential.

Nature Chemical Biology: doi:10.1038/nchembio.917

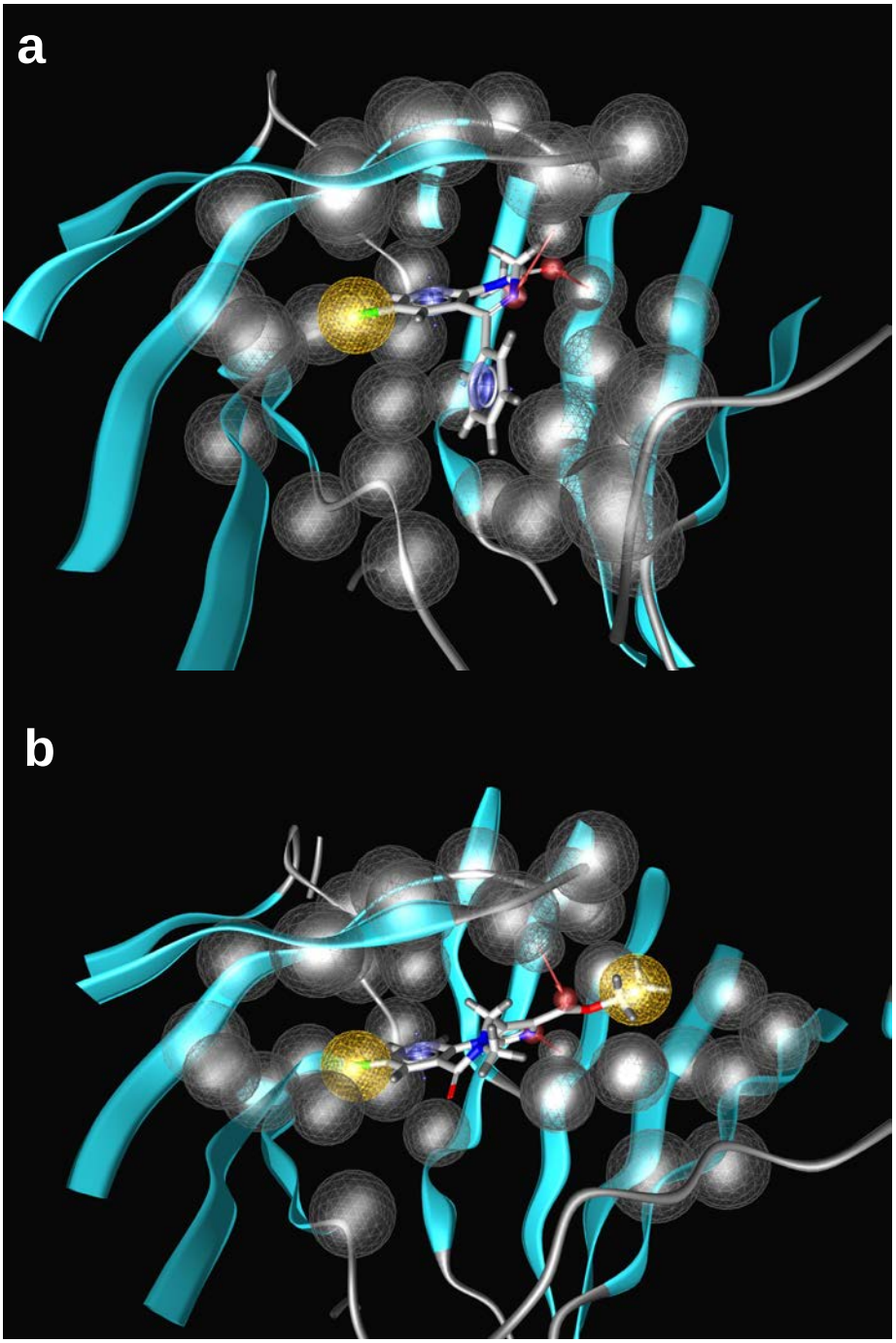

Supplementary Fig. 10 – Depiction of structure-based pharmacophore models based on CBM I diazepam (panel **a**, *Pharmacophore D*) and flumazenil (panel **b**, *Phamacophore F*) bound structures. Yellow spheres represent hydrophobic features, blue slices represent aromatic features and red arrows indicate h-bond acceptor features. Grey spheres represent exclusion volumes and roughly resemble steric binding site topology.

Nature Chemical Biology: doi:10.1038/nchembio.917

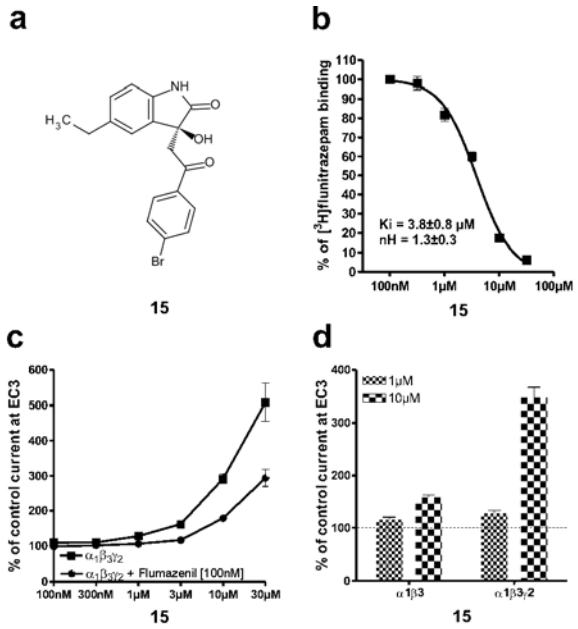

Supplementary Fig. 11 – Structure of the 3-hydroxy-oxindole **15,** and its action on $GABA_A$ receptors.(**a**) Chemical structure. **(b)** Inhibition of 2nM [^{3}H]flunitrazepam binding to mouse cerebellar membranes by **15.** Data represent means±SD from three experiment performed in triplicate **(c)** Dose response curve of **15** on GABA EC3 currents in the absence (■), or presence of100nM flumazenil (●), obtained from Xenopus laevis oocytes expressing recombinant $GABA_A$ receptors composed of $\alpha1\beta3\gamma2$ subunits. Data represent means±SD from three separate experiments performed in different oocytes from 2 different batches. It can be seen that the modulatory action of **15** is incompletely blocked by co-application of the benzodiazepine null modulator flumazenil. **(d)** Effect of compound **15** at 1 µM and 10 µM concentration on $\alpha1\beta3$ and $\alpha1\beta3\gamma2$ (rat) receptors recombinantly expressed in Xenopus laevis oocytes at GABA EC3 (n=4-6). The gamma-subunit independent action seen in $\alpha1\beta3$ receptors indicates a second site of interaction of this compound with these receptors and is consistent with the incomplete flumazenil sensitivity of modulation seen in **(c)**.

Nature Chemical Biology: doi:10.1038/nchembio.917

Supplementary References

49. Notredame, C., Higgins, D.G. & Heringa, J. T-Coffee: A novel method for fast and accurate multiple sequence alignment. *J. Mol. Biol.* **302**, 205-217 (2000).
50. Shi, J., Blundell, T.L. & Mizuguchi, K. FUGUE: sequence-structure homology recognition using environment-specific substitution tables and structure-dependent gap penalties. *J. Mol. Biol.* **310**, 243-257 (2001).
51. Sali, A. & Blundell, T.L. Comparative protein modelling by satisfaction of spatial restraints. *J. Mol. Biol.* **234**, 779-815 (1993).
52. Huang, N., Shoichet, B.K. & Irwin, J.J. Benchmarking sets for molecular docking. *J. Med. Chem.* **49**, 6789-6801 (2006).
53. Irwin, J.J. & Shoichet, B.K. ZINC--a free database of commercially available compounds for virtual screening. *J. Chem. Inf. Model.* **45**, 177-182 (2005).
54. Brejc, K. et al. Crystal structure of an ACh-binding protein reveals the ligand-binding domain of nicotinic receptors. *Nature* **411**, 269-276 (2001).
55. Celie, P.H.N. et al. Nicotine and carbamylcholine binding to nicotinic acetylcholine receptors as studied in AChBP crystal structures. *Neuron* **41**, 907-914 (2004).
56. Unwin, N. Refined structure of the nicotinic acetylcholine receptor at 4A resolution. *J. Mol. Biol.* **346**, 967-989 (2005).
57. Hansen, S.B. et al. Structures of Aplysia AChBP complexes with nicotinic agonists and antagonists reveal distinctive binding interfaces and conformations. *EMBO J.* **24**, 3635-3646 (2005).
58. Dellisanti, C.D., Yao, Y., Stroud, J.C., Wang, Z. & Chen, L. Crystal structure of the extracellular domain of nAChR alpha1 bound to alpha-bungarotoxin at 1.94 A resolution. *Nat. Neurosci.* **10**, 953-962 (2007).
59. Hibbs, R.E. & Gouaux, E. Principles of activation and permeation in an anion-selective Cys-loop receptor. *Nature* **474**, 54-60 (2011).
60. Salvadori, P., Bertucci, C., Ascoli, G., Uccello-Barretta, G. & Rossi, E. Direct resolution, characterization, and stereospecific binding properties of an atropisomeric 1,4-benzodiazepine. *Chirality* **9**, 495-505 (1997).
61. Gilman, N.W., Rosen, P., Earley, J.V., Cook, C. & Todaro, L.J. Atropisomers of 1,4-benzodiazepines. Synthesis and resolution of a diazepam-related 1,4-benzodiazepine. *J. Am. Chem. Soc.* **112**, 3969-3978 (1990).
62. Gilman, N.W. et al. Atropisomers of 1,4-benzodiazepines. 2. Synthesis and resolution of imidazo[1,5-a][1,4]benzodiazepines. *J. Org. Chem.* **58**, 3285-3298 (1993).
63. Lee, S. et al. Axial chirality and affinity at the GABA(A) receptor of pyrimido[1,2-a][1,4]benzodiazepines and related compounds. *Bioorg. Med. Chem.* **16**, 9519-9523 (2008).
64. Blount, J.F., Fryer, R.I., Gilman, N.W. & Todaro, L.J. Quinazolines and 1,4-benzodiazepines. 92. Conformational recognition of the receptor by 1,4-benzodiazepines. *Mol. Pharmacol.* **24**, 425-428 (1983).
65. Simonyi, M.s. et al. Conformational recognition by central benzodiazepine receptors. *Bioorg. Chem.* **18**, 1-12 (1990).
66. Maksay, G., Tegyey, Z. & Simonyi, M. Central benzodiazepine receptors: in vitro efficacies and potencies of 3-substituted 1,4-benzodiazepine stereoisomers. *Mol. Pharmacol.* **39**, 725-732 (1991).

Nature Chemical Biology: doi:10.1038/nchembio.917

67. Ernst, M., Bruckner, S., Boresch, S. & Sieghart, W. Comparative models of GABAA receptor extracellular and transmembrane domains: important insights in pharmacology and function. *Mol. Pharmacol.* **68**, 1291-1300 (2005).
68. Krissinel, E. & Henrick, K. Secondary-structure matching (SSM), a new tool for fast protein structure alignment in three dimensions. *Acta Crystallogr. D Biol. Crystallogr.* **60**, 2256-2268 (2004).
69. Mysinger, M.M. & Shoichet, B.K. Rapid context-dependent ligand desolvation in molecular docking. *J. Chem. Inf. Model.* **50**, 1561-73 (2010).
70. Wolber, G. & Langer, T. LigandScout: 3-D pharmacophores derived from protein-bound ligands and their use as virtual screening filters. *J. Chem. Inf. Model.* **45**, 160-169 (2005).
71. Rarey, M., Kramer, B., Lengauer, T. & Klebe, G. A fast flexible docking method using an incremental construction algorithm. *J. Mol. Biol.* **261**, 470-489 (1996).
72. Claussen, H., Buning, C., Rarey, M. & Lengauer, T. FlexE: efficient molecular docking considering protein structure variations. *J. Mol. Biol.* **308**, 377-395 (2001).
73. Larkin, M.A. et al. Clustal W and Clustal X version 2.0. *Bioinformatics* **23**, 2947-2948 (2007).
74. Sigel, E., Schaerer, M.T., Buhr, A. & Baur, R. The benzodiazepine binding pocket of recombinant alpha1beta2gamma2 gamma-aminobutyric acidA receptors: relative orientation of ligands and amino acid side chains. *Mol. Pharmacol.* **54**, 1097-1105 (1998).
75. Sieghart, W. & Schuster, A. Affinity of various ligands for benzodiazepine receptors in rat cerebellum and hippocampus. *Biochem. Pharmacol.* **33**, 4033-4038 (1984).
76. Sigel, E., Mamalaki, C. & Barnard, E.A. Isolation of a GABA receptor from bovine brain using a benzodiazepine affinity column. *FEBS Lett.* **147**, 45-48 (1982).
77. Zhang, W., Koehler, K.F., Harris, B., Skolnick, P. & Cook, J.M. Synthesis of benzo-fused benzodiazepines employed as probes of the agonist pharmacophore of benzodiazepine receptors. *J. Med. Chem.* **37**, 745-757 (1994).
78. Kilpatrick, G.J. et al. CNS 7056: a novel ultra-short-acting Benzodiazepine. *Anesthesiology* **107**, 60-66 (2007).
79. Berezhnoy, D. et al. On the benzodiazepine binding pocket in GABAA receptors. *J. Biol. Chem.* **279**, 3160-3168 (2004).
80. Kucken, A.M., Teissére, J.A., Seffinga-Clark, J., Wagner, D.A. & Czajkowski, C. Structural requirements for imidazobenzodiazepine binding to GABA(A) receptors. *Mol. Pharmacol.* **63**, 289-296 (2003).
81. Tan, K.R. et al. Proximity-accelerated chemical coupling reaction in the benzodiazepine-binding site of gamma-aminobutyric acid type A receptors: superposition of different allosteric modulators. *J. Biol. Chem.* **282**, 26316-26325 (2007).
82. Tan, K.R., Baur, R., Charon, S., Goeldner, M. & Sigel, E. Relative positioning of diazepam in the benzodiazepine-binding-pocket of GABA receptors. *J. Neurochem.* **111**, 1264-1273 (2009).
83. Wang, R., Lai, L. & Wang, S. Further development and validation of empirical scoring functions for structure-based binding affinity prediction. *J. Comput. Aided Mol. Des.* **16**, 11-26 (2002).
84. Labute, P. The generalized Born/volume integral implicit solvent model: Estimation of the free energy of hydration using London dispersion instead of atomic surface area. *J. Comput. Chem.* **29**, 1693-1698 (2008).

85. Wei, B.Q., Baase, W.A., Weaver, L.H., Matthews, B.W. & Shoichet, B.K. A model binding site for testing scoring functions in molecular docking. *J. Mol. Biol.* **322**, 339-355 (2002).
86. Huang, Q. et al. Pharmacophore/receptor models for GABA(A)/BzR subtypes (alpha1beta3gamma2, alpha5beta3gamma2, and alpha6beta3gamma2) via a comprehensive ligand-mapping approach. *J. Med. Chem.* **43**, 71-95 (2000).
87. Im, W.B. et al. Differential affinity of dihydroimidazoquinoxalines and diimidazoquinazolines to the alpha 1 beta 2 gamma 2 and alpha 6 beta 2 gamma 2 subtypes of cloned GABAA receptors. *Br. J. Pharmacol.* **110**, 677-680 (1993).
88. Ulrich Schacht, G.B. Effects of clobazam in benzodiazepine-receptor binding assays. *Drug Dev. Res.* **S1**, 83-93 (1982).
89. Jennings, A.S. et al. Imidazo[1,2-b][1,2,4]triazines as alpha2/alpha3 subtype selective GABA A agonists for the treatment of anxiety. *Bioorg. Med. Chem. Lett*. **16**, 1477-1480 (2006).
90. Atack, J.R. et al. In vitro and in vivo properties of 3-tert-butyl-7-(5-methylisoxazol-3-yl)-2-(1-methyl-1H-1,2,4-triazol-5-ylme thoxy)-pyrazolo[1,5-d]-[1,2,4]triazine (MRK-016), a GABAA receptor alpha5 subtype-selective inverse agonist. *J. Pharmacol. Exp. Ther.* **331**, 470-484 (2009).
91. Sethy, V.H. & Oien, T.T. Role of cGMP in the mechanism of anxiolytic activity of U-78875. *Pharmacol. Biochem. Behav.* **39**, 379-382 (1991).
92. Mickelson, J.W. et al. High-affinity alpha-aminobutyric acid A/benzodiazepine ligands: synthesis and structure-activity relationship studies of a new series of tetracyclic imidazoquinoxalines. *J. Med. Chem.* **39**, 4654-4666 (1996).
93. Hanson, S.M., Morlock, E.V., Satyshur, K.A. & Czajkowski, C. Structural requirements for eszopiclone and zolpidem binding to the gamma-aminobutyric acid type-A (GABAA) receptor are different. *J. Med. Chem*. **51**, 7243-7252 (2008).
94. Lewis, R.T. et al. A pyridazine series of alpha2/alpha3 subtype selective GABA A agonists for the treatment of anxiety. *J. Med. Chem.* **49**, 2600-2610 (2006).
95. Cox, E.D. et al. Synthesis and evaluation of analogues of the partial agonist 6-(propyloxy)-4-(methoxymethyl)-beta-carboline-3-carboxylic acid ethyl ester (6-PBC) and the full agonist 6-(benzyloxy)-4-(methoxymethyl)-beta-carboline-3-carboxylic acid ethyl ester (Zk 93423) at wild type and recombinant GABAA receptors. *J. Med. Chem*. **41**, 2537-2552 (1998).
96. Primofiore, G. et al. 3-Aryl-[1,2,4]triazino[4,3-a]benzimidazol-4(10H)-ones: tricyclic heteroaromatic derivatives as a new class of benzodiazepine receptor ligands. *J. Med. Chem.* **43**, 96-102 (2000).
97. Dubinsky, B. et al. 5-ethoxymethyl-7-fluoro-3-oxo-1,2,3,5-tetrahydrobenzo[4,5]imidazo[1,2a]pyr idine-4-N-(2-fluorophenyl)carboxamide (RWJ-51204), a new nonbenzodiazepine anxiolytic. *J. Pharmacol. Exp. Ther*. **303**, 777-790 (2002).
98. Wegner, F. et al. GABAA receptor pharmacology of fluorinated derivatives of the novel sedative-hypnotic pyrazolopyrimidine indiplon. *Eur. J. Pharmacol.* **580**, 1-11 (2008).
99. Guerrini, G. et al. Benzodiazepine receptor ligands. 8: synthesis and pharmacological evaluation of new pyrazolo[5,1-c] [1,2,4]benzotriazine 5-oxide 3- and 8-disubstituted: high affinity ligands endowed with inverse-agonist pharmacological efficacy. *Bioorg. Med. Chem.* **14**, 758-775 (2006).
100. Primofiore, G. et al. Novel N-(arylalkyl)indol-3-ylglyoxylylamides targeted as ligands of the benzodiazepine receptor: synthesis, biological evaluation, and molecular

modeling analysis of the structure-activity relationships. *J. Med. Chem.* **44**, 2286-2297 (2001).
101. Lager, E. et al. 4-quinolone derivatives: high-affinity ligands at the benzodiazepine site of brain GABA A receptors. synthesis, pharmacology, and pharmacophore modeling. *J. Med. Chem.* **49**, 2526-2533 (2006).
102. Takada, S. et al. Synthesis and structure--activity relationships of fused imidazopyridines: a new series of benzodiazepine receptor ligands. *J. Med. Chem.* **39**, 2844-2851 (1996).
103. Selleri, S. et al. Synthesis and benzodiazepine receptor affinity of pyrazolo[1,5-a]pyrimidine derivatives. 3. New 6-(3-thienyl) series as alpha 1 selective ligands. *J. Med. Chem.* **46**, 310-313 (2003).
104. Primofiore, G. et al. High affinity central benzodiazepine receptor ligands: synthesis and biological evaluation of a series of phenyltriazolobenzotriazindione derivatives. *J. Med. Chem.* **48**, 2936-2943 (2005).
105. Kahnberg, P. et al. Refinement and evaluation of a pharmacophore model for flavone derivatives binding to the benzodiazepine site of the GABA(A) receptor. *J. Med. Chem.* **45**, 4188-4201 (2002).
106. De Sarro, G. et al. Benzodiazepine receptor affinities, behavioral, and anticonvulsant activity of 2-aryl-2,5-dihydropyridazino[4,3-b]indol- 3(3H)-ones in mice. *Pharmacol. Biochem. Behav.* **65**, 475-487 (2000).
107. Marcel, D., Bardelay, C. & Hunt, P.F. Lesion of noradrenergic neurones with DSP4 does not modify benzodiazepine receptor binding in cortex and hippocampus of rat. *Neuropharmacology* **25**, 283-286 (1986).
108. Lippa, A. et al. Selective anxiolysis produced by ocinaplon, a GABA(A) receptor modulator. *Pro.c Natl. Acad. Sci. U S A* **102**, 7380-7385 (2005).
109. Ogris, W. et al. Affinity of various benzodiazepine site ligands in mice with a point mutation in the GABA(A) receptor gamma2 subunit. *Biochem. Pharmacol.* **68**, 1621-1629 (2004).
110. Bare, T.M. et al. Synthesis and structure-activity relationships of a series of anxioselective pyrazolopyridine ester and amide anxiolytic agents. *J. Med. Chem.* **32**, 2561-2573 (1989).
111. Szekeres, H.J. et al. 3,4-Dihydronaphthalen-1(2H)-ones: novel ligands for the benzodiazepine site of alpha5-containing GABAA receptors. *Bioorg. Med. Chem. Lett.* **14**, 2871-2875 (2004).
112. Carling, R.W. et al. 3-phenyl-6-(2-pyridyl)methyloxy-1,2,4-triazolo[3,4-a]phthalazines and analogues: high-affinity gamma-aminobutyric acid-A benzodiazepine receptor ligands with alpha 2, alpha 3, and alpha 5-subtype binding selectivity over alpha 1. *J. Med. Chem.* **47**, 1807-1822 (2004).
113. Chambers, M.S. et al. 6,7-Dihydro-2-benzothiophen-4(5H)-ones: a novel class of GABA-A alpha5 receptor inverse agonists. *J. Med. Chem.* **45**, 1176-1179 (2002).
114. Griebel, G. et al. SL651498: an anxioselective compound with functional selectivity for alpha2- and alpha3-containing gamma-aminobutyric acid(A) (GABA(A)) receptors. *J. Pharmacol. Exp. Ther.* **298**, 753-768 (2001).
115. Crawforth, J. et al. Tricyclic pyridones as functionally selective human GABAA alpha 2/3 receptor-ion channel ligands. *Bioorg. Med. Chem. Lett.* **14**, 1679-1682 (2004).
116. Davies, L.P., Barlin, G.B., Ireland, S.J. & Ngu, M.M. Substituted imidazo[1,2-b]pyridazines. New compounds with activity at central and peripheral benzodiazepine receptors. *Biochem. Pharmacol*. **44**, 1555-1561 (1992).

117. Mehta, A.K. & Shank, R.P. Interaction of abecarnil, bretazenil, and RO 19-8022 with diazepam-sensitive and -insensitive benzodiazepine sites in the rat cerebellum and cerebral cortex. *Life Sci.* **57**, 2215-2222 (1995).
118. Atack, J.R. et al. TPA023 [7-(1,1-dimethylethyl)-6-(2-ethyl-2H-1,2,4-triazol-3-ylmethoxy)-3-(2-fluor ophenyl)-1,2,4-triazolo[4,3-b]pyridazine], an agonist selective for alpha2- and alpha3-containing GABAA receptors, is a nonsedating anxiolytic in rodents and primates. *J. Pharmacol. Exp. Ther.* **316**, 410-422 (2006).
119. Wada, T. et al. Pharmacologic characterization of a novel non-benzodiazepine selective anxiolytic, DN-2327. *Jpn. J. Pharmacol.* **49**, 337-349 (1989).
120. Jain, A.N. & Nicholls, A. Recommendations for evaluation of computational methods. *J. Comput. Aided Mol. Des.* **22**, 133-139 (2008).
121. Boobbyer, D.N., Goodford, P.J., McWhinnie, P.M. & Wade, R.C. New hydrogen-bond potentials for use in determining energetically favorable binding sites on molecules of known structure. *J.Med. Chem.* **32**, 1083-1094 (1989).
122. Goodford, P.J. A computational procedure for determining energetically favorable binding sites on biologically important macromolecules. *J. Med. Chem.* **28**, 849-857 (1985).

Nature Chemical Biology: doi:10.1038/nchembio.917

II. A residue close to α1 loop F disrupts modulation of $GABA_A$ receptors by benzodiazepines while their binding is maintained

Journal of Neurochemistry JNC

JOURNAL OF NEUROCHEMISTRY | 2010 | 115 | 1478–1485 doi: 10.1111/j.1471-4159.2010.07052.x

A residue close to α_1 loop F disrupts modulation of $GABA_A$ receptors by benzodiazepines while their binding is maintained

Roland Baur,*[,1] Benjamin P. Lüscher,*[,1] Lars Richter† and Erwin Sigel*

*Institute of Biochemistry and Molecular Medicine, University of Bern, Bern, Switzerland

†Department of Medicinal Chemistry, University of Vienna, Vienna, Austria

Contribution of the thesis author to this article:

The author of the thesis performed a computational analysis on a homology model of the α1β2γ2 $GABA_A$ receptor (homology models were generated by Margot Ernst and Werner Sieghart). In more detail the intra molecular protein-protein H-bond networks in proximity to the benzodiazepine binding site of the $GABA_A$ receptor model were investigated. The results aided in the selection of α1Y168 as a candidate for receptor mutation.

Journal of Neurochemistry

JOURNAL OF NEUROCHEMISTRY | 2010 | 115 | 1478–1485 doi: 10.1111/j.1471-4159.2010.07052.x

A residue close to α_1 loop F disrupts modulation of $GABA_A$ receptors by benzodiazepines while their binding is maintained

Roland Baur,*[,1] Benjamin P. Lüscher,*[,1] Lars Richter† and Erwin Sigel*

*Institute of Biochemistry and Molecular Medicine, University of Bern, Bern, Switzerland

†Department of Medicinal Chemistry, University of Vienna, Vienna, Austria

Abstract

Benzodiazepines act at the major isoforms of GABA type A receptors where they potentiate the current evoked by the agonist GABA. The underlying mechanism of this potentiation is poorly understood, but hypothesized to be related to the mechanism that links agonist binding to channel opening in these ligand activated ion channels. The loop F of the α_1 and the β_2 subunit have been implicated in channel gating, and loop F of the γ_2 subunit in the modulation by benzodiazepines. We have identified the conservative point mutation Y168F located N-terminally of loop F in the α_1 subunit that fails to affect agonist properties. Interestingly, it disrupts modulation by benzodiazepines, but leaves high affinity binding to the benzodiazepine binding site intact. Modulation by barbiturates and neurosteroids is also unaffected. Residue α_1Y168 is not located either near the binding pockets for GABA, or for benzodiazepines, or close to the loop F of the γ_2 subunit. Our results support the fact, that broader regions of ligand gated receptors are conformationally affected by the binding of benzodiazepines. We infer that also broader regions could contribute to signaling from GABA agonist binding to channel opening.

Keywords: benzodiazepine binding, benzodiazepine modulation, channel gating, F loop, GABA, $GABA_A$ receptor.

J. Neurochem. (2010) **115**, 1478–1485.

In the family of ligand-activated ion channels that includes nicotinic acetylcholine receptors, GABA type A ($GABA_A$) receptors, glycine receptors and serotonin 5-HT_3 receptors, binding of the agonist is followed by a conformational change leading to the opening of the inherent ion channel. The mechanism by which binding leads to channel opening is highly controversial. One concept envisages a direct functional link between the binding site and the channel region by a random coil polypeptide stretch called loop F. The function of loop F in linking binding and gating is disputed some observations pointing in favor of the hypothesis (Lyford *et al.* 2003; Newell and Czajkwski 2003; Hansen *et al.* 2005; Thompson *et al.* 2006; Williams *et al.* 2009) and others against (Khatri *et al.* 2009; Pless and Lynch 2009). This controversy has recently been reviewed (Khatri and Weiss 2010). Beside loop F, residues located at the outer membrane surface have been implicated in the binding/gating process (Sigel *et al.* 1999; Brejc *et al.* 2001; Kash *et al.* 2003; Lummis *et al.* 2005; Unwin 2005; Mercado and Czajkowski 2006), but it is far from clear how the information of binding site occupancy is transferred to these residues.

GABA type A receptors are pseudosymmetric proteins consisting of five subunits, thus containing five F loops. The pharmacological properties of a $GABA_A$ receptor depend on subunit composition (Sieghart and Sperk 2002) and arrangement (Minier and Sigel 2004). In this study we concentrated on the major form of adult $GABA_A$ receptors $\alpha_1\beta_2\gamma_2$ (Macdonald and Olsen 1994; Rabow *et al.* 1995; Sieghart 1995), whose subunits are arranged $\alpha_1\gamma_2\beta_2\alpha_1\beta_2$ counterclockwise around the central ion channel (Baumann *et al.* 2001, 2002; Baur *et al.* 2006). In the $GABA_A$ receptor, the F Loop of the α_1 subunit as well as the F loop of the β_2 subunit have been reported to play an important role in linking binding to gating of the $GABA_A$ receptor (Newell and Czajkwski 2003; Williams *et al.* 2009).

Many drugs act at $GABA_A$ receptors among them benzodiazepines. Benzodiazepines are clinically important

Received August 31, 2010; revised manuscript received September 24, 2010; accepted October 5, 2010.

Address correspondence and reprint requests to Erwin Sigel, Institute of Biochemistry and Molecular Medicine, University of Bern, Bühlstrasse 28, CH-3012 Bern, Switzerland. E-mail: erwin.sigel@mci.unibe.ch

[1]These authors contributed equally to this study.

Abbreviations used: DMCM, methyl 6, 7-dimethoxy-4-ethly-beta-carboline-2-carboxylate; $GABA_A$ receptor, GABA type A receptor; HEK, human embryonic kidney.

drugs and are used mainly for their sedative/hypnotic and anxiolytic action. They bind to a high affinity binding site, located at the α/γ subunit interface, that is homologous to the two GABA agonist sites, located at β/α subunit interfaces (for review see Sigel and Buhr 1997). Benzodiazepines potentiate responses of the major $GABA_A$ receptor isoforms to the agonist GABA. In this case high affinity binding of benzodiazepines induces a structural change to the receptor, leading to potentiation. Again, the underlying structural change is poorly understood. In this case, loop F of the γ_2 subunit has been suggested to be involved in this process (Hanson and Czajkowski 2008; Padgett and Lummis 2008). Residues located at the outer membrane surface may also play a role (Boileau and Czajkowski 1999).

We report here on a conservative point mutation located at the N-terminal end of loop F in the α_1 subunit of the $GABA_A$ receptor, which does not affect the response to GABA and high affinity binding of benzodiazepines to their site, but strongly decreases modulation by benzodiazepines. This residue is distant from loop F of the γ_2 subunit, arguing for the fact that receptor regions outside this loop F are essential for signaling from the benzodiazepine binding site to the channel portion. We hypothesize that the same may be the case for signaling from agonist binding to channel opening in the ligand gated ion channel family.

Methods

Construction of the mutated receptor subunit

The mutant subunit α_1Y168F was prepared using the QuikChange™ mutagenesis kit (Stratagene, Agilent Technologies, Basel, Switzerland). For cell transfection, the cDNAs were subcloned into the polylinker of pBC/CMV (Bertocci *et al.* 1991). This expression vector allows high-level expression of a foreign gene under control of the cytomegalovirus promoter. The α subunit was cloned into the *Eco*RI and the β and γ subunits were subcloned into the *Sma*I site of the polylinker by standard techniques.

Expression in Xenopus oocytes

Capped cRNAs were synthesized (Ambion, Applied Biosystems, Rotkreuz, Switzerland) from the linearized vectors containing the different subunits, respectively. A poly-A tail of about 400 residues was added to each transcript using yeast poly-A polymerase (United States Biologicals, Cleveland, OH, USA). The concentration of the cRNA was quantified on a formaldehyde gel using Radiant Red stain (Bio-Rad Laboratories, Reinach, Switzerland) for visualization of the RNA. Known concentrations of RNA ladder (Invitrogen, Basel, Switzerland) were loaded as standard on the same gel. cRNAs were precipitated in ethanol/isoamylalcohol 19 : 1, the dried pellet dissolved in water and stored at −80°C. cRNA mixtures were prepared from these stock solutions and stored at −80°C.

Xenopus laevis oocytes were prepared, injected and defolliculated as described previously (Sigel 1987; Sigel and Minier 2005). They were injected with 50 nL of the cRNA solution containing wild type or mutated α_1 and wild type β_2 and γ_2 subunits at a concentration of 10 nM : 10 nM : 50 nM (Boileau *et al.* 2002), and then incubated in modified Barth's solution [10 mM HEPES, pH 7.5, 88 mM NaCl, 1 mM KCl, 2.4 mM $NaHCO_3$, 0.82 mM $MgSO_4$, 0.34 mM $Ca(NO_3)_2$, 0.41 mM $CaCl_2$, 100 units/mL penicillin, 100 μg/mL streptomycin] at 18°C for at least 24 h before the measurements.

Functional characterization in Xenopus oocytes

Currents were measured using a home-built two-electrode voltage clamp amplifier in combination with a XY-recorder (90% response time 0.1 s) or digitized at 100 Hz using a MacLab/200 (AD Instruments, Spechbach, Germany). Tests with a model oocyte were performed to ensure linearity in the larger current range. The response was linear up to 20 μA. Electrophysiological experiments were performed at a holding potential of −80 mV. The perfusion medium contained 90 mM NaCl, 1 mM KCl, 1 mM $MgCl_2$, 1 mM $CaCl_2$, and 5 mM Na-HEPES (pH 7.4). The perfusion solution (6 mL/min) was applied through a glass capillary with an inner diameter of 1.35 mm, the mouth of which was placed about 0.4 mm from the surface of the oocyte (Baur and Sigel 2007). The experiments were performed after the measured currents became constant. Concentration response curves for GABA were fitted with the equation $I(c) = I_{max}/(1 + (EC_{50}/c)^n)$, where c is the concentration of GABA, EC_{50} the concentration of GABA eliciting half maximal current amplitude, I_{max} is the maximal current amplitude, I the current amplitude and n the Hill coefficient. Allosteric modulation via the benzodiazepine site were measured at a GABA concentration eliciting 2–5% of the maximal GABA current amplitude. GABA was applied for 20 s alone or in combination with allosteric compound. The prototype positive allosteric modulator diazepam, the prototype negative allosteric modulator methyl 6, 7-dimethoxy-4-ethyl-beta-carboline-2-carboxylate (DMCM) and the prototype benzodiazepine antagonist Ro15-1788 were used. Additionally, a positive modulator with a different chemical structure from classic benzodiazepines, the imidazobendiazepine zolpidem was tested. Relative current potentiation by benzodiazepines (BZ) was determined as $(I_{1\ \mu M\ BZ\ +\ GABA}/I_{GABA} - 1) * 100\%$. The perfusion system was cleaned between drug applications, by washing with dimethylsulfoxide to avoid contamination.

Transfection of recombinant $GABA_A$ receptor in cultured cells

The cells were maintained in minimum essential medium (Invitrogen, Basel, Switzerland) supplemented with 10% fetal calf serum, 2 mM glutamine, 50 units/mL penicillin and 50 μg/mL streptomycin by standard cell culture techniques. Equal amounts (total of 20 μg DNA/90 mm dish) of plasmids coding for $GABA_A$ receptor subunits were transfected into human embryonic kidney (HEK) 293 cells (ATCC no. CRL 1573) by the calcium phosphate precipitation method (Chen and Okayama 1987). After overnight incubation, the cells were washed once with serum free medium and reefed with medium.

Membrane preparation

Approximately 60 h after transfection the cells were harvested by washing with ice-cold phosphate-buffered saline, pH 7.0, and centrifuged at 150 *g*. Cells were washed with buffer containing 10 mM K phosphate, 100 mM KCl, 0.1 mM K EDTA, pH 7.4. Cells were homogenized by sonication in the presence of 10 μM

phenyl-methyl-sulfonyl-fluoride and 1 mM EDTA. Membranes were collected by three centrifugation-resuspension cycles (100 000 *g* for 20 min), and then used for ligand binding or stored at −20°C.

Binding assays

Binding assays were carried out as before (Baur *et al.* 2008). Briefly, resuspended cell membranes (0.2–0.5 mL) were incubated for 60 min on ice in the presence of [^{3}H]Ro15-1788 (87 Ci/mmol, PerkinElmer, Schwerzenbach, Switzerland) or [^{3}H]flunitrazepam (86 Ci/mmol, PerkinElmer) and various concentrations of competing ligands. Membranes were collected by rapid filtration on GF/C filters (Whatman, Dassel, Germany). After three washing steps with 5 mL of buffer, the filter-retained radioactivity was determined by liquid scintillation counting. Non-specific binding was determined in the presence of 10 μM Ro15-1788 or 20 μM flunitrazepam, respectively. Displacement assays were carried out with [^{3}H]Ro15-1788 as radioactive ligand and increasing concentrations of diazepam or DMCM. Data were fitted by using a nonlinear least-squares method to the equation $B(c) = B_{max}/(1 + K_d/c)$ for binding curves and $B(c) = B_{max}/(1 + (c/IC_{50}))$ for displacement curves, where c is the concentration of ligand, B, binding, B_{max}, maximal binding, K_d, dissociation constant and n, Hill coefficient. All fitting procedures were performed with the Kaleidagraph software. IC_{50} values of displacement curves were converted to K_i values according to the Cheng-Prusoff equation (Cheng and Prusoff 1973).

Alignment and model building

A multiple sequence alignment was performed using the clustalX (Thompson *et al.* 1994) program. Based on this sequence alignment and the X-ray crystal structure of acetylcholine binding protein (AChBP) (Hansen *et al.* 2005), the homology model was built by MODELLER (Sali and Blundell 1993) as described in Ernst *et al.* (2005).

Results

Response to GABA

The conservative mutation to Phe was introduced into residue α_1Y168. Tyrosine side chains differ from phenylalanine side chains by the potential to form a hydrogen bridge. The mutated subunit was expressed together with β_2 and γ_2 subunits in Xenopus oocytes and the resulting receptor compared to wild type receptors. The mutation did not significantly affect functional expression levels (not shown) and only weakly affected the response to GABA (Fig. 1). The concentration-response curves of wild type $\alpha_1\beta_2\gamma_2$ and mutant α_1Y168F$\beta_2\gamma_2$ receptors were characterized by EC_{50}s of 16 ± 2 μM (n = 6) and 18 ± 10 μM (n = 7) and a Hill coefficients of 1.36 ± 0.06 and 1.06 ± 0.18, respectively.

To ensure presence of the γ_2 subunit in both receptors, we performed concentration-response curves for wild type $\alpha_1\beta_2$ and mutant α_1Y168Fβ_2 receptors. Omission of the γ_2 subunit is known to lead to a shift of the concentration response curve for GABA to the left (Sigel *et al.* 1990). These curves

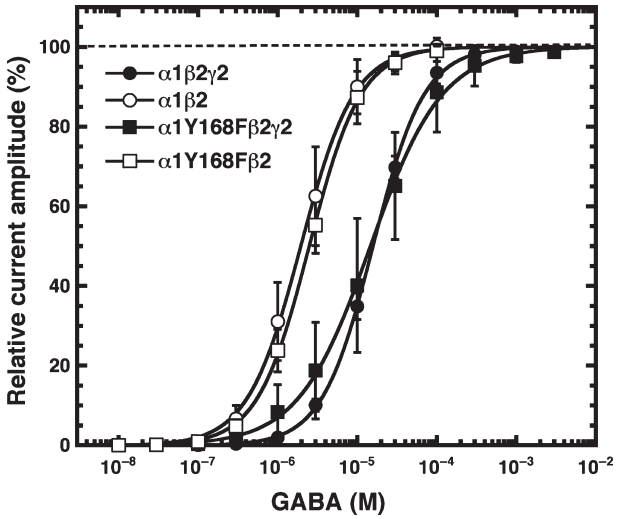

Fig. 1 Concentration response curves for GABA at wild type $\alpha_1\beta_2\gamma_2$ and $\alpha_1\beta_2$ and mutant α_1Y168F$\beta_2\gamma_2$ and α_1Y168Fβ_2 receptors. Receptors were expressed in Xenopus oocytes and exposed to increasing concentrations of GABA. Individual curves were first normalized to the observed maximal current amplitude and subsequently averaged. Mean ± SD of at least five experiments carried out with different oocytes from at least two batches for each subunit combination is shown.

were characterized by EC_{50}s of 2.1 ± 0.8 μM (n = 5) and 2.6 ± 0.7 μM (n = 5) and Hill coefficients of 1.36 ± 0.12 and 1.36 ± 0.13, respectively (Fig. 1). Thus, in mutant α_1Y168F$\beta_2\gamma_2$ receptors a similar leftward shift of the concentration-response curves was observed as in wild type $\alpha_1\beta_2\gamma_2$ receptors, confirming the presence of the γ_2 subunit in both receptors.

Potentiation by ligands of the benzodiazepine binding site

Large differences between wild type and mutant receptors were observed for the potentiation by diazepam. Current traces are shown in Fig. 2. Potentiation of about 200% in wild type $\alpha_1\beta_2\gamma_2$ receptors was reduced to 30% in mutant α_1Y168F$\beta_2\gamma_2$ receptors. This decrease in potentiation was also observed for other ligands of the benzodiazepine binding site (Fig. 3). A quantitative analysis showed that current potentiation was reduced by the mutation for 1 μM diazepam from 200 ± 44% in wild type receptors to 28 ± 26% in mutant receptors, for 1 μM flunitrazepam from 187 ± 13% to 28 ± 12% and for 1 μM zolpidem from 424 ± 21% to 64 ± 30%. Inhibition by DMCM was reduced from −60 ± 1% to 0 ± 11% (Fig. 3). All data were derived from four experiments carried out with oocytes from two independent batches. Ro15-1788 did not significantly affect the current amplitudes elicited by GABA. Data shown below indicate that Ro15-1788 binds with high affinity irrespective of the mutation. Thus, Ro15-1788 is an antagonist in both wild type and mutant receptors (Fig. 3).

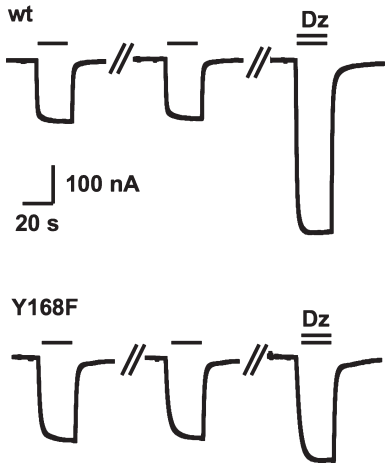

Fig. 2 Diazepam potentiates α_1Y168F$\beta_2\gamma_2$ receptors less than wild type receptors. Receptors were expressed in Xenopus oocytes and exposed twice to 1 μM GABA alone followed by combined application of 1 μM GABA and 1 μM diazepam.

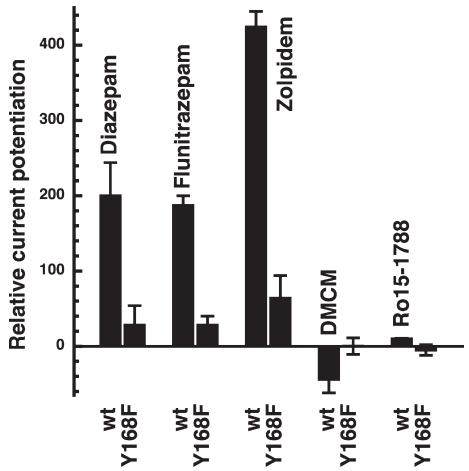

Fig. 3 Ligands of the benzodiazepine binding site potentiate α_1Y168F$\beta_2\gamma_2$ receptors less than wild type receptors. Similar experiments as shown in Fig. 2 were carried out with 1 μM diazepam, 1 μM flunitrazepam, 1 μM zolpidem, 1 μM DMCM or 1 μM Ro15-1788. Means ± SD of experiments carried out with four oocytes from two batches for each subunit combination are shown.

The concentration dependence of the potentiation by diazepam and zolpidem at wild type $\alpha_1\beta_2\gamma_2$ and mutant α_1Y168F$\beta_2\gamma_2$ receptors was also determined (Fig. 4). Potentiation by diazepam was fitted with an EC_{50} of 0.059 ± 0.013 μM (n = 3) and a maximal potentiation of 285 ± 29% for wild type receptors, and 3.7 ± 2.4 μM (n = 4) and 53 ± 9% for mutant receptors (Fig. 4a). Potentiation by zolpidem was fitted with an EC_{50} of 0.17 ± 0.01 μM (n = 3) and a maximal potentiation of 392 ± 29% for wild type receptors, and 5.8 ± 2.6 μM (n = 3) and 64 ± 14% for mutant receptors (Fig. 4b). Thus, for both ligands of the

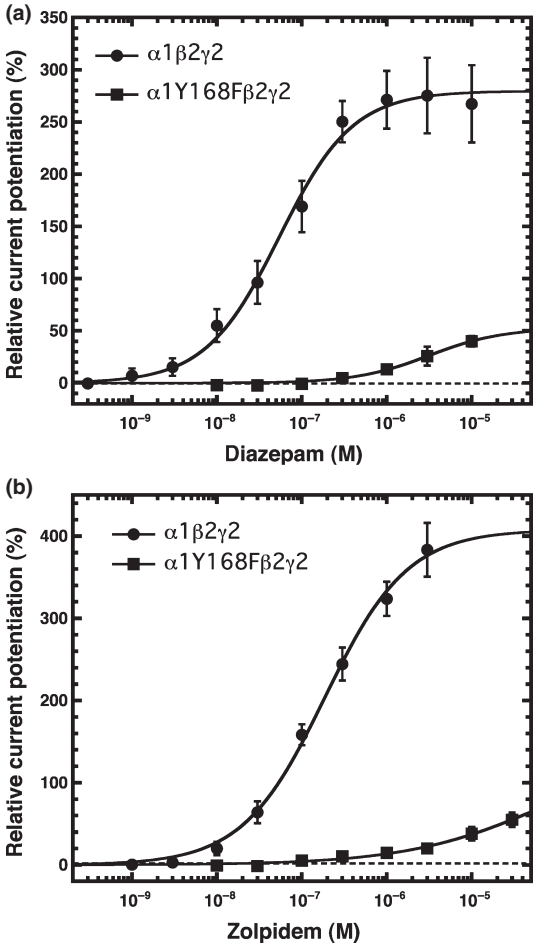

Fig. 4 Concentration-dependent potentiation of wild type $\alpha_1\beta_2\gamma_2$ and mutant α_1Y168F$\beta_2\gamma_2$ receptors by diazepam and zolpidem. Receptors were expressed in Xenopus oocytes and exposed to 0.5 μM or 1.0 μM GABA in combination with increasing concentrations of diazepam (a) or zolpidem (b), respectively. Individual curves were first normalized to the observed maximal current amplitude and subsequently averaged. Mean ± SD of experiments carried out with four oocytes from two batches for each subunit combination are shown.

benzodiazepine binding site, there was a decrease in apparent affinity amounting to more than 30-fold, and a decrease in the maximal potentiation amounting to more than 5-fold. It was interesting to see whether the apparent decrease in affinity for function was reflected in a decrease in binding affinity.

Radioactive ligand binding to the benzodiazepine binding site

Wild type $\alpha_1\beta_2\gamma_2$ and mutant α_1Y168F$\beta_2\gamma_2$ receptors were expressed in HEK293 cells and their benzodiazepine binding sites probed with several ligands. Radioactive ligands were tested in binding assays and non-radioactive ligands in displacement assays. Figure 5(a) shows as an example the binding of [^{3}H]Ro15-1788 to mutant receptors. The affinity

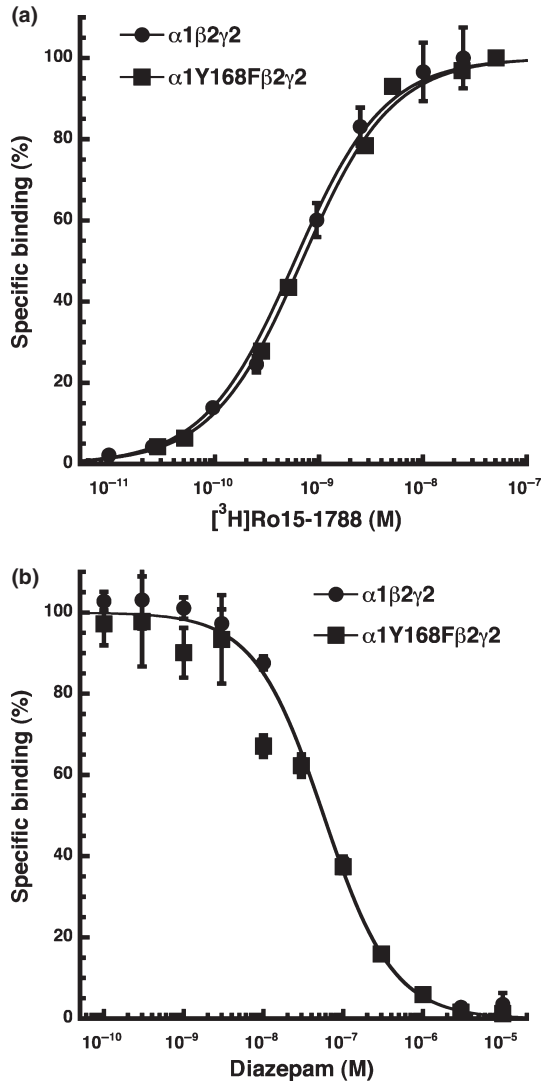

Fig. 5 Binding of [^{3}H]Ro15-1788 to (a) and displacement of [^{3}H]Ro15-1788 by diazepam from (b) wild type $\alpha_1\beta_2\gamma_2$ and mutant α_1Y168F$\beta_2\gamma_2$ receptors. Receptors were expressed in HEK293 cells, membranes harvested and subjected to a radioactive ligand binding assay. Individual experiments are shown. Fitted curves for wild type and mutant receptor overlap. Mean ± SD from experiments carried out in triplicate.

of mutant receptors was with 0.8 nM in the range of that of wild type receptors, indicating that the point mutation did not disrupt the binding affinity. Displacement by diazepam of [^{3}H]Ro15-1788 binding also remained unaffected by the mutation (Fig. 5b). Table 1 summarizes these experiments. Wild type and mutant receptors were compared in their respective affinities for [^{3}H]Ro15-1788, [^{3}H]flunitrazepam, diazepam and DMCM. For none of the tested ligands more than a 1.8-fold difference between wild type and mutant receptors was observed.

Lack of an effect of mutation of the homologous residue in the β_2 subunit

The homologous residue to α_1Y168 in the β_2 subunit, F166 was mutated to Y. $\alpha_1\beta_2$F166Yγ_2 receptors were expressed in Xenopus oocytes and functionally characterized. Neither the EC_{50} for GABA nor modulation by 1 μM diazepam was affected by the mutation (results not shown). Very similar results were obtained with mutation of the neighboring residues of β_2F166, β_2E165D and β_2Y167F.

Lack of an effect of the mutation α_1Y168Y on channel gating and modulation by pentobarbital, neurosteroids and inhibition by zinc ions

The mutation α_1Y168Y mutation did not affect channel gating by GABA or binding of benzodiazepines, but disrupted modulation of the channel by benzodiazepines. It was interesting to see if the action of other modulatory compounds was affected by the mutation or whether the effect was specific for modulation by benzodiazepines. Therefore, we investigated if channel modulation by pentobarbital, the neurosteroid THDOC (3α,21-dihydroxy-5α-pregnan-20-one) or inhibition by zinc ions was affected by the α_1Y168Y mutation. As Fig. 6 shows, neither concentration dependent gating (Fig. 6a) or potentiation (Fig. 6b) by pentobarbital, nor concentration dependent gating (Fig. 6c) or potentiation (Fig. 6d) of the channel, nor its concentration dependent inhibition by zinc ions was affected (not shown). Inhibition by 1 μM and 1 mM Zn^{2+} was 24 ± 11% (n = 3) and 86 ± 1% (n = 3) for wild type receptors and 22 ± 10% (n = 3) and 82 ± 6% (n = 3) for mutant receptors, respectively.

Table 1 Summary of the binding properties of the benzodiazepine binding site in wild type $\alpha_1\beta_2\gamma_2$ and mutant α_1Y168F$\beta_2\gamma_2$ receptors

Receptor	[^{3}H]Ro15-1788, K_d (nM)	[^{3}H]flunitrazepam, K_d (nM)	Diazepam, K_i (nM)	DMCM, K_i (nM)
$\alpha_1\beta_2\gamma_2$	0.70 ± 0.11	2.0 ± 0.4	14.5 ± 3.7	1.3 ± 0.3
α_1Y168F$\beta_2\gamma_2$	0.73 ± 0.05	1.6 ± 0.3	8.2 ± 2.0	2.1 ± 0.4

Binding of [^{3}H]Ro15-1788 and of [^{3}H]flunitrazepam to and displacement of [^{3}H]Ro15-1788 by diazepam and DMCM was determined. Receptors were expressed in HEK293 cells, membranes harvested and subjected to a radioactive ligand binding assays. Individual curves were first normalized to the observed maximal binding level and subsequently averaged. Mean ± SD from two to four experiments each carried out in triplicate.

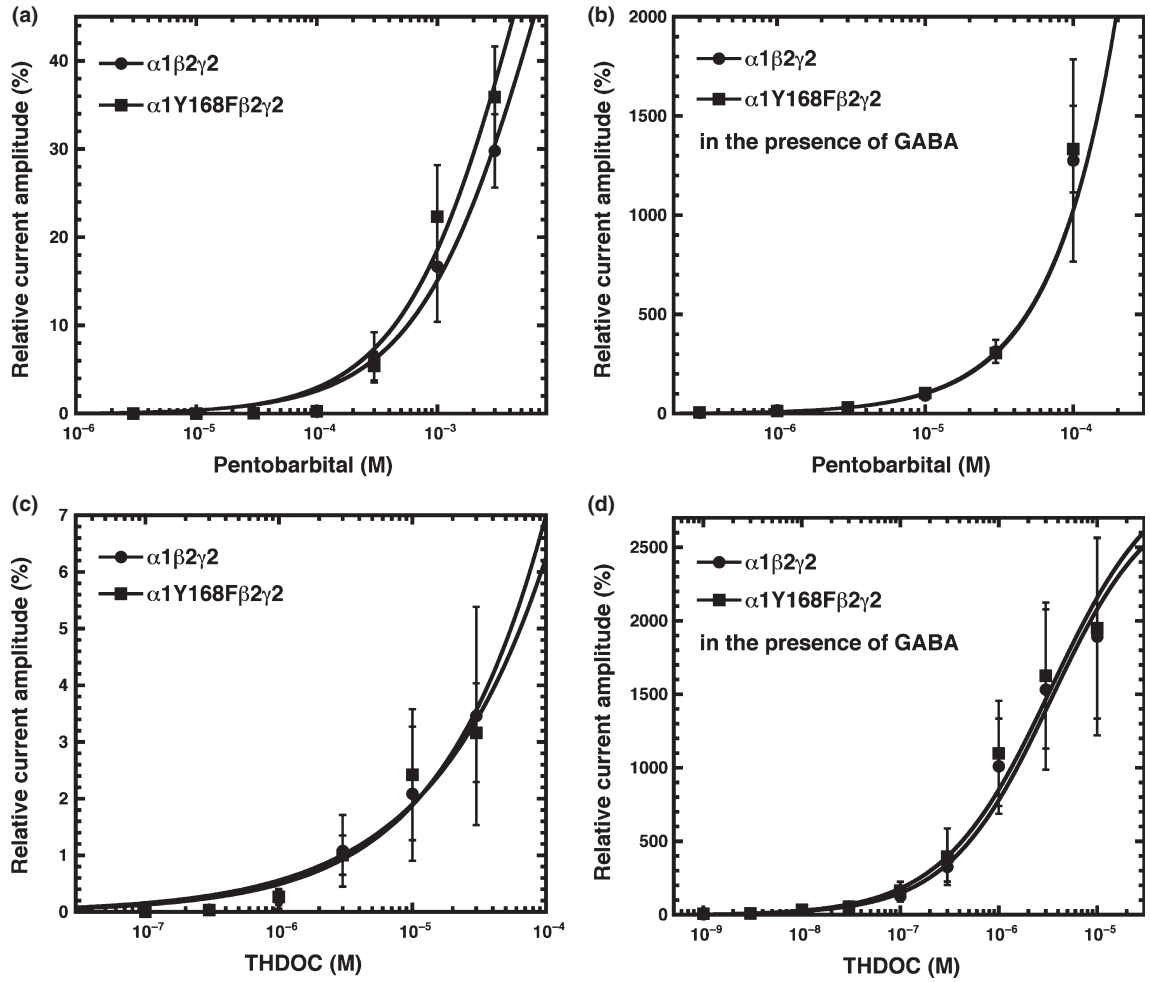

Fig. 6 Modulation of wild type $\alpha_1\beta_2\gamma_2$ and mutant α_1Y168F$\beta_2\gamma_2$ receptors by pentobarbital and THDOC (3α,21-dihydroxy-5α-pregnan-20-one) (a) Increasing concentrations of pentobarbital were applied to wild type and mutant receptors in the absence GABA. (b) Increasing concentrations of pentobarbital were applied to wild type and mutant receptors in combination with 1.5 μM GABA. (c) Increasing concentrations of THDOC were applied to wild type and mutant receptors in the absence GABA. (d) Increasing concentrations of THDOC were applied to wild type and mutant receptors in combination with 1.5 μM GABA. Mean ± SD of experiments carried out with three oocytes for each subunit combination are shown.

Location of α_1Y168 in the receptor

Figure 7 is based on a homology model of part of the extracellular domain of the $\alpha_1\beta_2\gamma_2$ $GABA_A$ receptor. The α_1 subunit is shown in yellow and the γ_2 subunit in bright blue. The amino acid residue α_1Y168 (atoms as spheres) is neither located in the binding site for GABA or that for benzodiazepines, nor is it located in the loop F of the γ_2 subunit (dark blue). It is located neighboring the N-terminal end of loop F as defined in Hanson and Czajkowski (2008) in the α_1 subunit (orange).

Discussion

We made observations relevant for the question how the signal induced by binding of benzodiazepines is propagated to an altered channel function in $GABA_A$ receptors. As amino acid residues located in the benzodiazepine binding site are homologous to amino acid residues located in the agonist site for GABA (reviewed in Sigel and Buhr 1997) our observations may be relevant for the question how the signal induced by binding of GABA is propagated to the ion channel. If this is the case, the experimental findings could concern the entire cys-loop ligand-activated receptor family.

Introduction of the conservative point mutation α_1Y168F into $\alpha_1\beta_2\gamma_2$ leaves channel gating by GABA and high affinity binding of benzodiazepines unaltered while channel modulation by benzodiazepines is strongly reduced. Channel gating and modulation by pentobarbital and THDOC and current inhibition by zinc ions are all unaffected by the mutation, pointing to a specificity of the mutation for benzodiazepine modulation. We observe a strong reduction of efficacy and potency of the current potentiation by

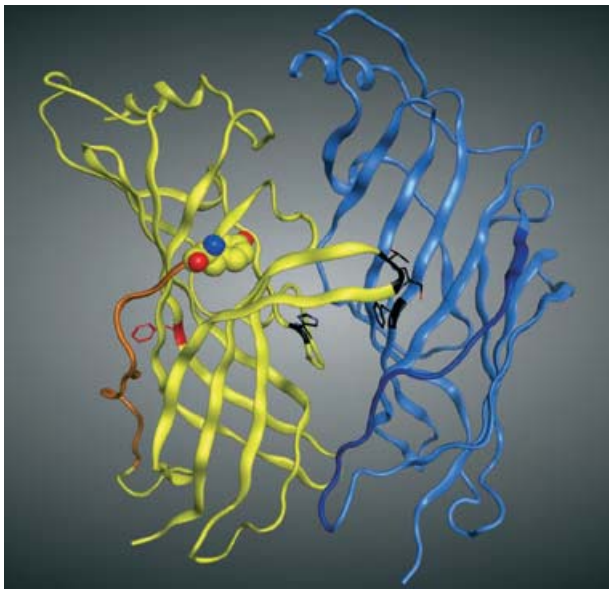

Fig. 7 Scheme of part of the extracellular domain of the $\alpha_1\beta_2\gamma_2$ $GABA_A$ receptor. The channel part that would be in the bottom extension is not shown. The α_1 subunit is colored in yellow and the γ_2 subunit in bright blue. α_1Y168 is shown in the space fill representation. Residues α_1H101 α_1S205 α_1T206 and γ_2F77 in the binding site for benzodiazepines highlighted in black and residue α_1F64 in the binding site for GABA in red are all shown in the stick representation. Loop F of the α_1 subunit is colored in orange and loop F of the γ_2 subunit in dark blue.

diazepam and zolpidem. Interestingly, not only positive but also negative allosteric modulators were affected.

The mutation has little influence on the binding properties of benzodiazepines to recombinant $\alpha_1\beta_2\gamma_2$ $GABA_A$ receptors expressed in HEK293 cells. As the observations on receptor function were made with receptors expressed in Xenopus oocytes, it may be argued that the γ_2 subunit essential for the formation of the benzodiazepine binding pocket was missing in the large majority of these receptors. We therefore expressed $\alpha_1\beta_2$ and α_1Y168Fβ_2 receptors and compared their apparent agonist affinities with $\alpha_1\beta_2\gamma_2$ and α_1Y168F$\beta_2\gamma_2$ receptors. Inclusion of the γ_2 subunit lowered the affinity in a similar way in wild type and mutant receptors, showing its presence in wild type and mutant receptors.

The amino acid residue α_1Y168 locates outside of the binding pocket for benzodiazepines and does not take part in the formation of loop F of the γ_2 subunit. It is also not located in theoretical lines projecting from binding site towards the ion channel. Intriguingly, it is located neighboring the N-terminal end of the loop F of the α_1 subunit. It could be argued that the mutation allosterically affects loop F of the γ_2 subunit. However, in spite of the location of the mutation at the N-terminal to the end of loop F of the α_1 subunit, somewhat unexpectedly gating of the channel by GABA remains unaffected. This loop has been implicated in the signaling from agonist site to channel. Newell and Czajkwski (2003) used the substituted cysteine accessibility method to characterize Pro174-Asp191 of the F-loop of the α_1 subunit. They suggested that this protein segment is aqueous-exposed and adopts a random coil conformation. Their findings also indicate that a part of this segment may act as a dynamic element during channel-gating transition. Occupation of the binding site for benzodiazepines in wild type receptors leads to an increase in the affinity for GABA binding. It may be hypothesized that α_1Y168 is involved in this process. Specifically a hydrogen bridge between the side chain of residue 168 with some unknown partner may be important as the mutation from Y to F compromises the ability of this side chain to form such a bridge. Indeed, in the mutant receptor potentiation by benzodiazepines is strongly blunted and consequently an increase in the apparent affinity for GABA may also be blunted.

Padgett and Lummis (2008) introduced point mutations independently into the C-terminal residues of loop F of the γ_2 subunit, Asp192-Arg197. Radioactive ligand binding of benzodiazepines to receptors expressed in HEK293 cells was unaffected by the mutations. In contrast, after expression in Xenopus oocytes, apparent affinity and maximum of modulation by diazepam was affected by mutation of each residue. The authors concluded that loop F contributes to the modulation by benzodiazepines and that its mobility may be a key to modulation.

On the basis of similar work, Hanson and Czajkowski (2008) also suggested, that 'γ_2 Loop F is a specific transducer of positive benzodiazepine modulator binding'. They reached this conclusion by studying receptors in which all residues of loop F of the γ_2 subunit were individually mutated to cysteine. After expression in HEK293 cells, binding properties for benzodiazepine ligands remained unaffected, while after expression in Xenopus oocytes mutation of some selected residues led to an increase or decrease in flurazepam potency and/or efficacy of modulation.

Our observations do not confirm or contradict observations that implicate loop F of the γ_2 subunit in linking binding of benzodiazepines to channel communication. But they challenge the notion that the conformational change linking binding and channel modulation is restricted to loop F of the γ_2 subunit. More likely, a large portion of the receptor is conformationally affected by the binding of benzodiazepines and contributes to signaling to the channel portion. Similar considerations may apply to the question, how the binding of agonists of the ligand gated ion channel family is communicated to receptor activation.

Acknowledgements

We thank Dr. V. Niggli for carefully reading the manuscript. This work was supported by the Swiss National Science Foundation grant

3100A0-105272/2. L.R. is grateful to the Austrian Academy of Sciences for financial support under the framework of the DOC programme (grant 2021).

References

Baumann S. W., Baur R. and Sigel E. (2001) Subunit arrangement of γ-aminobutyric acid type A receptors. *J. Biol. Chem.* **276**, 36275–36280.

Baumann S. W., Baur R. and Sigel E. (2002) Forced subunit assembly in $\alpha_1\beta_2\gamma_2$ $GABA_A$ receptors. *J. Biol. Chem.* **277**, 46020–46025.

Baur R. and Sigel E. (2007) Replacement of histidine in position 105 in the α_5 subunit by cysteine stimulates zolpidem sensitivity of $\alpha_5\beta_2\gamma_2$ $GABA_A$ receptors. *J. Neurochem.* **103**, 2556–2564.

Baur R., Minier F. and Sigel E. (2006) A $GABA_A$ receptor of defined subunit composition and positioning, Concatenation of five subunits. *FEBS Lett.* **580**, 1616–1620.

Baur R., Tan K. R., Lüscher B. P., Gonthier A., Goeldner M. and Sigel E. (2008) Covalent modification of $GABA_A$ receptor isoforms by a diazepam analogue provides evidence for a novel benzodiazepine binding site that prevents modulation by these drugs. *J. Neurochem.* **106**, 2353–2356.

Bertocci B., Miggiano V., Da Prada M., Dembic Z., Lahm H.-W. and Malherbe P. (1991) Human catechol-O-methyltransferase: cloning and expression of the membrane-associated form. *Proc. Natl Acad. Sci. USA* **88**, 1416–1420.

Boileau A. J. and Czajkowski C. (1999) Identification of transduction elements for benzodiazepine modulation of the GABA(A) receptor: three residues are required for allosteric coupling. *J. Neurosci.* **19**, 10213–10220.

Boileau A. J., Baur R., Sharkey L. M., Sigel E. and Czajkowski C. (2002) The relative amount of cRNA coding for γ2 subunits affects stimulation by benzodiazepines in $GABA_A$ receptors expressed in Xenopus oocytes. *Neuropharmacology* **43**, 695–700.

Brejc K., van Dijk W. J., Klaassen R. V., Schuurmans M., van Der Oost J., Smit A. B. and Sixma T. K. (2001) Crystal structure of an ACh-binding protein reveals the ligand-binding domain of nicotinic receptors. *Nature* **411**, 269–276.

Chen C. and Okayama H. (1987) High-efficiency transformation of mammalian cells by plasmid DNA. *Mol. Cell. Biol.* **7**, 2745–2752.

Cheng Y. C. and Prusoff W. H. (1973) Relationship between the inhibition constant (K1) and the concentration of inhibitor which causes 50 per cent inhibition (I50) of an enzymatic reaction. *Biochem. Pharmacol.* **22**, 3099–3108.

Ernst M., Bruckner S., Boresch S. and Sieghart W. (2005) Comparative models of $GABA_A$ receptor extracellular and transmembrane domains: important insights in pharmacology and function. *Mol. Pharmacol.* **68**, 1291–1300.

Hansen S. B., Sulzenbacher G., Huxford T., Marcot P., Taylor P. and Bourne Y. (2005) Structures of Aplysia AChBP complexes with nicotinic agonists and antagonists reveal distinctive binding interfaces and conformations. *EMBO J.* **24**, 3635–3646.

Hanson S. M. and Czajkowski C. (2008) Structural mechanisms underlying benzodiazepine modulation of the GABA(A) receptor. *J. Neurosci.* **28**, 3490–3499.

Kash T. L., Jenkins A., Kelley J. C., Trudell J. R. and Harrison N. L. (2003) Coupling of agonist binding to channel gating in the $GABA_A$ receptor. *Nature* **421**, 272–275.

Khatri A. and Weiss D. S. (2010) The role of Loop F in the activation of the GABA receptor. *J. Physiol.* **588**, 59–66.

Khatri A., Sedelnikova A. and Weiss D. S. (2009) Structural rearrangements in loop F of the GABA receptor signal ligand binding, not channel activation. *Biophys. J.* **96**, 45–55.

Lummis S. C., Beene D. L., Lee L. W., Lester H. A., Broadhurst R. W. and Dougherty D. A. (2005) Cis-trans isomerization at a proline opens the pore of a neurotransmitter-gated ion channel. *Nature* **438**, 248–252.

Lyford L. K., Sproul A. D., Eddins D., McLaughlin J. T. and Rosenberg R. L. (2003) Agonist-induced conformational changes in the extracellular domain of alpha 7 nicotinic acetylcholine receptors. *Mol. Pharmacol.* **64**, 650–658.

Macdonald R. L. and Olsen R. W. (1994) $GABA_A$ receptor channels. *Annu. Rev. Neurosci.* **17**, 569–602.

Mercado J. and Czajkowski C. (2006) Charged residues in the α1 and β2 pre-M1 regions involved in $GABA_A$ receptor activation. *J. Neurosci.* **26**, 2031–2040.

Minier F. and Sigel E. (2004) Positioning of the alpha-subunit isoforms confers a functional signature to gamma-aminobutyric acid type A receptors. *Proc. Natl Acad. Sci. USA* **101**, 7769–7774.

Newell G. J. and Czajkwski C. (2003) The $GABA_A$ receptor α_1 subunit Pro^{174}-Asp^{191} is involved in GABA Binding and channel gating. *J. Biol. Chem.* **278**, 13166–13172.

Padgett C. L. and Lummis S. C. (2008) The F-loop of the GABA A receptor gamma2 subunit contributes to benzodiazepine modulation. *J. Biol. Chem.* **283**, 2702–2708.

Pless S. A. and Lynch J. W. (2009) Ligand-specific conformational changes in the alpha1 glycine receptor ligand-binding domain. *J. Biol. Chem.* **284**, 15847–15856.

Rabow L. E., Russek S. J. and Farb D. H. (1995) From ion currents to genomic analysis, recent advances in $GABA_A$ receptor research. *Synapse* **21**, 189–227.

Sali A. and Blundell T. L. (1993) Comparative protein modelling by satisfaction of spatial restraints. *J. Mol. Biol.* **234**, 779–815.

Sieghart W. (1995) Structure and pharmacology of gamma-aminobutyric acidA receptor subtypes. *Pharmacol. Rev.* **47**, 181–233.

Sieghart W. and Sperk G. (2002) Subunit composition, distribution and function of $GABA_A$ receptor subtypes. *Curr. Top. Med. Chem.* **2**, 795–816.

Sigel E. (1987) Properties of single sodium channels translated by Xenopus oocytes after injection with messenger ribonucleic acid. *J. Physiol.* **386**, 73–90.

Sigel E. and Buhr A. (1997) The benzodiazepine binding site of GABAA receptors. *Trends Pharmacol. Sci.* **18**, 425–429.

Sigel E. and Minier F. (2005) Educational paper: the Xenopus oocyte: system for the study of functional expression and modulation of proteins. *Mol. Nutr. Food Res.* **49**, 228–234.

Sigel E., Baur R., Trube G., Mohler H. and Malherbe P. (1990) The effect of subunit combination of rat brain GABAA receptors on channel function. *Neuron* **5**, 703–711.

Sigel E., Buhr A. and Baur R. (1999) The conserved lysine residue in the middle of the predicted extracellular loop between M2 and M3 in the $GABA_A$ receptor is involved in channel gating. *Neurochem* **73**, 1758–1764.

Thompson J. D., Higgins D. G. and Gibson T. J. (1994) CLUSTAL W: improving the sensitivity of progressive multiple sequence alignment through sequence weighting, position-specific gap penalties and weight matrix choice. *Nucleic Acids Res.* **22**, 4673–4680.

Thompson A. J., Padgett C. L. and Lummis S. C. (2006) Mutagenesis and molecular modeling reveal the importance of the $5\text{-}HT_3$ receptor F-loop. *J. Biol. Chem.* **281**, 16576–17582.

Unwin N. (2005) Refined structure of the nicotinic acetylcholine receptor at 4A resolution. *J. Mol. Biol.* **346**, 967–989.

Williams C. A., Bell S. V. and Jenkins A. (2009) A Residue of the β2-subunit stabilizes the closed state of the $GABA_A$ receptor. *J. Biol. Chem.* **285**, 7281–7287.

C. Concluding Discussion

The main part of this thesis (*Richter et al., 2012,* **B.I**) is concerned with the elucidation of the binding mode of 1,4-benzodiazepines at the benzodiazepine binding site in α1β2γ2 $GABA_A$ receptors. In the absence of a crystal structure of the ligand-bound benzodiazepine binding site of $GABA_A$ receptors, protein homology modeling and computational ligand docking are the only source of structure-based hypotheses for the interaction of benzodiazepines with their binding site. However, accurate prediction of membrane protein structures and ligand interactions remains a challenge[1], and requires accurate modeling of structurally divergent regions and extensive use of experimental evidence, as shown recently in a community-wide GPCR structure prediction assessment. In the article *(Richter et al., 2012,* **B.I***)* the workflow for identifying the binding mode of 1,4-benzodiazepines can be divided into two steps in order to overcome the obstacles of **"homology model ambiguity"** (*exploration step*) and **"docking scoring deficiences"** (*selection step*).

In the first *exploration step,* the local uncertainty resulting from structurally divergent regions of related cys-loop receptor family members was compensated by constructing a variety of homology models from different templates, resulting in an array of homology models with varying backbone conformations. Further variability was added by enabling flexible sidechains during the docking procedure and retaining the 100 best ranked poses per ligand per model. Inevitable this ends up with a multitude of possible binding modes, **but with a high likelihood of generating the correct ligand-receptor complex.**

The great challenge of the subsequent step, the *selection step,* was the identification of this correctly generated ligand-receptor complex out of an ocean of docking poses. The first selection criterion was based on the common binding mode (**CBM**) hypothesis. The CBM assumes that diazepam and its close structural analogues exhibit a common binding mode within the benzodiazepine binding pocket. Indeed,clustering of ligand poses according to a similar orientation of their common structure as well as according to similar interactions with pocket amino acid residues finally led to three common binding mode geometries, CBM I – III. The CBM hypothesis accomplished to integrate experimental knowledge (mutagenesis data, labeling data, structure-activity relationships) deriving from different ligands and even from an additional ligand class (flumazenil, belonging to the class of imidazobenzodiazepines) for binding mode evaluation.

Here, **CBM I is convincingly supported by a large variety of structural, computational and experimental evidence** and taken together, overwhelming evidence indicates that CBM I is the correct binding mode of diazepam in the benzodiazepine binding pocket.

Previous studies also featured docking poses of diazepam or its analogues. Overall, however, conclusions remained contradictory. Thus, in one study[2] a flunitrazepam orientation similar to CBM III poses was reported. Another study[3] identified a diazepam pose vaguely similar to CBM I, but apparently with a very different interaction pattern due to a different pocket topology. A pharmacophore derived diazepam pose[4] is in a position intermediate between CBM II and I. Most recently, binding modes vaguely resembling our CBM II were proposed based on modeling structures from a single template and covalently incorporated ligands.[5] In a study more concerned with zolpidem[6], flunitrazepam poses featured the P-conformation, which has been demonstrated to be inactive at the benzodiazepine binding site.

Ultimately, two virtual screening runs were applied based on the structures of CBM I ligand-receptor complexes that finally lead to the identification of three new, experimentally validated, benzodiazepine binding site ligand classes. The first screen was based on a structure-based pharmacophore model derived from CBM I while the second was a docking-based virtual screening run against CBM I structures. This was, for the very first time, the application of structure-based methods in the successful identification of new benzodiazepine binding site ligands. Further exploration of in silico screening results presumably will identify additional novel ligand classes for the benzodiazepine binding site.

Next to the identification of the binding mode, the structural model of the benzodiazepine binding site was also used for investigating the mechanism of the allosteric transduction from modulator binding to altered channel gating. For this reason, a computational analysis of the intra-molecular protein-protein interactions in the proximity to the benzodiazepine binding site was undertaken. This procedure finally aided in the selection of α1Y68 as a candidate for receptor mutation. Subsequent experimental studies then proved that α1Y168 plays an important role in the allosteric coupling mechanism. The whole study was published in the article of Baur et al.[7](**B.II**), with the thesis author contributing as a co-author.

In order to gain more detailed insights into the allosteric coupling mechanism, molecular dynamic studies will identify the flexible and rigid parts of the pocket and define their ligand-

pocket interactions as well as the mechanism of allosteric modulation of positive, negative and neutral interactors.

In a broader view, the gained structural model of the benzodiazepine binding site (*Richter et al., 2012*)[8] can also be used for modelling of the benzodiazepine-binding sites of other $GABA_A$ subtypes. Docking of unselective and subtype-selective ligands into their binding sites will ultimately lead to an improvement of our understanding of the molecular determinants for subtype selectivity of ligands on $GABA_A$ receptors. This knowledge will aid the development of subtype selective benzodiazepine binding site ligands, avoiding interactions with subtypes known to be responsible for benzodiazepine addiction[9].
Finally, the underlying computational workflow can stimulate other groups, aiming to integrate various information sources for binding mode evaluation of structurally unresolved membrane proteins.

References:

1. Michino, M. et al. Community-wide assessment of GPCR structure modelling and ligand docking: GPCR Dock 2008. *Nat. Rev. Drug Discov.* **8**, 455-463 (2009).
2. Mokrab, Y. et al. Exploring ligand recognition and ion flow in comparative models of the human GABA type A receptor. *J. Mol. Graph. Model.* **26**, 760-774 (2007).
3. Ci, S., Ren, T. & Su, Z. Investigating the putative binding-mode of GABA and diazepam within GABA A receptor using molecular modeling. *Protein J.* **27**, 71-78 (2008).
4. Clayton, T. et al. An updated unified pharmacophore model of the benzodiazepine binding site on gamma-aminobutyric acid(a) receptors: correlation with comparative models. *Curr. Med. Chem.* **14**, 2755-2775 (2007).
5. Berezhnoy, D., Gibbs, T.T. & Farb, D.H. Docking of 1,4-benzodiazepines in the alpha1/gamma2 GABA(A) receptor modulator site. *Mol. Pharmacol.* **76**, 440-450 (2009).
6. Sancar, F., Ericksen, S.S., Kucken, A.M., Teissére, J.A. & Czajkowski, C. Structural determinants for high-affinity zolpidem binding to GABA-A receptors. *Mol. Pharmacol.* **71**, 38-46 (2007).
7. Baur, R., Luscher, B.P., Richter, L. & Sigel, E. A residue close to alpha1 loop F disrupts modulation of GABAA receptors by benzodiazepines while their binding is maintained. *J Neurochem* **115**, 1478-85 (2010).
8. Richter, L. et al. Diazepam-bound GABA(A) receptor models identify new benzodiazepine binding-site ligands. *Nat Chem Biol* (2012).
9. Tan, K.R., Rudolph, U. & Luscher, C. Hooked on benzodiazepines: GABAA receptor subtypes and addiction. *Trends Neurosci* **34**, 188-97 (2011).

CURRICULUM VITAE

LARS RICHTER

Postal address	Sprögnitz 1 3910 Zwettl
Telephone number	0664/ 183 72 60
E-Mail address	lars.richter@univie.ac.at

Date of birth	23.02.1982
Place of birth	Hannover
Citizenship	Deutsch
Marital status	ledig

EDUCATION

10/2007	Beginning with "Doktoratsstudium Pharmazie" at the University of Vienna
05/2007	Completion of pharmacy study at the University of Vienna
05/2007	3.Diplomprüfung with excellence, grade: 1,0
03/2007	2.Diplomprüfung with excellence, grade: 1,25
01/2004	1.Diplomprüfung with excellence, grade: 1,5
10/2002	Beginning with pharmacy study at the University of Vienna
1993 – 2002	Bundesrealgymnasium Zwettl / lower austria
1989 – 1993	Volksschule Groß Globnitz / lower austria

TEACHING ACTIVITIES

10/2008 – 03/2012	Teaching activity at the Department of Pharmaceutical Chemistry
03/2007 – 09/2008	Tutor at the Department of Pharmaceutical Chemistry
08/2006 – 09/2008	Tutor at the Department of Pharmacology and Toxicology

AWARDS & PRIZES

01/2008	DOC-fellowship from the Austrian Academy of Sciences
12/2007	Würdigungspreis des Bundesministeriums für Wissenschaft und Forschung
11/2007	Leistungsstipendium der Pharmazeutischen Gehaltskasse

SPECIAL KNOWLEDGE AND SKILLS

foreign language english	very good knowledge	
foreign language portuguese	good knowledge	
computer knowledges	operating systems:	Windows, Linux
	programs:	MOE, FlexX, Schrödinger
	programming languages:	Scientific Vector Language (SVL)

LEBENSLAUF

LARS RICHTER

Adresse	Sprögnitz 1 3910 Zwettl
Telefon	0664/ 183 72 60
E-Mail	lars.richter@univie.ac.at
Geburtsdatum	23.02.1982
Geburtsort	Hannover
Staatsbürgerschaft	Deutsch
Familienstand	ledig

AUSBILDUNG

10/2007	Beginn Doktoratsstudium Pharmazie
05/2007	Abschluss des Pharmaziestudiums an der Universität Wien
05/2007	3.Diplomprüfung mit Auszeichnung, Note: 1,0
03/2007	2.Diplomprüfung mit Auszeichnung, Note: 1,25
01/2004	1.Diplomprüfung mit Auszeichnung, Note: 1,5
10/2002	Beginn des Pharmaziestudiums an der Universität Wien
1993 – 2002	Bundesrealgymnasium Zwettl / NÖ
1989 – 1993	Volksschule Groß Globnitz / NÖ

LEHRTÄTIGKEITEN

10/2008 – 03/2012	Lehrtätigkeit am Department für Medizinische Chemie
03/2007 – 09/2008	Tutor am Department für Medizinische Chemie
08/2006 – 09/2008	Tutor am Department für Pharmakologie und Toxikologie

AUSZEICHNUNGEN & PREISE

01/2008	DOC-Stipendium der Österreichischen Akademie der Wissenschaften
12/2007	Würdigungspreis des Bundesministeriums für Wissenschaft und Forschung
11/2007	Leistungsstipendium der Pharmazeutischen Gehaltskasse

BESONDERE KENNTNISSE UND FÄHIGKEITEN

Fremdsprache Englisch	sehr gute Kenntnisse	
Fremdsprache Portugiesisch	gute Kenntnisse	
Computerkenntnisse	Betriebssystem:	Windows, Linux
	Programme:	MOE, FlexX, Schrödinger
	Programmiersprachen:	Scientific Vector Language (SVL)